Co-funded by the European Union

DEBSEUz

"TIIAME" NATIONAL RESEARCH UNIVERSITY

A.Mirzabaev, J.Izzatillaev, D.Kodirov, T.Makhkamov

DESIGN OF ENERGY DEVICES AND STATIONS BASED ON ALTERNATIVE ENERGY SOURCES

“TIIAME” NATIONAL RESEARCH UNIVERSITY

A. Mirzabaev, J. Izzatillaev, D. Kodirov, T. Mahkamov

DESIGN OF ENERGY DEVICES AND STATIONS BASED ON ALTERNATIVE ENERGY SOURCES

Textbook / Study Guide for Higher Education Students

Tashkent 2025

This study book has been recommended for publication in accordance with Order № 409-a/f, dated December 31, 2025, of the Scientific Council of the “National Research University TIIAME”.

The study book has been prepared based on a new curriculum developed through the analysis of international educational plans and programs for higher education. The book entitled “Design of energy devices and stations based on alternative energy sources” is an educational and methodological guide devoted to the design, calculation, and practical installation of energy devices that operate using renewable energy sources.

This book is mainly intended for students, master’s degree students, and specialists studying in the fields of energy engineering, electrical engineering, and renewable energy.

The book provides detailed information about the types of alternative energy sources, their operating principles, and their role in modern energy systems. It also examines the possibilities of using energy sources such as solar energy, wind energy, biogas, biomass, and small hydropower, as well as their advantages and economic efficiency. In addition, the engineering calculations, technical requirements, and stages of designing renewable energy systems are also described.

This study book has been prepared as one of the practical outcomes of the project “Development of a Training Program for Targeted Engineers in Solar Energy in Uzbekistan” (101128871 – DEBSEUz – ERASMUS-EDU-2023-CBHE) implemented within the framework of the European Union’s Erasmus+ program.

Author:

A. Mirzabaev – Professor of the Department of Power Supply and Renewable Energy Sources, “TIIAME” National Research University.

J.O. Izzatillaev – Head of the Department of Power Supply and Renewable Energy Sources, “TIIAME” National Research University.

D.B. Kodirov – Dean of the Faculty of Energy, “TIIAME” National Research University.

A.A. Mahkamov – Deputy Director of “MIR SOLAR” LLC.

Reviewers:

M. Murodov – Associate Professor of the Department of Energy Engineering, Faculty of Energy, Namangan State Technical University, Candidate of Technical Sciences (PhD).

O. Matchonov – Head of the Department of Electrotechnology and Operation of Electrical Equipment, “TIIAME” National Research University, Doctor of Philosophy in Technical Sciences (PhD).

© TIIAME – National Research University, 2025

CONTECTS

INTRODUCTION 7
CHAPTER 1. FUNDAMENTALS OF SOLAR ENERGY 9
§1.1. SOLAR RADIATION 9
§1.2. ANALEMMA 14
§1.3. SOLAR RADIATION SPECTRUM 17
§1.4. ATMOSPHERE MASS 20
§1.5. PHOTOELECTRIC EFFECT 23
§1.6. THE SHOCKLEY-QUEISSER LIMIT 28
CHAPTER 2. PHOTOVOLTAIC MODULES 31
§2.1. PHOTOVOLTAIC MODULES 31
§2.2. TEST CONDITIONS (STC, NOCT, AND NMOT) 41
§2.3. ELECTRICAL PARAMETERS AND VOLT-AMPERE CHARACTERISTICS OF THE PHOTOVOLTAIC MODULE. 44
§2.4. REVIEW OF THE TECHNICAL SPECIFICATION OF THE PHOTOVOLTAIC MODULE 50
§2.5. INSTALLATION OF PHOTOVOLTAIC MODULES 54
§2.6. MAINTENANCE OF PHOTOVOLTAIC MODULES 68
CHAPTER 3. INVERTERS 73
§3.1. PULSE-WIDTH MODULATION 73
§3.2. PRINCIPAL CIRCUIT DIAGRAM OF THE INVERTER 76
§3.4. EFFICIENCY COEFFICIENT INVERTER 94
§3.5. HYBRID AND STANDALONE INVERTERS 99
§3.6. REQUIREMENTS AND RECOMMENDATIONS FOR INSTALLATION INVERTER 104
§3.7. EVOLUTION OF INVERTER ARCHITECTURES AND PROTECTION SYSTEMS 105
CHAPTER 4. DESIGN OF PHOTOVOLTAIC POWER PLANTS 114
§4.1. BASIC GEOMETRY IN ENGINEERING PRACTICE OF PHOTOVOLTAIC POWER PLANTS 114
§4.2. CLASSIFICATION OF PHOTOVOLTAIC POWER PLANTS 122
§4.3. BASIC PRINCIPLES AND GUIDELINES FOR DESIGNING PHOTOVOLTAIC POWER PLANTS 126
§4.4. ANALYSIS OF DESIGN SOLUTIONS FROM PRACTICAL EXPERIENCE 144

§4.5. Cable selection 161
§4.6. Interaction of the inverter with components of the power system 172
§4.7. Grounding 178
§4.8. Lightning protection 181
CHAPTER 5. DESIGN OF WIND POWER PLANTS 184
§5.1. Wind and its formation 184
§5.2. Prospects for the utilization of wind energy in Uzbekistan 188
§5.3. International standards for wind turbines published by the International Electrotechnical Commission (IEC) 191
§5.4. Components of a wind turbine 192
§5.5 Wind turbine tower 200
§5.6 Wind turbine blades 205
§5.7 Determination of the number of wind energy systems 217
CHAPTER 6. DESIGN OF HYDROELECTRIC POWER PLANTS 221
§6.1 Methods of utilizing energy of low-head water flows 221
§6.2 Determination of hydropower resources 228
§6.3. Structure and operating principle of a hydroelectric power plant 230
CHAPTER 7. DESIGN OF BIOGAS POWER PLANTS 243
§7.1. Biogas production units and their operation process. 243
§7.2. Anaerobic digestion process of organic biomass. 247
§7.3. Biogas: composition, formation process, and yield. 263
REFERENCES 270

INTRODUCTION

In recent years, rapid development has been observed in the field of solar energy both in the Republic of Uzbekistan and worldwide. In accordance with the Development Strategy of the Republic of Uzbekistan until 2030, it is planned to commission photovoltaic power plants (PVPPs) with a total installed capacity exceeding 12 GW and to increase the share of renewable energy sources (RES) in total electricity generation to 54% [1], [2], [3]. A significant portion of this capacity more than 1.2 GW will be provided by small and medium-scale photovoltaic power plants with capacities below 1 MW, which are intended for distributed and local power supply facilities.

The rapid growth of investments in solar energy has led to a significant increase in the number of companies operating in this sector, as well as growing interest among engineers, related field specialists, and students of technical higher education institutions. Under such conditions, the demand for qualified personnel and accessible educational materials that facilitate the rapid and effective acquisition of practical skills in the design, construction, and operation of photovoltaic power plants has sharply increased.

This учебное пособие is based on practical experience gained during the implementation of solar power plant projects in Uzbekistan and is aimed at improving the qualifications of engineers, designers, and technical specialists currently working in this field. At the same time, it may also be useful for students in the fields of power engineering and electrical engineering who intend to build a career in renewable energy.

The field of solar energy is developing rapidly: technical solutions, equipment, and the regulatory framework are continuously being improved. Accordingly, the main objective of this guide is not merely to present specific design solutions, but to explain the underlying logical and physical principles and laws behind them. Such an approach helps the reader develop a deep understanding of the processes and enables independent navigation in future technological advancements and regulatory requirements.

It should be noted that the numerical values provided in this guide are approximate in nature, and the technical examples are mainly used to illustrate engineering approaches; they should not be considered as final solutions to specific problems. A reader who thoroughly masters the material of this guide will be able to confidently study topics of interest in greater depth, as they will have a systematic understanding of the key principles and approaches to the design and operation of photovoltaic power plants.

This guide does not include instructions on modeling in specialized software such as PVSyst or PV*Sol, as detailed user manuals and training materials for these programs are available in open sources. It is assumed that the reader will independently acquire the skills to use these tools based on existing resources.

CHAPTER 1. FUNDAMENTALS OF SOLAR ENERGY

This chapter explores the physical phenomena associated with the Sun that form the basis of photovoltaic system operation. This section provides essential information on the characteristics of solar radiation, including its intensity, spectral composition, the Sun's trajectory across the celestial sphere, the analemma, and the effects of atmospheric factors such as pressure and radiation scattering. The fundamentals of the photoelectric effect, a key physical process underlying the conversion of solar energy into electricity and forming the basis of photovoltaic module operation, are also examined. Knowledge of these fundamental aspects is essential for engineers when designing and assessing the performance of photovoltaic power plants. Additional topics not covered in this section are recommended for independent study through specialized literature and professional sources.

§1.1. Solar radiation

Virtually all energy present on Earth originates from the sun in one way or another. Solar radiation is the fundamental energy source sustaining the planet’s climatic and biological processes. For example:

- Wind is generated due to the uneven heating of the Earth's surface by solar radiation, which causes temperature and pressure gradients, thereby forming air currents.
- Hydropower is based on the conversion of the potential energy of water, accumulated by means of solar energy, into electrical energy. Solar radiation causes the evaporation of water, which subsequently falls as precipitation and accumulates in elevated areas. This water, flowing downward, converts its potential energy into kinetic energy, and then through the turbines of hydropower plants into electrical energy.
- Biomass accumulates energy through photosynthesis - a process directly dependent on sunlight.
- Even fossil fuels (oil, gas, coal) are the result of accumulated solar energy in biomass, transformed over millions of years under pressure and heat.

Exceptions include geothermal and nuclear energy, whose origins are linked to

the Earth's internal heat and radioactive decay.

Another partial exception is tidal energy, which is chiefly based on the gravitational influence of the Moon. The Sun’s contribution to this process is also present but is secondary, serving only to amplify or diminish tidal fluctuations.

In the context of photovoltaic power plant design, our primary focus is the direct conversion of solar energy into electrical energy.

Solar radiation - is the flux of electromagnetic energy emitted by the Sun, utilized by photovoltaic modules (PV modules) for direct conversion into electrical energy. The intensity of solar radiation is determined by the solar radiation flux density.

The solar radiation flux density - is a physical quantity that indicates the amount of solar energy incident on a perpendicular surface of 1 m^2 area within 1 second. This parameter is fundamental in determining the efficiency and power output of photovoltaic power plants. The unit of measurement is watts per square meter (W/m^2).

The solar constant - is the solar radiation flux density at the outer boundary of the Earth's atmosphere, incident on a unit area perpendicular to the direction of solar rays, measured at the average Earth-Sun distance.

Despite its name, the solar constant is a conventionally constant average value that in practice varies from approximately 1320 to 1410 W/m^2, depending on the distance between the Earth and the Sun as well as the level of solar activity. However, calculations generally employ the average value of 1361 W/m^2 [13].

The Earth follows an elliptical orbit (see Fig. 1.1) and is closest to the Sun at the point of perihelion (approximately January 3 to 7), whereas the greatest distance occurs at the point of aphelion (approximately July 3 to 7).

Although in January the Earth is closer to the Sun and the value of the solar constant is slightly higher during this period, the actual level of solar radiation on the Earth's surface at this time, particularly in the northern hemisphere including Uzbekistan, remains low.

This is caused by unfavorable geometric and climatic conditions - a low solar elevation angle, short daylight duration, and increased cloud cover.

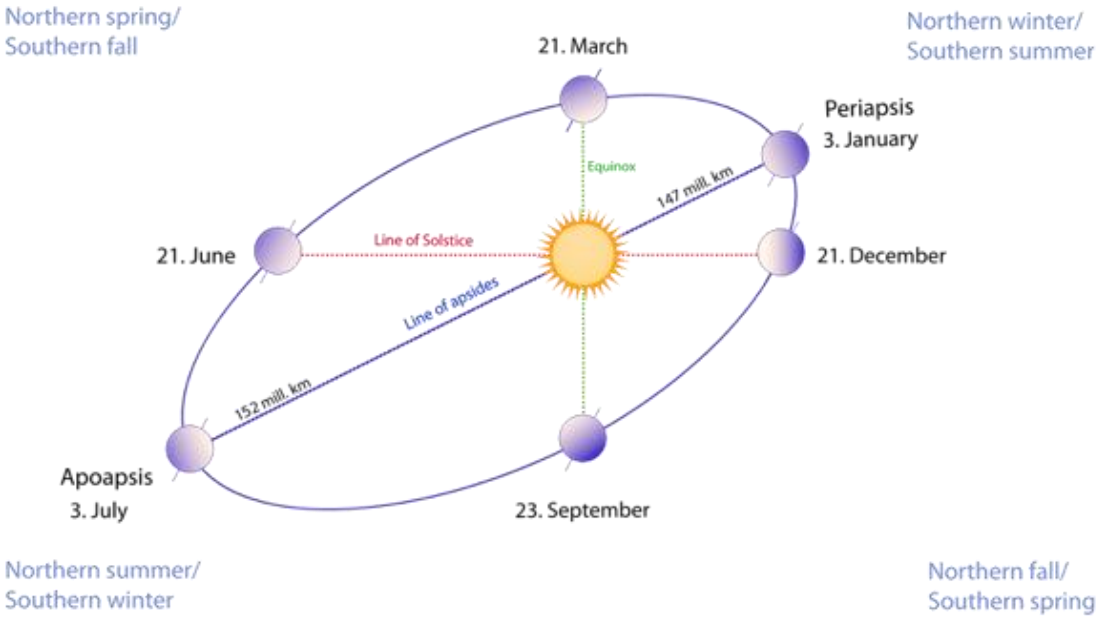

Figure 1.1. Earth's orbit.

The solar constant represents the theoretical maximum solar irradiance on a surface perfectly perpendicular to the Earth's rays in the complete absence of an atmosphere. However, in real conditions, this level is never attained, as a significant portion of solar radiation is attenuated, scattered, and reflected while passing through the atmosphere. Even in clear weather, some energy is lost due to interactions with air molecules, water vapor, dust, and clouds.

As a result, a mixed flux of solar radiation-comprising direct, diffuse and reflected components (see Fig. 1.2)-reaches the surface. Even under the most favorable conditions, such as at noon in ahigh-altitude location,

•the magnitude of direct radiation rarely exceeds 1000 W/m^2, which is considerably lower than the solar constant.

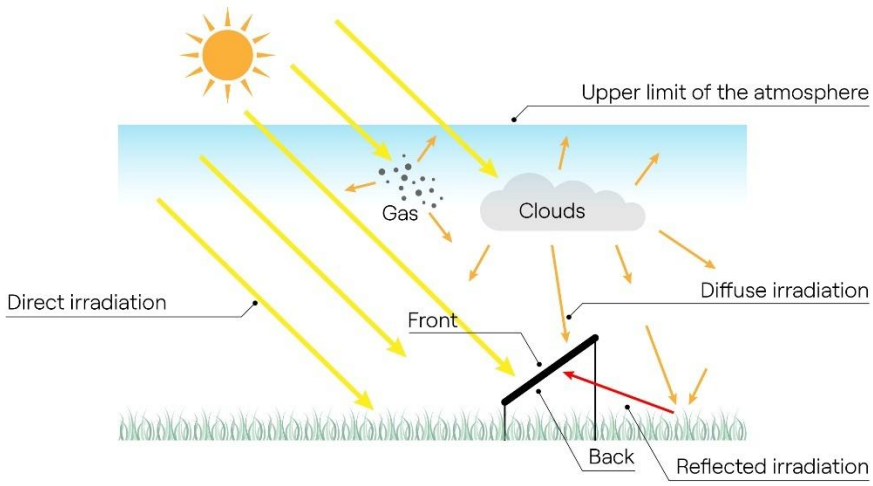

Figure 1.2. Components of solar radiation.

Direct solar radiation (DNI - Direct Normal Irradiance) is the component of solar radiation that passes through the atmosphere without scattering and reaches the surface along a straight line from the solar disk. It is measured on a surface oriented perpendicular to the direction of solar rays and attains maximum values under clear weather conditions.

Diffuse radiation (DHI - Diffuse Horizontal Irradiance) is the component of solar radiation scattered in the atmosphere (by air molecules, water vapor, dust, clouds, and other aerosols) and received on the Earth's surface from various directions within the sky hemisphere. Unlike direct radiation, diffuse light is present even during overcast conditions and supplies energy to the surface in the absence of the direct solar disk.

Reflected (from the surface) radiation (RHI-Reflected Horizontal Irradiance, also known as Albedo Irradiance) is the portion of solar radiation that is reflected from the earth's surface, water, snow, buildings, and other objects, and can additionally reach inclined photovoltaic modules. This component is especially significant when using bifacial modules, which are capable of capturing radiation from both sides. The magnitude of reflected radiation is determined by the albedo coefficient-he surface's ability to reflect sunlight.

As an example, the albedo values for some common surfaces are presented:

- fresh snow ~ 0.8–0.9
- asphalt (dark) ~ 0.05–0.10
- concrete (light-colored) ~ 0.25–0.35
- metal roof (galvanized, light-colored) ~ 0.35–0.55
- flat roof with bitumen membrane (dark) ~ 0.05–0.10
- white reflective roof (cool roof) ~ 0.65–0.85
- ceramic roof tiles (red) ~ 0.30–0.45

In cases where photovoltaic modules in stationary installations are not oriented strictly southward, the use of bifacial modules combined with measures to increase surface albedo significantly enhances the electricity generation of the photovoltaic power plant.

Global solar irradiance (GHI - Global Horizontal Irradiance for a horizontal surface, GTI - Global Tilted Irradiance for an inclined surface) represents the total

amount of solar energy incident on a given area. It includes direct solar radiation, diffuse radiation from the atmosphere, as well as, when necessary, reflected radiation from the Earth's surface. This indicator is crucial for assessing solar potential and calculating the output of photovoltaic power plants.

In practice, the parameter of global solar radiation at optimal tilt and azimuth (OPTA) for photovoltaic module installation in a specific region (GTI OPTA - Global irradiance at optimal tilt) is also utilized. This parameter is utilized to estimate the maximum attainable level of solar radiation based on the geographic location of the site.

Azimuth - the horizontal angle defining the direction in which photovoltaic modules are oriented relative to geographic north. It is measured clockwise as follows:

- *0° - PV modules are oriented north,*
- *90° - PV modules are oriented east,*
- *180° - PV modules are oriented south,*
- *270° - PV modules are oriented west.*

In the northern hemisphere, including Uzbekistan, PV modules are generally oriented south (azimuth 180°) to maximize their annual energy production.

The tilt angle of the photovoltaic module is the angle between the module plane and the horizontal surface.

Table 1.1 presents the values of direct, diffuse, and global solar radiation, as well as an approximate annual electricity generation of the photovoltaic power plant per unit of installed capacity for various cities in Uzbekistan. The data are provided solely for informational purposes to offer a general understanding of the solar resource level and the potential output of a stationary photovoltaic power plant depending on the installed capacity (source: https:// globalsolaratlas.info / [14]).

Table 1.1 – Solar radiation and specific annual photovoltaic power plant output in Uzbekistan.

City	DNI, kW/m^2	DHI, kW/m^2	GHI, kW/m^2	GTI OPTA kW/m^2	OPTA degrees	PV Gen kWh/kW
Tashkent	1663	655	1670	1918	33/180	1544
Namangan	1296	765	1579	1792	32/180	1433
Fergana	1173	781	1524	1713	32/180	1380
Andijan	1223	773	1543	1744	32/180	1398
Gulistan	1440	722	1629	1841	32/180	1471

Jizzakh	1547	694	1664	1881	32/180	1509
Samarkand	1809	648	1753	2013	33/180	1616
Bukhara	1809	681	1778	2057	34/180	1639
Navoi	1857	655	1776	2057	34/180	1642
Karshi	1824	677	1800	2062	33/180	1641
Termez	1665	757	1811	2042	31/180	1614
Urgench	1680	692	1689	1984	35/180	1606
Nukus	1593	700	1641	1930	36/180	1571

Figure 1.3 shows the average annual electricity output of the photovoltaic power plant in Uzbekistan, normalized per unit of installed capacity, calculated based on solar radiation data from 1999 to 2018 [14].

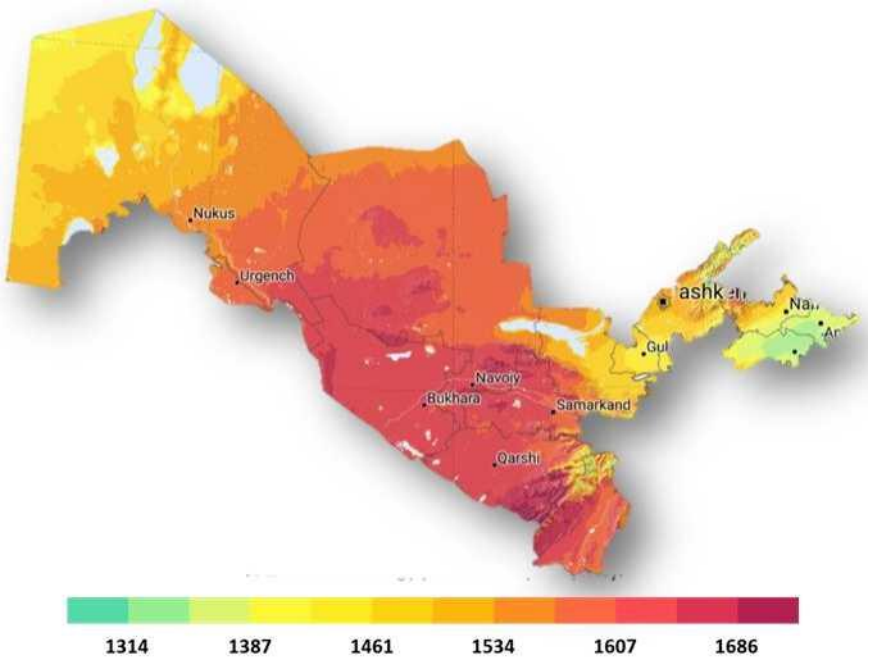

Figure 1.3. Average specific annual output of photovoltaic power plants in Uzbekistan.

§1.2. Analemma

Analemma is a curve illustrating the apparent position of the Sun in the sky at the same time of day (for instance, at solar noon) throughout the year. Graphically, it typically appears as an elongated figure eight (see Fi1.4), although its precise shape depends on the observer's latitude and the coordinate system.

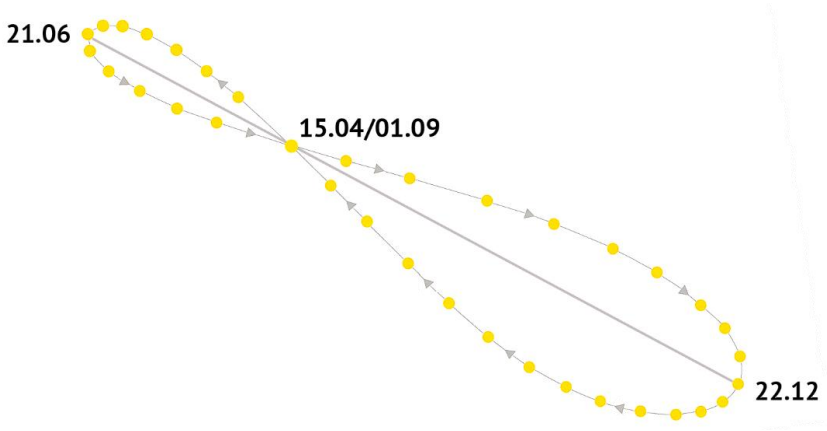

Figure 1.4. Analemma.

The formation of the analemma is related to two principal astronomical factors:

- The tilt of the Earth's axis, causing the Sun's altitude above the horizon to vary throughout the year;

- The ellipticity of the Earth's orbit, whereby the Earth moves around the Sun at a variable speed.

The analemma can be constructed by regularly photographing the Sun's position from a single location at the same time of day throughout the year.

The analemma is of significant importance in the design of photovoltaic power plants. It serves as the basis for determining the optimal tilt angle of photovoltaic modules, considering the specified objectives, system type, and the seasonal variability of loads. Moreover, the analemma directly influences the determination of spacing between rows of photovoltaic modules to prevent mutual shading.

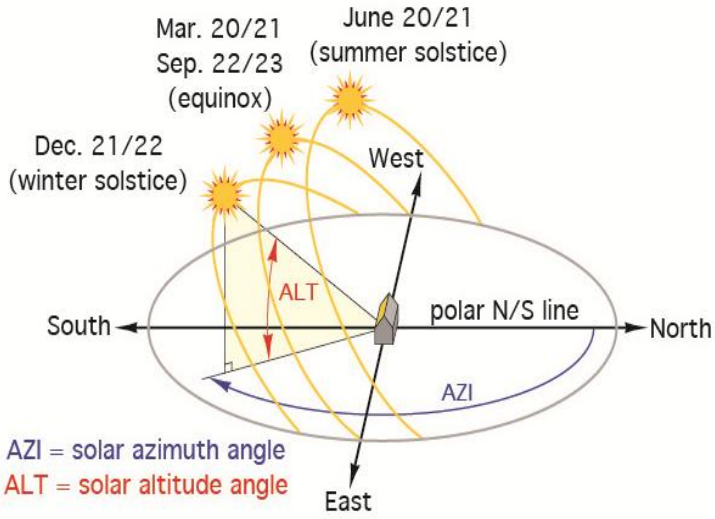

Figure 1.5. The trajectory of the Sun relative to the horizon at the observation point.

Figure 1.5 illustrates the apparent trajectory of the Sun's movement relative to the horizon at the observation point. In the Northern Hemisphere, the Sun reaches its maximum altitude on the day of the summer solstice (June 21), and its minimum altitude on the day of the winter solstice (December 22).

The Sun’s altitude above the horizon depends on the geographic latitude: the closer to the equator, the higher the Sun ascends during the day; The closer to the poles, the lower its maximum altitude.

For example, in Tashkent, the maximum solar altitude at noon on the summer solstice is slightly above 72°, whereas at the equator at this time, the Sun is nearly at the zenith at an elevation of 90°.

The zenith is the point on the celestial sphere located directly above the observer's head, i.e., along the vertical line extending upward from their position on the Earth’s surface.

Since the solar altitude depends on geographic latitude and season, the optimal tilt angle of photovoltaic modules is determined through calculations and simulations based on the defined objectives.

Nevertheless, for a simplified assessment under mid-latitude conditions, including

those in Uzbekistan, the following approximate guidelines can be applied:

- Balanced winter /summer generation: φ= latitude;
- Maximum annual generation: φ = latitude - 10^0;
- Maximum summer generation: φ = latitude - (150...20^0);
- Maximum winter generation: φ = latitude + (100...20^0)

Photovoltaic modules installed at an angle equal to the geographic latitude ensure uniform and balanced electricity generation throughout the year. However, during summer, the Sun rises higher above the horizon, resulting in increased levels of solar radiation. Consequently, reducing the tilt angle by approximately 10° enables an increase in total annual generation due to more efficient output during the spring-summer period, which accounts for the majority of the annual energy balance.

The reduction in the Sun’s altitude during winter creates a risk of shading on the surface of photovoltaic modules, potentially causing a significant drop in generation

precisely when the power system critically requires solar resources.

Therefore, at the design stage, it is essential to consider the minimum solar altitude and calculate the corresponding distance between rows of modules, as well as the influence of external objects causing shading.

It should be noted that during the day the Sun inevitably descends below the horizon (from sunset to sunrise); hence, in calculations, it is advisable to base considerations on the minimum solar altitude near solar noon - for instance, within two hours before and after solar noon.

For example: in Tashkent, on the day of the winter solstice:

- At 10:20, the solar altitude is 19.5°.
- At 12:20, the solar altitude is 25.3°.
- At 14:20, the solar altitude is 19.7°.

Accordingly, when designing a photovoltaic power plant in the city of Tashkent, it is advisable to arrange the modules so that shading is avoided at solar altitudes not lower than 20°.

Geographical (true) noon - *the moment when the Sun reaches its highest elevation above the horizon and is due south (in the northern hemisphere). It does not always coincide with 12:00 standard time, as it depends on the geographical longitude of the specific location.*

For example, on the day of the winter solstice, geographical noon occurs around 12:10 in Andijan, 12:20 in Tashkent, and 13:00 in Nukus.

Additionally, due to the ellipticity of the Earth’s orbit and the tilt of the Earth's axis, the time of geographical noon varies throughout the year - for instance, in Tashkent it occurs at 12:20 on the winter solstice and 12:25 on the summer solstice.

§1.3. Solar radiation spectrum

The solar radiation spectrum is the distribution of solar energy across different wavelengths λ (or frequencies υ). In simple terms, it indicates which types of light and in what quantities arrive from the Sun to the Earth.

Sunlight - is a flux of photons, that is, elementary particles of electromagnetic radiation. Photons have no rest mass or charge but possess energy and momentum, and

it is they who carry the energy of light. Each photon can be represented as a quantum of light the smallest portion of energy that can be absorbed or emitted by matter.

The energy of a single photon is determined by the following formula:

$$\mathbf{E = h \cdot v}$$

where: E - photon energy, J; h - Planck's constant (h = 6.62640^{-34} J·s); v - radiation frequency, Hz.

There is a strict correlation between frequency and wavelength:

$$\mathbf{v = \frac{c}{\lambda}}$$

where: v - radiation frequency, Hz; c - speed of light (c = $3\text{-}10^{8}$ m/s); A - wavelength, m.

Thus, the shorter the wavelength (and correspondingly, the higher the frequency), the greater the photon energy. Conversely, the longer the wavelength (and the lower the frequency), the less energy carried by the photon. Table 1.2 presents the primary wavelength ranges of the solar spectrum.

Table 1.2. Primary wavelength ranges of the solar spectrum

Radiation range	Wavelength	Photon energy (approximate)
Gamma radiation (γ)	<0.01 nm	>100,000 eV
X-ray radiation	0.01 – 10 nm	124 – 100,000 eV
Far ultraviolet (UV-C)	10 – 280 nm	4.5 – 124 eV
Medium ultraviolet (UV-B)	280 – 315 nm	3.9 – 4.5 eV
Near ultraviolet (UV-A)	315 – 400 nm	3.1 – 3.9 eV
Visible light	400 – 700 nm	1.8 – 3.1 eV
Near Infrared (IR-A)	700 – 1400 nm	0.9 – 1.8 eV
Mid Infrared (IR-B)	1400 – 3000 nm	0.4 – 0.9 eV
Far Infrared (IR-C)	3000 nm – 1 mm	0.001 – 0.4 eV
Microwaves	1 mm – 10 cm	<0.001 eV
Radio Waves	>10 cm	<<0.001 eV

The photon energy in traditional units is indicated in electronvolt (eV). To convert electronvolt (eV) to joules (J), the following formula is used:

$$1\ eV = 1.602 \cdot 10^{-19}\ J$$

As shown in Table 1.2, photons of ultraviolet radiation have greater energy than photons in the infrared range, due to their shorter wavelength and higher frequency.

However, the intensity of light is determined not by the energy of an individual photon, but by the total number of photons passing through a unit area per unit time. The greater the number of photons incident on the surface per second, the higher the luminous flux and, consequently, the more intense the radiation. Even if all photons have the same energy (i.e., the same wavelength), the light will appear brighter where their flux density is greater.

Figure 3.6 shows a graph of the relative intensity of the solar radiation spectrum as a function of wavelength. The smallest proportion of energy corresponds to:

- Visible light - approximately 43%.
- Near-infrared light accounts for approximately 49%.
- Ultraviolet light accounts for approximately 7%.
- Other ranges (X-rays, gamma rays, radio waves, etc.) constitute less than 1%.

The maximum spectral density of solar radiation occurs at a wavelength of about 500 nm, corresponding to the green-blue region of the visible spectrum. Human visual sensitivity also peaks within this range, likely as a result of evolutionary adaptation to natural solar lighting conditions.

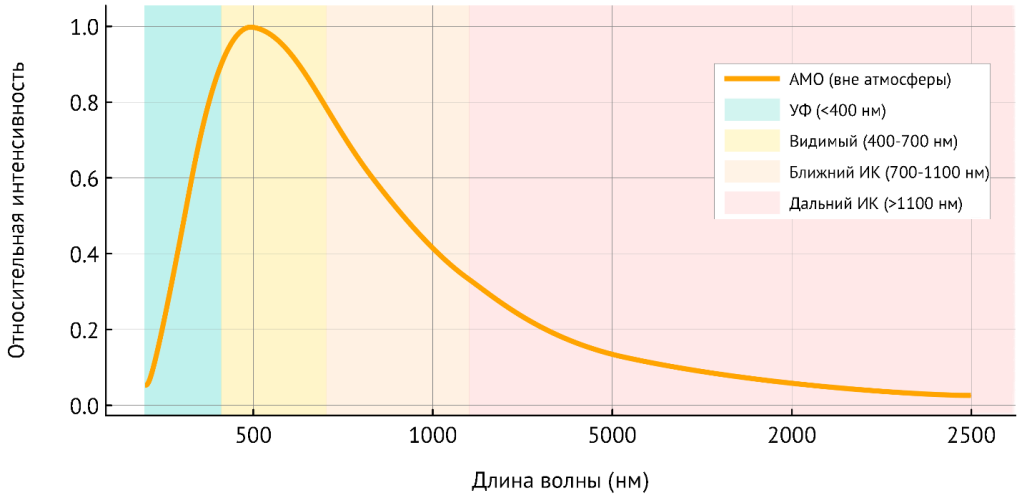

Figure 1.6. Solar radiation spectrum at AM0 (outside the atmosphere).

The solar radiation spectrum changes as it passes through the atmosphere:

The shortwave part (especially ultraviolet and blue light) is attenuated due to scattering by air molecules and aerosols, while characteristic absorption dips occur in the infrared region caused by water vapor and carbon dioxide.

The longer the path of solar radiation through the atmosphere, the greater the distortion in its spectral composition.

§1.4. Atmosphere mass

Atmospheric mass (or Air Mass, abbreviated as AM) is a dimensionless quantity indicating how many times longer the path of solar radiation through the Earth's atmosphere is compared to the path taken when passing vertically (i.e., when the Sun is at the zenith, directly overhead).

The formula for calculating air mass can be simplified as follows:

$$\mathbf{AM} \approx \frac{\mathbf{1}}{\mathbf{cos}\emptyset}$$

where: AM - air mass; ∅ - zenith angle, defined as the angle between the direction to the Sun and the perpendicular to the horizontal surface at a specific point on the Earth's surface.

The simplified formula for calculating air mass offers sufficiently high accuracy for solar elevations above 15°, thus making it applicable to midlatitude conditions, including those in Uzbekistan. For more precise analysis, empirical models are employed, which the reader may examine independently.

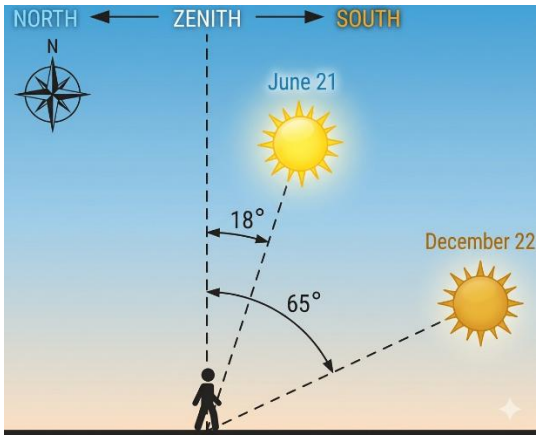

Figure 1.7. Zenith angle illustrated by the example of Tashkent city.

The higher the AM value, the longer the path of solar radiation through the atmosphere, and consequently, the lower the intensity of the solar flux at the surface. This directly affects the reduction in photovoltaic (PV) power generation, especially in the morning and evening hours when AM is at its highest. At noon, AM is minimal, while in the morning and evening it tends toward infinity.

To improve the accuracy of calculations, this expression can be further adjusted by taking into account atmospheric pressure, which is determined by the altitude of the location above sea level. The need for this correction arises from the fact that AM is proportional to the mass of air per unit area through which solar radiation passes. As altitude increases, atmospheric pressure and air density decrease, resulting in a reduction of the effective thickness of the atmosphere and a decrease in the absorption and scattering of solar radiation. Taking this factor into account, the AM calculation can be expressed as follows:

$$\boldsymbol{AM \approx \frac{1}{cos\emptyset} \cdot \frac{P}{P_0}}$$

where: P – local atmospheric pressure; P_0 – standard atmospheric pressure at sea level.

In general, determining the local atmospheric pressure requires taking into account the actual temperature stratification of the atmosphere in the area where the PV system is installed, which varies with altitude. However, in engineering practice, when estimating atmospheric pressure as a function of altitude, it is acceptable to use a simplified barometric formula, provided that a standard atmospheric temperature is assumed:

$$\mathbf{P(h) = P_0 \cdot e^{-h/H}}$$

where H – the characteristic height of the atmosphere, taken as 8434 m.

The given simplified barometric relationship is applicable for engineering calculations at altitudes up to 1 km, where the approximation error remains acceptable. For most practical engineering problems under the conditions of the Republic of Uzbekistan, this altitude range is sufficient.

Taking into account atmospheric pressure and using the simplified barometric formula, the air mass calculation can be expressed as follows:

$$\mathbf{AM \approx \frac{1}{cos\emptyset} \cdot e^{-\frac{h}{H}}}$$

Example. Let us calculate the minimum value of the atmospheric mass (AM) for g. Tashkent. The geographical latitude of Tashkent is 41.30° north. The maximum solar altitude is observed on the day of the summer solstice and is approximately 72.15° for this latitude. Accordingly, the zenith angle at this moment is equal to:

$$\emptyset = \mathbf{90^0 - \varphi = 90^0 - 72,15^0 = 17,85^0}$$

where: **φ** - solar altitude above the horizon (the angle between the direction to the Sun and the horizontal plane).

Formal minimum atmospheric mass on the day of the summer solstice in Tashkent:

$$\mathbf{AM} \approx \frac{\mathbf{1}}{\mathbf{cos}\emptyset} = \frac{\mathbf{1}}{\mathbf{cos(17,85)}} = \frac{\mathbf{1}}{\mathbf{0,951}} = \mathbf{1,05}$$

Let us determine the correction coefficient for the city of Tashkent. The altitude of Tashkent above sea level is on average 440-480 m. In engineering calculations, an average value of 455 m is often used. The correction coefficient at an altitude of h=455 m is:

$$\mathbf{P_0/P_0 = e^{-h/H} = e^{-455/8434} \approx 0,95}$$

Atmospheric mass - one of the three primary parameters included in the standard testing conditions (STC - Standard Test Conditions) for photovoltaic modules, alongside solar irradiance and cell temperature. The value of atmospheric mass affects the spectral composition of solar radiation at the Earth's surface, which in turn directly influences the efficiency of the modules, as their sensitivity varies according to the wavelength of light (see section 1.5 for further details).

Thus, when evaluating the characteristics of photovoltaic modules, it is essential to consider not only the radiation flux density but also its spectral composition. Outside the atmosphere (AM=0), the solar radiation spectrum remains relatively stable; however, it undergoes changes when passing through the atmosphere-changes that intensify with increasing atmospheric mass. Under STC conditions, a standardized solar radiation spectrum known as AM1.5 Global (AM1.5G) is used this is a reference solar spectrum at an atmospheric mass of 1.5, corresponding to the Sun’s position at

an angle of 48.2° from the zenith. The specified spectrum is regulated by the international standard IEC 60904-3.

The average solar zenith angle in Tashkent during the period of maximum solar radiation is approximately 41°, corresponding to an air mass of approximately AM1.41. This value is close to the standard AM1.5 adopted under STC conditions.

The conclusion is illustrated by Fig. 1.8, which clearly displays the azimuth, solar altitude, and zenith angle within a single schematic.

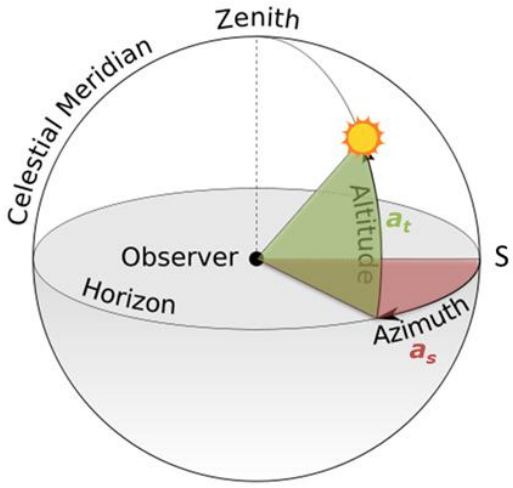

Figure 1.8. Azimuth, altitude and zenith angle.

The celestial meridian is a vertical plane extending from north to south through the zenith, dividing the sky into eastern and western halves.

§1.5. Photoelectric effect

The photoelectric effect or photoeffect, is a physical phenomenon in which electrons are emitted from a substance under the influence of light (electromagnetic radiation).

There are two primary types of the photoelectric effect:

- The external photoelectric effect is a process in which electrons absorb photon energy and leave the surface of a material, typically a metal;
- The internal photoelectric effect is a process in which, under illumination, electrons within a semiconductor transition from the valence band to the conduction band without exiting the material. This generates electron-hole pairs, the movement of which produces an electric current.

Let us examine the mechanism of the photoelectric effect by considering the example of the external photoelectric effect. Free electrons are always present in metal and can move freely within its structure. When a photon with energy E=h·v strikes the metal, this energy is utilized to liberate an electron from the material that is, to overcome the attraction between the electron and the metal atoms and to impart a specific kinetic energy to it (see Fig. 1.9).

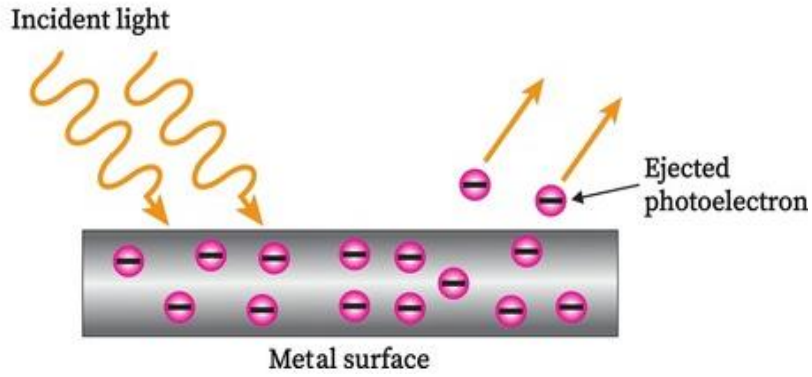

Figure 1.9. External photoelectric effect.

The energy required to release the electron from the metal is called the work function. The work function is a characteristic property of the material. It is independent of the light's frequency or intensity.

Einstein's equation for the photoelectric effect, based on the conservation of energy principle, is given as follows:

$$\mathbf{h \cdot v = h \cdot \frac{c}{\lambda} = A + E}$$

where: A - work function, J; E - kinetic energy of the electron, J.

As stated, only photons with specific energies (i.e., wavelength/frequency) can eject an electron from the metal. Initially, energy is expended to perform work (to release the electron from the metal) and only afterwards to accelerate it (impart kinetic energy). Therefore, a certain threshold wavelength of light exists at which the photoelectric effect occurs. This is the wavelength at which the photon energy is just sufficient to release an electron from the metal (to overcome the work function), while it is insufficient to impart kinetic energy. The wavelength at which the photoelectric effect ceases is called the red boundary of the photoelectric effect.

A single photon can release only one electron if its energy exceeds the work

function (i.e., surpasses the red boundary of the photoelectric effect). Accordingly, the number of ejected electrons is proportional to the number of incident photons and thus depends on the light intensity, provided the light frequency exceeds the threshold.

During the photoelectric effect in a metal, an electron is “ejected” outside the material, making it difficult to use for generating useful current, since the operation of an electrical circuit requires a directed flow of charge within a closed system. Moreover, the work function of metals is relatively high, and the energy of photons in the visible and infrared ranges-which constitute the main part of the solar spectrum - is often insufficient for an effective photoelectric effect on a metallic surface.

This is precisely why photovoltaic modules utilize the internal photoelectric effect characteristic of semiconductors: here, electrons do not leave the material, but under the influence of the internal electric field, they move directionally within the structure, generating electric current in the external circuit.

A solar cell (or photoelement) is a semiconductor device composed of two layers of doped silicon with different conductivity types:

- n-type - a layer with an excess of free electrons (doped, for example, with phosphorus);
- p-type - a layer with an excess of holes (doped, for example, with boron).

Doping is the process of introducing a small number of impurities into pure semiconductor material (for example, silicon) to modify its electrical properties. Depending on the type of added dopant, two primary types of semiconductors are distinguished:

- N-type (from "negative”) - arises when elements with one more electron than silicon atoms are introduced. For instance, phosphorus or arsenic. Such dopants are termed donors, as they supply additional electrons charge carriers.
- P-type (from "positive") — occurs when elements with one less electron than silicon are added. For example, boron or indium. These impurities create holes — the absence of electrons — which also act as positive charge carriers.

At the interface between these two layers, a p-n junction is formed - a distinct region where an internal electric field arises. This field plays a crucial role: it directs charge carriers - electrons toward the n-region and holes toward the p-region, thereby

ensuring their spatial separation and preventing rapid recombination.

Within the p-n junction, a depletion layer forms - a region nearly devoid of free charges. It establishes a potential barrier that prevents the movement of carriers in the reverse direction. Owing to this internal electric field, electrons and holes are separated into opposite directions before recombination can occur.

This separation is what enables the generation of an electric voltage at the terminals of the solar cell. Upon connecting an external load, a directed current arises, and the photovoltaic element commences its primary function - converting light into electrical energy (see Fig. 1.10).

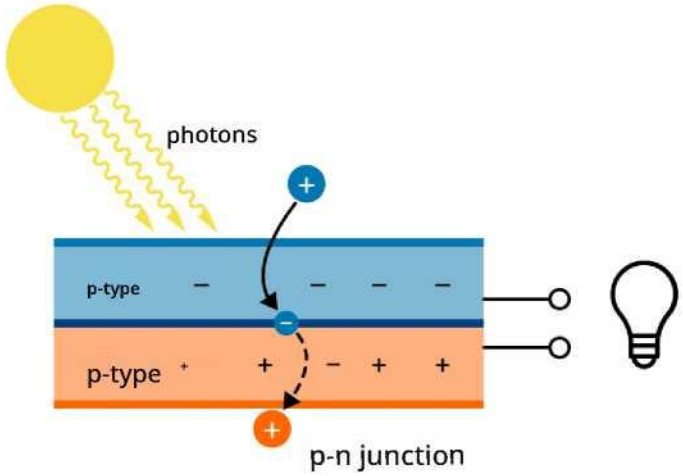

Figure 1.10. Internal photoeffect.

In the atomic structure of a crystal, an electron may exist only in one of two energy bands:

- Valence band - the region where electrons are tightly bound to atoms and do not participate in conduction;
- Conduction band —is the region where electrons can freely move through the crystal and generate electric current.

Between these two bands lies the so-called forbidden band —an energy gap in which electrons cannot exist. An electron either remains in the valence band or transitions to the conduction band; no intermediate states exist.

For current to appear in a semiconductor, certain electrons must acquire sufficient energy to transition from the valence band to the conduction band, thereby overcoming the forbidden energy gap. This transition is possible if, for example, the photon energy of the incident light is equal to or exceeds the width of this gap. Upon entering the

conduction band, the electron becomes a free charge carrier capable of moving under the influence of an electric field and contributing to the generation of electric current.

The silicon forbidden band gap is approximately 1.1 electron-Volts (eV). This indicates that for an electron in silicon crystal to transition from the valence band to the conduction band (and thereby participate in current flow), it must gain energy not less than 1.1 eV.

The photon energy, expressed in electron-volts (eV), is calculated by its wavelength using the following formula:

$$\mathbf{E} = \frac{\mathbf{1240}}{\boldsymbol{\lambda}}$$

where: E - photon energy in electron-volts (eV), X - wavelength in nanometers (nm).

Substituting E = 1. 1 eV, we obtain:

$$\boldsymbol{\lambda} = \frac{\mathbf{1240}}{\mathbf{1,1}} = \mathbf{1127\ nm}$$

Thus, photons with wavelengths longer than approximately 1100-1127 nm have insufficient energy to overcome the silicon bandgap. Such photons do not excite electrons in the semiconductor and therefore do not participate in electricity generation - their energy is generally converted into heat. Consequently, infrared photons with wavelengths exceedingly approximately 1100 nm either pass through the cell or are converted into heat, without contributing to electricity generation. This indicates that not only the total solar irradiance is important, but also its wavelength composition, i.e., the spectral distribution.

The optimal absorption range of radiation for silicon solar cells lies between 300 and 1100 nm. The contributions of different spectral regions to generation are distributed as follows:

- Ultraviolet (300-400 nm) - approximately 5%;
- Visible light (400-700 nm) - approximately 50-55%;
- Near-infrared range (700-1100 nm) - approximately 40-45%.

Photons with wavelengths less than 280 nm:

- Are absorbed by glass or a protective coating and do not reach the semiconductor;
- Even if they reach it, their excess energy is dissipated as heat;

- Ultraviolet photons can damage the material; therefore, panels are often equipped with filters that block this range.

Photons with wavelengths greater than 1100 nm (far-infrared range):

- Their energy is insufficient to excite an electron (to overcome the band gap);
- These photons are neither absorbed nor involved in generation, but are scattered or absorbed as heat.

§1.6. The Shockley-Queisser limit

The nature and mechanism of the photoelectric effect are inevitably accompanied by energy losses, which raises a fundamental question about the efficiency of this process-namely, its coefficient of performance. The efficiency of a solar cell reflects the fraction of incident solar radiation converted into electrical energy. However, this parameter is constrained by physical factors-both the characteristics of the solar radiation and the properties of the semiconductor material and is defined by the so-called Shockley-Queisser limit.

The Shockley–Queisser limit (Shockley–Queisser limit) is the theoretically calculated maximum efficiency of a single-junction (single-junction) solar cell, based on the photoelectric effect and the law of conservation of energy. This limit is approximately 33.7% when a standard solar irradiance (AM1.5) at a temperature of 25°C is incident on the solar cell. It was first described in 1961 by scientists William Shockley and Hans Queisser.

The Shockley-Queisser limit of 33.7% applies not only to silicon but to any single junction solar cell operating under standard illumination conditions. (AM1.5) and a temperature of 25°C. This value is valid for an optimal bandgap width which, according to calculations, should be about 1.34 eV. Silicon has a bandgap width of approximately 1.1 eV; accordingly, its theoretical limit is lower, about 29-31%.

The given value is valid for illumination without concentration. With optical concentration of solar radiation, the theoretical maximum efficiency for a single-junction cell increases to approximately ~41% under extremely high concentration, ideal optics, and so on.

The Shockley–Queisser limit represents the theoretical maximum efficiency of

an ideal single-junction semiconductor without optical losses, with complete quantum yield and absence of reflections or recombination. Let us examine why, even under ideal conditions, a single-junction p-n junction has a fundamental efficiency limit.

Reason № 1. Losses due to photons with insufficient energy.

Every semiconductor has a specific bandgap width — the minimum photon energy required to "excite" an electron and transition it from the valence band to the conduction band. As previously mentioned, for silicon, this energy is approximately 1.1 eV, corresponding to a wavelength of about 1100 nm. Photons with energy below this threshold (i.e., with a wavelength longer than 1100 nm) cannot initiate the generation of electric current-they either pass through the material or are absorbed as heat. Consequently, a portion of the infrared radiation in the solar spectrum remains unutilized during the conversion into electrical energy.

Reason № 2. Losses during relaxation of the 'excess' photon energy.

Photons with energy exceeding the minimum required to overcome the bandgap are also utilized inefficiently. For example, photons with a wavelength of approximately 500 nm, corresponding to the peak intensity of the solar spectrum, possess an energy of 2.48 eV. In silicon, only 1.1 eV of this energy is utilized to promote an electron to the conduction band, while the remaining 1.38 eV is lost as heat during relaxation. Thus, more than half of the energy of such a photon is dissipated as waste.

Reason №3. Losses due to thermodynamic equilibrium.

Even in an ideal solar cell, equilibrium is established between carrier generation and their radiative recombination-some electrons and holes inevitably recombine.

Reason №4. Losses due to thermal emission.

Even at a temperature of 25°C, some charge carriers can overcome the p-n junction due to thermal energy, resulting in leakage currents the so-called dark current. As temperature increases, this effect intensifies, further reducing the output voltage of the solar cell.

Thus, the Shockley-Queisser limit constitutes a natural barrier for conventional solar cells with a single p-n junction. This limit can only be surpassed by employing multi-junction cells or tandem technologies that utilize photons of different energies

more efficiently.

In a multi-junction cell, each photon is matched to a semiconductor material with a bandgap width closely aligned to its energy. This approach minimizes losses associated with thermal relaxation and enables efficient utilization of photons across different parts of the spectrum, substantially enhancing overall efficiency. Under ideal conditions, employing an infinite number of p-n junctions, the theoretical maximum efficiency can reach approximately 86.8%. However, currently in industry, single-junction silicon solar cells are predominantly used; therefore, a detailed examination of the operating principles of multi-junction structures is beyond the scope of this material.

Interested readers may independently explore this topic further.

In conclusion, an approximate estimate of energy losses in silicon solar cells is provided to form a general understanding:

- Photons with energy below 1.1 eV do not participate in current generation, as they cannot overcome the silicon bandgap. Losses amount to approximately 19-20% (according to the AM1.5 Global standard).
- Thermal losses during relaxation occur when photons with energy greater than 1.1 eV transfer excess energy as heat during the electron transition to the conduction band. These losses are approximately 33-35%.
- Optical losses - reflection, scattering, and absorption in materials not associated with current generation (glass, anti-reflective coating, etc.). Losses amount to approximately 6-10%, depending on the module design.
- Electrical losses - carrier recombination, contact resistance, conductor resistance, and other internal losses. These losses are approximately 10-15%.

CHAPTER 2. PHOTOVOLTAIC MODULES

This chapter examines the design and historical development of photovoltaic modules, including modern technologies and materials employed in their production. Conditions for standard tests (STC, NOCT, NMOT) are presented, enabling the assessment of module parameters under controlled conditions. Key electrical characteristics are described, including voltage and current at maximum power, open-circuit voltage, short-circuit current, as well as the current-voltage characteristic and its dependence on external factors such as temperature, solar radiation, and surface contamination. Special attention is devoted to the correct installation of photovoltaic modules, electrical connections, and the fundamental requirements for their maintenance and diagnostics.

§2.1. Photovoltaic modules

A photovoltaic module (PV module), commonly known in everyday life as a solar panel, is a device designed to convert sunlight into electrical energy through the photoelectric effect in semiconductor materials (internal photoelectric effect). It consists of several interconnected solar cells enclosed within a protective structure that provides mechanical strength, sealing, and resistance to external influences.

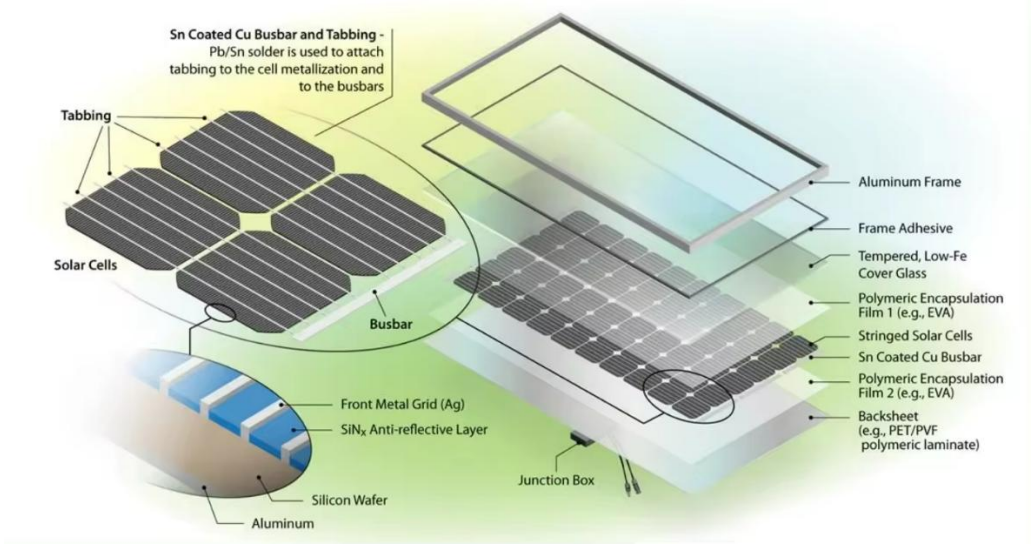

Figure 2.1. Main structural components of a photovoltaic module.

The main structural layers (elements) of the photovoltaic module (PVM), presented in Fig. 2.1, include [15], [16]:

- Aluminum frame (Aluminum Frame) - typically anodized, meaning it is coated with a protective oxide layer that ensures high resistance to corrosion, moisture, salts, and ultraviolet radiation. Anodizing also enhances the surface hardness and its resistance to mechanical damage.
- Adhesive gasket (Frame Adhesive) - used to secure the aluminum frame to the glass surface of the photovoltaic module;
- Protective glass (Front (Cover) Glass) - typically tempered, with a thickness of 2 mm (for bifacial PV modules) and 3.2 mm (for monofacial PV modules), providing protection for the photovoltaic cells against mechanical impacts, hail, dust, moisture, and ultraviolet radiation. Modern PV modules utilize high-transparency or anti-reflective glass with a low reflection coefficient (ARC - Anti-Reflection Coating), which increases the overall module efficiency. The glass effectively attenuates ultraviolet radiation with wavelengths below approximately 300 nm, which does not contribute to generation but may cause degradation of polymer layers.
- The top encapsulant layer (Encapsulant) is a protective transparent polymer situated between the glass and the photovoltaic cells. Typically manufactured from ethylene vinyl acetate (EVA) - a specialized thermosetting material. Ensures fixation and sealing of photovoltaic cells, and fulfills the function of electrical insulation, preventing electrical breakdown between the cells. Exhibits high optical transparency - approximately 95% within the 400-1100 nm wavelength range;
- Photovoltaic elements (Solar Cells) - are generally monocrystalline or poly-crystalline silicon cells designed to convert solar radiation into electrical energy through the photoelectric effect.
- The main (Main Bus) and current-collecting (BB- busbar) busbars are designed to collect and transmit electric current from the photovoltaic cells within the module.
- The lower encapsulant layer (Encapsulant), similar to the upper one, is a transparent polymer material that provides fixation and sealing of the photovoltaic cells, protects them from external impacts, and serves as electrical insulation.
- The back protective layer (Back sheet) is a multilayer polymer film on the rear side of the module, manufactured from fluoropolymers (PVF, PVDF), PET, or their combinations. Provides protection against moisture, UV radiation, mechanical, and

thermal effects, and also functions as an electrical insulator. Typically, white in color (to enhance light reflection), less commonly black (for decorative purposes).

In bifacial PV modules, instead of a rear protective layer, a transparent heat-strengthened glass (Heat Strengthened Glass) is used, allowing electricity generation from both sides.

The junction box (Junction Box) is a sealed module on the rear side of the panel, containing bypass diodes to prevent overheating during shading and contacts for cable connection. Ensures the electrical connection of the panel to the external circuit and protects against reverse currents.

Depending on the type of silicon crystal used, photovoltaic modules are classified as monocrystalline (Mono-Si) and polycrystalline (Poly-Si). Without delving into technical details, it should be noted that monocrystalline modules have now virtually supplanted polycrystalline ones in the market. This is attributable to their higher efficiency, improved temperature stability, greater durability, and extended service life. Even the lower cost of polycrystalline panels does not offset their technical limitations, making them uncompetitive under current conditions, particularly given the decreasing production costs of monocrystalline panels.

In addition to crystalline modules, thin-film modules are also available on the market (Thin-film photovoltaic modules, fabricated from amorphous silicon (a-Si), cadmium telluride (CdTe), or copper indium gallium selenide (CIGS), offer significant advantages including low weight, flexibility, resistance to degradation under shading, and superior performance under diffuse light conditions. Nevertheless, owing to their lower efficiency, susceptibility to moisture, and difficulties in scaling, thin-film technologies are presently applied in a limited scope, predominantly in niche applications such as facade integration, autonomous devices, or light weight structural installations.

In modern space power engineering, multijunction photovoltaic cells based on gallium arsenide (GaAs) and its combinations with indium phosphide and germanium substrate (GaInP/GaAs/Ge) are most widely used, providing a high efficiency (exceeding 30-35%) and resistance to radiation, temperature fluctuations, and the conditions of outer space [17], [18]. Their primary advantage over traditional silicon

cells lies in the combination high specific efficiency, durability, and low degradation under radiation exposure, which are critically important for the long-term operation of satellites and spacecraft in orbit. In several projects, flexible thin-film elements based on CIGS are also being tested, offering lower weight and mechanical flexibility; however, III-V multi-junction structures remain the standard in space today due to their optimal balance of efficiency and reliability [19]. However, due to their high cost, such components are virtually unused in ground-based solar energy systems, where silicon remains the primary material.

III–V denotes a class of semiconductor materials composed of elements from groups III and V of the Periodic Table (e.g., Ga, In, As, P). These include compounds such as GaAs, InP, GaSb, and others, which are used to manufacture highly efficient multi-junction photovoltaic cells.

Photovoltaic modules can be distinguished by their external appearance: single crystal modules have a uniform dark coloration and cells with beveled corners (see Fig. 2.2 A), whereas polycrystalline modules exhibit a bluish-metallic tint and cells with right-angled corners (see Fig. 2.2 B). Thin-film modules, unlike crystalline ones, feature a smooth matte surface without a visible pattern of individual cells, most commonly exhibiting dark blue, purple, or black coloration (see Fig. 2.2 C).

A. Monocrystalline cell B. Polycrystalline cell C. Thin-film module

Figure 2.2. Monocrystalline (A), polycrystalline (B) cell, and thin-film module (C).

Before proceeding to the classification of photovoltaic modules (PVM), it is necessary to enumerate the primary types of their degradation:

- LID (Light-Induced Degradation - light degradation) - occurs within the first

hours or days after installation. Caused by the interaction of oxygen and boron in silicon, resulting in a 2-3% power loss.

- LeTID (Light and Elevated Temperature Induced Degradation - degradation under light and elevated temperature) - manifests during prolonged exposure to light and temperatures above 50°C. May cause a power loss of up to 3% within 1-2 years. In some cases, it is reversible through thermal regeneration.
- PID (Potential Induced Degradation - potentially induced degradation) -Occurs at high voltage between cells and ground (typically in systems of 1000 V and above). Leads to current leakage and the formation of localized zones with reduced output.
- UV degradation (Ultraviolet Degradation - degradation caused by ultraviolet exposure) - affects front cover materials, especially EVA laminate, resulting in yellowing and decreased light transmittance. It does not directly affect the cell itself but reduces the module's output power.
- Mechanical Degradation (Mechanical Degradation) — occurs due to microcracks caused by transportation, improper installation, or impacts (e.g., hail).

Such damage can cause localized hot spots and a reduction in power generation.

- Thermal Degradation (Thermal Degradation) — repeated heating and cooling cycles over time lead to solder joint failure, delamination, and degradation of electrical connections.

Mechanical degradation - one of the most concealed and difficult-to- detect types of damage. It often arises from improper installation practices: excessive pressure on panels, walking on modules, and careless handling of equipment. The consequences of such damage do not appear immediately but manifest months or even years later as microcracks, localized hot spots, and decreased generation. Therefore, it is imperative to regularly monitor the construction site, conduct briefings for installers, ensure adherence to installation standards, and assess the quality of work completed at every stage - from unloading to final securing of equipment.

Photovoltaic modules are classified by the type of silicon employed as follows:

- P-type (Positive type — positive type) – the most historically utilized and traditional type. This type is based on doping silicon with boron, resulting in an excess of "holes" as the primary charge carriers. The primary drawback of P-type modules is

their susceptibility to LID and LeTID degradation, which causes decreased efficiency and a shorter operational lifespan compared to more advanced alternatives.

- N-type (Negative type — negative type) – currently considered the primary promising direction. It is based on doping silicon with phosphorus, resulting in electrons being the main charge carriers. It is not susceptible to LID and LeTID, and it offers a longer service life along with improved stability at high temperatures.

Photovoltaic modules are classified according to cell manufacturing technology as follows:

- PERC (Passivated Emitter and Rear Cell - emitter with rear-side passivation) is an enhanced classical technology, whereby a dielectric layer is applied to the cell's rear surface to reduce charge carrier recombination and improve efficiency.
- TOPCon (Tunnel Oxide Passivated Contact - a passivated contact through a tunnel oxide) - a thin tunnel oxide layer and a passivating layer are applied to the silicon surface, enhancing conductivity and significantly reducing degradation, particularly in n-type cells.
- HJT (Heterojunction Technology - heterojunction technology) - a structure that combines crystalline silicon (c-Si) and thin layers of amorphous silicon (a-Si:H) on both sides of the cell, providing high efficiency and stable operation at elevated temperatures.
- IBC (Interdigitated Back Contact - interdigitated rear contacts) - all current collecting elements are located on the rear side of the cell, allowing maximum utilization of the front surface for light absorption and achieving the highest efficiency values; however, this requires complex and costly manufacturing.

PERC technology based on P-type silicon has long been the mass standard in photovoltaic module production (approximately until 2023). However, with the development of the industry, it has gradually been supplanted by more advanced solutions based on N-type silicon, in particular - the TOPCon technology. For instance, by early 2025, the entire product line of one of the world’s leading manufacturers - Jinko Solar - fully transitioned to producing modules based on n-type TOPCon.

The primary reasons for abandoning P-type PERC are its susceptibility to degradation types LID and LeTID, lower thermal stability, limited potential for efficiency

enhancement, and a shorter service life compared to N-type technologies.

Photovoltaic modules are classified by cell construction into:

- Full-Cell (Full-Cell or Full-Cut) - the classic format, in which the solar cell is used whole, without division (Fig. 2.3 A).
- Cut (half) cells (Half-Cell or Half-Cut) - in this design, each solar cell is cut in half, and the halves are then connected in strings, similarly to full - sized cells (Fig. 2.3 B).

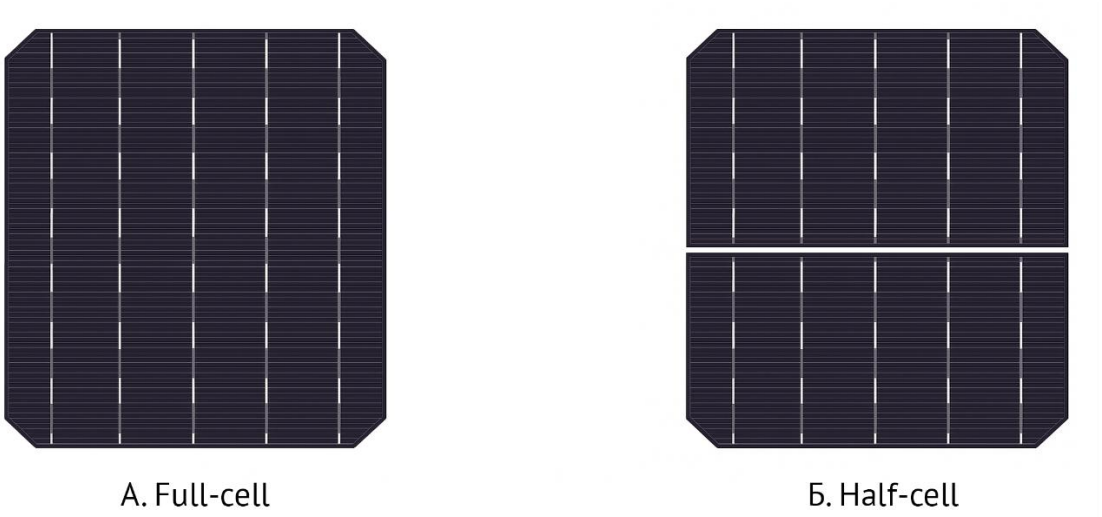

Figure 2.3. Photovoltaic modules with full (Full-Cell) and half (Half-Cell) cells.

Full-Cell photovoltaic cells (Full-Cell) have long been employed in all photovoltaic modules; however, today they have been almost entirely replaced by more efficient solutions based on Half-Cell technology (Half-Cell).

Advantages of Half-Cell technology (Half-Cell):

- The electric current in Half-Cells is reduced by half compared to Full-Cells, resulting in internal losses decreasing fourfold and reduced heating, The risk of hot spot formation (Hot Spot) is reduced, and the overall module efficiency is increased.
- From an electrical connection standpoint, the module with Half-Cell cells is divided into two independent halves. In the event of partial shading (for example, on the lower part of the module during winter when the Sun is low), the upper half continues to operate without restrictions. Thus, unlike modules with full cells (Fig. 2.4 A), only half of the power output is lost (Fig. 2.4 B).

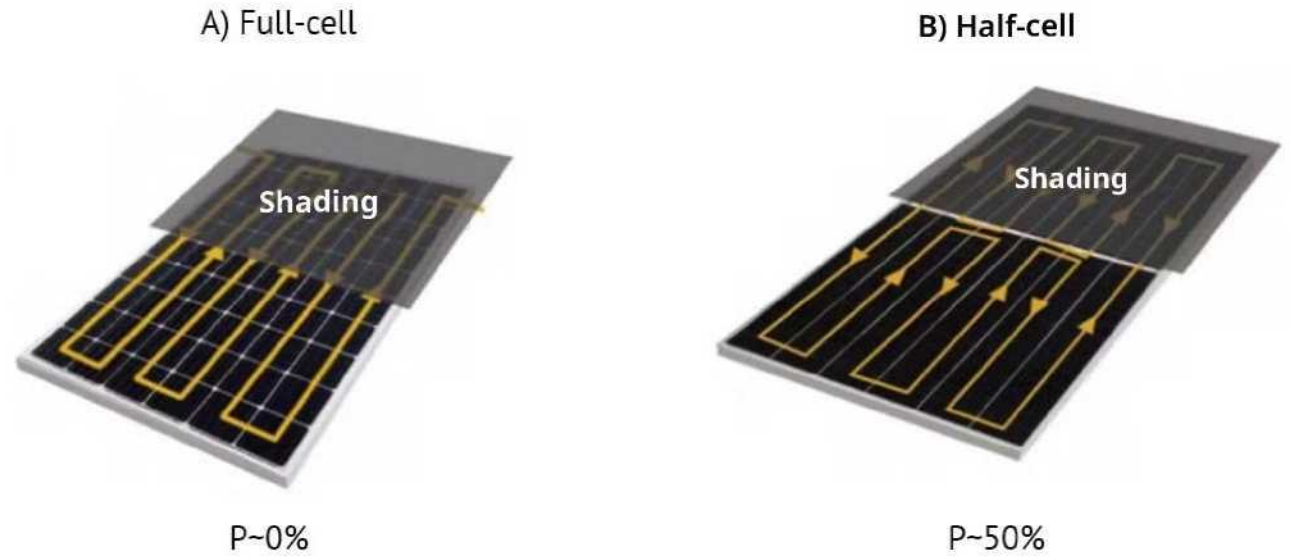

Figure 2.4. Generation of modules with full (A) and half-cut (B) cells under partial shading.

Thermal losses and the efficiency of photovoltaic modules largely depend on the configuration of the current-collecting busbars (BB — Busbar) printed on the surface of the solar cell. As the number of BB increases, the distance between the busbars and the so-called current-collecting "fingers" (Finger Grid), which are thin metal lines evenly distributed across the cell surface, decreases. They collect the electric current generated over the entire surface of the silicon layer and channel it to the thicker busbars (BB). Reducing the distance between busbars decreases the finger length, reduces resistance and thermal losses, and consequently enhances the overall module efficiency.

Initially, configurations with 2BB or 3BB (Fig. 2.5 A) were employed, which were later replaced by 4BB and 5BB (Fig. 2.5 B) to minimize losses and improve reliability. Currently, the majority of modern modules utilize the Multi Busbar (MBB) configuration with up to 16 busbars (Fig. 2.5 B) or more, which substantially reduces losses, enhances efficiency, and improves resistance to microcracks. An increase in the number of busbars results in a reduction of distance.

Currently, busbar-less technologies are actively advancing; notably, the Shingled technique is an advanced method of connecting solar cells wherein they are overlapped similarly to roof shingles (hence the name: shingled - 'laid like shingles'). In this technology, cells are pre-cut into narrow strips, and connections between them are

made not by soldering but by using conductive adhesive (ECA - Electrically Conductive Adhesive).

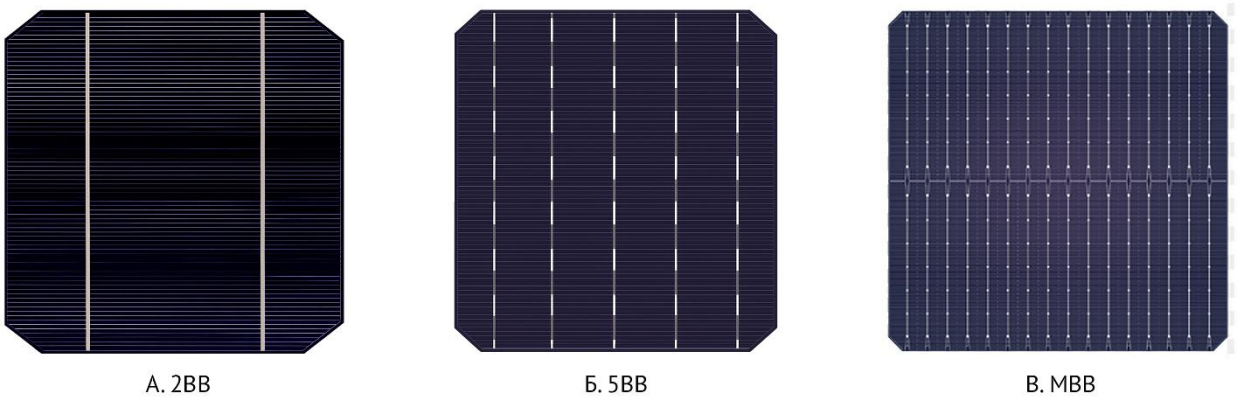

Figure 2.5. Types of photovoltaic cells based on the number of busbars (BB - Busbar).

This approach results in:

- the entire cell surface remaining active due to the absence of shading busbars, thereby enhancing efficiency;
- the elimination of soldering, which reduces thermal stresses and improves reliability;
- a design that is more resistant to partial shading, as cells are connected in parallel and can operate independently.

Photovoltaic modules are classified according to the number of light-receiving sides as follows:

- Monofacial (Monofacial)- photovoltaic modules in which electricity generation occurs exclusively on the front (illuminated) side. These modules feature an opaque back layer (typically a backsheet made of fluoropolymer), which provides protective functions but does not participate in generation. This is the classic type that has long dominated the market (see Fig. 2.6).
- Bifacial modules are capable of capturing solar radiation on both their front and rear sides. The rear side consists of tempered glass, allowing photons to penetrate to the cell. Reflected light (from the ground, roofs, snow, etc.) provides additional generation the power increase can range from 5% to 25% or more, depending on installation conditions (albedo, distance to the surface, height, orientation, etc.) (see Fig. 2.6).

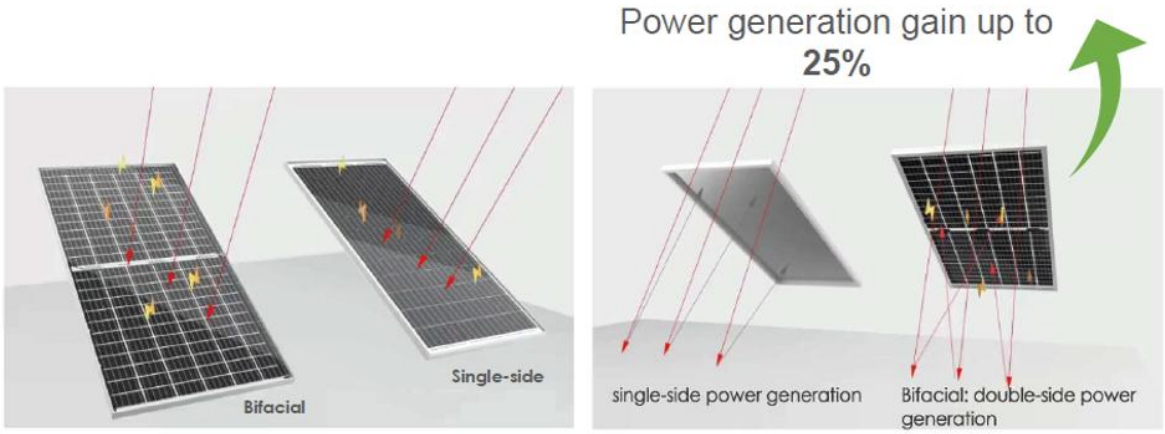

Figure 2.6. Monofacial and bifacial photovoltaic modules.

An additional advantage of bifacial photovoltaic modules is the accelerated melting of snow. This is because the panels are capable of generating electricity and heating up even from sunlight reflected onto their rear side. This effect becomes more pronounced as the azimuth of the PV module deviates further from south (180°), since the flux of reflected solar radiation incident on the rear side of the module increases accordingly.

of technological progress.

Figure 2.7. Graph illustrating the development of solar cells and photovoltaic modules.

Figure 2.7 shows a graph of the development of solar cells and module technologies, presented for informational purposes — to provide a general

understanding of the dynamics of technological progress.

Currently, monocrystalline photovoltaic modules based on N-type silicon, manufactured using TOPCon technology, featuring half-cut cells (Half-Cut) and multi-busbar structures (MBB), are predominantly employed in practice.

Promising directions include technologies based on N-type silicon, specifically HJT and IBC, which offer higher efficiency, low degradation, and stable performance at elevated temperatures. Moreover, shingle-less designs (Shingled), back-contact cells, and multi-section formats (e.g., 1/3-cut) are under active development.

§2.2. Test conditions (STC, NOCT, AND NMOT)

The output power and generation of a photovoltaic power plant depend on multiple factors: the density and spectral composition of solar radiation, the tilt angle and orientation of the modules, wind speed, the ventilation gap between the module and the surface, cell temperature, and other conditions. For standardized comparison and performance evaluation of modules, their parameters are specified in technical documentation under defined test conditions [20]. As these conditions substantially influence output power and performance, engineers must understand their differences and accurately compare modules based on the obtained data. In practice, three types of test conditions are most frequently employed: STC, NOCT, and NMOT [21], [22], [23]. Let us examine them in greater detail.

STC (Standard Test Conditions - standard laboratory conditions) are the defined parameters under which the nominal characteristics of photovoltaic modules are measured. They include solar irradiance at a flux density of 1000 W/m^2, a cell temperature of 25°C, and a spectral distribution of radiation corresponding to an air mass of AM1.5. These conditions are idealized and are used for comparing different module models; however, they do not represent actual operational conditions on site. According to international standards, specifying the electrical parameters of a module under STC is mandatory and must be included in the technical documentation for each photovoltaic module.

The primary drawback of STC conditions is their disconnection from real operational conditions. During laboratory testing, the cell temperature is maintained at 25°C,

typically by forced cooling, whereas in real installations under solar irradiation, modules can heat up to 50-75°C or higher. Furthermore, the solar irradiance density of 100 0 W/m^2 adopted in STC corresponds to peak values, which in most regions occur only briefly on clear days. Moreover, the spectral composition of solar radiation, defined by air mass AM1.5, is a conventional standard and does not reflect actual meteorological and geographical conditions. Collectively, these factors result in characteristics specified under STC significantly overestimating the expected module performance under real conditions.

To evaluate the impact of actual operating conditions on module performance, at the end of the 1980s and beginning of the 1990s, the parameter NOCT (Nominal Operating Cell Temperature) was introduced — representing the nominal cell temperature under typical ambient conditions and open-circuit operation.

The primary distinction between NOCT and STC conditions lies in that, instead of a fixed cell temperature (25 °C in STC), the ambient temperature is fixed at 20 °C, while the cell temperature is determined naturally as a consequence of standardized test conditions: solar irradiance of 800 W/m^2, wind speed of 1 m/s at the module's rear surface, a tilt angle of 45°, and operation of the module under open-circuit conditions, i.e., without electrical load.

These conditions more closely approximate actual operational environments, and the resulting cell temperature value indicates the degree to which the module will heat during operation. The lower the NOCT value, the lower the module's operating temperature and the higher its efficiency.

NOCT does not constitute comprehensive conditions for module testing but serves as an additional parameter characterizing the module's thermal behavior. It should be understood that NOCT is not the precise cell temperature but an average value dependent on the module's design and the materials used, which define its heat dissipation capacity.

Under real conditions, the temperature of solar cells can exceed the ambient temperature by 15-30°C. High-quality modules generally exhibit good heat dissipation properties and do not heat above 40-45°C (under NOCT test conditions, with an ambient temperature of 20°C), which helps minimize power losses associated with

temperature increases. Conversely, modules with low thermal conductivity tend to overheat, adversely affecting their efficiency. For example, the technical specification of the JKM5 65N-72HL4 module indicates a NOCT value of 45±2°C, which demonstrates its stable thermal characteristics.

NOCT measurement conditions assume an open rear surface of the module, enabling free cooling through natural air circulation. Therefore, to ensure effective heat dissipation and prevent overheating of components-particularly when modules are installed horizontally in direct contact with the roof-it is essential to provide a ventilation gap between the module and the surface. This prevents heat accumulation and preserves the operational efficiency of the photovoltaic module. Manufacturers emphasize in their technical manuals that the minimum distance between the module and the roof must be at least 100 mm.

The NOCT parameter, specified in the technical documentation, enables an approximate calculation of the cell temperature based on the ambient temperature according to the following formula:

$$\mathbf{T_c = T_{amb} + \frac{G}{800} \cdot (NOCT - 20)}$$

where: T_c - cell temperature, 0°C; T_{amb} - ambient temperature, 0°C; G - solar irradiance, W/m^2.

Example. Let us calculate the cell temperature at an ambient temperature of 40 degrees, with a solar irradiance density of 1000 W/m^2 and NOCT=45 ^{0}C:

$$\mathbf{T_c = T_{amb} + \frac{G}{800} \cdot (NOCT - 20) = 40 + \frac{1000}{800} \cdot (45 - 20) = 71,25C}$$

Thus, the NOCT parameter allows for an approximate estimation of how much the

cell temperature exceeds the ambient air temperature under a given solar irradiance. This information is essential for calculating power losses due to temperature and for determining the operating voltage of modules, particularly under elevated summer temperatures

However, a drawback of the NOCT parameter is that it is determined under open-circuit module operation, i.e., without an electrical load, which does not reflect actual operating conditions in which the module is connected to a load and operates at the

maximum power point. Accordingly, since 2016, the international standard IEC 6 1215 has introduced a more realistic indicator instead of NOCT - NMOT (Nominal Module Operating Temperature), where the module operates under load and the cell temperature is determined under conditions more closely representing actual operation [24], [25]. Meanwhile, the other test parameters - solar radiation intensity (800 W/m^2), ambient temperature (20°C), wind speed (1 m/s at the rear surface), and tilt angle (45°) - remained constant.

Although the air mass (AM) is not formally regulated under NMOT and NOCT conditions, unlike STC where it is strictly fixed at AM1.5, most leading manufacturers still specify the AM1.5 value in technical documentation as a reference parameter to ensure data comparability and a consistent approach in calculations.

The temperature at NMOT, under comparable conditions, is always higher than at NOCT because it is measured with the module operating at the maximum power point (MPP - maximum power point), where current flows through the cells and actual energy dissipation occurs within the internal resistances. This results in additional heating of the module compared to the NOCT mode, where the module is in an open-circuit state and no current flows.

Although NOCT has formally been replaced by NMOT, many leading manufacturers still specify NOCT instead of NMOT in their technical specifications due to established industry practices, market inertia, the lack of mandatory transition requirements, and marketing considerations, as the NOCT values are higher than those at NMOT.

§2.3. Electrical parameters and Volt-Ampere characteristics of the photovoltaic module.

The electrical parameters of a photovoltaic module characterize its ability to generate electrical power under specified irradiance and temperature conditions.

The primary parameters include [13], [26], [27]:

- short-circuit current (I_{sc}, short-circuit current) - the maximum current that a photovoltaic module can deliver at zero voltage, i.e., in the event of a direct short circuit between the positive and negative terminals without load. Physically, this current is

determined by the number of photons absorbed by the solar cells and directly depends on the intensity of solar radiation: the higher the irradiance flux density (W/m^2), the greater the current generated. The I_{sc} is also affected by the cell temperature - the current slightly increases as the cells heat up;

- The open-circuit voltage (U_{oc}, open-circuit voltage) is the maximum voltage supplied by the photovoltaic module when no current flows, i.e., when the circuit is open and the module is disconnected from the load. Physically, the open-circuit voltage is determined by the characteristics of the p-n junctions in solar cells and depends on the accumulated charge resulting from the photoelectric effect. The primary external factor influencing the open-circuit voltage is the cell temperature: as temperature increases, the voltage decreases, and conversely, it increases as temperature decreases.
- Current at maximum power point (I_{mp}), current at maximum power point) - the current at which the module generates maximum electrical power. The value of I_{mp} is always slightly less than I_{sc}.
- Voltage at the maximum power point (Ump, voltage at maximum power point). The voltage at which the module delivers the highest power. The value of U_{mp} is always less than U_{oc}, since when the load is connected and current flows, part of the voltage is lost due to the internal resistances of the solar cell and contact connections.
- Maximum power (P_{max} or P_{mp}, maximum power) is the maximum electric power that the module can deliver under specified conditions (by default, STC). It is calculated as the product of I_{mp} and U_{mp}.
- Fill factor (FF) is the ratio of the maximum power of a module to the product of the short-circuit current and the open-circuit voltage:

$$\mathbf{FF} = \frac{\mathbf{P_{max}}}{\mathbf{I_{sc} \cdot U_{oc}}}$$

The fill factor characterizes the effectiveness of utilizing the module's maximum current and voltage capabilities. The FF depends on the quality of the cells, contact resistances, and the overall design of the module.

Efficiency (η) is the ratio of the electrical output power of the photovoltaic module to the incident solar radiation on its surface. It is expressed as a percentage and calculated using the formula:

$$\eta = \frac{P_{max}}{E \cdot S} \cdot 100\%$$

where: P_{max} — maximum electric power of the module, W; E - solar radiation flux density, W/m^2; S- module area, m^2.

Efficiency denotes the fraction of the incident solar energy that the module is capable of converting into electricity. It depends on the cell technology, their temperature, surface reflectivity, and manufacturing quality. The higher the efficiency, the more effectively the module utilizes solar radiation.

Note. *In practice, many users mistakenly believe that the higher the nominal power rating of a photovoltaic module, the better its quality. However, an increase in power rating is often achieved not by improving the efficiency of the solar cells but by increasing their total surface area. Meanwhile, the module's dimensions and weight increase, while structural elements, such as the frame, remain unchanged, rendering the module more susceptible to mechanical damage. Thus, a high Power alone does not necessarily signify a technological advantage. For an accurate comparison of modules, their efficiency should be considered, or power should be normalized per unit area.*

The operation of a photovoltaic module is graphically represented by the volt ampere characteristic (BAX, I-V curve), which depicts the dependence of output current on voltage under fixed conditions (most commonly STC). The characteristic I-V curve is bounded by two extreme points: the short-circuit current (I_{sc}) at zero voltage and the open-circuit voltage (V_{oc}) at zero current. Within the operational range between them lies the maximum power point (MPP — Maximum Power Point), corresponding to the optimal mode at which the module delivers maximum energy to the load. In real conditions, this point is tracked by inverters equipped with the MPPT function.

By multiplying the current and voltage values at each point of the I–V characteristic and plotting the result, the power curve (P-V curve) is obtained, which clearly indicates the location of the maximum power point. Figure 2.8 shows the current-voltage characteristic (I-V curve) and the power curve (P-V curve) for a monocrystalline photovoltaic module with a nominal power rating of 640 W, measured under standard test conditions (STC) at a solar irradiance of 1000 W/m ^{2}.

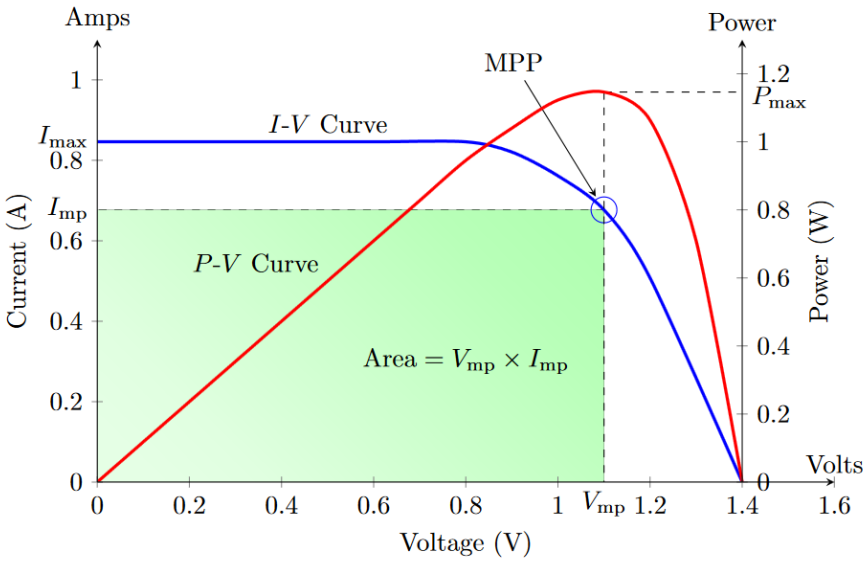

Figure 2.8. Volt-ampere characteristic (I-V curve) and power curve (P-V curve).

The volt-ampere characteristic is sensitive to variations in external conditions.

With an increase or decrease in solar irradiance, the output current of the photovoltaic module changes almost proportionally, since the light intensity determines the number of incident photons, and hence the number of generated charge carriers. The open-circuit voltage changes insignificantly under these conditions, as its dependence on irradiance follows a logarithmic relationship.

For instance, when solar radiation increases from 200 to 1000 W/m^2, the current can increase fivefold, while the voltage rises by only a few percent. As an illustration, Figure 2.9 displays the current-voltage characteristic (A) and the power curve (B) of a monocrystalline photovoltaic module with a nominal power rating of 640 W under various levels of solar radiation.

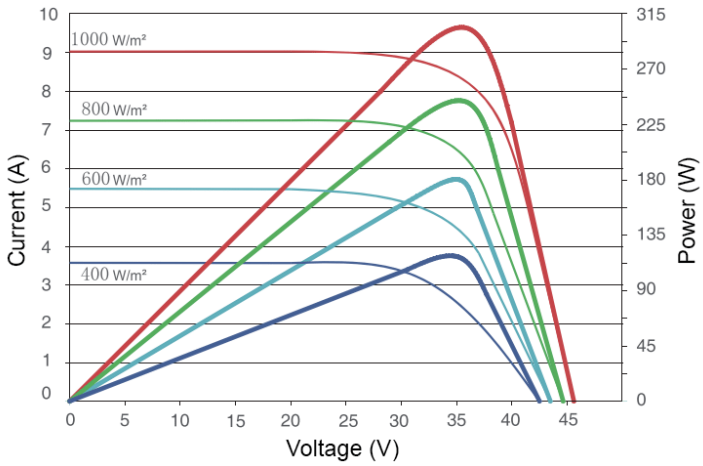

Figure 2.9. Dependence of the I–V characteristic (A) and the power curve (B) on

the level of solar radiation.

The volt-ampere characteristic is also sensitive to changes in solar cell temperature. As the temperature rises, the module voltage decreases; conversely, it increases as the temperature falls. This phenomenon is due to enhanced recombination in the p-n junction and a reduction in the internal potential, resulting in a voltage decrease. Simultaneously, the short-circuit current increases with temperature rise and decreases as temperature falls; however, this current variation is considerably less pronounced compared to voltage variation. Figure 2.10 presents the I-V characteristics of a monocrystalline photovoltaic module with a nominal power of 640 W at cell temperatures of 25°C, 50°C, and 75°C.

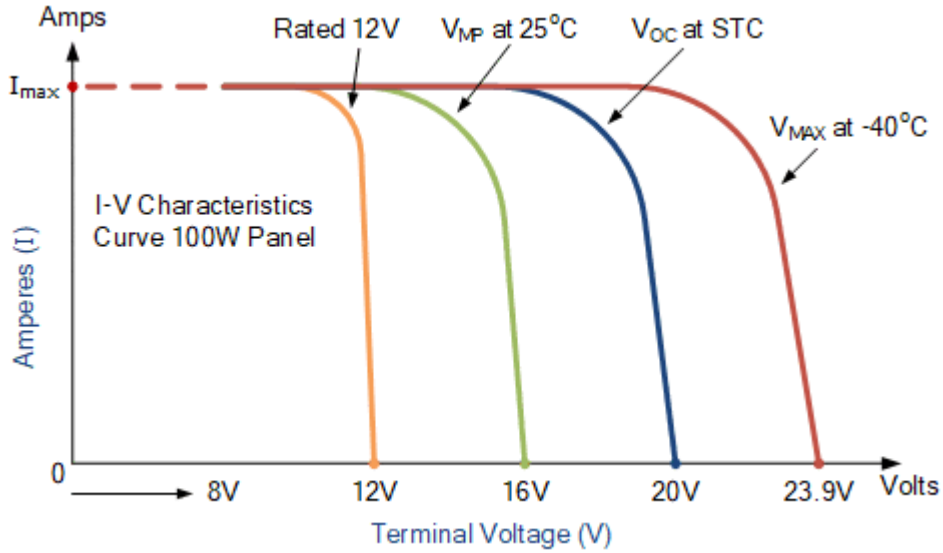

Figure 2.10. Dependence of the I-V characteristic on temperature.

To characterize the dependence of voltage, current, and consequently power on temperature, temperature coefficients are specified in the technical datasheet of the photovoltaic module:

- for open - circuit voltage (approximately -0.25%/0°C for modern PV modules);
- for short-circuit current (approximately +0.045%/^{0}°C for modern PV modules);
- and for maximum power (approximately -0.3%/^{0}°C for modern PV modules).

The approximate value of (V_{oc}) at any cell temperature can be determined by the following formula:

$$\mathbf{V_{OC}(t) = V_{OC\,STC} \cdot (1 + K_V \cdot \frac{(t - 25)}{100})}$$

where: $\mathbf{V_{OC}(t)}$ – open-circuit voltage (V) at a cell temperature of t; $\mathbf{V_{OC\,STC}}$ – open-circuit voltage (V) at a cell temperature of 25°C; $\mathbf{K_V}$ – temperature coefficient of voltage; $\mathbf{t}$ – cell temperature in degrees Celsius.

Example: let us calculate the open-circuit voltage for the photovoltaic module JKM-640-78HL4, where under STC it is 57.34 V and the temperature coefficient of voltage is -0.25%/°C. Let us determine the voltage values at cell temperatures of 65°C and -15°C:

$$\mathbf{V_{OC}(t = 65C) = 57,34 \cdot \left(1 - 0,25 \cdot \frac{(65 - 25)}{100}\right) = 51,26\ V}$$

$$\mathbf{V_{OC}(t = -15C) = 56,95 \cdot \left(1 - 0,25 \cdot \frac{(-15 - 25)}{100}\right) = 62,65\ V}$$

In simple terms, the open-circuit voltage changes by approximately 2.5% for every 10°C deviation in cell temperature from the standard test conditions (25°C according to STC). Specifically, with each 10°C rise in temperature, V_{oc} decreases by about 2.5%, and with a decrease in temperature, it increases by the same amount.

With temperature variation, not only does the open-circuit voltage (V_{oc}) change, but so does the overall voltage, including the voltage at the maximum power point (V_{mp}). However, according to international standards, the mandatory parameter for publication is specifically the temperature dependence of V_{oc}, as this parameter is critically important for ensuring system safety. When designing a photovoltaic power plant, it is essential to calculate the open-circuit voltage at the minimum design temperature to ensure that it does not exceed the permissible limits for the cables, inverters, fuses, and other equipment used.

The temperature coefficient of the voltage at the maximum power point (V_{mp}) is usually not specified in datasheets; however, for an approximate assessment of V_{mp} at various temperatures, the temperature coefficient of the open-circuit voltage (V_{oc}) can be utilized. Although these coefficients differ slightly, this method enables an approximate calculation of the operating voltage on the inverter's DC side depending on temperature, including determining the minimum V_{mp} value during the summer period, which is crucial for verifying compliance with the inverter's MPPT range (further

details are provided in the INVERTERS chapter).

The maximum power of a photovoltaic module (P_{max}) and the short-circuit current (I_{sc}) at deviations of the cell temperature from the standard 25°C are determined by a similar formula. Unlike voltage and power, the short-circuit current increases with rising temperature. Therefore, from a system safety perspective, it is essential to verify the maximum possible current level at the calculated elevated temperature to ensure compliance with the permissible current ratings of cables, fuses, switching devices, and protective equipment.

§2.4. Review of the technical specification of the photovoltaic module.

For the accurate design of a photovoltaic power plant, it is essential to thoroughly study the technical documentation for a specific series of photovoltaic modules. To prevent errors arising from the use of unreliable data, it is recommended to rely solely on specifications published on the manufacturer's official website. As an example, consider the information contained in the specification for the Tiger Neo 78HL4-BDV module with a power rating of 625-650 W from Jinko Solar [28].

Note. *During production, solar cells do not always possess strictly identical characteristics due to technological deviations, and therefore, after testing, they are sorted by their output power. Consequently, photovoltaic modules with identical design and the same number of cells may vary in nominal power, for example, ranging from 625 to 650 W.*

The first page of the specification customarily provides a summary of the technical and structural characteristics of the photovoltaic module series. Specifically, the following are indicated:

- the name of the product line, for example: Tiger Neo JKM 625-650N-78HL4 - BDV;
- the range of nominal powers characteristic of modules in this series (in the present case - from 625 W to 650 W);
- the applied technology and its features, such as N-type TOPcon;
- the type of module - bifacial or monofacial, with half-cut cells or full-size cells;

International standards and certifications to which the product complies (for

example, IEC 61215:2021, IEC 61701, and others).

Concise advantages of the product line include high specific power, improved resistance to thermal effects, a low temperature coefficient, and durability against degradation.

In practice, an engineer must be capable of interpreting the module's code designation, as it encodes information regarding the module’s design, technology, and characteristics. This ability facilitates rapid navigation of specifications and supports the initial sorting of modules. For example, in the module designation JKM 640-78HL4 -BDV the key information is encoded: the nominal power is 640 W, the number of cells is 78, half-cut cells are used (denoted by H-half-cut), the module features bifacial generation (the letter B-bifacial), and it is manufactured with a glass-glass construction (denoted by D - double glass).

The first page of the specification also contains information pertaining to warranty obligations and degradation rates. Specifically, for the considered series of modules, the product warranty is 12 years, with the declared degradation during the first year of operation not exceeding 1%, and the guaranteed average annual degradation over the expected service life limited to 0.4% per year for 30 years (see Fig. 2.11).

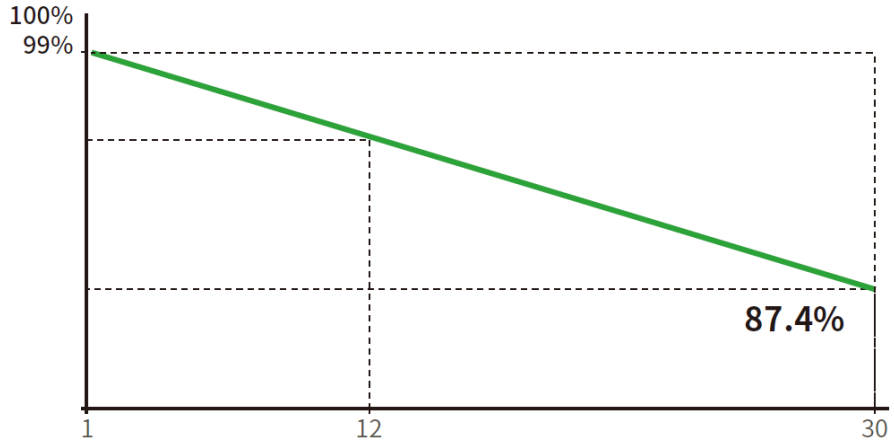

Figure 2.11. Limit degradation of the photovoltaic module.

The residual nominal power of the photovoltaic module is calculated by the formula:

$$\mathbf{P_n = P_0 \cdot (1 - D_1) \cdot \left(1 - D_{year} \cdot (n - 1)\right)};$$

where: P_n - residual power of the PV module after n years, W; P_0 - initial power

of the PV module, W; D_1 - degradation during the first year; D_{year} - annual degradation after the first year; n - number of years.

For the considered photovoltaic module model, the guaranteed residual nominal power after 30 years is 87.4% of the initial value.

The degradation of photovoltaic modules must be taken into account when conducting economic calculations, particularly when determining the project's payback period. As the power output of modules decreases over time, this directly impacts the amount of electricity generated in subsequent years and, consequently, the revenue from its sale or the associated cost savings. Ignoring degradation can result in an over estimation of generation capacity and an inaccurate projection of investment returns.

For the photovoltaic module JKM525M-72HL4-TV with P-type silicon and PERC technology, degradation in the first year is 2%, with an annual degradation rate of 0.45%, corresponding to a guaranteed residual power of 84.95% after 30 years.

The second page of the specification typically provides detailed technical information about the module, including overall dimensions, mounting points, mechanical characteristics (frame type, weight, glass thickness, and other parameters), packaging details (number of modules per pallet and container), as well as electrical characteristics under Standard Test Conditions (STC).

Table 3.1 presents, as an example, the characteristics of the module JKM-640-78 HL4-BDV, measured under STC conditions.

Table 2.1. Electrical characteristics of the photovoltaic module JKM-640-78HL4-BDV

Parameter	Symbol	STC
Maximum Power, W	P_{max}	640
Voltage at Maximum Power, V	V_{mp}	48,02
Current at Maximum Power, A	I_{mp}	13,33
Open-Circuit Voltage, V	V_{oc}	57,34
Short-Circuit Current, A	I_{sc}	13,98
Module Efficiency under STC Conditions	η	22,90%
Allowable power tolerance	δ	0 ~ +3 %
Temperature coefficient of P_{max}	KP	-0,29 %/0C
Temperature coefficient of V_{oc}	KV	-0,25 %/0C
Temperature coefficient of I_{sc}	KI	0,045 %/0C

For bifacial photovoltaic modules, the technical specification additionally specifies the parameter under BNPI (Bifacial Nameplate Power Index the nameplate power index for bifacial panels). Unlike standard STC conditions, BNPI accounts not only for frontal irradiation of 1000 W/m^2 but also for the additional radiation incident on the rear surface of the module, typically assumed to be 135 W/m^2.

Table 2.2 presents the parameters specified in the technical specification of the JKM-640-78HL4-BDV module under BNPI conditions, alongside the corresponding values under STC conditions for clear comparison.

Table 2.2. Comparison of characteristics of single-sided and double-sided modules.

Parameter	Symbol	BNPI	STC
Maximum Power, W	P_{max}	704	640
Voltage at Maximum Power, V	V_{mp}	48,06	48,02
Current at Maximum Power, A	I_{mp}	14,65	13,33
Open-Circuit Voltage, V	Voc	57,42	57,34
Short-Circuit Current, A	I_{sc}	15,43	13,98

As shown, the addition of radiation on the rear side of the photovoltaic module increased the short-circuit current (I_{sc}), current at the maximum power point (I_{mp}), and consequently the power (P_{max}), while the open-circuit voltage (V_{oc}) and voltage at the maximum power point (V_{mp}) remained practically unchanged. This is because additional illumination increases the number of absorbed photons, which leads to the generation of a greater number of electrons and, consequently, to an increase in current (I_{sc} and I_{mp}). Simultaneously, the voltage level is determined by the properties of the p-n junction and is practically independent of the photon count; therefore, the voltage remains nearly constant with changing illumination. Thus, under bifacial illumination, the increase in output power is achieved through an increase in current.

For bifacial photovoltaic modules, the technical specification also specifies the bifaciality coefficient (Bifaciality Coefficient) for the parameters V_{oc}, I_{sc}, and P_{max}. This characteristic indicates the capability of the module's rear side to generate electricity relative to the front side under identical illumination conditions.

In other words, this coefficient represents the proportion of voltage, current, or

power that the rear side can produce compared to the front side when both surfaces receive equal illumination intensity.

The bifaciality coefficient is calculated using the following formula:

$$\boldsymbol{\beta = \frac{X_{rear}}{X_{front}} \cdot 100\%}$$

where**:** β - bifaciality coefficient, %; X_{rear} - the value of the short-circuit current (I_{sc}), open-circuit voltage (V_{oc}) or maximum power (P_{max}) under illumination of the rear side only (1000 W/m$^{2)}$; X_{front} - the value of the current (I_{sc}), voltage (V_{oc}), or power (P_{max}) under illumination of the front side only (1000 W/m^2)·

The bifaciality coefficient for voltage is virtually identical when illuminating both the front and rear sides. Illumination of the rear side generates current in a smaller volume, consequently reducing the power output. To substantiate this, Table 2.3 presents the bifaciality coefficients (Bifaciality Coefficient) for the JKM-625-78HL4-BDV module.

Table 2.3. Bifaciality coefficient of the JKM-625N-78HL4-BDV module

Module	$\beta_{Voc,}$ %	$\beta_{Isc,}$ %	$P_{max,}$ %
JKM-625-78HL4-BDV	98±5%	80±5	80±5

Thus, if the photovoltaic module JKM-625-78HL4-BDV generates 500 W of power at a given moment when illuminated only on its front side (without incident radiation on the rear surface), and then the module is flipped so that its rear side faces the sun (maintaining the same tilt angle and azimuth) while preventing radiation from reaching the front side, the output power will be approximately 375-425 W, corresponding to 75-85% of the power under frontal illumination.

§2.5. Installation of photovoltaic modules

While the matching of technical and electrical parameters of modules and inverters influences the overall system efficiency, the correct installation of photovoltaic modules is crucial to ensuring the reliability, longevity, and safety of the entire installation. Improper installation-such as mechanical damage to cells, excessive force during fastening, uneven support, or overheating of components due to incorrect orientation or shading-can result not only in reduced efficiency but also in module

failure, and in certain cases, fire hazards.

Furthermore, improper installation can cause deformation of structural elements: panels may sag, shift, or suffer damage from wind and snow loads, accelerating degradation and reducing the overall service life of the photovoltaic power plant.

The following sections will address specific aspects that must be taken into account during installation. However, prior to beginning installation, it is strongly advised to thoroughly consult the installation manual (Installation Manual) provided by the photovoltaic module manufacturer.

1. Transportation and handling of photovoltaic modules. To prevent damage, it is recommended to deliver the modules to the construction site in their original factory packaging. Further handling of modules on-site must be performed with utmost care: avoid bending and deformation; preferably, transport the modules in a vertical position (on edge) to minimize the risk of bending.

Important! Safe handling of photovoltaic modules requires the involvement of at least two people. The handling of modules by a single worker is strictly prohibited. In practice, this requirement is often neglected by installation personnel, particularly due to limited experience, when modules have already been moved single-handedly and apparently without consequence.

However, this practice is highly dangerous: damage sustained during careless transportation may be latent and not immediately visible, potentially manifesting only after months or even years in the form of localized overheating, microcracks, cell degradation, reduced performance, or complete module failure. Strict control must be implemented to ensure compliance with safe handling requirements for the modules, and disciplinary measures must be applied immediately in the event of violations.

2. Provide a technological passage between the modules.

It is essential to provide a technological passage between the modules to avoid stepping on the surface of photovoltaic modules during installation or maintenance.

Do not stand on or step over photovoltaic modules. This may cause damage to the glass, cells, or frame, as well as pose a risk of injury due to slipping or surface failure of the module under load.

Figure 2.12. Do not stand on or step on photovoltaic modules.

3. Requirements for photovoltaic module installation sites. From a fire safety perspective, photovoltaic modules should be installed on surfaces that are not combustible. During operation, especially in cases of contact connection failure or damage to the cable network, arc discharge may occur, which can lead to localized heating and, in some cases, ignition.

Furthermore, placing photovoltaic power plants near highly flammable materials such as hay, straw, petroleum products, gasoline, and other combustible substances is strictly prohibited. Adherence to fire safety distances and the requirements for foundations and surroundings is an essential component of the safe operation of photovoltaic power plants.

4. Installation of photovoltaic power plants on ground-mounted structures. When installing photovoltaic modules on soil foundations, potential soil subsidence or erosion must be taken into account, as these phenomena can, over time, cause deformation of the supporting structures and the modules themselves, thereby reducing system reliability and shortening its operational lifespan.

This is especially pertinent when installing photovoltaic modules on loose or inclined soil prone to seasonal shifts, erosion, or washout. Uneven foundation settlement may result in tilting of supports, distortion of module geometry, loosening of fastenings, increased load on frames and glass, as well as alteration of tilt angles, which diminishes generation efficiency.

Moreover, structural deformation can lead to disruption of electrical connections,

formation of cracks in components, or compromise of sealing integrity. In the case of long linear arrays of modules, it is particularly important to control longitudinal sagging and support bending.

To minimize these risks, an engineering and geodetic assessment of the site must be carried out prior to installation, along with provisions for drainage, reinforcement, and/or foundation construction (bored piles, screw piles, or concrete supports), especially in areas with unstable or weak-bearing soils.

5. Minimum distance between the rear side of the module and the roof. One common method for installing photovoltaic modules on roofs is the direct attachment of modules to mounting rails secured to the roof surface. This method is particularly prevalent when the roof slope ranges from 15° to 30°, as in such cases the modules are installed parallel to the surface without requiring additional inclined structures.

In practice, photovoltaic power plants sometimes employ modules mounted on two black metal rails with a 40×40 mm cross-section, fixed directly to the roof (see Fig. 2.13). In this configuration, the ventilation gap between the rear surface of the module and the roof is approximately 40 mm, which is categorically insufficient for adequate heat dissipation.

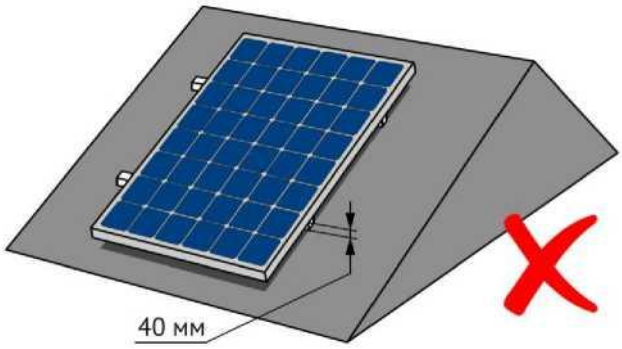

Figure 2.13. Example of insufficient ventilation clearance between the module and the roof.

Limited ventilation leads to module overheating, resulting in reduced performance, accelerated degradation, and, in the long term, may compromise the reliability of the entire system.

To ensure proper ventilation and effective heat dissipation, photovoltaic module manufacturers specify that the minimum distance between the rear surface of the

module and the roof surface must be at least 100 mm, including any potential deflection of the module under its own weight. To ensure the required ventilation gap, it is recommended to use longitudinal and/or transverse mounting rails with an increased cross-section (see Fig. 2.14), or to provide for the installation of vertical supports that elevate the modules to the necessary height above the roof surface.

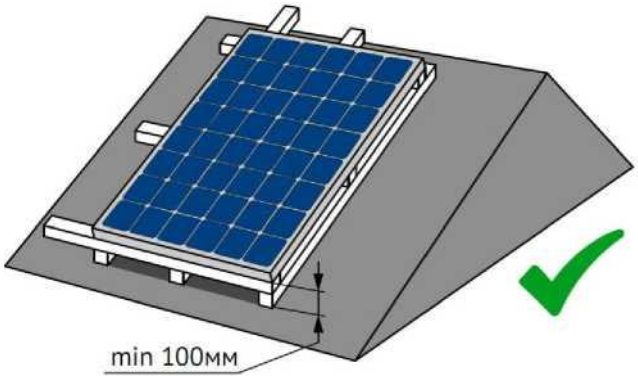

Figure 2.14. Example of maintaining the minimum ventilation gap (100 mm).

A 100 mm gap is the minimum permissible, however, when installing modules on roofs with a low slope angle, this gap may be insufficient. The smaller the tilt angle, the slower the natural heat dissipation occurs, as convection worsens and ventilation efficiency decreases.

Therefore, it is recommended to provide a ventilation gap of 200-300 mm, which ensures more effective cooling of the modules and reduces the risk of overheating. This is particularly relevant under the conditions in Uzbekistan, where elevated ambient temperatures in summer further increase the thermal load on the equipment.

Note. *In the case of installing photovoltaic (PV) modules in a horizontal ("flat-lying") position on a roof, it is preferable to use monofacial panels. The use of bifacial modules in such a configuration is impractical for two reasons: firstly, there is no reflected radiation reaching the rear side, and secondly, the glass–glass construction of bifacial panels promotes greater heat accumulation in the gap between the module and the roof.*

However, at present, the market in Uzbekistan is predominantly supplied with bifacial modules, and in some cases, it is not possible to obtain monofacial panels. In such situations, when the use of bifacial PV modules is unavoidable, it is recommended to provide a ventilation gap of at least 300 mm between the rear surface of the module

and the roof. This significantly improves heat dissipation, reduces the operating temperature of the modules, and thereby helps maintain their efficiency and reliability over the long term.

Requirements for the module tilt angle relative to the horizontal plane.

The tilt angle of photovoltaic modules relative to the horizontal surface is chosen based on the type of system being designed and its priorities.

For autonomous stations not connected to a centralized power supply system, it is especially important to ensure maximum generation during the winter period, when daylight duration is minimal and solar incidence angles are low. During the summer period, such plants typically generate surplus energy (except when energy intensive consumers, such as irrigation pumps, are connected to the system).

It is preferable for the support structure of an autonomous photovoltaic power plant to allow adjustment of the module tilt angle according to the season - increasing the angle during winter and decreasing it in summer. If the structure is stationary, the tilt angle is chosen based on the seasonal load profile of the autonomous consumers. If significant energy consumption also occurs during the winter period, it is recommended to set the tilt angle between 40° and 50° to compensate for the low solar elevation and enhance generation efficiency during this season.

For grid-connected photovoltaic power plants, the primary objective is to maximize annual energy generation. In the context of Uzbekistan, the optimal tilt angle of modules for these purposes is between 30° and 35°, corresponding to the region's geographic latitude and ensuring balanced energy production throughout the year.

When installing modules on a roof, the tilt angle is often determined by the roof’s slope - this facilitates installation and reduces wind load. However, this approach has certain limitations. For example, horizontal installation of modules results in two significant issues:

- Decreased energy generation due to an inefficient angle of solar incidence, particularly during the autumn and winter seasons.
- Accumulation of contaminants on the module surfaces, especially on the lower areas, since with little or no tilt, rain and meltwater are unable to effectively remove dust and dirt. This results in local shading, reduced generation, and potential cell

overheating.

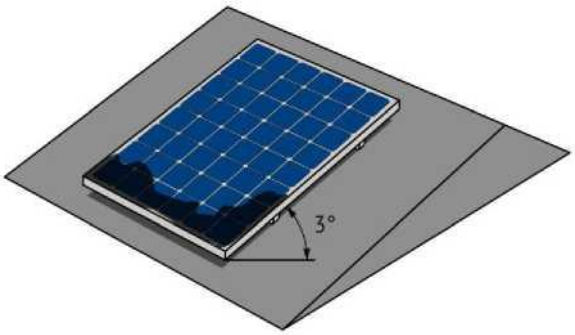

Figure 2.15. Deposition of dust and dirt on the lower edge of the module at a low tilt angle.

Accordingly, photovoltaic module manufacturers recommend ensuring a minimum tilt angle of no less than 10°, even for installations on flat roofs this facilitates natural self-cleaning of the modules and mitigates the risk of degradation caused by soiling.

6. Mounting of photovoltaic modules to the support structure. Photovoltaic modules can be mounted on the support structure using bolts with anti-corrosion protection (see Fig. 2.16 A), or by means of special intermediate (see Fig. 2.16 B) and end clamps (see Fig. 2.16 C).

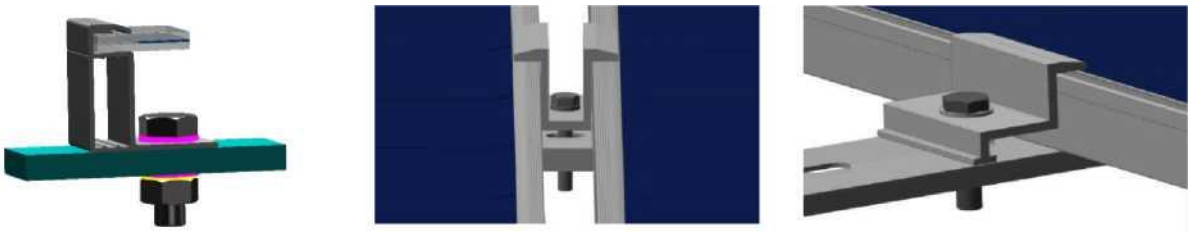

A B C

Figure 2.16. Methods of securing a photovoltaic module to the support structure.

For bolted mounting, the photovoltaic module frame is provided with special installation holes (see Fig. 2.17). However, in practice, especially during the construction of small- and medium-power photovoltaic power plants, this method is rarely used due to greater labor intensity, the need for precise marking, and reduced flexibility compared to the use of standard mounting clamps.

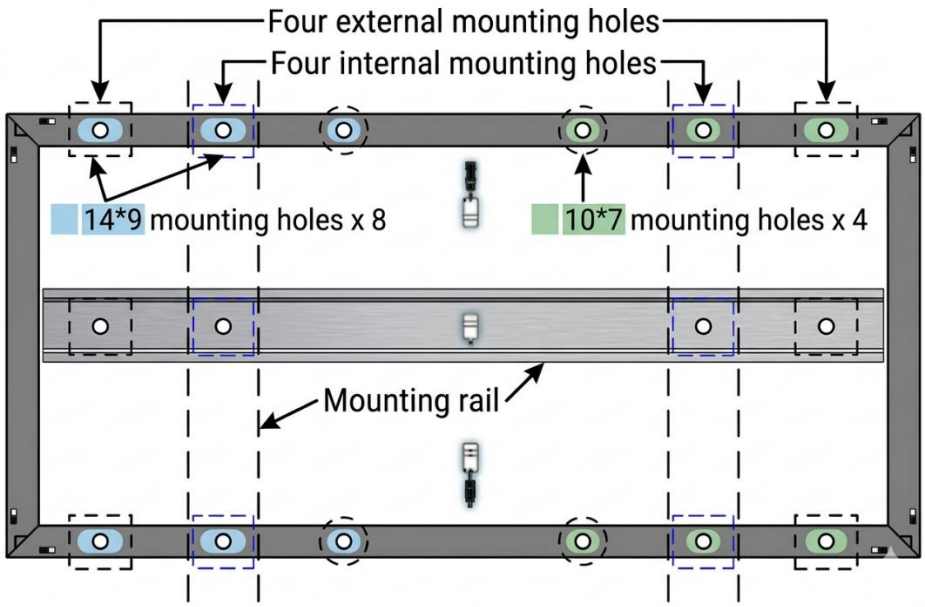

Figure 2.17. Mounting holes in the module frame for bolt fastening.

Bolt fastening requires more installation time, increases the risk of frame damage due to improper tightening, and is less convenient for mass installation.

Therefore, in most cases, preference is given to end and intermediate clamps, which ensure reliable fixation and considerably accelerate installation work.

According to the installation manual for PV modules by Jinko Solar, the following requirements are specified for mid clamps and end clamps (see Fig. 2.18):

- thickness (a) – not less than 3 mm;
- clamp length (b) – not less than 50 mm;
- width of the mid clamp (c) – 20 mm;
- clamping zone overlapping the PV module frame (d) – 10–11 mm.

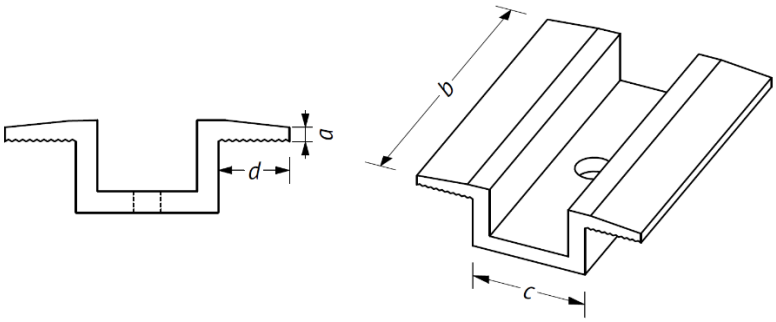

Figure 2.18. Clamp for securing the PV module.

Some installers use large clamping washers up to 100 mm in diameter to mount photovoltaic modules, positioning them on the module frame. This method of fastening

is unacceptable because part of the washer inevitably extends beyond the frame and shades a portion of the solar cells (see Fig. 2.19). This causes localized power loss, may induce cell overheating (hot-spot), and ultimately can lead to module damage.

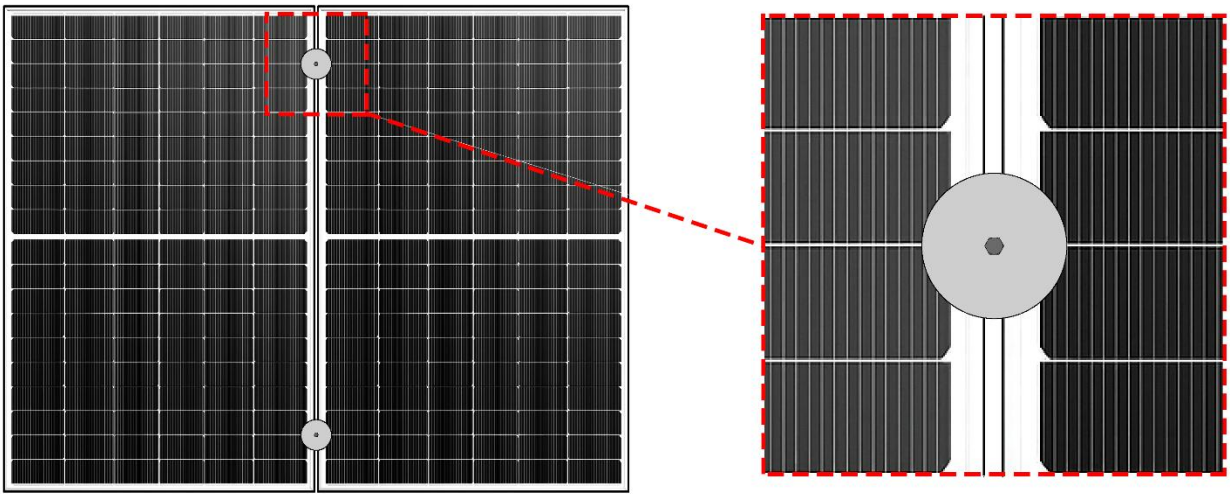

Figure 2.19. Fastening of the photovoltaic module using a washer.

A round clamp design is fundamentally unsuitable for fastening photovoltaic modules, as it does not simultaneously ensure both reliability and the absence of shading.

If the washer has a small diameter to avoid extending onto the active surface of the module, the contact area becomes insufficient for secure fixation, especially under high wind loads. Conversely, if a washer of adequate diameter is used to provide firm fastening, it inevitably extends beyond the frame boundaries and shades part of the solar cells, resulting in reduced generation and an increased risk of hot-spot effects.

Therefore, specially designed clamps should be used for mounting the modules, with shapes and dimensions that comply with the manufacturer’s specifications and prevent shading.

Excessive torque applied when tightening the clamp bolt may cause damage to the photovoltaic module’s aluminum frame, including deformation of the profile or the development of microcracks. To prevent this, it is advisable to use a torque wrench for the final tightening of fasteners to ensure strict compliance with the recommended torque values.

In practice, M8 bolts (preferred due to higher strength) and M6 bolts are most commonly used for mounting modules. The recommended tightening torques are as

follows:

- for M8 bolts — 16–20 N·m;
- for M6 bolts — 9–12 N·m.

The installation manual for photovoltaic (PV) modules describes more than nine different mounting configurations, which vary in the number and orientation of mounting rails. The reader may independently familiarize themselves with all available methods if necessary; however, this section will cover the two most popular and widely used mounting methods in Uzbekistan.

- a two-rail mounting system with four fixing points (see Fig. 2.20 A): $L = A/4 \pm 50$;
- a three-rail mounting system with six fixing points (see Fig. 2.20 A): $L_1 = 400$, $L_2 = (A/2 - L_1 + 50)$, $L_3 = (A/2 - L_1 - 50)$.

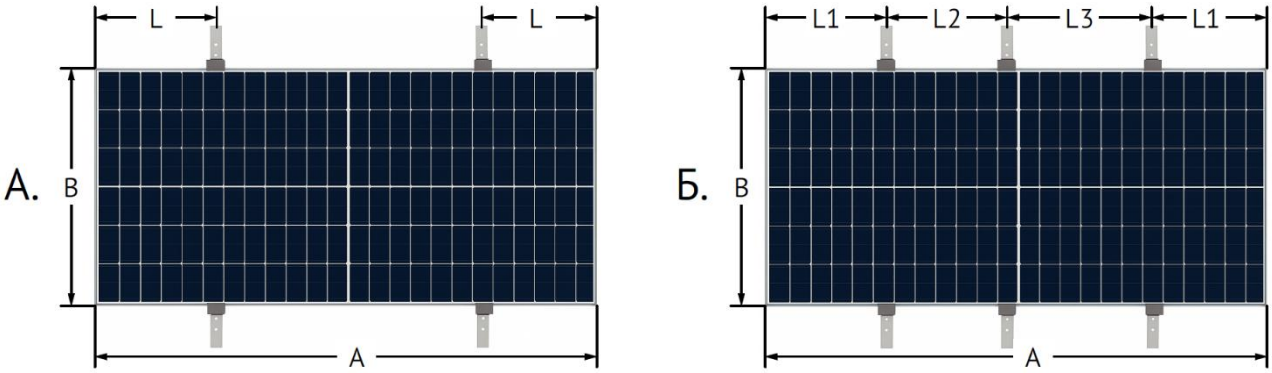

Figure 2.20. Fastening of the PV module at four (A) and six (B) points.

Considering that the cost of an additional mounting rail is negligible compared to the total cost of the photovoltaic power plant, it is recommended to employ module fastening at six points (Method B). This method enhances the structural reliability:

- the risk of module deflection under snow load is significantly reduced;
- improved resistance to wind loads is ensured;
- and in the event of inadequate fastening at one point, the system remains operational due to the presence of five additional support points, thereby increasing the overall mechanical reliability.

When using method, A, that is, fastening the photovoltaic module at four points, it is necessary to adhere to the manufacturer's recommendations regarding the permissible distance between fastening points.

Unfortunately, in practice, photovoltaic power plants are often encountered where these requirements are disregarded, and the distance between rails reaches two meters, which significantly exceeds the permissible limits. Such a violation may cause the module to bend under snow load and, in the long term, lead to damage to the glass, frame, or a reduction in the overall structural reliability.

7. Spacing between photovoltaic modules. The frame of the photovoltaic module is subject to thermal expansion; therefore, it is recommended to leave compensation gaps between modules during installation.

Along the short side of the modules, a gap of approximately 10-20 mm should be provided, which is typically ensured automatically by using intermediate clamps with a standard width of 20 mm. Along the long side, maintaining a gap of 20-30 mm is recommended (see Fig. 2.21).

Such gaps are necessary for:

- compensating thermal deformation of the frames,
- ensuring natural drainage of water from the module surfaces, and creating conditions for ventilation that mitigate the risk of overheating and contamination.

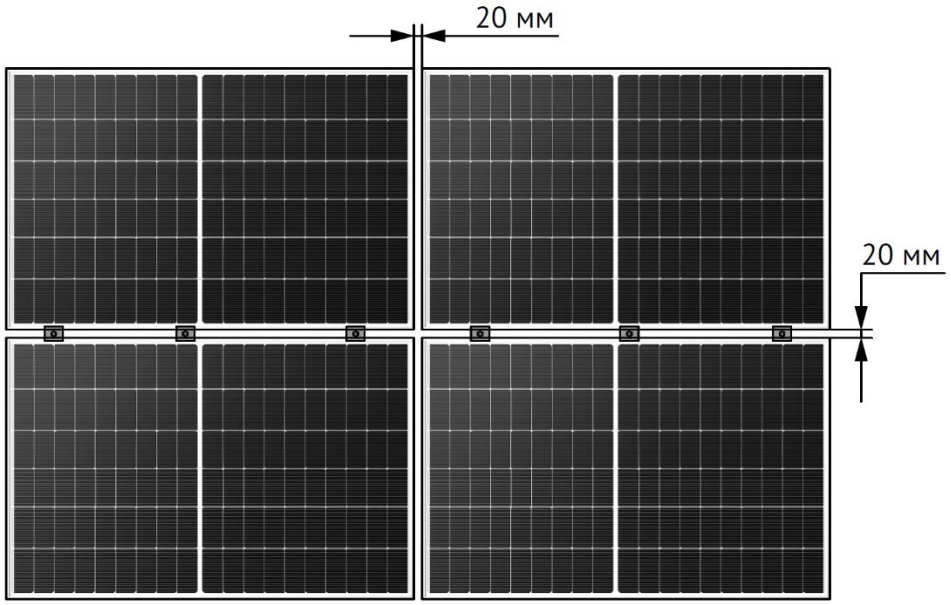

Figure 2.21. Compensation gaps between photovoltaic modules.

8. MC4 connector. For connecting photovoltaic modules, it is recommended, whenever possible, to purchase original MC4 connectors from the module manufacturers themselves. This guarantees full compatibility and compliance with the

required electrical and mechanical specifications.

In the event of using third-party MC4 connectors, their technical specifications must be carefully examined. Each reputable manufacturer provides a product datasheet on their official website, specifying nominal currents and voltages, along with compliance with IEC 62852 and UL 6703 standards.

For modern high-power photovoltaic modules, the use of MC4 connectors with the following characteristics is recommended:

- a nominal current of 35–40 A (depending on the cable cross-section — 4 or 6 mm^2);
- a nominal voltage of up to 1500 V.

Using connectors that do not comply with the current and voltage requirements may result in overheating, deteriorated contact, and an increased risk of failure or fire.

Important! When connecting MC4 connectors, they must be firmly and securely snapped together until a distinct clicking sound is heard (see Fig. 2.22 A). An incomplete connection leads to a loose contact (see Fig. 2.22 B), which can cause serious consequences.

In the best-case scenario, this will trigger the DC arc fault protection in the inverter. In the worst case, it can lead to overheating, melting of the connector, or even a fire, especially under high currents and high ambient temperatures.

Figure 2.22. Reliable (A) and weakened (B) MC4 connection.

9. Protective measures for MC4 module connectors against dust, moisture, and corrosion. Although MC4 connectors inherently provide an IP67 degree of protection by design, they remain vulnerable during installation. Until the final connection is completed, connectors often remain unprotected against dust and moisture ingress, which risks compromising their functionality.

The ingress of dust can cause a reduction in the electrical contact area, while moisture can result in oxidation of the contact surface, increased contact resistance, localized heating, contact burn-out, and, consequently, even fire.

Therefore, special attention must be given to protecting MC4 connectors during installation. Recommended:

- Prior to installation on the supporting structure, the modules should be stored in their factory packaging or in a dry, enclosed room that excludes exposure to dust and moisture.
- Immediately after installing the module on the structure, it is necessary to connect the MC4 connectors as soon as possible to ensure the sealing of the connections.
- If immediate connection is not possible, the connectors must be temporarily protected with special caps (see Fig. 2.23), especially when working in conditions of high dust levels, such as in desert environments.

Figure 2.23. Caps for protecting MC4 connectors from dust or moisture ingress.

Adhering to these recommendations enhances the reliability of the connections, prevents latent damage, and prolongs the service life of the entire system.

10. Cable length of the photovoltaic module. In most modern photovoltaic modules, the junction box is located at the center of the rear surface. This is partly due to the use of Half-Cut cells in most modules; the module essentially consists of two symmetrical halves, each connected to its corresponding section within the junction box.

Photovoltaic modules are manufactured with cables of varying lengths both short and long. If the project allows for a choice, the cable length should be selected according to the method of module connection.

For example, when connecting modules along the short side (see Fig. 2.24), it is advisable to use modules with short cables. For this type of connection, a length of 1520 cm is sufficient, whereas longer cables (1 meter or more) will only complicate installation, create unnecessary loops, impair aesthetics, increase thermal losses, and

raise the risk of damage.

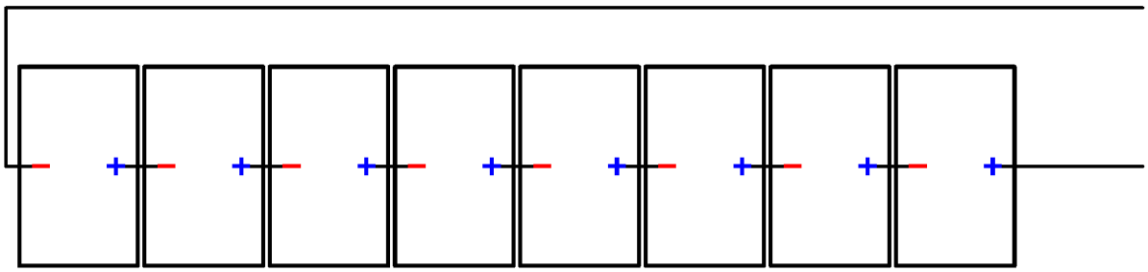

Figure 2.24. PV module connection along the short side.

If the connection scheme requires connecting modules along the long side (see Figure 2.25), it is necessary to use modules with long cables. Otherwise, additional intermediate extension cables will need to be installed, resulting in a twofold increase in the number of connections via MC4 connectors.

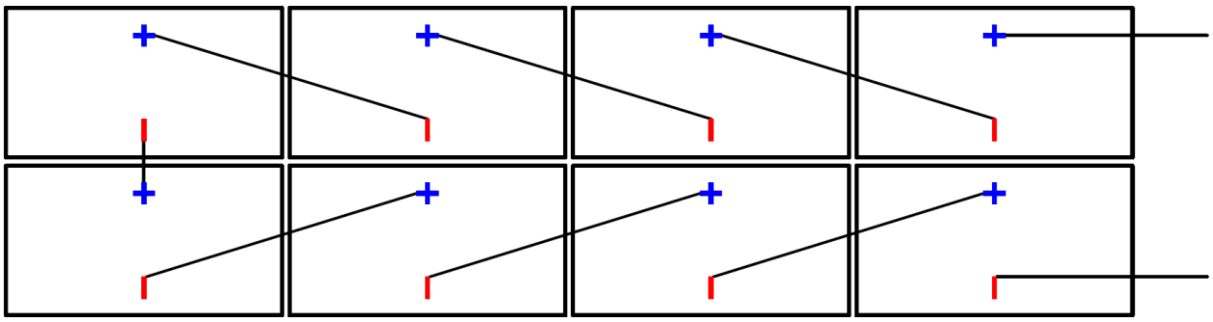

Figure 2.25. PV module connection along the long side.

An increase in the number of contact connections reduces the overall reliability of the system, elevates the risk of transitional resistances, local overheating, and consequently decreases efficiency, as well as increases the risk of failures during operation.

Therefore, the correct selection of cable length at the module procurement stage prevents unnecessary connections, simplifies installation, and enhances the reliability of the entire photovoltaic installation.

11. Protective grounding. The frame of photovoltaic modules is manufactured from aluminum and treated with a special anodized coating that ensures long-term corrosion protection. However, such a coating possesses dielectric properties and does not provide reliable electrical contact; therefore, grounding the module through the frame surface is inadmissible.

Special grounding holes are provided on the module frame for connecting the grounding conductor, where the anodized layer has been removed or conductive

contact pads are available. These holes are typically located at four positions near the corners of the frame, ensuring convenient connection of the grounding conductor regardless of the module's orientation on the structure.

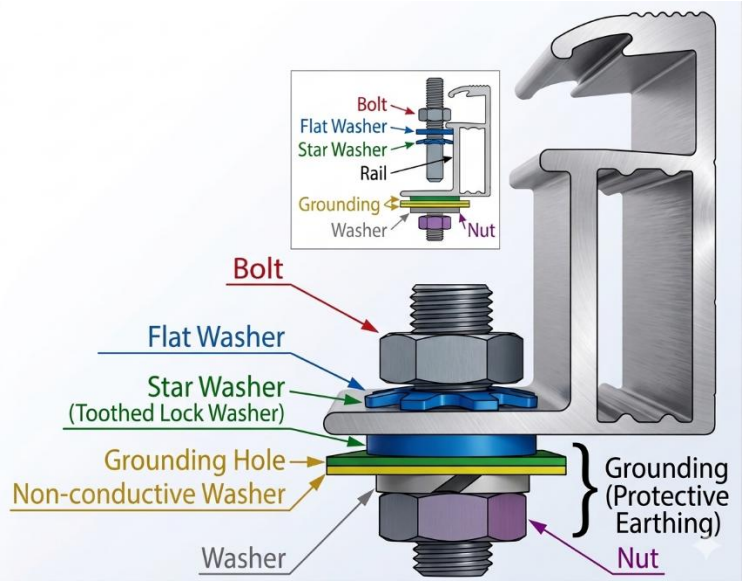

Figure 2.26. PV module grounding.

Grounding must be performed only at manufacturer-designated points, using bolts, clamps, or certified terminals to ensure reliable contact and compliance with standards such as IEC 61730, UL 1703, and NEC 690.43. Failure to follow these recommendations may lead to reduced protective performance, increased resistance, and a higher risk of electrical faults.

§2.6. Maintenance of photovoltaic modules.

To promptly detect faults and prevent emergency situations, it is recommended to conduct regular visual inspections and maintenance of photovoltaic modules.

1. Visual inspection.

During the visual inspection, attention should be given to the following aspects:

- Evaluate the module's appearance under light: slight variations in color tones between cells at different viewing angles are normal for modules with anti-reflection coating technology. However, if the shades differ within the same cell, this may indicate an internal defect.

In such cases, it is necessary to contact the manufacturer.

- Check the glass for cracks, chips, or other mechanical damage.
- Inspect the current-collecting busbars of the cells for signs of corrosion.

Corrosion may result from moisture penetration through the rear surface of the module. If corrosion is detected, it is necessary to further inspect the rear side of the module for damage.

- Inspect the distribution boxes (junction boxes) for any signs of melting, charring, or fire damage.
- Check all MC4 connectors: ensure they are fully snapped in and show no signs of melting, charring, or deformation of plastic components.
- Verify that all bolted connections (including grounding) are in proper condition and securely tightened.

It is recommended to conduct a visual inspection of photovoltaic modules at least twice annually-preferably in spring and autumn. This enables the timely detection of potential malfunctions before the summer period, when increased temperature and current impose additional stress on the system, as well as before the onset of winter, when snow loads increase and voltage in the circuits rises due to the reduction in ambient temperature.

2. Cleaning of the photovoltaic module surface.

Contamination of photovoltaic module surfaces is one of the most common causes of decreased efficiency in solar power plants.

Even minor contamination-such as dust, sand, leaves, bird droppings, or soot can significantly impact the performance of a module and the entire string.

Soiled areas obstruct the passage of solar radiation, causing some cells to cease participating in power generation. This results in a reduction of output power not only in an individual module but throughout the entire string, particularly when modules are connected in series.

To evaluate the effect of soiling on the surfaces of photovoltaic modules on the electricity output of a solar power plant, an experiment was conducted in the city of Tashkent.

To eliminate the influence of external factors (other than the degree of contamination of the PV module surface) on the results, two virtually identical photovoltaic power plants, located in close proximity to each other, were selected for comparison. Both plants are equipped with identical modern inverters and modules,

installed on roofs with the same orientation (azimuth 185°) and identical tilt angles relative to the horizon (30°). The inverters of both plants are connected to the same bus section of a single transformer, with all operational and protective parameters configured identically.

To evaluate the effect of cleaning on electricity generation by photovoltaic modules, a thorough cleaning of the surfaces of all modules was conducted at the first plant, whereas at the second plant, the surfaces of the PV modules remained uncleaned (see Fig. 2.27).

Following the cleaning, daily electricity output increased by 12.8%. The testing methodology, data analysis approach, and results are detailed in reference [29].

Figure 2.27. Photovoltaic modules before and after cleaning.

In addition to reduced power generation, surface contamination of photovoltaic modules presents another serious issue local overheating of cells due to disruption of their normal operating mode. When some cells are shaded or contaminated, they stop generating energy, but current continues to flow through the circuit. In this scenario, the cell operates in load mode, converting the incoming energy into heat instead of electricity.

This results in:

- local overheating (hot-spot);
- accelerated degradation of cell materials;
- insulation damage and risk of fire.

Long-term consequences:

- continuously soiled modules age faster and lose efficiency.

- the risk of damage to glass and lamination increases due to thermal expansion.
- generation mismatches between modules within the same string increase, adversely affecting the operation of the MPPT controller.

The frequency of cleaning photovoltaic modules depends on the installation region, environmental contamination level, and amount of precipitation.

In areas with high dust accumulation, as well as during the summer period when rain is absent for extended durations, it is recommended to perform cleaning more frequently than usual, since natural removal of dust and contaminants does not occur.

Before cleaning photovoltaic modules, it is essential to familiarize yourself with the equipment manufacturer's recommendations as specified in the technical documentation or maintenance manual. Failure to adhere to these instructions may result in damage to the module surfaces, reduced operational efficiency, and, in certain cases, voiding of the warranty.

Below are some standard recommendations included in the instructions of most manufacturers:

- For cleaning the glass, it is recommended to use water with a neutral pH level between 6.5 and 8 to avoid damaging the protective coating on the glass surface. Water with a high mineral content can cause deposits on the glass surface; therefore, its use is not advisable.
- Under no circumstances should abrasive materials be used.
- To minimize the risk of electrical and thermal shock, it is recommended to clean photovoltaic modules during early morning or late evening hours, when solar radiation is minimal and the modules are cooler. This is particularly important when operating in regions with high ambient temperatures.
- Applying cold water to the heated surface of the module may cause thermal shock and damage to the glass, especially if microcracks are present. There is also the possibility of temporary evaporation followed by condensation: rapid cooling can cause moisture to form between the glass layers and the protective film, which subsequently leads to oxidation of the current-collecting busbars and accelerated degradation of the module. Therefore, moderately warm water should be used for cleaning, avoiding abrupt temperature changes.

- Never attempt to clean photovoltaic modules with damaged glass or signs of exposed wiring, as this constitutes a risk of electric current shock.

3. Thermographic diagnostics

Thermographic diagnostics is among the most effective and non-invasive methods for evaluating the technical condition of photovoltaic modules. It enables the detection of hidden defects that are not visible during visual inspection but may significantly impact system performance and safety.

Thermal imaging diagnostics enable the detection of:

- "Hot spots" (Hot-Spots) — localized overheated areas arising from microcracks in cells, point contaminations, damaged connections, degradation of EVA film, or current-collecting busbars;
- Increased resistance in contact connections - overheating of MC4 connectors, junction boxes, terminals, and bolted connections.
- Uneven operation of cells within a single module (e.g., due to degradation of individual sections or poor-quality lamination).
- Presence of diode defects in bypass circuits—overheating of one module section while others function properly.

The temperature difference between normal and overheated areas should not exceed 10-15°C. If the difference exceeds 15°C, additional diagnostic testing is recommended. Individual cells heated by 20°C or more relative to neighboring cells unambiguously indicate a hot-spot or internal defects.

Thermographic diagnostics should be conducted on a sunny day, with a solar radiation level of at least 600 W/m^2, to ensure sufficient current in the circuit.

The module surface must be dry and clean to obtain accurate results.

The inspection is conducted from both the front side of the module and, if necessary, from the distribution box side.

CHAPTER 3. INVERTERS

An inverter is an electrical device designed to convert direct current generated by photovoltaic modules into alternating current with specified voltage and frequency parameters. It is justifiably regarded as the 'heart' of the photovoltaic plant, ensuring its connection to the load or the power grid. This chapter reviews the fundamental operating principles of inverters, their typical schematic configurations, and structural features. Key factors affecting energy conversion efficiency are outlined, including the architecture of the power stage, MPPT algorithms, and thermal operating modes. The chapter also addresses practical aspects related to inverter installation, selection, interaction with other system components, and the implementation of integrated protection and control functions.

§3.1. Pulse-width modulation

An inverter is an electrical device designed to convert direct current (DC) into alternating current (AC) with specified voltage and frequency parameters.

To understand how an inverter generates an alternating sinusoidal voltage from direct current, it is first necessary to examine the concept of pulse-width modulation (PWM). This method forms the basis of operation for most modern inverters and allows precise control over the amplitude, waveform, and frequency of the output signal. This section addresses only those aspects of PWM that are directly relevant to the design of photovoltaic power plants. Topics related to the component base, diode bridge construction, filter topologies, and circuit design are beyond the scope of this material and may be studied independently by the reader [30], [31], [32].

Pulse Width Modulation (PWM) is a method for controlling power electronic switches (such as MOSFETs or IGBTs) used in inverters to generate alternating sinusoidal voltages from a direct current source. The principle involves generating a sequence of rectangular pulses of variable width, the shape of which corresponds to the instantaneous values of the sine wave. After passing through LC filters, such a pulse signal is converted into a smoothed sinusoidal voltage suitable for powering a load or feeding into the grid.

Note. *Filters used in industry are significantly more complex and may feature different circuit configurations, including resistors.*

According to the fundamental laws of electrical engineering, the current in an inductance coil and the voltage across a capacitor cannot change abruptly. The characteristics of transient processes depend on the values of inductance and capacitance, as well as on the connection scheme and external conditions. To smooth the signal in inverters, the coil is typically connected in series, while the capacitor is connected in parallel with the load, forming an L-C low-pass filter. Consequently, the pulsating signal is smoothed.

Figure 3.1 illustrates an example of an output signal obtained by smoothing a sequence of rectangular pulses with an LC filter.

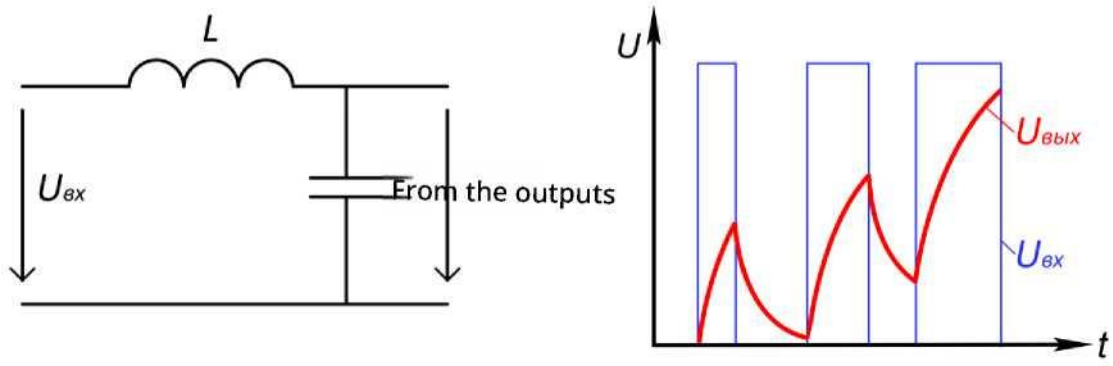

Figure 3.1. Input pulse and output smoothed signals on the L-C filter.

The PWM operation algorithm can be simplified as follows:

- The inverter controller (typically a microcontroller or digital signal processor - DSP) generates a sinusoidal reference signal at a specified frequency (e.g., 50 Hz);
- A high-frequency triangular or sawtooth waveform is generated (the carrier frequency of the PWM is typically 10-20 kHz); The PWM frequency is typically chosen to be 200-400 times higher than the frequency of the output sinusoidal signal. For example, at an output frequency of 50 Hz, the PWM frequency is approximately 10 kHz. The higher the PWM frequency, the easier it is to smooth the signal using a filter; however, this is accompanied by increased switching losses in the power switches.
- In each cycle, the control circuit compares the amplitude of the sinusoid and the triangular wave, generating a sequence of pulses whose widths vary according to the sinusoid's shape with wider pulses at the center of the half wave and narrower

pulses near the zero crossings (see Fig. 3.2).

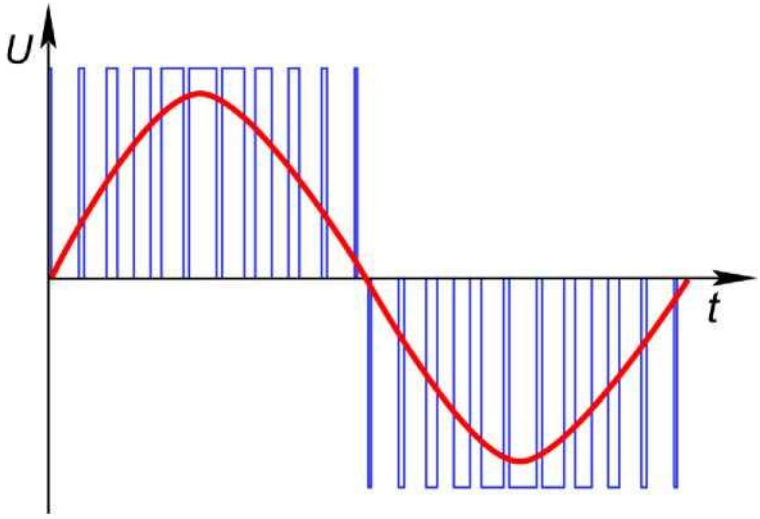

Figure 3.2. PWM modulation of a sinusoidal signal.

The L-C filter smooths the signal, extracts the fundamental harmonic component, and suppresses higher harmonic components (see Fig. 3.3).

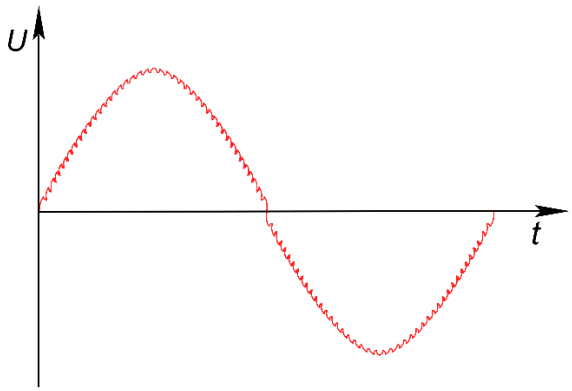

Figure 3.3. Output signal after smoothing.

To generate a sinusoidal output voltage, the voltage magnitude on the inverter's DC bus (DC BUS), from which the PWM pulses are formed, must exceed the sinusoid amplitude by 10-20%. Thus, for a single-phase system with an RMS voltage of 230 V, the sinusoidal amplitude is approximately 325 V; accordingly, the DC bus voltage must be at least 360 V. In the case of three-phase inverters, calculations are generally performed based on line voltage, and the voltage on the direct current bus should be approximately 600 V.

During the design and construction of photovoltaic power plants, modules are connected in series to form a photovoltaic block (PVB or String), which is then connected to the inverter's direct current input (DC Input). If the PVB voltage is below the required level for full PWM operation, a DC-DC converter (direct current

converter) is used to increase it. In this case, part of the energy is consumed in the voltage boosting process, which reduces the overall system efficiency and, importantly, leads to increased thermal losses and a rise in the inverter's temperature, which in turn may cause the inverter's power rating to be thermally limited.

Therefore, in the design process, it is recommended to configure the PV array with a V_{mpp} as close as possible to the inverter's nominal operating voltage.

Typically, this value is:

- approximately 360 VDC for single-phase inverters;
- approximately 600 VDC for three-phase models.

§3.2. Principal circuit diagram of the inverter

Figure 3.4 presents the principal circuit diagram of a single-phase grid-tied inverter. A description of its key components follows below.

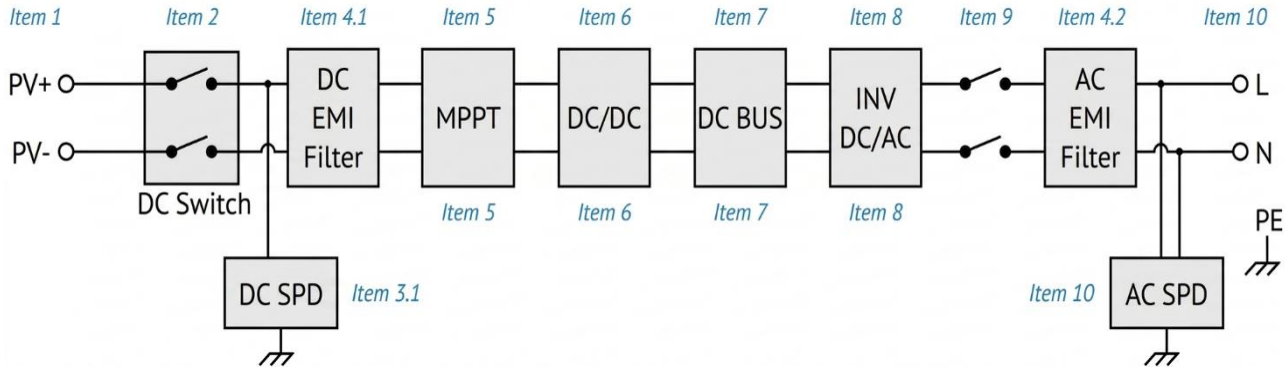

Figure 3.4. Schematic diagram of a single-phase grid-tied inverter.

Position №1. – PV+ and PV− connection terminals.

They are intended for connecting the positive and negative conductors of a photovoltaic array (PV array) — a group of photovoltaic modules (PV modules) connected in series to form the required DC voltage level needed at the input of a solar inverter. In practice, the English term "String" is most commonly used, which literally means "chain" or "thread," reflecting the series connection of modules into a single electrical line.

Each input has a maximum PV input current limitation, so the connected string must have a current I_{mp} that does not exceed this value.

Important! Only original MC4-type connectors supplied with the inverter must be used for connecting wires to the PV+ and PV- terminals.

Position №2. DC switch (DC Switch) - is used to disconnect the circuit between the PV modules and the inverter.

Important! It is not recommended to switch off the DC Switch while the inverter is operating unless absolutely necessary, especially during periods of peak solar radiation. Before switching off, the inverter should be placed into standby mode via the service menu to preliminarily reduce the current to zero and eliminate the risk of damage.

Position №3. Surge Protection Device (SPD) in the direct and alternating current circuits.

Designed to divert high-energy impulse over voltages to the grounding system, thereby preventing equipment damage. SPDs are installed on both the DC side (SPD DC) and the AC side (SPD AC) of the inverter.

Important! Surge Protective Devices (SPDs) for DC and AC circuits differ significantly in design and operating principles; therefore, the device must be selected according to the circuit type. Moreover, DC-SPDs feature a more complex arc quenching system due to the absence of current zero crossing.

SPDs are classified by type as follows:

- Type I - designed to divert current during direct lightning strikes, rated for currents up to 65-100 kA (impulse waveform 10/350 mks - with a rise time to peak value of 10 mks and a decay time from peak to 50% of 350 mks).
- Type II - used for protection against induced over voltages caused by remote discharges, designed for currents up to 20 kA (pulse waveform 8/20 mks).
- Type III - used as additional protection for end equipment against residual impulses. Typically applied in combination with types I and II.

Generally, inverters on both the DC and AC sides are equipped with Type II surge protective devices, which are intended not for protection against direct lightning strikes, but against induced impulse over voltages arising from nearby lightning discharges or switching operations in the network.

Important! In the event of overvoltage, the internal components of the SPD (varistors, surge arresters) instantly transition to a conductive state, significantly reducing resistance and directing the impulse energy to the grounding system.

However, in the absence of grounding or when its resistance is high, the overvoltage energy cannot be efficiently dissipated, resulting in a high level of residual voltage. Under these conditions, the inverter may sustain damage despite the presence of the SPD.

DC-SPDs are produced for nominal voltages of 600 V, 1000 V, and 15 00 V, whereas AC -SPDs are designed for voltages of 230 V (single-phase) and 400 V (three-phase circuits).

Position №3. Electromagnetic Interference Filter (EMI, Electro Magnetic Interference).

Designed to suppress high-frequency electromagnetic interference generated by the inverter during operation. The installation of the EMI filter reduces the level of interference propagated through cable lines, thereby:

- Enhance the quality of electric power in the network;
- Ensure compliance with electromagnetic compatibility (EMC) standards;
- Mitigate the risk of mutual interference with other electronic devices, particularly in sensitive loads (such as measuring instruments, communication systems, etc.).

EMI filters for direct current (DC) and alternating current (AC) circuits differ in design, function, and operational characteristics. AC filters are intended to suppress high-frequency interference in 230/400 V networks with sinusoidal voltage. Unlike these, DC filters are employed in circuits with voltages up to 600,1000, or 1500 V and are designed to suppress impulse noise generated by converters and PWM controllers

Important! The EMI filter is designed to suppress high-frequency interference generated by the inverter and to divert it to the grounding circuit. Without grounding, such interference cannot dissipate effectively, significantly reducing the filtering efficiency. Furthermore, grounding the enclosure or the filter shield helps to reduce the emitted electromagnetic interference level. Hence, reliable and high-quality grounding of the inverter is a critically important prerequisite for the correct operation of the EMI filter.

Position № 5. MPPT Controller (Maximum Power Point Tracking)

MPPT is a maximum power point tracking system integrated into the inverter,

intended to maximize energy generation from photovoltaic modules under varying illumination and temperature conditions.

Chapter 3.3 examined the current-voltage characteristic (I-V curve) of a single photovoltaic module. A photovoltaic array, composed of modules connected in series, also has its own I-V curve. Ideally, the I-V curve of the photovoltaic array is similar in shape to that of an individual module, but with the voltage increased proportionally to the number of connected PV modules.

However, in practice, the I-V curve of the photovoltaic array deviates from that of an ideal module, since individual modules within the string exhibit parameter variations caused by manufacturing tolerances, soiling, shading, and other factors. These differences cause the modules to interact with each other, resulting in the overall I-V characteristic of the photovoltaic array being somewhat distorted compared to the theoretically expected one. To enhance the efficiency of MPPT operation, it is essential to create an ideal I-V characteristic, that is, to form the photovoltaic array from identical PV modules, install them with the same tilt angle and azimuth, and eliminate shading on any of the PV modules.

When connecting two photovoltaic arrays to a single MPPT, the I-V characteristics of both arrays must be as identical as possible. This entails the use of identical modules, an equal number of PV modules in each string, as well as a uniform orientation: the angle
of inclination and azimuth. Discrepancies in these parameters lead to distortion of the overall I-V characteristic, complicate MPPT operation, and reduce the system's overall efficiency.

The MPPT controller regulates the operating voltage and current (U and I) by sequentially 'scanning' the I-V characteristic to identify the point at which maximum power is achieved (P=U*I). When solar irradiance varies or shading occurs, the maximum power point (MPP) shifts, and the MPPT controller automatically finds the new optimal value using an embedded algorithm, thereby ensuring efficient system operation.

When designing a photovoltaic system, it is essential to consider the following key characteristics of the MPPT controller:

- MPPT Operating Voltage Range (MPPT Operating Voltage Range) - the range of DC input voltages within which the MPPT controller can track the maximum power point. When the voltage exceeds this range, the MPPT either switches off or operates in a restricted mode.

- MPPT Full-Load Operating Voltage Range (MPPT Full-Load Operating Voltage Range) - the voltage range within which the MPPT can accept and convert the entire specified input power without a reduction in current. For correct operation, the operating voltage of the photovoltaic module (V_{mp}) must remain within this range both in summer (at high temperatures - minimum value) and in winter (at low temperatures - maximum value) to avoid power losses.

- Maximum Input Current per MPPT (Maximum Input Current per MPPT) is the highest current value that can safely be supplied to the MPPT controller input without risk of overload. It is essential that the current at maximum power (I_{mp}) from a single photovoltaic module does not exceed this limit. When connecting two parallel PV modules, the total current must not exceed the allowable limit. If the PV module current exceeds the specified maximum, the controller will limit the input current to its permissible threshold, causing power losses and a decrease in overall system efficiency.

- Maximum Short-Circuit Current per MPPT (Maximum Short-Circuit Current per MPPT) is the highest current that an MPPT can endure without damage during an input short circuit. To ensure reliable operation of the controller, it is recommended that its allowable short-circuit current be at least 1.25 times greater than the short-circuit current (I_{sc}) of the connected photovoltaic module.

When two PV modules are connected to a single input, the total I_{sc} of both modules is taken into account.

- Maximum allowable power at MPPT (MPPT Max Input Power) is the maximum input power that the MPPT can effectively process. If this value is exceeded, the controller limits the current received from the PV modules to prevent overload, resulting in reduced actual energy output. This characteristic may not be explicitly stated in the technical documentation, but it can be requested from the equipment manufacturer.

Position №6. DC-DC Converter (DC-DC Converter).

The DC-DC converter is intended to match the output voltage of the photovoltaic module (PV module) with the voltage on the direct current bus (DC-BUS), which is necessary for the subsequent conversion of direct current into alternating current using the inverter section of the device (see PWM modulation).

Although the converter is depicted as a separate unit in the schematic diagram, structurally, it is an integral part of the MPPT controller and performs the function of maximum power point tracking. Here, we have singled it out to emphasize that, in any case, voltage must be increased to the nominal level required for subsequent conversion to alternating current.

Most commonly, a boost converter is employed in grid-tied inverters (Boost mode), which increases the input voltage of the photovoltaic module to the level necessary for proper inverter operation. More versatile solutions use buck-boost mode).

Important! Many inverters feature two or more independent MPPT inputs, enabling photovoltaic modules with varying orientation, tilt, or string length to be connected. Although MPPT inputs operate independently, they are generally connected to a common direct current bus (DC-BUS) via their respective DC-DC converters.

Therefore, to ensure stable and reliable inverter operation, significant voltage imbalance should be avoided. Manufacturers typically permit a voltage difference of no more than 150 V between photovoltaic modules connected to different MPPT inputs.

When designing a system, it is essential to ensure the formation of blocks with operating voltages as close as possible or to limit the difference to one module (approximately 40-50 V). Some inverters, when the voltage difference at the MPPT is excessive, enter a fault mode and display an error message, for example: "DC BUS UNBALANCE".

Position № 7 - direct current bus (DC Bus)

The direct current bus (DC Bus) is a common bus within the inverter architecture, designed to connect all DC sources and loads inside the device. The DC bus supplies

power to the inverter bridge (DC-AC) for delivering energy to the load or to the grid. The voltage on the DC bus must exceed the amplitude of the AC output signal to ensure proper PWM modulation.

Position № 8 Inverter (DC/AC)

The inverter (DC/AC) is a power module that converts the direct voltage from the DC bus into a sinusoidal alternating voltage to supply the load or feed energy into the grid. Conversion is performed using a transistor bridge (typically based on IGBT or MOSFET) and pulse-width modulation (PWM). LC or LCL filters are installed at the inverter's output to smooth the pulsed waveform into a sine wave with minimal harmonics.

Position № 9 Output Isolation Relay

The output isolation relay is intended for hardware disconnection of the inverter from the AC network upon detection of emergency or unstable operating modes, as well as during generation shutdown.

The relay trips under conditions such as absence of voltage in the network, deviations of frequency or voltage beyond permissible limits, synchronization errors, or activation of insulation or frequency protection. Reclosing occurs only after network parameters are restored and the switching delay is observed in accordance with the applicable standards.

Note. *In several countries, requirements for isolating relays mandate a dual relay cascade with a Fail-Safe function, certified for operation in distributed generation systems (see Fig. 3.5).*

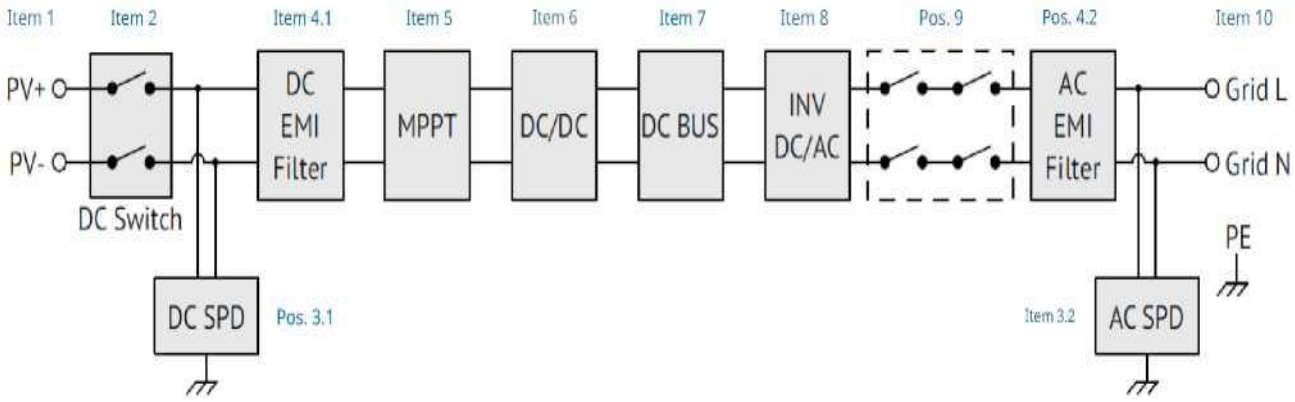

Figure 3.5. Schematic diagram of a single-phase grid-tied inverter with a dual relay stage (Fail-Safe).

Position № 10. Terminals «L», «N», and «PE», designated for connecting the

phase conductor, neutral, and grounding wires on the AC side.

In hybrid inverters, additional terminals are provided for connecting battery packs (position 11), as well as an integrated DC-DC converter (position 12), which ensures voltage matching between the batteries and the DC bus. Terminals (position 13) are also provided for connecting a diesel generator set (Gen), along with separate output terminals (position 14) for connecting a critical load (EPS), which is supplied with guaranteed power supply from batteries and/or photovoltaic modules in the event of a failure centralized power supply system. Furthermore, the inverter block contains a rectifier (AC/DC) that converts grid voltage into direct current, which is subsequently supplied to the DC bus and utilized by the charge controller to charge the batteries when powered from the external grid. The schematic diagram of a single-phase hybrid inverter is presented in Figure 3.6.

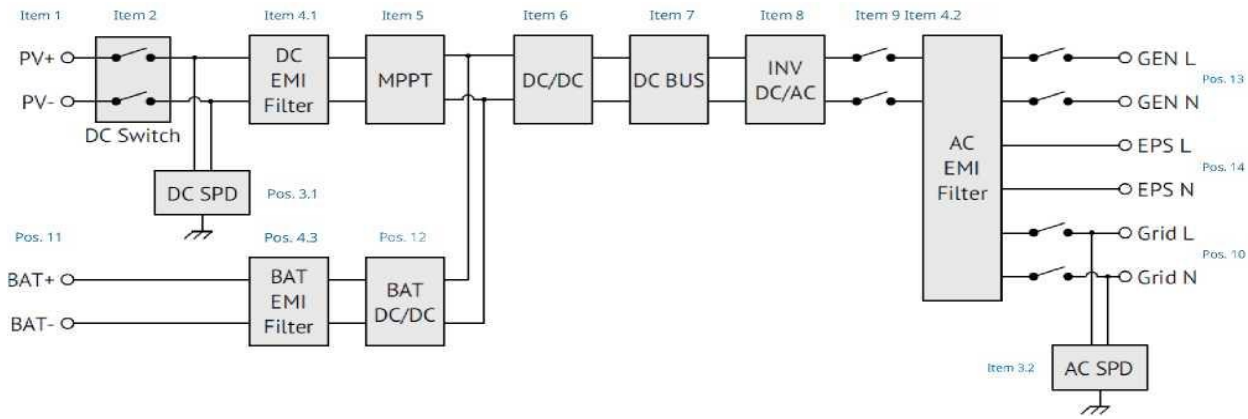

Figure 3.6. Schematic diagram of a single-phase hybrid inverter.

§3.3. Technical compatibility of modules and inverter

Substantial investments in the photovoltaic sector worldwide have facilitated not only increased production volumes but also a significant enhancement in the technical specifications of photovoltaic power plant components. In recent years, the power of photovoltaic modules (PVM) has increased significantly, primarily due to the rise in PVM current. Whereas in 2015-2017, the production standard consisted of M2 format elements (156×156 mm) with I_{SC} approximately 8–9 A, by 2020 the larger M6 (166×166 mm) and M10 (182×18 2 mm) formats had become widespread, allowing I SC to increase to 11-13 A. The implementation of the M12 format (210×210 mm), along with advanced technologies such as TOPCon and HJT, has facilitated current

increases in PVMs to the range of 18-20 A. A characteristic example is the bifacial module JKM730-66HL5-BDV, which has a short-circuit current (I_{SC}) of 18.81 A under STC conditions and reaches 20.79 A under BNPI conditions [28].

Thus, within a relatively short period, this parameter has nearly doubled, reflecting not only advancements in photovoltaic materials and component architecture but also the imperative to reconsider design methodologies. The observed growth trends in PV module parameters present new challenges in the design of photovoltaic power plants and in ensuring their technical conformity with inverter equipment specifications. Despite continuous development and refinement of inverters, the rate of increase in the maximum currents of their MPPT controllers generally lags slightly behind the growth of currents in modern modules.

Let us examine this issue by way of a typical and highly demanded photovoltaic power plant with a capacity of 10 kW, based on the three-phase grid-connected inverter Huawei SUN2000-10KTL-M1HC, which has a nominal power of 10 kW. Table 3.1 presents the primary technical specifications of the inverter related to the photovoltaic module connection side (PV Input) [33].

Note. *In practice, it is not always possible to find technical documentation for the inverter or photovoltaic module with an accurate translation. In such cases, knowledge of English and its continuous improvement prove especially valuable, as original specifications and manuals are typically published in English.*

Table 3.1. Main technical specifications of the HUAWEI SUN2000-10KTL-M1-HC grid-connected inverter

Parameter	Value
Recommended max. PV power	15,000 W
Max. input voltage	1100 V
MPPT voltage range	140 - 980 V
Full-load MPPT voltage range	140 - 850 V
Startup voltage	200 V
Rated input voltage	600 V
Max. input current per MPPT	13.5 A
Max. short-circuit current	19.5 A

Max. power per MPPT	8.8 kW
Number of MPP trackers	2
Max. input number per MPP tracker	1

Assume that only two PV module models are available on the market, identical in nominal power rating but differing in architecture and belonging to different product lines of the same manufacturer:

- JKM630N-78HL4, containing 156 cells (78x2);
- JKM630N-66HL4, containing 132 cells (66x2).

To convey the essence of the matter, design specifics related to single-sided or double-sided configurations (BDV) are disregarded we consider both modules, conditionally, as single-sided.

The main characteristics of photovoltaic modules are presented in Table 3.2.

Table 3.2. Main characteristics of the PV modules JKM630N-78HL4 and JKM630N-66HL4

Parameter	JKM630N-78HL4	JKM630N-66HL4
Maximum power (P_{max}), W	630	630
Voltage at maximum power (V_{mp}), V	47,70	41,02
Current at maximum power (I_{mp}), A	13,21	15,36
Open-circuit voltage (V_{oc}), V	57,08	49,48
Short-circuit current (I_{sc}), A	13,86	16,20
Efficiency, %	22,54	23,32
Temperature coefficient of V_{oc}, %/°C	-0,25	-0,25
Temperature coefficient of I_{sc}, %/°C	0,045	0,045

A distinctive feature of the models under consideration is the difference in electrical parameters: the module JKM630N-78HL4 has higher voltage and lower current (here in after, conventionally referred to as the high-voltage module), whereas the module JKM630N-66HL4 has lower voltage and higher current (hereinafter, conventionally referred to as the low-voltage module).

Determination of the Number of Photovoltaic Modules. According to the technical specifications of the inverter (Table 3.1), the recommended maximum power of connected modules is 15 kW. Simultaneously, the inverter's maximum output power is limited to 11 kW at a power factor of 1. This implies that when connecting excess PV module capacity, the inverter's output power may be limited (the so-called "clipping"), resulting in some of the energy generated by the modules not being utilized.

The practice of moderately oversizing the inverter is widely adopted globally: typically, the total installed capacity of connected PV modules exceeds the inverter's nominal power by approximately 20%. This approach enables to compensate for generation losses under conditions of low insolation, partial load, and gradual module degradation, thereby ensuring a more complete utilization of the inverter's capabilities and approaching its nominal output power for the majority of the day.

It should also be noted that the inverter's operational efficiency significantly decreases if the total power of the connected photovoltaic modules is substantially below its nominal power (less than 20%). This occurs because, at low load levels, the inverter operates outside its optimal range, leading to increased internal losses and a reduction in overall efficiency.

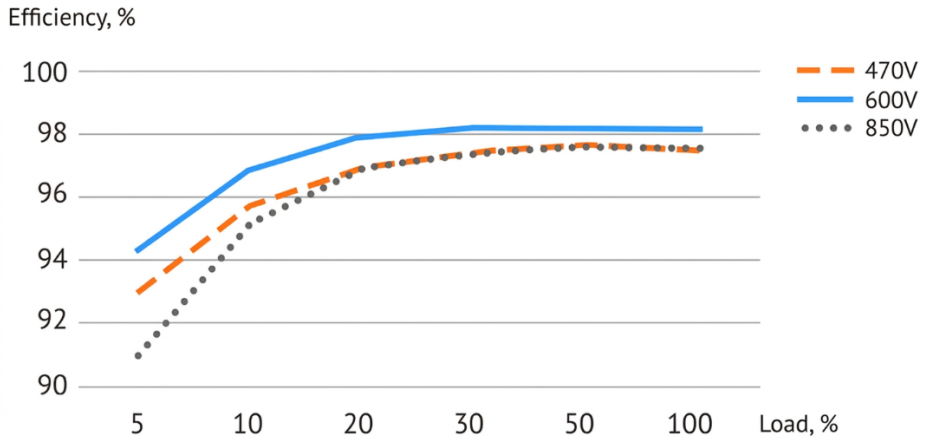

Figure 3.7. Dependence of the efficiency of the Huawei SUN2000-10KTL-M1 HC inverter on load.

Figure 3.7 illustrates the dependence of the efficiency of the Huawei SUN2000-10KTL-M1 HC inverter on load level and PV module voltage (the effect of PV module voltage on the inverter's efficiency will be analyzed separately). As shown in the graph, at load levels below 30%, the inverter's efficiency significantly decreases - a sharp

decline in its performance coefficient is observed.

The decision regarding the number of connected photovoltaic modules and their total installed power capacity is made individually for each project - considering the type of photovoltaic power plant, the orientation of the PV modules (azimuth and tilt angle), and climatic conditions of the geographical region, target generation metrics, as well as economic feasibility, including the cost of the modules themselves.

For example, the solar radiation level in the Fergana Valley is lower than in the Bukhara region; therefore, under the conditions of the Fergana Valley, it is advisable to provide a slightly higher installed power of PV modules compared to projects in the Bukhara region when using the same inverter. Moreover, climatic conditions also influence inverter performance: in cooler regions, at the same output power, the inverter's internal temperature is lower, reducing the risk of overheating and subsequent power limitation (Temperature Derating).

In general, based on operational experience with small and medium-capacity photovoltaic power plants in Uzbekistan, for inverters equipped with ventilation systems, it is recommended to connect photovoltaic modules with a total power rating 5-15% higher than the nominal power rating when using single-sided modules, and no more than 10% higher when employing bifacial modules. This approach enables optimal loading of the inverter, taking into account climatic conditions, and enhances system efficiency without significant losses due to output power limitation.

Note. *Single-phase inverters typically lack built-in fans for forced heat dissipation and are equipped solely with a natural cooling system. Operational experience indicates that on particularly hot summer days, when ambient temperatures exceed +38°C, the inverter temperature reaches 80°C, after which the device enters temperature derating mode. For this reason, it is not always advisable to connect photovoltaic modules with a total power exceeding the nominal power of the inverter in low-power single-phase photovoltaic power plants, or an external ventilation system must be provided.*

Considering the recommendations outlined above, as well as the presence of two independent MPPT inputs in the inverter and the desirability of maintaining the same voltage at each input (which requires an even number of modules for symmetrical

distribution), the design incorporates 18 photovoltaic modules rated at 630 W each, with a total installed capacity of 11.34 kW.

For clarity, let us compare the output power of the inverter when connecting modules JKM630N-78HL4 and JKM630N-66HL4 under conditions corresponding to the standard test conditions (STC).

First, consider a system comprising photovoltaic modules JKM630N-78HL4 and an inverter Huawei SUN2000-10KTL-M1 HC.

Voltage at the maximum power point (V_{mp}) of the PV array, assembled from 9 JKM630N-78HL4 modules connected in series:

$$\mathbf{V_{mp} = 9 \cdot 47,70 = 429,3\ V}$$

Since the modules are connected in series, the current at the maximum power point (I_{mp}) of the entire photovoltaic block will equal the I_{mp} of a single module. For the JKM630N-78HL 4 module, this value is 13.21 A, which is below the MPPT's maximum allowable input current of 13.5 A. Therefore, the inverter's MPPT controller will be capable of operating materials at the maximum power point of the photovoltaic block and delivering input power without current limitation. Thus, the total input power to the inverter, when operating from two photovoltaic blocks and excluding thermal losses in the cable lines, amounts to:

$$\mathbf{P_{вх} = 2 \cdot V_{mp} \cdot I_{mp} \cdot = 2 \cdot 429,3 \cdot 13,21 = 11342,1\ W}$$

Considering thermal losses in the cable lines, as well as losses within the inverter itself, the inverter's output power will be slightly less than 11 kW. As this value does not exceed the inverter's maximum allowable output power, no restrictions arise from the inverter.

Now let us consider a system comprising photovoltaic modules JKM630N-66HL4 and the inverter Huawei SUN2000-10KTL-M1 HC.

Voltage at the maximum power point (V_{mp}) of a PV array assembled from nine series-connected JKM630N-66HL4 modules:

$$\mathbf{V_{mp} = 9 \cdot 41,02 = 369,2\ V}$$

However, the module current I_{mp} is 15.36 A, which exceeds the maximum

allowable input current of the inverter's MPPT controller, set at 13.5 A. Consequently, upon reaching the corresponding level of solar radiation, the current at the MPPT input will attain the limiting value of 13.5 A (point 1 in Fig. 3.8), and any further increase in current will be impossible.

With a further increase in solar radiation intensity, the current-voltage characteristic (I-V curve) of the photovoltaic module will shift upward. If the current limitation were absent, the operating point would move to a new maximum power point (point 2 in Fig. 3.8), corresponding to the prevailing illumination conditions. However, due to the current limitation imposed by the MPPT controller, the operating point will be forced to shift rightward - into the region of higher voltages and lower current, i.e., outside the optimal operating point (point 3 in Fig. 3.8). Consequently, the photovoltaic module will operate away from the maximum power point, resulting in power generation losses.

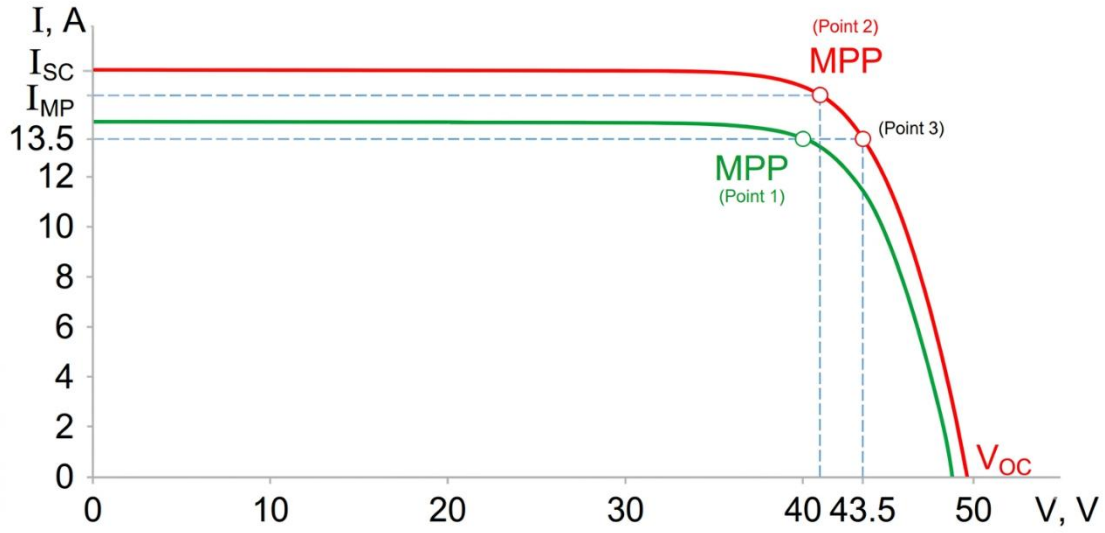

Figure 3.8. Current-voltage characteristic of the JKM630N-66HL4 module.

In the presented current-voltage characteristic (I-V curve) under STC conditions, it is evident that at a current of 13.5 A, corresponding to the maximum allowable value at the MPPT input, the voltage at point 3 is approximately 43.5 V, which exceeds the voltage at the maximum power point of 41.02 V. Therefore, the operating point shifts to a higher voltage region, and the PV module voltage is:

$$\mathbf{V_{(I=13,5A)} = 9 \cdot 43,5 = 391,5\ V}$$

Therefore, the total power at the inverter input during operation from two

photovoltaic units, considering the current limit imposed by the MPPT and excluding thermal losses in the cable lines, amounts to:

$$\mathbf{P_{вх} = 2 \cdot V_{(I=13,5A)} \cdot I_{max.inv} := 2 \cdot 391,5 \cdot 13,5 = 10570,5\ W}$$

The power losses under the considered conditions due to inverter current saturation were: $\mathbf{\Delta P_{losses} = 2 \cdot V_{mp} \cdot I_{mp} - P_{вх} = 2 \cdot 369,2 \cdot 15,36 - 10570,5 = 771\ W}$

Thus, under the considered conditions, the losses arising from reaching the inverter's maximum input current amounted to 771 W. Accordingly, from a technical standpoint, it is preferable to use JKM630N-78HL4 photovoltaic modules in conjunction with the Huawei SUN2000-10KTL-M1 HC inverter.

In reality, the voltage increases from the moment the current limit is reached until solar radiation attains its maximum value is somewhat less than indicated by calculations under STC conditions. This occurs because, after reaching the current limit, the cell temperature continues to rise, causing the I-V characteristic to shift leftward, resulting in a voltage decrease.

Figure 3.9 presents the current and voltage graphs, while Figure 3.10 shows the current and power graphs for a single-phase inverter with a maximum MPPT input current of 12.5 A. As shown in the graphs, at approximately 9 AM the current reaches its peak value of 12.5 A and ceases to increase. At this point, the voltage is approximately 260 V, and the output power is around 3.15 kW. Subsequently, as solar radiation intensifies, the current remains constant; however, the power continues to increase reaching approximately 3.4 kW due to the voltage rising to 280 V.

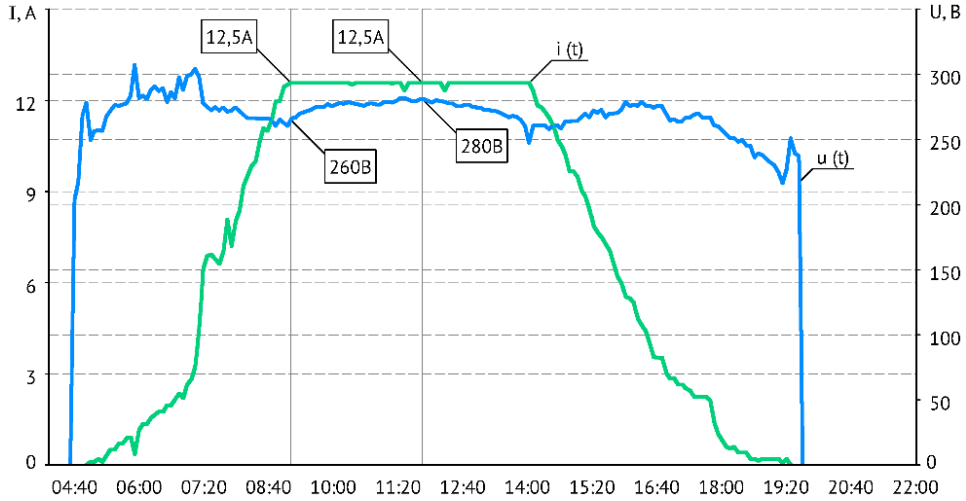

Figure 3.9. Graph of current and voltage on the inverter's DC side.

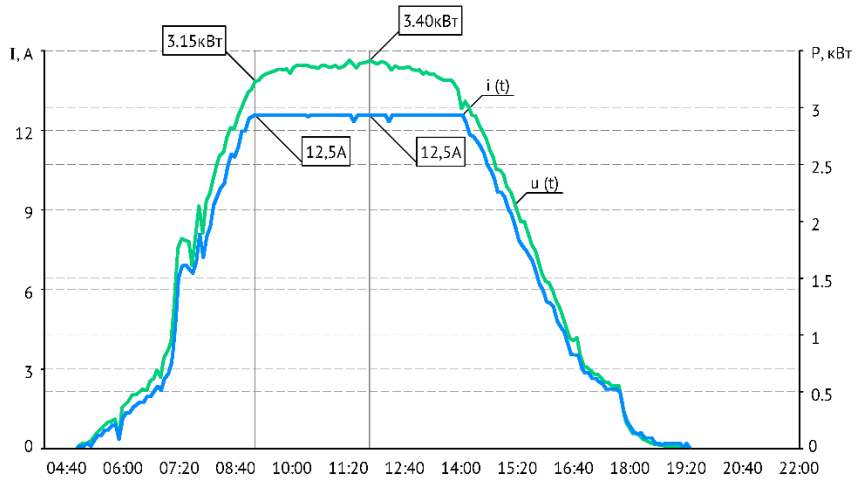

Figure 3.10. Graph of current on the DC side and output power on the AC side of the inverter.

Note. *As shown in the graph, the inverter's output power is slightly less than the product of the current and voltage of the PV module on the DC side. For instance, with a current of 12.5 A and a voltage of 280 V, the input power amounts to 3.5 kW, while the inverter's output power is approximately 3.4 kW. This discrepancy is due to internal losses within the inverter, whose efficiency (η) in this case is:*

$$\boldsymbol{\eta = P_{AC}/P_{DC} = 3,4/3,5 \approx 97,1\%}$$

In addition to reducing thermal losses, a key advantage of employing JKM630N-7

8HL4 modules is the decrease in current load on the MPPT controller. When these PV modules are used, the operating current remains below the maximum permissible value for the MPPT input throughout the entire working day. Conversely, when using JKM630N-66HL4 modules, the current at the maximum power point reaches the permissible limit for the MPPT input for several hours, resulting in power curtailment. Continuous operation at the permissible current limit can negatively impact the reliability and service life of the controller over the long term. Whenever it is possible to deliver the required power at a lower current load, this approach should always be employed.

An additional significant factor supporting the choice of JKM630N-78HL4 modules is their short-circuit current level. Without delving into technical specifics, it is important to note that, according to established guidelines, the short-circuit current permissible for the MPPT must exceed the combined short-circuit current of the

connected modules by at least 25%. For the Huawei SUN2000-10KTL-M1 HC inverter, this parameter is 19.5 A, which is approximately 40% higher than the short-circuit current of theJKM63 0N-78HL4 module, equal to 13.86 A. At the same time, the short-circuit current of the JKM630N-66HL4 module is 16.24 A, providing a margin of only about 20%. This further confirms that, in the case under consideration, using the JKM630N-78HL4 module ensures more reliable and safer inverter operation.

The arguments listed above become even more significant when only bifacial photovoltaic modules are available for installation. As previously noted, the increase in output power under reflected radiation occurs almost entirely due to the rise in current, while the voltage level remains practically unchanged. Under such conditions:

• generation losses associated with current limitation by the MPPT controller increase;

• the duration of MPPT operation in the mode of maximum current load increases, which may adversely affect its reliability in the long term;

• Furthermore, the short-circuit current margin is reduced, thereby compromising compliance with safe operation requirements.

In practice, low-power photovoltaic power plants are sometimes configured with all modules connected in series, forming a single photovoltaic string supplied to one MPPT controller. Let us examine the potential consequences of such a configuration using the example of the Huawei SUN2000-10KTL-M1 HC inverter and the JKM63 0N-78HL4 and JKM630N-66HL4 modules.

Initially, consider the case where 18 JKM630N-78HL4 modules are connected in series, forming a single photovoltaic string (PVS) connected to one input of the Huawei SUN2000-10KTL-M1 HC inverter.

First, we will verify the permissibility of such a connection with respect to a safe voltage level. For this purpose, we determine the open-circuit voltage of the entire PV module at the design minimum cell temperature of -20°C:

$$\mathbf{V_{OC.max} = 18 \cdot V_{OC\,STC} \cdot \left(1 + K_V \cdot \frac{(t - 25)}{100}\right)}$$

$$\mathbf{= 18 \cdot 57,08 \cdot \left(1 - 0,25 \cdot \frac{-20 - 25}{100}\right) = 1143\ V}$$

where: $\mathbf{V_{OC.max}}$– open-circuit voltage at the design minimum cell temperature of -20°C, V; $\mathbf{V_{OC\,STC}}$ – open-circuit voltage under STC conditions, V; $\mathbf{K_V}$ – temperature coefficient of voltage; $\mathbf{t}$ – the calculated cell temperature in degrees Celsius.

As can be observed, the open-circuit voltage of the photovoltaic module at the calculated minimum temperature is 1143 V, which exceeds the maximum permissible input level of the inverter (1100 V) and considerably surpasses the recommended voltage range for MPPT controller operation. Consequently, further analysis is rendered irrelevant, since one of the critically important criteria the allowable voltage level ensuring safe equipment operation is not satisfied.

Note. *When designing three-phase inverters, it is recommended to configure photovoltaic arrays so that the open-circuit voltage does not exceed 850 V — if not at the calculated minimum temperature, then at least at the most probable minimum operating temperature regularly encountered in the given climate.*

Now consider the scenario where 18 JKM630N-66HL4 modules are connected in series to form a single photovoltaic array (PVA), connected to one input of the Huawei SUN2000-10KTL-M1 HC inverter.

Let us verify the permissibility of this connection from the perspective of safe voltage levels. For this purpose, we determine the open-circuit voltage of the entire PV module at the design minimum cell temperature of -20°C:

$$\mathbf{V_{OC.max} = 18 \cdot V_{OC\,STC} \cdot \left(1 + K_V \cdot \frac{(t - 25)}{100}\right)}$$

$$\mathbf{= 18 \cdot 49,48 \cdot \left(1 - 0,25 \cdot \frac{-20 - 25}{100}\right) = 990\ V}$$

Although the calculated maximum voltage does not exceed permissible limits, the voltage level of the photovoltaic unit remains high, and such a configuration is not recommended. Nevertheless, in this example, we consider the potential consequences of such a connection particularly given that, in practice, photovoltaic power plant projects with a capacity of 10 kW, assembled from 16 modules of 630 W each with a total installed capacity of 10.1 kW, are frequently encountered. In the case of a series connection of all 16 modules, the calculated maximum voltage reaches 880 V:

In the case of a series connection of 18JKM630N-66HL4 modules, power losses caused by current limitation on the inverter side remain unchanged. The operating voltage of the photovoltaic array under the considered conditions for this connection is: $$\mathbf{V_{(I=13,5A)} = 18 \cdot V_{point\ 3} = 18 \cdot 43,5 = 783\ V}$$

where $\mathbf{V_{point\ 3}}$-voltage at the operating point under the considered solar radiation level, V.

Thus, the operating voltage remains below 850 V and stays within the MPPT range at full load. Therefore, compared to the configuration using two photovoltaic units of 9 modules each instead of a single 18-module unit, there are no additional current or voltage limitations under the specified conditions. Under such conditions, the total power should remain at approximately 10,5 kW.

Nevertheless, in this configuration, the power is limited by the maximum allowable MPPT power, which for the inverter under consideration is 8,8 kW. In practice, when configuring a photovoltaic power plant, this parameter is often overlooked largely because it is not always specified in publicly available technical documentation and can only be obtained upon special request from the manufacturer. Failure to verify this parameter often leads to significant power limitations, especially in projects where two photovoltaic arrays are connected to a single MPPT. A practical example illustrating this situation will be considered further in the analysis of various photovoltaic power plant configurations.

§3.4. Efficiency coefficient inverter

The inverter's efficiency is defined as the ratio of output alternating current (AC) power to input direct current (DC) power supplied by the photovoltaic modules:

$$\mathbf{\eta_{inverter} = \frac{P_{output}}{P_{input}} \cdot 100\%}$$

The inverter's maximum efficiency is usually indicated in its technical specification. However, under actual operating conditions, the inverter's effective efficiency is lower, as it depends on numerous factors. The characteristic dependency of efficiency on various parameters (load, voltage, temperature, etc.) is unique to each

model and can vary significantly even among inverters from the same manufacturer.

This section will examine typical dependencies that allow for an understanding of the general nature of the main factors' influence without reference to a specific model. Current efficiency charts for a specific inverter should be requested directly from the manufacturer.

Note. *Situations arising from mismatches between photovoltaic module characteristics and the inverter's parameters including constraints on maximum current and allowable MPPT power were examined in the preceding section. These constraints do affect the overall system efficiency; however, they are not directly related to the inverter's own efficiency. This phenomenon is explained by the fact that power reduction in such cases occurs prior to the inverter input, due to the operating point of the photovoltaic modules shifting away from the maximum power point.*

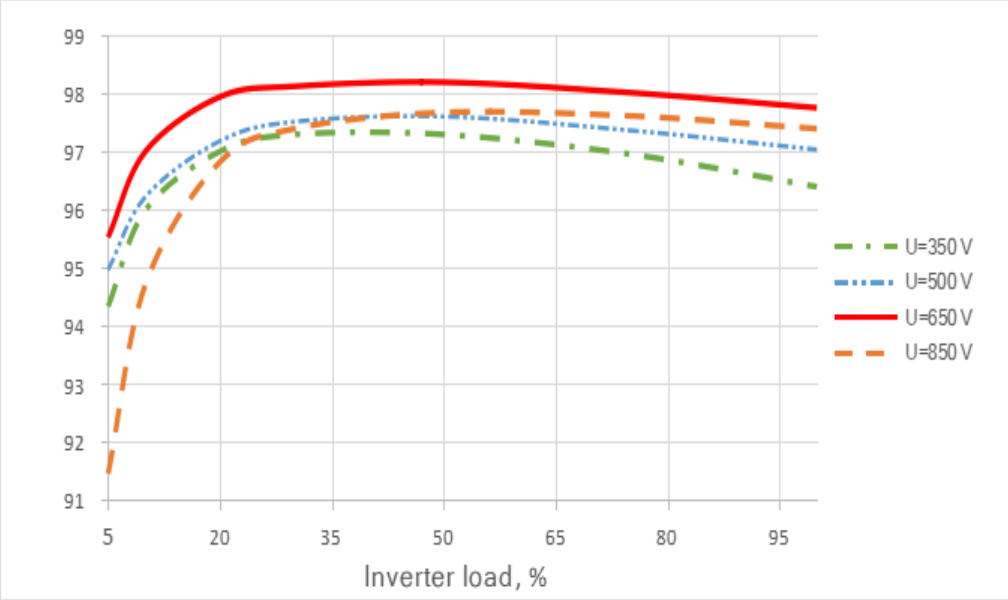

Figure 3.11. Dependence of the efficiency of a three-phase inverter on its load level.

The efficiency of the inverter depends on its load level as well as on the voltage of the photovoltaic array supplied to the inverter's DC input.

Figure 3.11 presents the efficiency curve of a three-phase inverter as a function of its load level at various DC input voltage levels. As evident from the graph, at any load level, maximum efficiency is achieved at an input voltage equal to the nominal value in this case, 650 V. Deviations from this voltage result in a decrease in efficiency by several percent.

Figure 3.12 also illustrates the dependence of the three-phase inverter's efficiency on the input voltage of the photovoltaic module at varying degrees of load. The graph indicates that throughout the entire range of operating voltages, maximum efficiency is attained when the inverter is loaded to approximately 50% of its nominal power rating.

The analysis of the graphs in Figures 3.11 and 3.12 shows that, for the studied three-phase inverter, the maximum efficiency of 98.2% is achieved at a load level of 50 % of the nominal power rating and at a DC input voltage equal to the nominal value- 6 50 V.

At the same input voltage, the inverter's efficiency within the load range of 20% to 100% deviates from its maximum value (at 50% load) by no more than 0.5%. Therefore, operating the inverter at only 50% power for a negligible improvement in efficiency is economically unjustifiable. Furthermore, due to the natural daily fluctuations in solar radiation, the inverter rarely operates at full load, functioning most of the time within a load range of 20% to 100%.

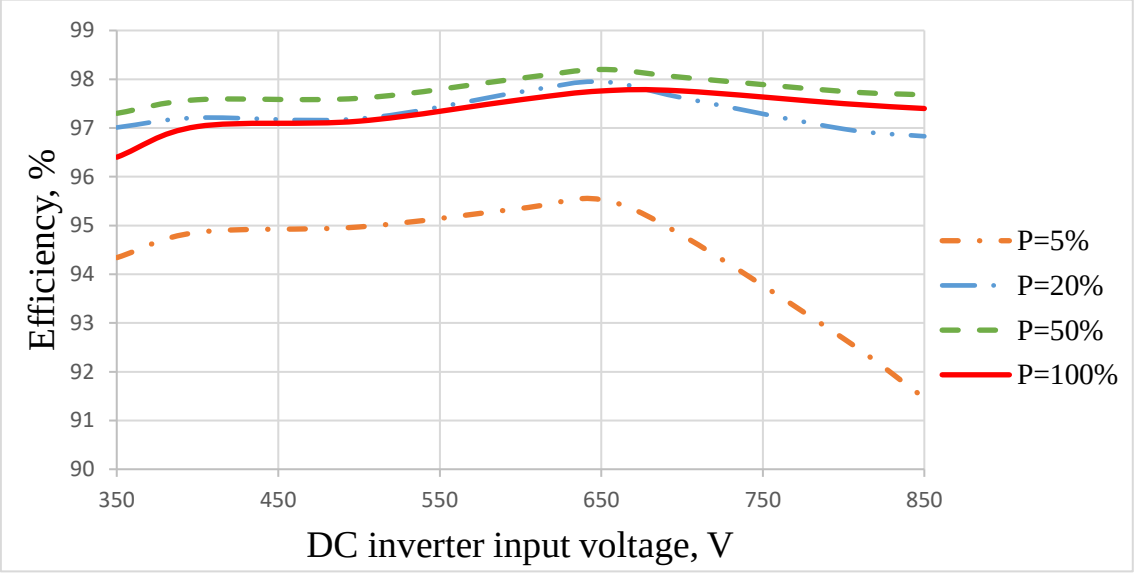

Figure 3.12. Efficiency dependence of a three-phase inverter on the DC input voltage.

Simultaneously, when the load falls below 20%, the inverter's efficiency begins to decrease significantly. Therefore, when designing a photovoltaic power plant, it is inadvisable to select an inverter with a large power margin "for the future" to allow for potential expansion of the installation. A more rational approach in such cases is to install an additional inverter of appropriate power during a subsequent increase in the

number of photovoltaic modules.

The decrease in inverter efficiency when the voltage of the photovoltaic unit deviates from its nominal value is explained by losses related to the need to adjust the input direct current voltage to a level optimal for subsequent conversion into alternating current. With the increase in nominal power ratings of PV modules and the shortage of low-power PV modules on the market, this issue becomes increasingly relevant, particularly for low-power stations.

As shown in the graphs in Figures 3.11 and 3.12, deviation of the photovoltaic block voltage from its nominal value results in a reduction of the inverter's efficiency by 1-2%. However, beyond the direct impact of voltage on conversion efficiency, there is also an additional indirect effect a decrease in the inverter's output power due to overheating. For example, a 2% drop in efficiency in a 50 kW inverter results in additional heat dissipation of approximately 1 kW. This causes the temperature inside the device to rise. When a critical temperature threshold is reached, the inverter activates the power reduction function (Temperature Power Derating) to protect the power electronics. Consequently, the actual losses of the entire photovoltaic power plant under such conditions may be substantially higher than the 1–2% losses attributed solely to efficiency reduction.

Furthermore, at low voltages of the PV module, currents increase, resulting in higher losses in the cable between the PV module and the inverter (according to the Joule-Lenz law). Therefore, the optimal approach is to design the PV module so that the voltage at the maximum power point (V_{mp}) under STC conditions is higher than the inverter's nominal voltage. This ensures that the actual operating voltage during the summer (accounting for the temperature-induced decrease in V_{mp}) corresponds to the inverter's optimal operating range. In this case, thermal losses and the risk of overheating are minimized specifically during the warm season, when the inverter's cooling conditions deteriorate.

Conversely, in winter, V_{mp} exceeds the nominal value, which may cause a slight reduction in the inverter's efficiency. However, owing to the low ambient temperature, overheating is prevented, and, unlike in the summer period, the inverter does not enter power derating mode (Temperature power derating). Consequently, such losses remain

negligible and do not impact the overall system energy production.

Note. *During the morning and evening hours, when the inverter's load is below 20%, its efficiency is significantly lower than optimal. However, this does not result in device overheating, as the absolute value of thermal losses during this period is minimal, and the inverter's cooling system effectively dissipates them.*

Figure 3.13 presents graphs of the single-phase inverter's efficiency as a function of its load at various input voltages on the direct current side. Figure 3.14 shows graphs of this same inverter's efficiency dependence on direct current input voltage at different load levels. The general characteristics of the curves are similar to those of a three-phase inverter, except that the nominal DC input voltage is 370 V for the single-phase inverter, compared to 650 V for the three-phase inverter (for the considered inverter model).

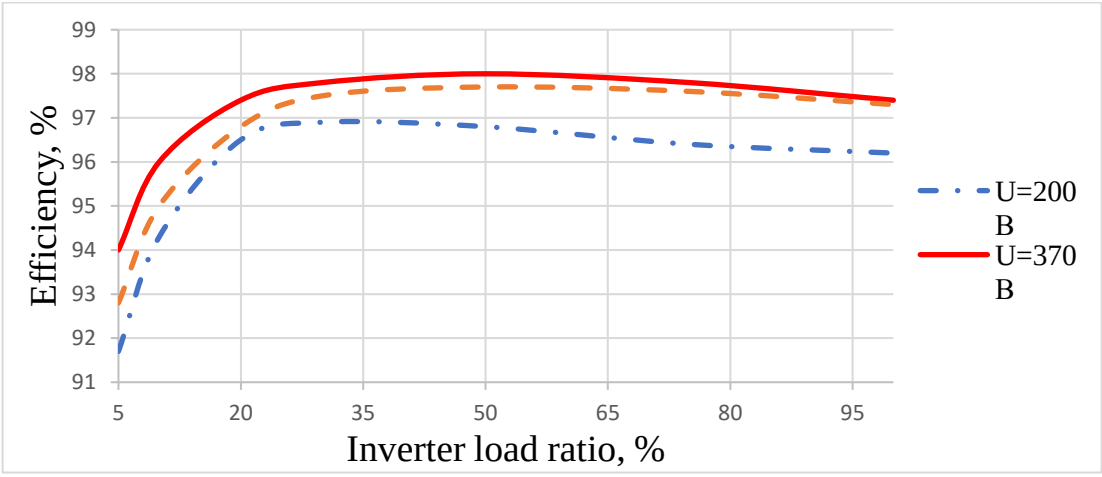

Figure 3.13. Dependence of the single-phase inverter's efficiency on its load level.

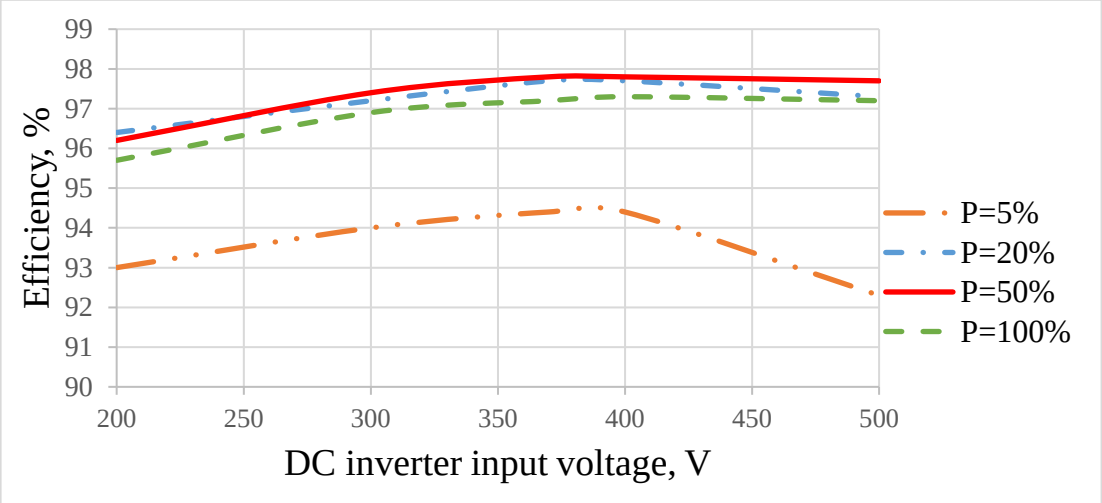

Figure 3.14. Dependence of the efficiency of a single-phase inverter on the DC input voltage.

The most representative example for single-phase systems is a 5 kW photovoltaic power plant based on a 5 kW grid-tied inverter equipped with two MPPT controllers and eight JKM630N-66HL4 photovoltaic modules with parameters V_{mp}=41.02 V. For this configuration, two connection options are possible:

- Option №1 – formation of two photovoltaic strings with a voltage V_{mp} around 200 V (4 photovoltaic modules per string), subsequently connected to two MPPT inputs;
- Option №2 – formation of a single photovoltaic string with a voltage V_{mp} around 400 V (8 photovoltaic modules per string) connected to one MPPT input.

Typically, the maximum allowable power of the MPPT in most single-phase inverters on the market permits connecting all modules to a single MPPT. For instance, the SUN2000-5KTL-L1 inverter has a maximum MPPT input power of 6.6 kW. Considering this, all other conditions being equal, the second connection option is more preferable, since the voltage of the photovoltaic module is closer to the nominal value -especially during the summer period. This allows avoiding additional losses of approximately 1.5% compared to the first option, which not only enhances efficiency but also positively affects the inverter's thermal mode.

§3.5. Hybrid and standalone inverters

As previously noted, hybrid inverters differ from grid-tied inverters by several additional functions. They include a rectifier for charging the battery from the grid, dedicated inputs for connecting the battery (pos. 11), as well as designated terminals (pos. 14) for connecting the emergency power supply output (EPS-Emergency Power Supply), intended to supply critical loads during external grid outages. Furthermore, some models include an additional input (pos. 13) for connection of a diesel generator (DG set).

All previously stated provisions concerning the matching of photovoltaic module parameters with MPPT controllers, as well as issues related to the inverter's efficiency in generation mode and power export to the grid, remain relevant for hybrid inverters. Next, we will consider parameters that are absent in grid-tied inverters and are specific to hybrid devices.

Conditions and limitations for operating batteries:

- Battery type (Battery type) - hybrid inverters support various battery types, including lead-acid (Lead-Acid), gel (GEL), AGM (absorbed glass mat), lithium-ion (Lithium -Ion), and lithium iron phosphate ($LiFePO_4$). The choice of an appropriate type depends on the inverter model and system requirements. It is especially important to ensure the inverter's compatibility with lithium battery, for which support of data exchange protocols with the Battery Management System (BMS) is required.

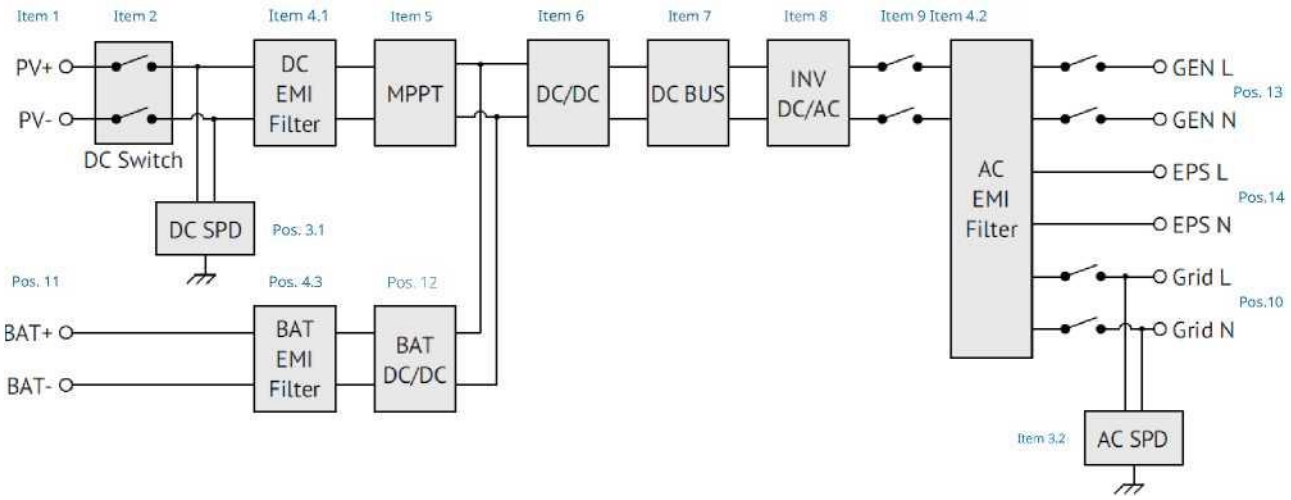

Figure 3.15. Schematic diagram of a single-phase hybrid inverter.

- Number of inputs for battery connection (Number of Connectable Batteries) - low-power hybrid inverters are typically equipped with a single battery input. More powerful solutions may feature two battery inputs, allowing connection of two separate battery blocks.

- Battery operating voltage range (Battery voltage range) - depending on the inverter class, low-voltage (LV) and high-voltage (HV) systems are distinguished. For LV inverters, the typical operating voltage range of batteries is 40-60 V, whereas for HV inverters it ranges from 120 to 800 V. The voltage of the connected battery must strictly conform to the specified range, as any deviation may cause startup errors, unstable operation, or equipment failure.

- Maximum charge and discharge current (Max. charge and discharge current) - each battery input has a limit on the maximum charge and discharge current. These values are critical for selecting the appropriate type of battery, calculating charging time, and determining permissible current loads on the cable line. Most models feature software-based current limitation, allowing the temporary use of batteries with lower

capacity and subsequent capacity expansion without inverter replacement.

- Available charging strategies (Charging strategies) – hybrid inverters support various battery charging algorithms, including prioritization of charging from solar generation or the grid, limitation by time and power, configuration of the permissible state of charge (SOC) range, as well as operation according to schedules or the utility company's tariff structure. Flexible configuration of charging strategies enhances efficiency and enables the system to be tailored to specific requirements.
- Supported communication interfaces (Supported communication interfaces) - for proper operation with modern lithium-ion batteries, the inverter must support digital data exchange interfaces such as RS485, CAN, or, in certain cases, Modbus TCP. The availability of such interfaces allows the inverter to receive information from the BMS of the battery (state of charge, temperature, current restrictions, etc.), thereby ensuring safe and optimized functioning of the energy storage system.
- Battery charge and discharge efficiency (Battery charge and discharge efficiency) - the efficiency of charging and discharging cycles typically ranges from 90% to 96%, depending on the inverter architecture, battery type, and operating conditions. Losses in this process are caused by energy conversion, the battery's internal resistance, and thermal losses in the inverter components.

Currently, standalone inverters, often referred to as On-Off Grid, possess the capability for grid support; however, unlike hybrid inverters, they lack the function of exporting electricity to the grid.

In both hybrid and standalone inverters, the critical load is connected to the EPS output. In the event of a mains voltage failure, the inverter automatically switches to backup power mode, ensuring uninterrupted power supply from the battery and/or photovoltaic modules.

To prevent inverter shutdown due to overload, the total power of all connected devices must comply with the EPS output specifications, including:

- Rated ESP apparent power;
- Peak apparent power.

Important! In the specifications of hybrid and standalone inverters, the apparent power (VA) is always specified, not the active power (W). Considering that the power

factor of household appliances typically ranges from 0.7 to 0.8, the permissible active load will be 20-30% lower than the declared apparent power of the EPS output.

Peak load is generally expressed as a percentage of the rated apparent power and is accompanied by a specification of the duration for which the inverter can operate in this mode. For example, a 100% overload is permissible for a duration of 10 seconds.

Important! In the event of an overload during nighttime, when there is no generation from photovoltaic modules, the entire load is supplied exclusively by the battery storage system. To ensure stable system operation and reduce the load on the batteries, it is recommended to select battery capacity at least twice the nominal power output of the EPS. For instance, with an EPS output power of 5 kW, it is optimal to provide a battery capacity of no less than 10 kWh ideally up to 20 kWh.

Although the inverter's rated power is specified without time limitation, when connecting heavy and prolonged loads such as electric vehicle charging, which takes several hours it is recommended that the power of such loads not exceed 60–7 0% of the inverter's rated power. This ensures reliable and stable operation of the equipment without overheating and degradation of its service life.

During the design and electrical installation of a hybrid or autonomous photovoltaic station, it is critically important to ensure the separate neutral (zero) connection of the critical load from the rest of the load. In practice, it is very common for a single common cable to be installed from the main switchboard to the distribution points, which makes separate connection of the neutral conductors for critical and non-critical loads impossible, necessitating the selection of a hybrid station based on the total load.

This requirement arises because, in autonomous mode, when the centralized power supply is disconnected, the inverter establishes its own isolated system with its own phase and neutral. Connecting the neutral of the EPS output to the neutral of the external (municipal) grid may result in leakage current circulation, improper operation of protective devices, emergency shutdowns, and potentially damage to the inverter. Therefore, the wiring (phase and neutral) for all critical load lines intended for connection to the EPS output must be installed separately and fully isolated from the rest of the electrical wiring associated with the external network (see Fig. 3.16).

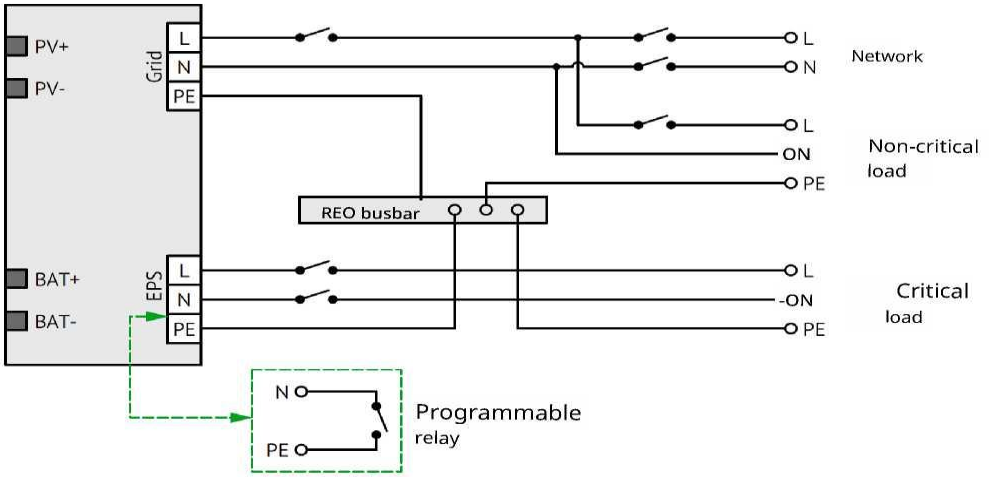

Figure 3.16. Power supply diagram in the presence of a hybrid inverter.

In autonomous mode, the inverter forms its own internal power supply system with a "floating" neutral, i.e., without a fixed connection of the neutral conductor to ground. In such a system, the phase and neutral conductors may have potentials of, for example, +110 V and -110 V relative to ground, depending on the inverter configuration. This causes the zero potential point to “float,” and certain devices, particularly those sensitive to grounding, may malfunction or fail to start altogether.

This issue most notably affects the majority of household gas boilers, which often employ spark ignition or a flame detection system sensitive to the position of the zero potential. In the absence of a solidly grounded neutral, such devices detect grounding faults or “reverse polarity” and refuse to operate.

To address this issue, certain inverter models are equipped with an integrated neutral-to-ground relay - N-G relay (Neutral-to-Ground relay). This relay automatically connects the neutral conductor of the EPS output to ground, establishing a proper neutral and ensuring the correct operation of sensitive equipment in standalone mode.

Important! For proper operation of such a grounding system, it is essential that the inverter's grounding loop (PE) is "clean" meaning it must have no electrical connection with the neutral conductor of the external (municipal) network. Any connection between the inverter’s grounding and the neutral conductor of the centralized power grid may cause parasitic currents, interconnection of different grounding systems, and consequently, unstable inverter operation, false protection activations, and even equipment damage.

§3.6. Requirements and recommendations for installation inverter

One of the key factors in installing a grid-tied or hybrid inverter is ensuring fire safety and effective heat dissipation. Incorrect placement of the inverter can lead to overheating, reduced service life, emergency generation shutdown, and, in some cases, a fire hazard.

The inverter must be installed:

- on a non-combustible and heat-resistant surface (e.g., concrete, metal, fire-resistant brick);
- Away from flammable materials (hay, wood, PVC insulation, fuel, etc.);
- In locations with natural or forced ventilation.

Modern inverters exhibit actual efficiency levels of 96-97%, meaning that 3-4% of the power supplied by photovoltaic modules is converted into heat. For example, a 100 kW inverter dissipates 3 to 4 kW of heat, which must be effectively removed to prevent component overheating and to prolong equipment lifespan.

Key recommendations for installation:

- Install the inverter strictly in a vertical orientation, as specified in the manufacturer's instructions. This ensures correct operation of the cooling system and ventilation channels.
- Maintain minimum clearances from walls, ceilings, and other objects to ensure free air circulation and access for maintenance. Figure 3.17 presents the clearance requirements for the Huawei SUN2000-50KTL-M3 inverter.
- Do not install the inverter in enclosed, poorly ventilated spaces such as attics or small storage rooms, especially those lacking windows and ventilation. In summer, temperatures there can reach 60-70°C, resulting in frequent activation of temperature protection and reduced efficiency.

The optimal solution is to install the inverter on the exterior wall of the building or on a technical structure beneath the PV modules, where it will be shielded from direct solar radiation. This is particularly critical between 10:00 and 15:00, when solar irradiance peaks, the inverter operates at maximum power mode, and heat dissipation reaches its highest levels.

If necessary, technical visors, canopies, or shading grids may be used to prevent

direct sunlight exposure while maintaining adequate ventilation.

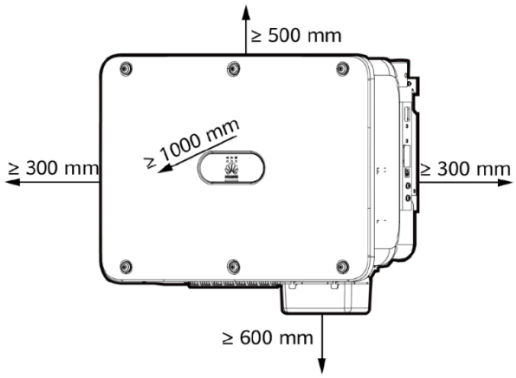

Figure 3.17. Clearance requirements around the Huawei SUN2000-50KTL-M3 inverter.

Hybrid inverters must be installed in close proximity to the battery storage location, as the proper operation of the energy storage system directly depends on the length and cross-section of the connecting cables between the batteries and the inverter. This is particularly critical for inverters operating with low-voltage batteries (e.g., 48 V), since at low voltages the currents in the circuit can be very high (up to 100-200 A or more). At the same time, each additional meter of cable results in significant energy losses and voltage drops, which affect the charging and discharging mode of the battery.

Therefore, hybrid inverters should be installed in the same room where the batteries are located, under the following conditions:

- the room must be ventilated, ensuring sufficient air exchange;
- additional heat dissipation must be provided during the summer;
- the temperature regime must comply with the requirements for both the inverter’s electronics and the batteries (typically from +15°C to +30°C).

It is also essential to consider fire safety requirements and, where necessary, to provide for the installation of smoke detection systems and emergency ventilation.

§3.7. Evolution of inverter architectures and protection systems

Along with the development of photovoltaic modules, inverters are also undergoing active advancement, resulting in the continuous evolution of photovoltaic power plant architecture.

Historically, inverters used a limited number of MPPT controllers, and some models frequently featured only a single MPPT for the entire inverter, irrespective of its power rating. Furthermore, at that time, the power rating of the PV modules was significantly lower. This was primarily due to the low current values at the maximum power point (I_{mp}), typically within the range of 5-7 A, whereas for modern PV modules this parameter can reach 16-20 A or more. Consequently, the power output of a single PV cell was considerably lower, requiring a greater number of PV cells to achieve the same installed capacity of the plant.

In ccollectively, the above factors resulted in a large number of PV cells being connected in parallel to a single MPPT controller. Furthermore, inverters of the previous generation were note quipped with integrated protection systems such as surge protective devices (SPDs), arc fault circuit interrupters (AFCI), smart string level disconnectors (SSLD), along with other features that enable monitoring and isolation of fault sections.

Consequently, to ensure reliable protection, it was always necessary to install a separate panel, known as the Combiner box, which comprised fuses and/or DC circuit breakers, as well as surge protective devices (SPDs). Such a panel served as the primary protective element on the DC circuit side.

To understand how changes in inverter architecture have impacted the overall safety system structure, it is necessary to consider the function of the fuse and/or circuit breaker on the direct current side, as well as analyze situations in which their installation is justified from the perspective of reliable operation and circuit protection.

It should be noted initially that the fuse on the DC side is not installed to protect the photovoltaic modules themselves but to prevent hazardous heating and ignition that may arise from reverse current feed for example, in the event of a short circuit in one of the parallel-connected photovoltaic strings.

If only one PV string is connected to the MPPT bus and a short circuit occurs within its circuit (see Fig. 3.18), the short-circuit current will circulate exclusively within the PV string itself between its modules and the point of the short circuit. In this case, the current does not pass through the fuses installed on the line connected to the inverter and, consequently, they will not operate even under high current within the

damaged circuit.

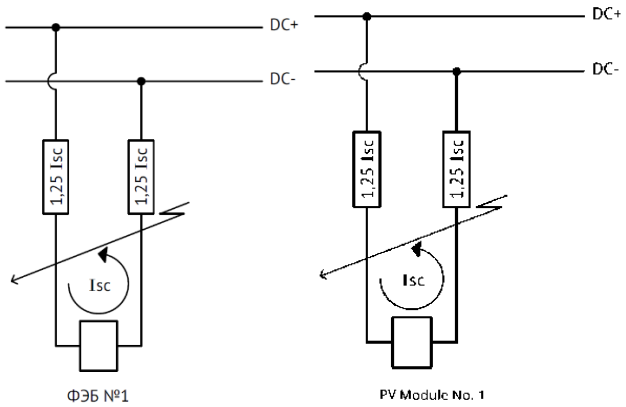

Figure 3.18. Current flow during a short circuit between conductors in a system with a single PV string.

In the event that other PV modules are connected in parallel to the MPPT bus, a reverse current feed arises from the operational units if a short circuit occurs in one of the modules. These PV modules continue to generate current, which will begin to flow toward the point of the short circuit. In this case, currents from the parallel-connected PV modules will pass through the fuses installed in their circuits, as shown in Figure 3.19.

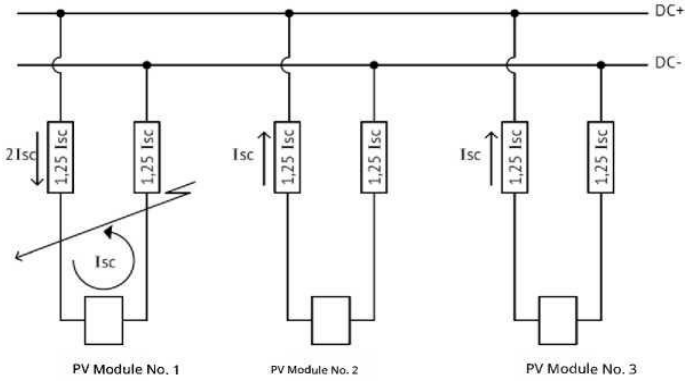

Figure 3.19. Current flow during a conductor short circuit in a system with three PV modules.

Important! The presence of a fuse in the direct current circuits of a photovoltaic system does not guarantee the automatic interruption of power supply at the short-circuit point, as is the case in alternating current circuits. In alternating current networks, a short circuit causes a sharp increase in current flowing from the source to the fault location. This increase in current activates the circuit breaker, which promptly opens the circuit and thereby eliminates the power supply.

In the direct current circuits of photovoltaic stations, the short-circuit current

typically exceeds the current at the maximum power point by only 5–1 0%. Fuses on the DC side are therefore selected with a margin of at least 25 % above the current at the maximum power point to prevent false tripping under conditions of high solar irradiance and elevated temperatures. This implies that even when a fuse is installed directly at the output of the PV module, in the event of a short circuit, the current does not reach the threshold required to activate the fuse and continues to flow within the closed loop, causing localized overheating at the fault site and presenting a subsequent risk of fire.

Thus, through the fuses installed on the inverter's DC side, a back-feed current flows from parallel-connected PV modules in the event of a short circuit in one of them. Now, let us examine the question: at what number of parallel PV modules does fuse operation become guaranteed in accordance with standard requirements and the physics of the process.

For reliable fuse operation, the back-feed current passing through it during a short circuit must exceed its nominal rating by at least 1.25 times:

$$\mathbf{I_{under} \geq 1,25 \cdot I_{fuse}}$$

According to NEC 690.8 and IEC 62548, to prevent false tripping caused by increased solar irradiation or a reduced fuse trip threshold at elevated temperatures, the rated fuse current must be at least 1.25 times greater than the short-circuit current of the PV module [34], [35]:

$$\mathbf{I_{fuse} \geq 1,25 \cdot I_{sc}}$$

Thus, for the reliable operation of the fuse, the back feed current must exceed the short-circuit current of the PV module by at least 1.56 times:

$$\mathbf{I_{under} \geq 1,25 \cdot I_{fuse} = 1,25 \cdot 1,25 \cdot I_{sc} = 1,56 \cdot I_{sc}}$$

Therefore, in accordance with the requirements of NEC 690.8 and IEC 62548, the installation of a fuse is mandatory if the back feed current from parallel PV modules exceeds the short-circuit current by a factor of 1.56. This is because, at such a current level, the fuse is highly likely to operate, thereby ensuring circuit interruption and cessation of feeding the damaged PV module from other PV modules.

Note. *In the considered cases, it is assumed that all parallel-connected photovoltaic modules are identical, which, nonetheless, is standard practice in correctly designed systems.*

In a system where parallel-connected PV modules possess identical characteristics, equal short-circuit currents (I_{sc}), and operate under comparable conditions, the feed current can reliably exceed the I_{sc} of the damaged PV module if three or more PV modules are connected in parallel. In this case, if a short circuit occurs in one of the blocks, the feed current from the two operational strings will be $2 \cdot I_{sc}$, exceeding the threshold of $1{,}56 \cdot I_{sc}$ required for reliable fuse activation.

The fuse will interrupt the circuit where the short circuit occurred and limit further feed from the remaining strings. It is important to understand that the feed from the photovoltaic modules of the damaged PV string remains active.

Therefore, in earlier generations of inverters, when the number of MPPT inputs was limited and each was connected to 3-5 PV strings, the installation of fuses was practically significant, as it reduced the back-feed power at the short circuit point and provided additional protection for the circuits.

Currently, modern inverters are equipped with an adequate number of MPPT controllers. For inverters with power ratings exceeding 20 kW, the architecture typically features one MPPT per 10 kW of power rating, with each MPPT equipped with two inputs (PV Inputs) to connect up to two photovoltaic modules. Conversely, inverters with power ratings below 20 kW are usually equipped with at least two independent MPPT controllers, such that each MPPT corresponds to less than 10 kW of installed power.

Considering the increasing capacity of modern photovoltaic modules, when configuring PV strings with a nominal voltage of approximately 600 V (typical for three-phase inverters), the power of a single PV string can reach 10 kW or more. In the case of single-phase inverters, where the nominal operating voltage is lower (typically 360-450 V), the power of a single PV string is approximately 5-6 kW. Thus, under current conditions, there is no need to connect more than two PV strings to a single MPPT; in certain cases, particularly when using high-power modules (exceeding 630 W), only one PV string is connected to each MPPT.

In accordance with the requirements of IEC 62109-1/2 standards, inverters are equipped with built-in mechanisms for reverse current protection [36], [37]. These measures include hardware solutions such as reverse-blocking diodes, which effectively prevent reverse current flow from the internal DC bus to the PV input terminals. For example, in inverters of the Huawei SUN2000 series, full galvanic isolation between MPPT controllers is implemented. In the event of a short circuit in a PV array connected to one MPPT, no reverse current is supplied from PV arrays connected to other MPPTs.

Each MPPT operates independently and has its own DC–DC converter, with no conductive path capable of providing current coupling between MPPT groups. Such an architecture ensures effective fault localization and enhances electrical safety.

For this reason, in most modern small- and medium-scale photovoltaic systems, fuses no longer perform the key protective function they once provided. In modern configurations, where no more than one or two PV strings are connected to each MPPT input, the risk of reverse current feeding is minimal. As a result, during short circuits in external circuits (outside the inverter), fuses may not operate under normal conditions.

Therefore, in such systems, it is necessary to implement enhanced measures to reduce the likelihood of short circuits between positive and negative conductors, including the separate routing of positive and negative cables.

Nevertheless, the installation of a fuse-disconnector and/or a circuit breaker remains advisable as an additional protective measure, primarily in the event of serious internal inverter faults. In such situations, the presence of a switching device enables rapid manual or automatic disconnection of the circuit, for example, in the case of water ingress into the inverter enclosure, which may occur when the inverter is installed in basements or other potentially flood-prone areas.

In addition, the presence of a fuse-disconnector simplifies the maintenance of a photovoltaic system (PV system), allowing circuit checks or testing on the DC side without the need to disconnect MC4 connectors from the inverter.

In large-scale PV systems, a different architecture is typically used, involving the combination of dozens of PV strings in combiner boxes, after which the energy is

transmitted to a centralized inverter via a single DC cable with an increased cross-section. In such configurations, in the event of a fault, the short-circuit current significantly exceeds the rated current of the fuses, ensuring their reliable and timely operation.

Important! Disconnection of the fuse-disconnector under load is strictly prohibited, as it constitutes a serious hazard to life.

To perform maintenance work during nighttime, it is necessary first to switch off the inverter's DC circuit breaker, and then disconnect the fuse. If work is conducted during daytime, the inverter should be switched to standby mode via software control, then the DC circuit breaker should be turned off, after which the absence of current in the cable should be verified using a tester, and only then should the fuse be disconnected.

Although in modern photovoltaic power plants typically only one photovoltaic module string is connected to a single MPPT thereby eliminating the possibility of reverse current feed from other strings the increase in the power ratings of the photovoltaic module strings leads to a rise in potential energy capable of reaching the fault point.

This means that even in the case of a single short circuit within one PV module, the high-power capacity of the unit can result in serious consequences if timely precautionary measures are not taken. Therefore, it is essential to implement technical solutions focused on preventing short circuits and ensuring their early detection.

In particular, it is recommended to:

- separate positive and negative conductors, especially along cable routes, to prevent their contact in the event of insulation damage;
- securely fasten cable lines, avoiding sags and mechanical damage;
- use inverters equipped with AFCI and SSLD functions;
- promptly respond to inverter warnings regarding potential short circuits or insulation degradation in any of the conductors.

The latter is particularly important, as the initial short circuit point may not cause an immediate fault, but the formation of a second point with opposite potential will create a closed current loop, resulting in localized heating, insulation melting, and potentially fire.

Thus, even when connecting a single PV module to the MPPT, ensuring insulation and operational reliability remains critically important for the overall safety of the system.

Modern inverters are equipped with built-in Type II surge protective devices (SPDs) on both the direct current (DC) and alternating current (AC) sides. These built-in SPDs provide effective protection against induced impulse over voltages, such as those caused by lightning strikes or switching surges.

The installation of additional external SPDs between the photovoltaic modules and the inverter inputs is generally not required under normal operating conditions, particularly for rooftop and ground-mounted installations of small and medium power ratings, provided that proper grounding and equipotential bonding systems are implemented.

Nevertheless, the use of external SPDs on the DC side may be warranted if the facility is situated in an area with high lightning activity, as determined by risk assessments [38], [39], [40].

In such cases, it is recommended to consider installing type I SPDs, which have an enhanced impulse current dissipation capacity and a faster response time, to ensure reliable protection against direct or nearby lightning strikes.

Important! When installing an SPD, a fuse or circuit breaker must be installed between the SPD and the power source. This requirement ensures that, in the event of a varistor failure during SPD operation and the presence of leakage current (ground fault), the damaged SPD is automatically disconnected from the network. This is particularly important in alternating current networks, where the single-phase short-circuit current can be substantial.

In conclusion, it should be emphasized that to ensure effective and reliable protection in photovoltaic systems, it is essential to clearly understand the purpose of each protective element and its operating principle, rather than merely replicating outdated solutions and mechanically applying them to modern photovoltaic power plants.

Such actions may not only prove ineffective but also reduce the overall reliability of the system. An example is when a standard electrical panel with a low IP protection

rating, not intended for outdoor operation, is installed on a roof and densely populated with fuses, circuit breakers, and surge protective devices.

This results in reduced spacing between positive and negative conductors, an increased number of contact points frequently made with inadequate clamping quality which significantly elevates the risk of local overheating, contact loosening, and ultimately, fire within the entire panel.

Thus, in the design and installation of protection systems, it is essential to rely not on standardized solutions but on a technically substantiated approach that considers the specific configuration of the photovoltaic power plant and its components.

It is also necessary to take into account that the technical characteristics of inverters generally lag somewhat behind those of modern photovoltaic modules. For example, the TRINA SOLAR TSM-NEG21C.20 module with a power rating of 725 W, manufactured in 2025, has a current at the maximum power point of 17.47 A under STC conditions, while BNPI calculations indicate up to 19.36 A, which exceeds the permissible current for a single PV input of the inverter. For high-power inverters, this limit typically reaches up to 16A, while for low-power inverters, it is 13.5A or even lower.

Accordingly, some inverter manufacturers have started recommending the connection of a single photovoltaic module to two inputs of one MPPT to reduce the current load on each input (see Fig. 3.20).

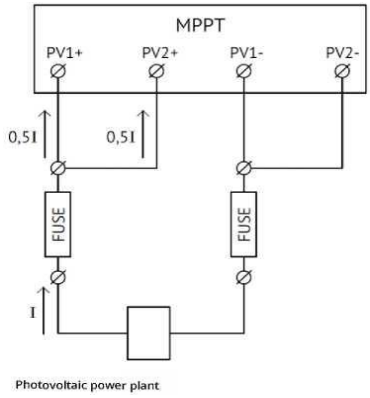

Figure 3.20. Connection of a single photovoltaic module with high current to two inputs of one MPPT.

However, these recommendations have appeared relatively recently and have not yet undergone thorough practical validation; therefore, their application demands a cautious approach and a technical assessment of equipment compatibility.

CHAPTER 4. DESIGN OF PHOTOVOLTAIC POWER PLANTS

This chapter examines the role of fundamental geometry in engineering practice and its impact on the efficiency of photovoltaic power plants. The key principles and guidelines to be followed in the design of photovoltaic power plants are presented, including module placement, tilt angles, and orientation. Technical solutions implemented in operational installations are analyzed based on real-world facilities.

Additionally, issues concerning the selection of solar and power cables, the interaction of the photovoltaic power plant with components of the electrical power system, as well as a brief review of grounding and lightning protection measures necessary to ensure the safe and reliable operation of the plant, are discussed.

§4.1. Basic geometry in engineering practice of photovoltaic power plants

Although modern photovoltaic power plants are modeled using specialized software and hardware complexes, knowledge of basic geometric principles remains an essential tool for verifying the accuracy of calculations and conducting approximate assessments at early design stages. In this section, the geometric relationships used in the design and commissioning of photovoltaic power plants will be presented.

1. Calculation of the area of a rectangle.

The area of a rectangle is determined as the product of its length and width. For example, the width of the photovoltaic module JKM590N-72HL4-BDV is 1134 mm, and its length is 2278 mm. Therefore, the area of the module is:

$$\mathbf{S_{PVM} = 1,134\ m \cdot 2,278\ m = 2,58\ m^2}$$

In practice, counterfeit photovoltaic modules with falsified markings and exaggerated nameplate specifications may be encountered. For instance, the actual power may be 500 W instead of the declared 600 W. Therefore, engineers should always reference the typical efficiency range for the respective class of modules and, if necessary, verify the declared power by considering the module area and efficiency.

Example. The photovoltaic module JKM590N-72HL4-BDV has a declared maximum power of 590 W under standard test conditions (STC) with an efficiency of

22.84%, which aligns with the expected range for modules of this class.

Let us verify whether this value corresponds to the geometric area of the module:

$$\mathbf{P_{mp} = S_{PVM} \cdot 1000 \frac{W}{m^2} \cdot \eta = 1,134\ m \cdot 2,278\ m \cdot 1000 \frac{W}{m^2} \cdot 0,2284 = 590\ W}$$

In the considered example, the module area corresponds to the declared power rating at the expected efficiency, which confirms the accuracy of the datasheet specifications regarding nominal power. Such a calculation does not guarantee that the module actually operates at the stated efficiency in practice; however, it enables the prompt identification of clearly incorrect data and the exclusion of modules with counterfeit markings, which occasionally occur in deliveries.

2. Calculation of the circumference. The classic formula for calculating the circumference includes the radius; however, in practice it is often more convenient to use the diameter. Therefore, the formula is often expressed as follows:

$$\mathbf{L = \pi \cdot D}$$

where: L - circumference length, m; D - diameter of the circle, m; $\boldsymbol{\pi \approx 3,14}$-the number Pi, a mathematical constant.

In practice, this formula is particularly useful for the approximate estimation of the residual cable length in a coil, given the diameter of the loop and the number of remaining turns.

Example. Let us determine the approximate length of the power cable wound on! drum №14 (see Fig. 3.16.1). Initial data:

- Diameter of the core (bushing) of the empty drum D_1 = 750 mm;
- The cable is laid in 3 rows of 20 turns each (a total of 60 turns);
- The outer diameter of the winding D_2 = 940 mm.

The diameter of each layer increases approximately by an amount equal to the diameter of the cable. Since each row contains the same number of turns, the average diameter of all turns can be assumed for a simplified estimation as:

$$\mathbf{D_{avr.} = \frac{750 + 940}{2} = 845\ mm = 0,845\ m}$$

Figure 4.1. Cable drum.

Let us calculate the length of the cable on the drum:

$$\mathbf{L = \pi \cdot D_{avr.} \cdot n \approx 3,14 \cdot 0,845\ m \cdot 60 \approx 159\ m}$$

Therefore, the approximate residual length of the cable on the drum is 159 meters.

3. The Pythagorean Theorem. The Pythagorean theorem is one of the fundamental theorems of geometry, applicable to a right triangle. It states that the square of the hypotenuse (side «c» in Fig. 4.2) is equal to the sum of the squares of the legs (sides «a» and «b» in Fig. 4.2), and is mathematically expressed as follows:

$$\mathbf{c^2 = a^2 + b^2}$$

The Pythagorean theorem is routinely applied in practice, especially during the engineering survey of a site designated for the installation of a photovoltaic power plant. It facilitates the rapid and accurate determination of distances, heights, and diagonal lengths, thereby simplifying site marking, cable laying, and equipment placement.

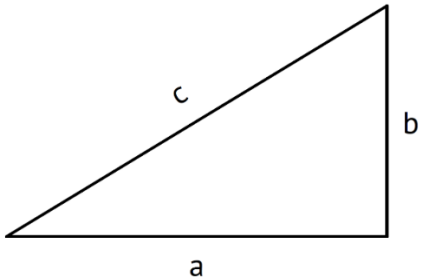

Figure 4.2. Right triangle.

Note. *Photovoltaic modules within a photovoltaic power plant are installed with*

a tilt relative to the horizontal surface. In this context, the leg 'a' corresponds to the horizontal component, while the leg 'b' corresponds to the vertical component of the inclined installation. Therefore, these legs are also referred to as the horizontal and vertical components, respectively.

Example. Let us consider a real example of the practical application of the Pythagorean theorem. Figure 4.3 presents a cross-section of the single-pitched roof of a production workshop facing south. Along the perimeter of the building are cinder block walls, between which metal trusses are installed that support a profiled sheet metal roof.

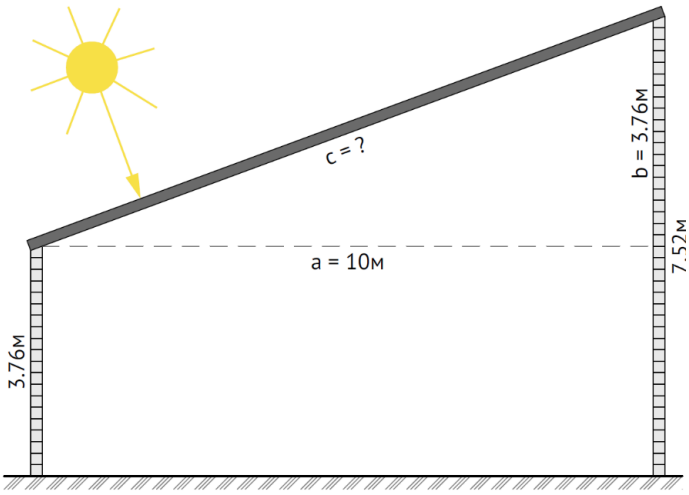

Figure 4.3. Practical application of the Pythagorean theorem to a single-pitch roof.

In practice, during an engineering survey, it is sometimes impossible to access the roof, for example, due to the lack of a ladder or roof access; however, it is necessary to estimate how many photovoltaic modules can be installed if installation is planned parallel to the roof slope. In this case, the key parameter is the actual working length of the slope (the inclined roof surface) between the walls.

A knowledge of basic geometry, specifically the Pythagorean theorem, enables a rapid and safe calculation of the roof slope length without the necessity of ascending onto the roof.

To do this, it is necessary to measure the height of one cinder block (or brick) and count the number of cinder blocks (or bricks) on the lower and upper sides of the

roof. Suppose the height of a single cinder block is 188 mm.

On the lower wall, 20 cinder blocks are laid, while on the upper wall, 40 cinder blocks are laid, respectively (see Fig. 4.3). This indicates that the height difference between the walls is 20 cinder blocks, or: $\mathbf{(40-20)\cdot 0,188=3,76\ m}$

Therefore, the vertical leg of the triangle representing the roof cross section measures 3.760 m.

Next, the horizontal distance between the walls is measured; assuming it is 10 meters, this will constitute the second leg (horizontal).

By applying the Pythagorean theorem, we calculate the length of the roof slope (the triangle's hypotenuse) designated for the installation of photovoltaic modules:

$$c=\sqrt{\mathbf{a^2+b^2}}=\sqrt{\mathbf{3,760^2+10^2}}\approx\mathbf{10,68\ m}$$

Therefore, the length of the inclined surface of the slope is approximately 10.68 meters, which enables an estimation of the available area for the placement of photovoltaic modules.

The slope angle relative to the horizontal plane can be calculated using trigonometric relationships combined with the Pythagorean theorem. This method will be discussed in detail in the following section.

Similarly, when access to the attic space is available but it is not possible to reach the roof to directly measure the slope length, it can be determined indirectly. To do this, the height (vertical distance) from the attic floor to the lowest point of the slope is measured, as well as separately, the height to the ridge. The difference between these two values yields the vertical leg. The corresponding horizontal distance between the lower point and the ridge determines the second leg. These two quantities form a right triangle, for which the length of the slope (the hypotenuse «c») can be easily calculated using the Pythagorean theorem (see Fig. 4.4); in the examples considered, it amounts to:

$$c=\sqrt{\mathbf{a^2+b^2}}=\sqrt{\mathbf{5^2+1,5^2}}\approx\mathbf{5,22\ m}$$

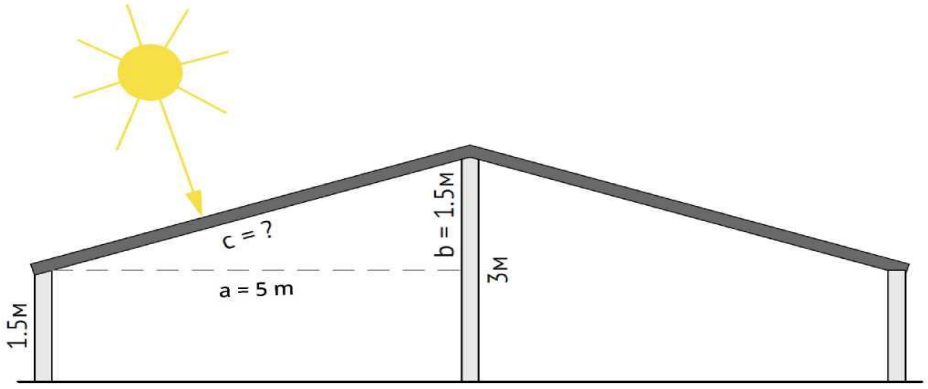

Figure 4.4. Practical application of the Pythagorean theorem for a gable roof.

4. Basic trigonometric formulas. Trigonometry - is a branch of mathematics that examines the relationships between the sides and angles of triangles, as well as trigonometric functions such as sine, cosine, and tangent.

The significance of trigonometry in the design of photovoltaic power plants cannot be overstated. Using it, an engineer can:

- Determine the height of the rear supports based on the specified tilt angle and module length;
- Calculate the shadow length given the solar elevation angle and object height;
- Determine the minimum allowable inter-row spacing between PV module rows to prevent self-shading;
- Calculate the necessary setbacks from shading objects (buildings, fences, trees, etc.);
- Construct a solar tracker or orient the panels at the specified angle.

Thus, fundamental knowledge of trigonometry is an integral part of engineering practice in the design and installation of photovoltaic power plants.

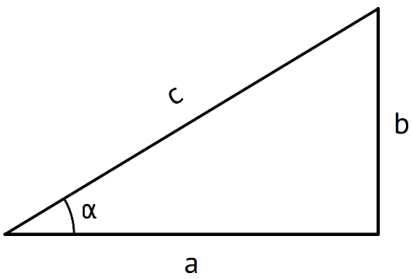

Figure 4.5. Determination of the tilt angle of a photovoltaic module installed on a horizontal surface.

We present the basic trigonometric relationships illustrated by the right triangle shown in Fig. 4.5, used in engineering calculations for the design and analysis of photovoltaic power plants (PV plants):

$$\mathbf{sin\alpha = b/c}; \quad \mathbf{cos\alpha = a/c}; \quad \mathbf{tg\alpha = b/a}; \quad \mathbf{ctg\alpha = b/a}$$

where: $\mathbf{in\alpha}, \mathbf{cos\alpha}, \mathbf{tg\alpha}$ **and** $\mathbf{ctg\alpha}$- the sine, cosine, tangent, and cotangent of the angle α, respectively.

The above trigonometric relationships enable the calculation of one side of a right triangle when the angle of inclination and the length of the other side are known. However, in practice, the inverse problem frequently arises - determining the angle of inclination from the known side lengths. In such cases, inverse trigonometric functions are employed:

$$\mathbf{\alpha = arcsi\,n(b/c)}; \quad \mathbf{\alpha = arccos\,(a/c)}; \quad \mathbf{\alpha = arctg(b/a)}; \quad \mathbf{\alpha = arcctg(b/a}$$

Note. *When using a calculator or computational software for trigonometric functions, it is essential not to confuse the units of angle measurement - degrees and radians. One radian corresponds to the number n, which is equivalent to 180 degrees. To verify the correctness of the unit selection in the program or calculator settings, it is recommended to perform a check using a known value, for example: sin(30°)=0.5. If the result differs, the argument may have been given in radians instead of degrees (or vice versa).*

Example. Let us determine the tilt angle of the single-pitch roof illustrated in Fig. 3.3. It is not necessary to calculate the length of the slope (c - the hypotenuse) to do this.

Roof slope angle relative to the horizontal plane:

$$\mathbf{\alpha = arctg(b/a) = arctg(3,76/10) \approx 20,6}\ \text{degrees}$$

Let us determine the roof slope angle depicted in 3.4:

$$\mathbf{\alpha = arctg(b/a) = arctg(1,5/5) \approx 16,7}\ \text{degrees}$$

Example. Calculate the required inter-row spacing for modules 2278 mm in length, installed at a 30° tilt on a horizontal surface, to prevent shading between rows at a solar elevation angle of 20° (see figure).

First, determine the height of the rear support b of a 2278 mm long module installed at a 30° angle to the horizontal surface.

$$\mathbf{b = L \cdot \sin(30°) = 2278 \cdot 0,5 = 1139\ mm}$$

Next, we determine the inter-row spacing X between the modules:

$$\mathbf{X = b \cdot ctg(20°) = 1139 \cdot 2,747 = 3128\ mm}$$

Thus, to avoid shading of the modules in the case under consideration at a solar altitude above 20°, the inter-row spacing must be at least 3128 mm. However, in practice, it is not always possible to maintain such a distance due to the limited available space. Therefore, the tilt angle of photovoltaic modules is often reduced to avoid winter shading, which generally has a greater impact on the photovoltaic power plant 's generation than deviation from the optimal tilt angle.

5. Calculation of the triangle's tilt angle based on the known lengths of its three sides. Sometimes, in practice, it is necessary to determine the tilt angle of a triangular structure when no angle-measuring tool is available. This situation is typical, for example, when installing support structures on sloped roofs, where a non-rectangular, arbitrary triangle is formed. We present the formula for determining the tilt angle a of the triangle shown in Fig. 4.6:

$$\mathbf{\cos\alpha = \frac{a^2 + c^2 - b^2}{2 \cdot a \cdot c}}$$

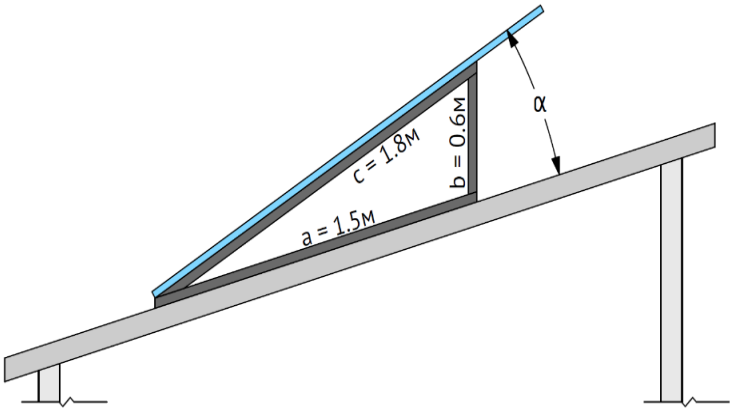

Figure 4.6. Determination of the support structure tilt angle relative to the roof.

Example. Determine the tilt angle of the triangular structure shown in Fig. 6.6 relative to the roof surface.

$$\boldsymbol{\alpha = \arccos\left(\frac{a^2 + c^2 - b^2}{2 \cdot a \cdot c}\right) = \arccos\left(\frac{1,5^2 + 1,8^2 - 0,6^2}{2 \cdot 1,5 \cdot 1,8}\right) \approx 18,2^\circ}$$

§4.2. Classification of photovoltaic power plants

Prior to addressing issues related to the design of photovoltaic power plants, it is appropriate to present their classification. Although this division is somewhat conventional, it enables the identification of typical configurations and a more precise definition of the target group for which the system is being developed.

Classification of photovoltaic power plants based on connection architecture and inverter type:

• A Grid on photovoltaic power plant (Grid on or Grid Tied) is a photovoltaic power plant integrated with a centralized electric power system (EPS). Such a plant operates only in the presence of a reference voltage from the grid, i.e., when voltage is available at the centralized power station. The primary objectives of a grid-connected photovoltaic power plant are to reduce electricity consumption from the external grid and/or to supply surplus electricity to the grid under contractual agreements or within incentive programs (for example, the 'green tariff').

A grid inverter, designed exclusively to operate in the presence of a reference

voltage, is used in a grid-connected photovoltaic power plant. In the event of voltage loss in the network or when its parameters exceed permissible limits, the inverter automatically ceases generation.

Note: *As a reference voltage source for a grid-tied inverter, not only the voltage of a centralized power system can be used, but also alternative sources, such as a diesel generator set. In this case, the grid-tied inverter can continue operating; however, additional measures are required to ensure power balance, as well as to maintain stable frequency and voltage parameters under isolated power system conditions (see Chapter 4.6 for details).*

A hybrid photovoltaic power plant (Hybrid) - is a photovoltaic power plant integrated with a centralized power station, but, unlike a grid-tied photovoltaic power plant, it can operate in the absence of a reference voltage in the network. In the event of a centralized power station shutdown, the hybrid system ensures uninterrupted power supply to the critical load connected to the output of the EPS (Emergency Power Supply), by means of generation from the photovoltaic modules and batteries, which serve the functions of energy storage, power balancing, and system parameter stabilization. A hybrid inverter is employed as part of such a plant.

Most modern hybrid inverters are equipped with dedicated terminals for connecting a diesel generator set (DGS), as well as a relay output designed for the automatic start of the DGS if the battery charge level falls below a specified threshold in the absence of power from the centralized power plant.

An autonomous photovoltaic power plant (Off-Grid) - in the classical sense is a photovoltaic power plant not connected to a centralized power plant and fully independent of external power sources. The power supply to consumers is provided exclusively by the generation of photovoltaic modules and batteries, which store energy and supply it during periods without solar radiation. Simultaneously, modern standalone inverters often allow connection to an external grid or diesel generator unit (DGU) for battery charging, without enabling reverse energy flow to the grid. Such devices are commonly referred to as on/off-grid inverters, as they can operate both in fully autonomous mode and with the grid solely as a backup power source. The

availability of a charging function from an external source allows for reduced battery capacity requirements, as it enables recharging during extended periods of cloudy weather or increased consumption.

Classification by the number of phases:

- Single-phase - used in residential houses and small facilities equipped with single-phase input and a single-phase electricity meter. Typically installed at power ratings up to 5-10 kW. The voltage on the alternating current side is 220 V. A single phase inverter is applied in such systems.
- A three-phase system - is employed in commercial, administrative, and industrial facilities, typically with an installed capacity of 10 kW or higher.

The voltage on the alternating current side is 380 V. It ensures even load distribution across phases and is used in facilities with three-phase power supply. It is also utilized in private residences equipped with a three-phase input and a three-phase electricity meter. A three-phase inverter is employed in such systems.

Classification of photovoltaic power plants by scale of application:

- Private sector (Residential level) - typically includes photovoltaic systems with power ratings up to 6 kW for single-phase and up to 20 kW for three-phase configurations. In certain cases, power ratings may be increased up to 10 kW for single phase and up to 50 kW for three-phase systems; however, such installations can impose increased load on the local distribution network, particularly under conditions of limited capacity of the existing line. In such cases, separate technical coordination with the grid operator is required, and, if necessary, the installation of a dedicated supply cable to the transformer substation.
- The commercial and industrial sector (C&I-Commercial & Industrial) includes -three-phase photovoltaic power plants installed on commercial buildings, warehouses, manufacturing facilities, and other infrastructure sites.

The installed power capacity generally ranges from 20 to 1000 kW. Such systems are typically connected to the facility's input-distribution device (IDD) or directly to the low-voltage (0.4 kV) busbars of the transformer substation.

The industrial sector (Utility-Scale) - comprises large grid-connected

photovoltaic power plants with capacities of 1 MW and above, primarily intended for electricity supply to the grid under power purchase agreements or within the wholesale electricity market. Such facilities are regarded as fully operational generating units. Inverter equipment utilized in Utility-Scale systems typically falls into the category of Medium Voltage Inverters, with an output voltage of 0.8 kV on the AC side. Step-up power transformers are used to integrate into the power system, converting the inverter output voltage to 10 kV, 35 kV, or 110 kV-depending on the facility category and the external electrical supply scheme. The connection point of such photovoltaic power plants is typically located on the medium or high voltage side and necessitates the development of a bespoke technological connection project that considers the parameters of the power system.

Classification of hybrid photovoltaic power plants by battery type:

- Hybrid systems with low voltage battery (LV — Low Voltage)- are typically characterized by a battery operating voltage ranging from 40 to 60 V. These solutions are primarily employed within single-phase hybrid photovoltaic power plants intended for the private sector. The typical installed power rating is up to 12 kW, although inverter models with higher power ratings up to 16 kW are also available on the market.
- Three-phase hybrid inverters supporting low-voltage battery banks are also available, used in systems with power ratings up to 20 kW, enabling the use of low-voltage architectures not only in residential but also in small commercial or private three-phase installations. However, as power increases, the current on the battery side rises significantly, resulting in increased losses, the requirement for cables with large cross-sections, and a decrease in overall efficiency. In this regard, systems with an installed capacity above 10–15 kW more frequently employ high-voltage (HV) battery architectures, which ensure more stable and efficient inverter operation at lower currents.
- Hybrid systems with high-voltage batteries (HV — High Voltage) utilize batteries with nominal voltages generally ranging from 120 V up to 600 V and higher. These systems are primarily implemented within three-phase hybrid photovoltaic plants designed for medium to high capacities — starting from 10 kW and above. The

high-voltage architecture on the battery side enables the reduction of currents, decreases power losses, allows the use of wires with smaller cross-sections, and simplifies thermal and switching solutions, which is particularly important for the stable operation of powerful inverters. Hybrid HV systems are extensively employed in private three-phase facilities as well as in small commercial installations.

Important! Battery banks intended for low-voltage (LV) systems must never be used in high-voltage (HV) configurations. Such batteries have design limitations concerning the operating voltage level, insulation class, and internal commutation.

Attempting to connect a low-voltage battery to a high-voltage inverter or to use it within a high-voltage architecture may lead to insulation break down, overheating, component failure, and consequently, ignition or fire. Therefore, when designing hybrid systems, it is essential to ensure voltage compatibility between the inverter and the battery system, following the manufacturers' technical documentation and applicable safety regulations.

§4.3. Basic principles and guidelines for designing photovoltaic power plants

The previous section presented a classification of photovoltaic power plants. In general, for all the above-mentioned system types, the principles of photovoltaic array formation and their connection to the inverter are similar, as they adhere to unified electrical engineering requirements and standards.

There is one fundamental distinction between hybrid and autonomous photovoltaic power plants and grid-connected photovoltaic power plants, which pertains to their purpose and design methodology. For grid-connected power plants, the primary objective is to maximize annual electricity generation, as these installations are generally aimed at commercial efficiency either reducing costs or selling energy to the grid. Under fixed tariff conditions, installation parameters such as the tilt angle and azimuth of the PV modules are chosen to maximize annual electricity production, typically with a south-facing orientation and an optimal angle relative to the horizon.

In hybrid systems, in addition to maximizing generation, a key function is to provide backup power supply to critical loads during an emergency shutdown of the

centralized power system. Since power outages are particularly critical for consumers during abnormally cold winter periods, the design of a hybrid photovoltaic power plant often necessitates increasing the tilt angle of the photovoltaic modules to enhance winter generation even if this entails some reduction in output during the summer months.

For autonomous systems, design is carried out solely on the basis of consumption profile analysis, as there is no support from the external power grid. In this case, the focus is not so much on maximum production as on the even distribution of generation throughout the day and ensuring reliable power supply.

Therefore, whenever possible, some photovoltaic arrays are oriented southeast and others southwest, which allows for increased generation during the morning and evening hours. Furthermore, it is recommended to employ an increased tilt angle, which enhances energy production during the winter, when days are short and it is essential to maximize the utilization of the available solar window, even if this results in reduced generation in the summer period.

However, all the aforementioned characteristics primarily pertain to the orientation of PV modules - their tilt angle, azimuth, and consequently, the inter-row spacing; in other words, parameters that influence the generation profile throughout the day and year. Meanwhile, the selection of the optimal number of PV arrays, the number of PV modules within each array, and the alignment of their electrical characteristics with the inverter's parameters remain consistent regardless of the plant type - whether grid-connected, hybrid, or standalone. For this reason, further discussion of these issues will be conducted using the example of a grid-connected photovoltaic power plant as the most universal and typical solution.

Fundamental differences in system architecture arise when transitioning from single-phase to three-phase implementation, primarily concerning voltage matching on the direct current side. For three-phase inverters, the nominal operating voltage at the direct current input is typically approximately 1.7 times higher than that of single - phase models. This dictates the formation of a PV array with a greater number of PV modules in series to attain an optimal voltage level.

Furthermore, in hybrid systems, the battery architecture depends on the number of phases. Typically, single-phase solutions utilize low-voltage (LV) battery systems, whereas three-phase systems employ high-voltage (HV) battery configurations. Nevertheless, low-power three-phase hybrid systems based on low-voltage batteries are also present on the market.

The development of photovoltaic modules in recent years has been rapid, especially regarding the increase in their power ratings, primarily achieved by raising the current. Whereas a few years ago, the market was dominated by photovoltaic modules with maximum power currents of approximately 10-11 A, today this figure exceeds 16 A and, accounting for the bifacial effect, can reach up to 20 A.

Inverter technology is also advancing, adapting to new requirements mainly by increasing the number of MPPT trackers and broadening their operating current ranges. However, the development pace of inverters somewhat lags behind the growth rate of the electrical characteristics of modules, particularly concerning permissible input currents to the MPPT.

In this context, ceteris paribus, preference should be given to photovoltaic modules with lower current, as this provides a wider selection of compatible inverters and reduces the risk of exceeding permissible input currents at the MPPT inputs.

Under these circumstances, rather than seeking to develop typical solutions for photovoltaic power plants, a more rational educational approach is to establish a system of basic requirements and technical recommendations upon which real practical situations can be analyzed. This approach enables not only a deeper understanding of the design principles but also the adaptation of the acquired knowledge to a broad spectrum of real-world conditions and challenges encountered in the implementation of modern photovoltaic systems.

Fundamental principles and guidelines for the design of photovoltaic power plants.

1. Based on the type of installed meter, determine the required number of phases for the photovoltaic power plant being designed. This issue is particularly pertinent in the design of photovoltaic power plants for the private sector, although similar

situations may also arise in small commercial facilities. Before commencing the design, it is necessary to independently verify the type of the installed electricity meter. This is important because, in practice, confusion often occurs between the number of input phases supplied to the building and the number of metering phases registered by the meter.

Quite often, three phases and a neutral conductor are supplied to the main distribution board of the house; however, they may then be routed through a phase selector switch, after which only one phase is connected to a single-phase meter. In such cases, despite the existence of a three-phase supply, it is necessary to design a single-phase photovoltaic power plant, unless the customer consents to the installation of a separate three- phase meter specifically designated for connecting the photovoltaic power station.

2. Assessment of the Distribution Network's Readiness for Photovoltaic Power Plant Connection. Before designing a photovoltaic power plant, it is necessary to assess the feasibility of integrating it into the existing distribution network. Primarily, the parameters of the supply cable from the inverter to the connection point at minimum, up to the 0.4 kV busbars of the transformer substation (TS)- must be verified. It is imperative to confirm that the cable's cross-section and length ensure permissible levels (continuous allowable current and allowable voltage drop) under conditions of zero self-consumption and full export of the photovoltaic power plant's generated power:

Unfortunately, in practice these issues often arise only at the final stage, after the equipment installation, when it becomes clear that the distribution network is unprepared to accept the photovoltaic power plant's power output. This causes a local voltage increase and possible deviations beyond permissible limits [41].

For example, Figure 3.7 presents the daily output power profiles of the same grid-connected photovoltaic power plant with a nominal capacity of 100 kW on a clear day, connected to two different parallel 0.4 kV distribution networks fed from different distribution points (DPs).

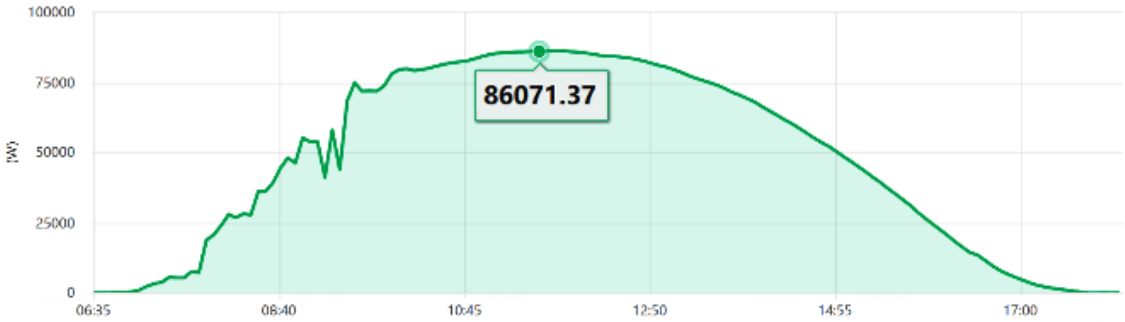

A. Integration to network №1.

B. Integration to Network № 2.

Figure 4.7. Output power curve of the photovoltaic power plant when connected to different distribution networks.

As illustrated in Figure 4.7, Network Configuration №1 provides favorable conditions for photovoltaic power plant integration, whereas Network №2 does not, since the line's throughput capacity is limited and does not permit transmission of the plant's full power to the power system.

As the inverter’s output power increases, a sharp rise in voltage is observed on the 0.4 kV side, and when the line voltage exceeds the overvoltage protection trip threshold (in this case, 439 V), the inverter automatically ceases generation and subsequently restarts after the network voltage stabilizes.

Note. *It should be noted that, in this example, the dynamic voltage control function (P-U function) in the inverter is not activated; this function enables the inverter to automatically reduce the photovoltaic power plant’s output power as the output voltage increases according to a predefined characteristic. Thus, voltage stabilization at a specified level is ensured without triggering emergency protection or inverter shutdown.*

In the given example, several serious problems arise immediately upon

connecting the photovoltaic power plant to network №2. Firstly, the power plant practically does not generate electricity because the inverter regularly shuts down due to exceeding the permissible voltage level, rendering the system inoperative. Secondly, multiple shutdowns and repeated synchronization attempts may cause damage to the inverter or significantly shorten its operational lifespan. Moreover, the photovoltaic power plant itself becomes a source of local voltage increases in the network: with insufficient line capacity and inadequate local consumption, the inverter begins to elevate the voltage in nearby sections of the network. More detailed information on this topic can be found in [42].

If overvoltage protection is disabled, the voltage may theoretically reach 500 V or higher, creating a risk of serious damage to household and industrial electrical equipment connected to this network.

Therefore, the assessment of the network condition and connection parameters must be performed prior to the initiation of the design process. If necessary, the installation of a dedicated line (cable) from the inverter to the distribution point or another appropriate network node should be provided. With the increasing density of photovoltaic power plant (PV plant) connections, where multiple PV plants may be connected to a single distribution line, a comprehensive assessment of their cumulative impact on the distribution network and the power system as a whole is required.

This issue becomes especially pertinent when integrating PV plants into rural distribution networks, which often feature extended power line configurations and limited conductor capacity. In many cases, the length of the distribution line from the distribution point to the consumer may reach 600 meters or more, and when connecting a photovoltaic power plant to the house farthest from the distribution point, there is a risk of significant voltage increase along the line segment during full power export from the station.

3. Evaluation of the throughput capacity of the electricity metering system. Although this issue could be included in the previous section, it is advisable to consider it separately. Since a photovoltaic power plant is always connected downstream of the electricity meter, in the case of power export, all generated power will pass through the

meter either directly (in the event of direct connection) or via current transformers.

The permissible load characteristics of the meter are specified in its technical passport; however, for approximate calculations, the following values may be used:

- For a single-phase meter, the maximum permissible current is typically 60 A;
- For a three-phase direct connection meter, the maximum current is up to 100 A per phase; however, the recommended current for an evenly distributed load across all three phases is no more than 30 A per phase.

It should be noted that the values of 60 A and 100 A are specified by manufacturers under ambient temperatures not exceeding +25°C, with adequate ventilation and the use of high-quality terminal blocks and connectors that ensure reliable contact and minimize heat generation.

It is also necessary to consider that under conditions of undervoltage in the network, the inverter will compensate for the voltage drop by increasing the output current (up to its maximum), unless undervoltage protection is activated.

Recommendations for the maximum permissible inverter power ratings for direct connection:

- For single-phase meters, it is recommended to connect an inverter with a power rating not exceeding 10 kW, with a maximum output current of up to 45 A;
- For three-phase meters with direct connection, it is advisable to use inverters up to 20 kW, with a maximum phase output current of 33-35 A;
- For photovoltaic power plants with power ratings exceeding 40 kW, corresponding to a phase current above 64 A, the use of intermediate current transformers is recommended.

4. Determine the optimal connection point to the distribution network. The selection of the optimal connection point for the photovoltaic power plant directly influences the overall efficiency of the power supply system and significantly reduces power losses. The optimal connection point should be determined individually for each project, taking into account the installed capacity of the photovoltaic power plant, the calculated load of the facility, and the configuration of the existing network.

The majority of small and medium photovoltaic power plants are primarily

designed to meet internal demand; in such cases, connecting the plant to the nearest point of consumption is a logical solution. This approach reduces thermal losses in the cable line and, consequently, enhances the overall energy efficiency of the power supply system.

Nevertheless, in certain cases, technical specifications may impose a strict requirement to connect directly to the 0.4 kV busbars of the transformer substation, even if this is not the optimal solution from an engineering and economic feasibility standpoint. In such situations, it is possible to renegotiate the connection point with the relevant grid organizations, after preliminarily substantiating the proposed changes for example, by indicating the reduction of losses, increased energy efficiency, cost savings, and the absence of technical necessity for laying a new line.

Example. A grid-connected photovoltaic power plant with a capacity of 50 kW is installed on the roof of an industrial building. The grid inverter is located in the electrical engineering room on the first floor, in direct proximity to the main distribution board (MDB) the distance is 5 meters (see Fig. 4.8 A). According to the design documentation, the calculated load on the main switchboard (MS or MDB) is 140 kW, while the calculated power of the photovoltaic power plant (PV plant) is 42.5 kW, indicating that the entire station generation is consumed internally without exporting to the grid. Therefore, the optimal point for connecting the inverter is the switchboard (MS), which provides the shortest path and minimal losses.

Simultaneously, the cross-section and length of the existing cable from the switchboard (MS) to the distribution point (DP) ensure the safe transmission of the full power of the PV plant to the centralized power system (EPS) - including instances when internal consumption is absent, such as on weekends and holidays.

However, according to the issued technical specifications, a mandatory condition for connection is the installation of a dedicated cable to the 0.4 kV busbars of the transformer substation located 150 meters from the inverter (see Fig. 4.8 B). This requirement results in unjustified power losses up to 4% of the total photovoltaic power plant output due to additional losses in the cable section from the inverter to the distribution point and subsequently from the distribution point to the switchgear.

Furthermore, laying a new cable involves technical risks, including potential damage to underground utilities, particularly in the absence of current as-built documentation.

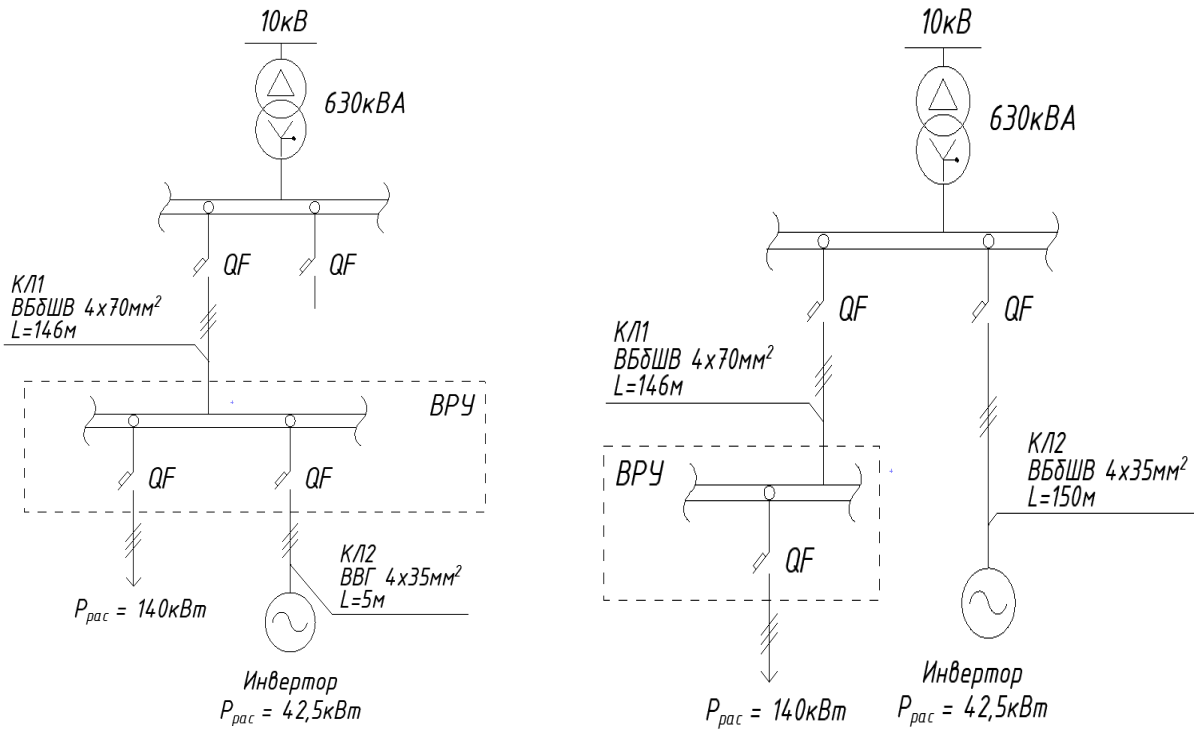

A. Connection Point – MS

B. Connection Point – Distribution Point

Figure 4.8. Connection options for a photovoltaic power plant to the existing power supply system.

5. Assess the site's potential for placement. One of the most complex and simultaneously critically important stages of design is the selection of the location and method for placing photovoltaic modules (PVM).

At the design stage, it is necessary to determine the photovoltaic power plant's capacity based on the number of PVMs that can be optimally arranged on the available area, considering orientation, tilt angle, and row spacing. An unacceptable approach is the reverse method, whereby the desired power of the plant is initially specified according to the customer's request, and then the placement of the modules is artificially adjusted accordingly, which often results in technical errors, inefficient use of equipment, or violations of shading and thermal mode regulations.

In the case of installing PV modules on flat, open terrain, particularly in rural

areas where there are no space limitations, the conditions are simplified. For network-oriented photovoltaic power plants aimed at maximizing annual generation, it is recommended to install modules at an inclination angle of approximately 30° relative to the horizontal plane, which is close to optimal for the latitudes of Uzbekistan.

The inter-row distance should be selected so that no shading occurs between rows when the sun's altitude exceeds 20°. This condition allows for ensuring Direct solar radiation incident on the active surface of the modules for at least four hours per day - approximately from 10:30 to 14:30 - even during the winter solstice, when the sun’s altitude is minimal. Further increases in inter-row spacing are generally impractical, as they result in inefficient land usage and a substantial enlargement of the occupied area, without yielding a significant increase in electricity generation.

It is also recommended to maintain a minimum clearance of at least 40 cm between the ground and the lower edge of the photovoltaic module to prevent snow accumulation and shading of the lower cells, especially in regions with winter precipitation.

Figure 4.9 shows a schematic diagram of the optimal arrangement of photovoltaic modules (PV modules) for ground-mounted installations where there are no restrictions on available space.

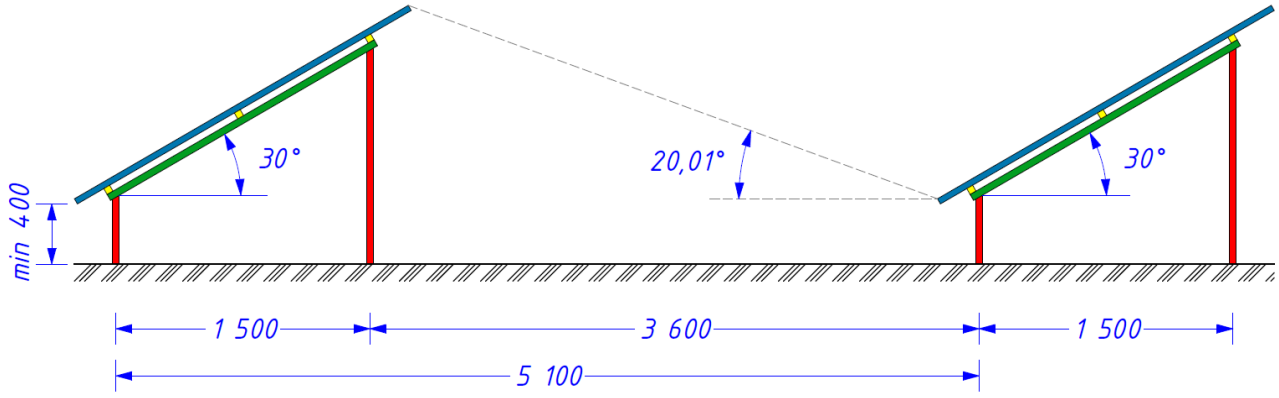

Figure 4.9. Option for the optimal placement of photovoltaic modules for ground-mounted installation.

The situation is considerably more complex when installing PV modules on a building roof, as standard design solutions cannot be applied in this case. Each roof has unique characteristics, including geometric shape, orientation relative to cardinal directions, tilt angle, load-bearing capacity, as well as the presence of engineering

utilities, ventilation equipment, and shaded zones. Therefore, each roof necessitates a separate engineering analysis and technical evaluation, accounting for both structural features and solar illumination patterns throughout the year.

Recommendations for PV module placement when installing on a roof:

- If the roof pitch exceeds 15°, modules may be installed parallel to the roof surface, provided that a ventilation gap of at least 100-300 mm between the rear side of the module and the roof is maintained for natural cooling.
- Photovoltaic arrays should be composed of modules installed under identical conditions, with uniform tilt angles and azimuths this ensures correct MPPT operation and consistent power generation.
- Whenever possible, modules should be installed vertically (with the long side upwards) - this recommendation is particularly pertinent for Half-Cut modules, where one half can continue generating electricity even if the lower part is shaded (e.g., by snow).
- Modules with differing azimuth orientations should not be combined within the same photovoltaic block (PVB), as this causes MPPT operation imbalance and negates the advantages of increasing the number of modules (see Fig. 4.10).

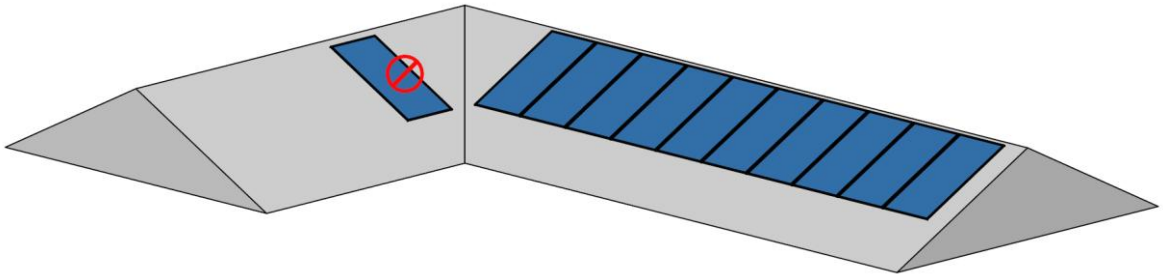

Figure 4.10. Photovoltaic block containing one module with a different installation azimuth.

In the examined case, it is more appropriate to retain a photovoltaic block (PVB) with fewer modules but under identical installation conditions than to add an additional module with a different azimuth.

- It is not recommended to arrange modules in multiple vertical tiers (one beneath another) in an attempt to increase the number of PV modules, as modules located in

the lower row are more prone to heavy contamination and prolonged snow coverage during winter, resulting in a complete or partial decrease in power generation.

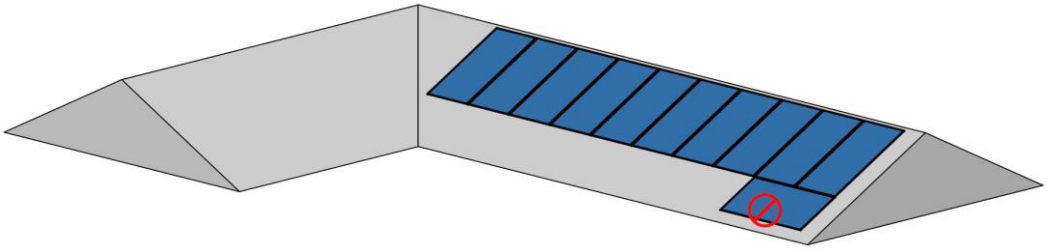

Figure 4.11. Photovoltaic block consisting of a single module with optimal orientation.

An example from practical experience is presented, illustrating the crucial importance of assembling a photovoltaic power plant block from modules operating under identical conditions. Consider a photovoltaic power plant installed on a pitched roof, whose central axis is oriented southwest with an azimuth of 193° (see Figure 4.12). Photovoltaic modules are arranged in three horizontal rows on both roof slopes - eastern and western. All modules are oriented identically: azimuth 193°, tilt angle relative to horizontal - 30°.

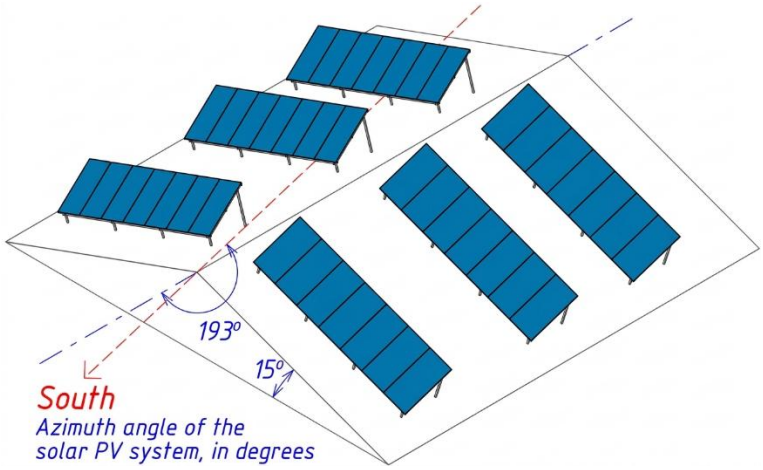

Figure 4.12. Photovoltaic power plant installed on a gable roof.

The design accounted for the geometric parameters of the roof: the distance between rows, as well as the setback from the ridge to the upper row of PV modules, were optimized to minimize mutual shading. Calculation results indicated that the maximum mutual shading angle between rows, at a sun azimuth of 193°, does not exceed 20°, which is within acceptable limits to ensure stable generation.

For the purposes of the experiment, three different photovoltaic electric blocks (PEBs) were formed using the same modules but with different connection logics (see Fig. 3.13):

- PEB №1 — comprised of 7 photovoltaic modules (PVMs) installed on two slopes (eastern and western);
- PEB № 2 — comprised of 14 PVMs located exclusively on the eastern slope;
- PEB № 3 — comprised of 14 PVMs located exclusively on the western slope.

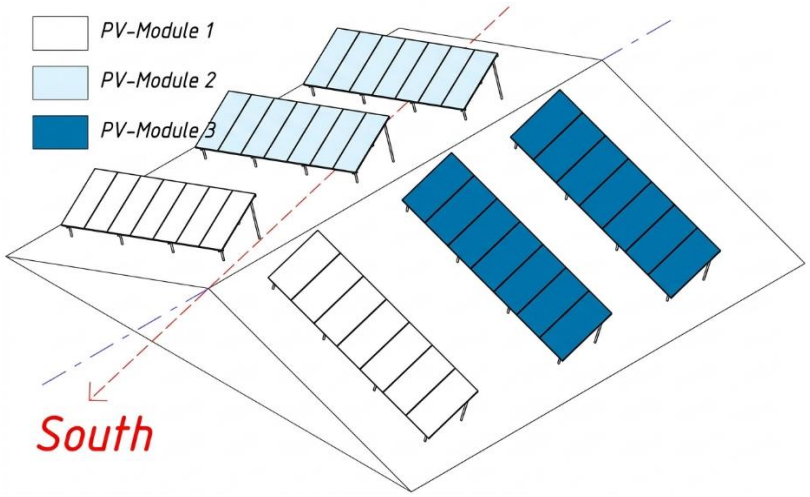

Figure 4.13. Diagram of photovoltaic block formation.

Each PV array was connected to a separate MPPT controller, eliminating mutual interference and ensuring independent operation. Table 4.1 presents the annual generation data for each PV array. As evident, the generation of PV array №2 and PV array № 3 was higher by 26% and 19%, respectively, compared to PV array №1, which comprised modules with different orientations and directions. The higher generation of PV array №2, consisting solely of modules installed on the eastern side, compared to PV array №3 (western side), is attributed to the building's azimuth.

The reduction in generation by PVB №1 is attributed to the operational characteristics of the MPPT controller, which encounters increased difficulty in identifying the maximum power point when some modules are mounted on the eastern slope (receiving greater reflected solar radiation during the first half of the day), while others are positioned on the western slope (exposed to similar illumination in the second half of the day). Consequently, the modules within a single PV string operate under

heterogeneous illumination conditions, including varying ratios of direct and reflected solar radiation, which complicates the tracking of the MPPT optimal operating mode. This results in voltage fluctuations and a reduction in output power.

Table 4.1. Electricity generation of PVB Nos. 1, 2, and 3 for the period from September 1, 2023, to August 31, 2024.

Date	Electricity generation, kWh		
	PV Module №1	PV Module №2	PV Module № 3
09/01/2023 – 11/30/2023	2302	2925 (+27%)	2642 (+15%)
12/01/2023 – 02/29/2024	1309	1790 (+37%)	1616 (+24%)
03/01/2024 – 05/31/2024	2449	2897 (+28%)	2797 (+14%)
06/01/2024 – 08/31/2024	2705	3441 (+27%)	3343 (24%)
01.09.2023 – 31.08.2024	8765	11053 (+26%)	10398 (+19%)

Figure 4.14 presents voltage and current curves for all three PV strings on August 31, 2024. As observed, PV string №1 experiences voltage drops, leading to decreased generation.

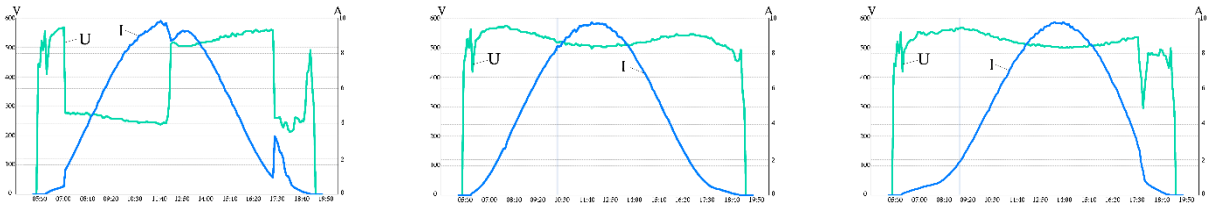

A. PVB №1 B. PVB №2 C. PVB №3

Figure 4.14 – Voltage and current graph of PV batteries №1, №2, and №3 on the DC side for August 31, 2024.

Similar MPPT controller behavior was recorded in other photovoltaic power plants installed similarly on pitched roofs, where modules of one photovoltaic block are located on different slopes. This confirms that multidirectional illumination within a single PV block systematically causes unstable MPPT operation and reduces overall electricity output.

Unfortunately, in practice, photovoltaic power plants are most often designed with modules interconnected according to the principle similar to PVB №1, as this solution considerably simplifies electrical installation work. However, installation convenience should not take precedence over the requirements for energy efficiency.

Another important advantage of grouping modules located on the same roof slope

is the localization of generation losses caused by mutual shading. Naturally, the optimal solution is the complete elimination of mutual shading; however, under real conditions, especially during winter, shading of the rear rows may occur from modules installed closer to the roof ridge due to the low solar elevation angle and limited spacing between rows. In such cases, when forming separate PV string blocks for each roof slope, generation losses are confined solely to the respective blocks: morning shading affects the modules on the western side (see Fig. 4.15 A), whereas evening shading affects those on the eastern side (see Fig. 4.15 B). However, if modules from different roof slopes are combined into a single PV string block, shading of any section results in a decrease in the overall block efficiency, as the MPPT controller tracks the least illuminated module.

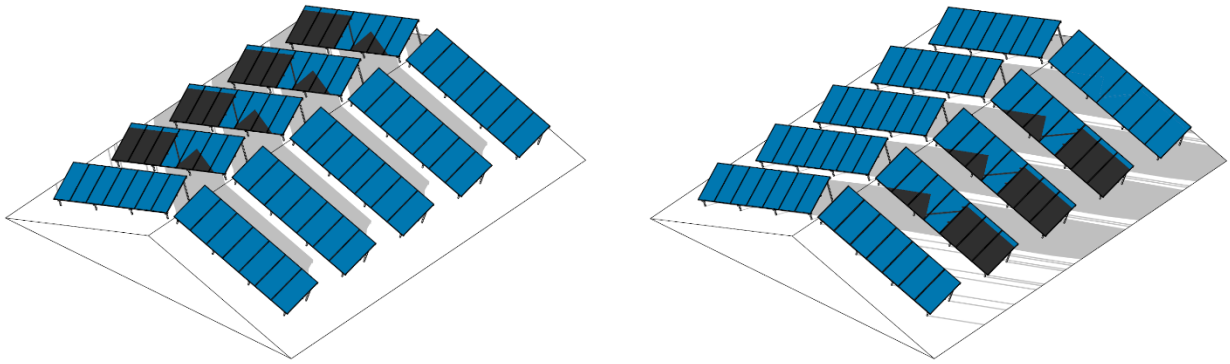

A. Morning shading B. Evening shading

Figure 4.15. Possible mutual shading of photovoltaic modules during the winter period.

Ensure the compatibility of PV module and inverter characteristics. For the safe and stable operation of a photovoltaic power plant, it is essential to ensure the compatibility of the electrical characteristics of the PV module, and correspondingly of individual photovoltaic cells, with the inverter's parameters. The main points are as follows:

- The PV module voltage at maximum power (U_{mp}) must fall within the inverter's MPPT voltage range.

Failure to comply with this condition may cause the inverter to be unable to accurately track the maximum power point, resulting in the photovoltaic power plant operating inefficiently or failing to initiate generation altogether.

- The maximum voltage of the photovoltaic module at the calculated minimum temperature (U_{OC}) must not exceed the inverter's maximum permissible input voltage.

Non-compliance with this condition may result in inverter failure, as exceeding the allowable input voltage compromises the electrical integrity of components and can cause damage to the input circuits.

- The current at the maximum power point of the photovoltaic module (I mp) must not exceed the maximum allowable current of the MPPT controller and its corresponding PV input. If two parallel photovoltaic modules are connected to a single MPPT, the calculation must consider the combined current of both modules, which must not exceed the specified limit.

Non-compliance with this condition may result in current being limited to the permissible maximum, thereby causing a loss of potential energy generation. Furthermore, exceeding the current limit causes increased heat dissipation within the MPPT circuits, potentially leading to overheating, reduced component lifespan, and, in some cases, emergency shutdown or damage of the inverter. All other conditions being equal, preference should be given to photovoltaic modules with lower current.

- The short-circuit current of the PV cell (I_{sc}) must not exceed the maximum permissible short-circuit current at the inverter input. Furthermore, it is recommended to maintain a current margin of at least 25%, meaning the actual short-circuit current should not exceed 80% of the maximum allowable value, thereby ensuring the reliability and thermal stability of the input circuits. In most cases, this condition is automatically satisfied if the current requirements at maximum power (I_{mp}) are met. When two PV modules are connected in parallel to a single MPPT, the total short-circuit current of both strings must be considered in the calculation.

Non-compliance with this condition may result in overloading of the inverter's input circuit, tripping of protective devices, overheating of power components, and, in certain cases, equipment damage.

- The total power rating of the PV modules must not exceed the maximum allowable power that the MPPT controller can process. When two PV modules are connected in parallel to a single MPPT, the combined installed power of both modules

must be taken into account in the calculation.

Failure to adhere to this condition may result in generation losses due to forced power limitation by the controller when the MPPT deviates from the maximum power point towards lower currents. Moreover, operating the MPPT at its power limit increases thermal stress, which can lead to accelerated degradation of circuit components, reduced cooling efficiency, and a shortened inverter lifespan. Therefore, it is recommended not to load the MPPT up to its maximum capacity, but to maintain a margin of at least 10-20%, particularly under high ambient temperature conditions.

- When connecting two PV arrays to a single MPPT, it is essential to use identical blocks composed of modules with matching characteristics, tilt angle, and azimuth.

Non-compliance with this requirement may lead to generation losses, as the MPPT controller will be unable to accurately track the overall maximum power point under unequal operating conditions of the two blocks. Furthermore, when voltage differences exist between parallel-connected PV arrays, backfeed current may occur between the strings, potentially causing local overheating, circuit imbalance, and additional energy losses. To prevent this phenomenon, it is recommended to connect only electrically and geometrically identical arrays to a single MPPT.

- The voltage of PV modules connected to a single MPPT controller must be identical. The voltage difference between PV modules connected to different MPPT controllers must not exceed 150 V to avoid internal current redistribution or the triggering of protective circuits (DC BUS UNBALANCE). However, the most preferred option is voltage equality among all PV modules, as this simplifies balancing and enhances inverter stability.

- All else being equal, it is recommended to configure the system so that only one PV module string is connected to each MPPT controller. This approach ensures maximum MPPT efficiency, simplifies maximum power point tracking, and eliminates the risk of circulating currents between parallel PV module strings. Moreover, it enhances the overall stability and reliability of the system by reducing the likelihood of cross-interference between strings. Under fault conditions, such as a short circuit, the absence of a second parallel-connected PV module string prevents current back

feeding from an adjacent circuit, thereby reducing the resulting current at the fault location.

6. Implement measures to improve the inverter's efficiency.

This is one of the most critical, yet regrettably often overlooked, aspects by engineers. The factors affecting the inverter's efficiency were discussed in Section 2.4. One of the most effective ways to enhance overall system efficiency is to design the PV array such that the voltage at maximum power (U_{mp}) closely matches the inverter's nominal operating voltage. This enables minimizing losses during the voltage step-up stage within the inverter and, consequently, increasing the overall conversion efficiency.

All else being equal, it is advisable to configure the photovoltaic module array so that the voltage at maximum power (V_{mp}) is as close as possible to the nominal voltage specifically during the summer period when the thermal conditions are most severe and the inverter's cooling efficiency significantly decreases. Under these conditions, it is particularly important to maximize efficiency and minimize heat generation to prevent overheating, power limitations, and reduction of the equipment's service life.

In winter, the voltage of the photovoltaic module is somewhat higher than nominal due to the decrease in temperature, which indeed leads to an increase in thermal losses; however, thanks to more favorable cooling conditions, this does not significantly affect the operation of the inverter.

Unfortunately, the rapid increase in photovoltaic module power ratings in recent years has primarily resulted from growth in current, while the operating voltage has remained practically unchanged. Consequently, the power of photovoltaic modules assembled at a standard voltage close to the inverter's nominal voltage has significantly increased. Thus, when utilizing modern high-power photovoltaic cells, the total power of a single photovoltaic module with a voltage V_{mp} around 600 V easily reaches and, in some cases, exceeds 10 kW.

The critical consequence of the mismatch between the operating parameters of photovoltaic modules and the inverter's nominal conditions is not so much a 1-2% reduction in efficiency due to losses incurred while raising the voltage to the nominal

level, but rather an increase in heat generation and, subsequently, a rise in temperature inside the inverter. For example, in a photovoltaic power plant with a capacity of 100 kW, a reduction in the inverter’s efficiency by only 2% results in additional thermal losses of approximately 2 kW. The thermal balance of the inverter is designed to operate at the optimal (nominal) voltage, and deviations from this result in an increase in the device's internal temperature, especially during summer. This, in turn, can lead to a sharp decrease in the inverter’s output power due to overheating. (temperature derating), as well as accelerated wear and degradation of electronic components, which adversely affect the equipment's service life and overall system reliability.

§4.4. Analysis of design solutions from practical experience

This section examines design solutions grounded in practical experience, considering the photovoltaic modules and inverters currently available on the Uzbekistan market.

1. Grid-connected photovoltaic system with a capacity of 100 kW. Design solution: Huawei SUN2000-100KTL-M2 inverter (Table 4.2) and 160 photovoltaic modules Jinko Solar JKM630N-66HL4M-BDV (Table 4.3).

Table 4.2. Main electrical characteristics of the Huawei SUN2000-100KTL-M2 inverter.

Parameter	Value
Rated active power	100 kW
Max. active power cosφ=1	110 kW
Max. input voltage	1100 V
MPPT voltage range	200-1000 V
Full-load MPPT voltage range	540-800 V
Startup voltage	200 V
Rated input voltage	600 V
Max. input current per MPPT	30 A
Max. short-circuit current	40 A
Max. power per MPPT	21 kW
Number of MPP trackers	10

Parameter	Value
Max. input number per MPP tracker	2
Max. input current per string	20 A

Table 4.3. Main electrical characteristics of the JKM630N-66HL4M-BDV

Parameter	STC	BNPI
Maximum power (Pmax), W	630	630
Voltage at maximum power (Vmp), V	41,02	41,04
Current at maximum power (Imp), A	15,36	16,95
Open-circuit voltage (Voc), V	49,48	49,46
Short-circuit current (Isc), A	16,20	17,90
Efficiency, %	23,32	
Temperature coefficient of Voc, %/°C	-0,25	
Temperature coefficient of Isc, %/°C	0,045	
Temperature coefficient of Pmp, %/°C	-0,29	

Solution: Formation of 10 photovoltaic blocks, each consisting of 16 PV modules. Photovoltaic modules within a single PV block have identical tilt angles and azimuths and are installed in a single row.

1.1. Power of all photovoltaic modules under STC conditions:

$$\mathbf{P_{mp\ STC} = 160 \cdot P_{mp} = 160 \cdot 630 = 100,8\ kW}$$

For general information, the theoretical output power at the minimum design temperature of minus 20 degrees is presented as follows:

$$\mathbf{P_{mp} = N \cdot P_{mp\ STC} \cdot \left(1 + K_P \cdot \frac{(t - 25)}{100}\right) = 160 \cdot 630 \cdot \left(1 - 0,29 \cdot \frac{-20 - 25}{100}\right) = 114\ kW}$$

It should be noted that such output power is practically unattainable under the conditions prevailing in Uzbekistan. This phenomenon occurs because when current flows through the cells, they heat up, causing the actual temperature to exceed the

calculated minimum. Furthermore, the solar radiation level in the region is typically below the standard 100 0 W/m^2 upon which the STC parameters are based. Even under rare conditions where the module temperature approaches -20°C and the solar radiation reaches 1000 W/m^2, the inverter will limit the output power by shifting the operating point along the current-voltage characteristic.

For general reference, the theoretical output power at the maximum calculated cell temperature of +70 degrees is as follows:

$$\mathbf{P_{mp}} = \mathbf{N} \cdot \mathbf{P_{mp\,STC}} \cdot \left(\mathbf{1} + \mathbf{K_P} \cdot \frac{\mathbf{(t-25)}}{\mathbf{100}}\right) = \mathbf{160} \cdot \mathbf{630} \cdot \left(\mathbf{1} - \mathbf{0,29} \cdot \frac{\mathbf{70-25}}{\mathbf{100}}\right) = \mathbf{87,6}$$

kW

As shown, during the summer period, the power generated by photovoltaic modules decreases due to elevated temperatures, which facilitates the partial unloading of the inverter. It is important not to confuse temperature-induced generation degradation on the direct current side with the inverter's internal conversion losses.

1.2. Maximum calculated open-circuit voltage of the PV module at the minimum design temperature of minus 20 degrees Celsius:

$$\mathbf{V_{OC}} = \mathbf{N} \cdot \mathbf{V_{OC\,STC}} \cdot \left(\mathbf{1} + \mathbf{K_V} \cdot \frac{\mathbf{(t-25)}}{\mathbf{100}}\right) = \mathbf{16} \cdot \mathbf{49,48} \cdot \left(\mathbf{1} - \mathbf{0,25} \cdot \frac{\mathbf{-20-25}}{\mathbf{100}}\right) = \mathbf{880}\ \text{V}$$

The maximum calculated open-circuit voltage does not exceed the operational voltage range of the MPPT, whose upper limit is 1000 V.

1.3. Voltage at maximum power (V_{mp}) of the PV module at the minimum design temperature of minus 20 degrees Celsius:

$$\mathbf{V_{mp}} = \mathbf{N} \cdot \mathbf{V_{mp\,STC}} \cdot \left(\mathbf{1} + \mathbf{K_V} \cdot \frac{\mathbf{(t-25)}}{\mathbf{100}}\right) = \mathbf{16} \cdot \mathbf{41,02} \cdot \left(\mathbf{1} - \mathbf{0,25} \cdot \frac{\mathbf{-20-25}}{\mathbf{100}}\right) = \mathbf{730\ V}$$

V_{mp} at the minimum design temperature lies within the full-load MPPT voltage range, ensuring the inverter's capability to deliver maximum power.

1.4. Voltage at maximum power (V_{mp}) of the photovoltaic module at the maximum design cell temperature of +70 degrees:

$$\mathbf{V_{mp} = N \cdot V_{mp\,STC} \cdot \left(1 + K_V \cdot \frac{(t - 25)}{100}\right) = 16 \cdot 41,02 \cdot \left(1 - 0,25 \cdot \frac{70 - 25}{100}\right)}$$
$$\mathbf{= 582\ V}$$

The voltage at maximum power (V_{mp}) at the calculated maximum cell temperature closely matches the nominal voltage, thereby ensuring enhanced inverter efficiency and preventing additional thermal stress. This is particularly important under high-temperature conditions, where effective heat dissipation is hindered.

Note. *The calculated maximum cell temperature may vary depending on the installation region. In the provided examples, a value of 70°C is adopted, as it corresponds to the upper limit of the operating temperature range specified in the photovoltaic module datasheet. Meanwhile, representatives of the manufacturer assert that module testing is performed at temperatures up to +85°C; however, this information is not documented in the official technical specifications and has not been included in the product datasheet.*

1.5. Maximum short-circuit current at the maximum design cell temperature of +7 0 degrees Celsius:

$$\mathbf{I_{sc} = I_{sc\,STC} \cdot \left(1 + K_I \cdot \frac{(t - 25)}{100}\right) = 16,20 \cdot \left(1 + 0,045 \cdot \frac{70 - 25}{100}\right) = 16,52}\ \text{A}$$

Maximum short-circuit current at the maximum design cell temperature of +70 degrees Celsius under BNPI conditions:

$$\mathbf{I_{sc} = I_{sc\,BNPI} \cdot \left(1 + K_I \cdot \frac{(t - 25)}{100}\right) = 17,90 \cdot \left(1 + 0,045 \cdot \frac{70 - 25}{100}\right) = 18,3}\ \text{A}$$

Given that the maximum permissible short-circuit current at the MPPT inverter input is 40A, and each MPPT is connected to only one photovoltaic module, a current margin exceedingly twice the value is ensured.

1.6. Verification of the conformity between the inverter input (PV input) and the current at the maximum power point (Imp) of the photovoltaic modules, as well as the photovoltaic array: $\mathbf{I_{max\,PV\,input} = 20A > I_{mp\,STC} = 15,36}$A

Accordingly, connecting a single PV array to the inverter input will not cause overheating of the PV input, provided that compatible MC4-type connectors are employed and reliable fixation of the connections is ensured.

1.7. Verification of compliance between the PV module current and the maximum permissible MPPT current, considering the connection of only one PV module to each MPPT:

$$\mathbf{I_{max\ MPPT} = 30A > I_{mp\ STC} = 15,36}\text{A}$$

The maximum permissible current at the MPPT input exceeds the photovoltaic module current at the maximum power point by more than a factor of two. Accordingly, losses related to current limitation on the inverter side are avoided.

1.8. Verification of compliance between the PV module power rating and the maximum permissible MPPT power rating, considering the connection of only one PV module per MPPT:

$$\mathbf{P_{max\ MPPT} = 21\ kW > P_{mp\ STC\ PVB} = 16 \cdot 630 = 10,08\ kW}$$

The maximum allowable power at the MPPT input exceeds the installed power rating of the photovoltaic block (PV module) by more than twice. Accordingly, losses associated with power limitation on the inverter side are eliminated.

Conclusion

The proposed solution is optimal because:

- It ensures maximum MPPT efficiency, as each MPPT tracks the maximum power point of only one photovoltaic module (PVM).
- It provides enhanced electrical safety, as the short-circuit point feed from neighboring PVMs is prevented by connecting only one PVM to each MPPT.
- Optimal operating voltage of the PV modules is ensured, particularly during the summer period, which enhances inverter efficiency and reduces thermal losses;
- The voltage of all PV modules connected to different MPPTs is identical, which not only simplifies system design, commissioning, and operation but also ensures an even load on the common DC bus, thereby improving inverter stability.
- A current margin exceeding double is provided, which, given the quadratic dependence of heat generation on current, results in a thermal margin exceeding four-

fold, thus contributing to the prolonged lifespan of the MPPT and other inverter components.

Considering the level of solar radiation in Uzbekistan, and subject to sufficient area and the Client's approval, it is possible to increase the number of modules in all photovoltaic power plant (PVPP) blocks from 16 to 17 units. Thus, it is feasible to assemble 10 PVPP blocks with 17 modules each, which will increase the installed capacity of the plant with minimal additional costs and accordingly enhance the annual generation of the photovoltaic power plant. Adding one photovoltaic module to each PVPP block results in an increase in both output power and voltage, while the current remains unchanged, as the modules are connected in series. Accordingly, an additional verification of the connection feasibility is required concerning the permissible power and the maximum input voltage at the MPPT inverter.

1.9. Total power of all photovoltaic modules under STC conditions:

$$\mathbf{P_{mp\,STC} = 170 \cdot P_{mp} = 170 \cdot 630 = 107,1}\ \text{kW}$$

The maximum output power of the inverter, assuming cosφ=1, is 110 kW. Accordingly, the inverter is capable of delivering the full power of the photovoltaic station, amounting to 107.1 kW, provided that the corresponding level of solar radiation is attained.

1.10. Maximum calculated open-circuit voltage of the PV module at the minimum design temperature of minus 20 degrees:

$$\mathbf{V_{OC} = N \cdot V_{OC\,STC} \cdot \left(1 + K_V \cdot \frac{(t - 25)}{100}\right) = 17 \cdot 49,48 \cdot \left(1 - 0,25 \cdot \frac{-20 - 25}{100}\right) = 936\ V}$$

The maximum calculated open-circuit voltage does not exceed the operational voltage range of the MPPT, whose upper limit is 1000 V.

1.11. Voltage at maximum power (V_{mp}) of the PV module at the minimum design temperature of minus 20 degrees:

$$\mathbf{V_{mp} = N \cdot V_{mp\,STC} \cdot \left(1 + K_V \cdot \frac{(t - 25)}{100}\right) = 17 \cdot 41,02 \cdot \left(1 - 0,25 \cdot \frac{-20 - 25}{100}\right) = 776\ V}$$

V_{mp} at the minimum design temperature lies within the full-load MPPT voltage range, ensuring the inverter's capability to deliver maximum power.

1.12. Voltage at maximum power (V_{mp}) of the photovoltaic module at the maximum calculated cell temperature of +70 degrees:

$$\mathbf{U_{mp} = N \cdot V_{mp\,STC} \cdot \left(1 + K_V \cdot \frac{(t - 25)}{100}\right) = 17 \cdot 41,02 \cdot \left(1 - 0,25 \cdot \frac{70 - 25}{100}\right) = 618\ V}$$

The voltage at maximum power (V_{mp}) at the calculated maximum cell temperature closely matches the nominal voltage, thereby ensuring enhanced inverter efficiency and preventing additional thermal stresses.

1.13.Verification of compliance between the photovoltaic module power rating and the maximum allowable MPPT power, taking into account that only one photovoltaic module is connected to a single MPPT:

$$\mathbf{P_{max\,MPPT} = 21\ kW > P_{mp\,STC\,PVB} = 17 \cdot 630 = 10,7\ kW}$$

The maximum allowable input power to the MPPT is nearly twice the rated power of the photovoltaic module (PV module). Accordingly, losses associated with power limitation on the inverter side are eliminated.

Thus, the configuration involving 17 photovoltaic modules per photovoltaic unit is more optimal for the chosen combination of inverter and PV modules, taking into account the high solar radiation levels in Uzbekistan. This enables the most efficient utilization of the equipment's power capacity without exceeding the allowable electrical parameters.

In practice, although rarely, photovoltaic stations exist where all available inverter inputs are fully utilized. For a photovoltaic power plant with a capacity exceeding 10 kW, this can only be achieved by irrationally reducing the number of modules in each

photovoltaic block (PFB). For instance, in the analyzed case, connecting to 20 inputs would require assembling a PFB with only 8 modules. This solution is technically unsound, as it results in a twofold reduction in voltage and, consequently, a decrease in inverter efficiency due to the need to further increase the voltage to the nominal level. Additionally, it causes a twofold increase in current, reaching the maximum allowable current at the inverter input, and leads to increased thermal losses. Additionally, this results in increased costs for the solar cable both due to the greater quantity required.

2. Photovoltaic power plants with capacities ranging from 20 to 60 kW employ inverters equipped with one MPPT for every 10 kW of power. As the power of photovoltaic modules increases, inverter configurations are progressively adapted accordingly. Currently, inverters available on the market feature one MPPT controller for every 10 kW of power. Consequently, models with power ratings of 20, 30, 40, 50, and 60 kW typically have 2, 3, 4, 5, and 6 MPPTs, respectively. In such cases, it is advisable to follow the approach proposed in the example of a 100-kW plant — connecting one photovoltaic module string to a single MPPT.

Special attention should be given to the maximum allowable current per string (Max. input current per string). Although many inverters permit a total current on one MPPT of up to 32 A, manufacturers (including via technical consultations) recommend not exceeding a current greater than 16 A per input. This value is acceptable for most PV modules on the market, particularly considering the actual solar irradiation levels.

However, recently, modules with power ratings of 700 W and above have increasingly appeared, where the current at the maximum power point approaches 18-20 A. The use of such modules requires increased attention because:

- their high power is achieved not so much by an increase in efficiency but by an increase in area (housing),
- they become heavier and bulkier,
- the elevated currents can lead to overheating of the inverter’s input circuits, connectors, and cable connections.

In this regard, it is recommended, whenever possible, to always prioritize modules

with lower power and a current up to 16A. If the use of such modules is unavoidable for any reason, it is necessary to consult the inverter manufacturer's technical support in advance and clarify the maximum allowable current per input. In such cases, some manufacturers recommend connecting one PV module to two inputs of a single MPPT, thereby reducing the current supplied to each input by half (see Fig. 4.16).

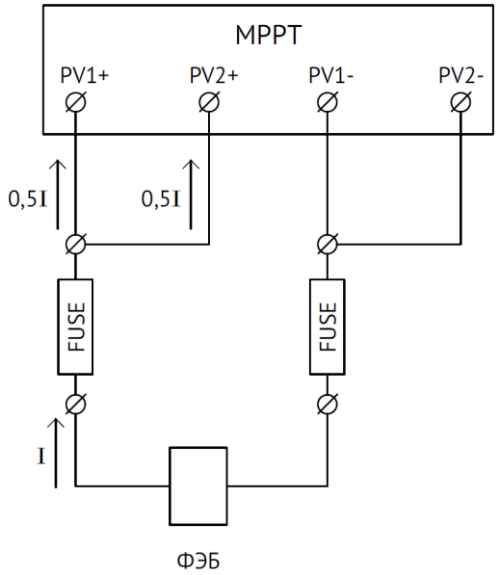

Figure 4.16. Connection of a single PV module with high current to two inputs of one MPPT.

3. A photovoltaic power plant with a capacity of 50 kW using inverters equipped with four MPPTs. There are inverters on the market that have fewer MPPT controllers than one per 10 kW of power rating. As an example, consider a design solution based on one of the most common inverters the Huawei SUN2000-50KTL-M3, featuring four MPPTs and a nominal power rating of 50 kW. The main electrical characteristics of the inverter are presented in Table 3.4.

Focusing on Jinko Solar products, the Uzbekistan market currently mainly features two types of photovoltaic modules: configurations based on 66 cells (series 66HL4) and on 72 cells (series 72HL4). Subsequently, both options will be examined regarding their compatibility with the Huawei SUN2000-50KTL-M3 inverter.

To begin with, let us consider a proven and optimal solution based on the Jinko Solar module JKM630N-66HL4M-BDV (Table 4.3), previously employed in the configuration of a photovoltaic power plant with a capacity of 100 kW, which remains

relevant when using inverters equipped with one MPPT controller per each 10 kW of installed power.

Table 4.4. Principal electrical characteristics of the Huawei SUN2000-50KTL-M3 Inverter.

Parameter	Value
Rated active power	50 kW
Max. active power cosφ=1	55 kW
Max. input voltage	1100 V
MPPT voltage range	200–1000 V
Full-load MPPT voltage range	530–800 V
Startup voltage	200 V
Rated input voltage	600 V
Max. input current per MPPT	30 A
Max. short-circuit current	40 A
Max. power per MPPT	18.3 kW
Number of MPP trackers	4
Max. input number per MPP tracker	2
Max. input current per string	20 A

The solution based on the JKM630N-66HL4M-BDV module involves the use of 80 photovoltaic modules with a total installed capacity of 50.4 kW, assembled into 5 photovoltaic blocks (PVB), each consisting of 16 modules. With regard to input voltages, the characteristics of the Huawei SUN2000-100KTL-M2 and SUN2000-50KTL-M3 inverters are practically identical. Since the number of modules in each PV array has not changed, all calculations previously performed for a 100 kW station remain valid and applicable in this case.

However, considering that the total number of PV arrays is five, and the inverter has four MPPT controllers, two PV arrays must be connected to a single MPPT controller. Accordingly, it is necessary to re-verify the conformity of current and power ratings at the input of the respective MPPT.

As previously calculated, the maximum short-circuits current of a single

photovoltaic block (PVB) at the design maximum cell temperature of +70°C is 16.52 A under STC conditions and 18.3 A under BNPI conditions. Since two PV blocks are connected to one MPPT, the combined current must be considered. Therefore, the short circuit current at the MPPT input amounts to 33 A (STC) and 36.6 A (BNPI), which remains below the allowable maximum of 40 A.

Although the recommended 25% margin is not provided in this case, the values remain within acceptable limits, particularly considering the actual climatic conditions in Uzbekistan, where solar radiation seldom reaches the calculated BNPI peaks.

A more critical verification concerns the maximum allowable operating current for the MPPT. The combined current of two PV modules at the maximum power point is 30.7 A under STC conditions and 33.9 A under BNPI conditions. As observed, at certain levels of solar radiation, currents exceeding the MPPT's maximum permissible value (30A) may occur. However, the MPPT controller will not physically allow the current to exceed the established limit; upon reaching 30A, it shifts the operating point toward reduced power, thereby limiting the output generation. This results in partial losses, particularly during periods of peak insolation.

Nevertheless, under conditions in Uzbekistan, such modes occur infrequently and are of short duration. According to practical observations, the current does not exceed 15A for the majority of the year. Thus, formally, no significant generation losses are expected, and such a solution is deemed acceptable for implementation.

However, a more significant issue is that the MPPT will operate near the maximum current limit (30A), which may cause accelerated wear of power components, increased heat dissipation, and reduced long-term reliability of the inverter. Therefore, it is recommended to avoid such solutions when alternative configuration options are available.

Let us verify the total power of two PV modules for compliance with the maximum allowable power of a single MPPT:

$$\mathbf{P_{max\ MPPT}} = \mathbf{18,3}\ \text{кВт} < \mathbf{2 \cdot P_{mp\ STC\ PVB}} = \mathbf{2 \cdot 16 \cdot 630} = \mathbf{20,2\ kW}$$

As demonstrated, the power of the two PV modules exceeds that of a single MPPT;

therefore, the MPPT will limit the power at 18.3 kW and will operate under this constraint most of the time. to operate at maximum power.

As can be seen, the total power of the two photovoltaic blocks (PVB) exceeds the maximum permissible input power of a single MPPT. Consequently, the MPPT will 220 limit the output power (power clipping) to approximately 18.3 kW and will operate in a maximum load mode for the majority of the time.

This issue can be addressed by redistributing the load between MPPT controllers through the formation of six photovoltaic blocks (PVB): four photovoltaic blocks consisting of 13 modules each and two photovoltaic blocks with 14 modules each. In this configuration, the four photovoltaic blocks of 13 modules can be paired and connected to two MPPT controllers, resulting in a total power of approximately 16.4 kW per controller.

However, this solution does not eliminate the problem of elevated input currents to these MPPT controllers, which still reach 30 A, and simultaneously creates a new technical issue - a decrease in the voltage of the photovoltaic blocks (PVB). This, in turn, leads to additional thermal losses in the inverter, especially during the summer period, when the voltage of the PV array, assembled from 13 modules, can drop below 500 V.

Note. *In the considered examples, the number of PV modules is selected so that the total installed power of the plant is as close as possible to the inverter's nominal power rating. This is because, in most commercial projects in Uzbekistan, the contractual power, and consequently the installation cost, are determined based on the nominal power rating of the photovoltaic plant.*

In the absence of such restrictions from the client, it is advisable to use a greater number of PV arrays - calculated so that all photovoltaic batteries (PVB) contain an identical number of modules. This approach simplifies design, installation, as well as current and voltage balancing, while also ensuring a more uniform and efficient operation of the inverter.

Now, let us consider an alternative design solution based on 72-cell photovoltaic modules-Jinko Solar JKM600N-72HL4-BDV, whose main electrical parameters are

presented in Table 6.5. This design solution involves using 84 modules assembled into 6 photovoltaic batteries (PVBs), each comprising 14 modules. Of these, four photovoltaic blocks will be connected to two MPPTs, with two PV blocks per MPPT, while the remaining two blocks will be connected to two other MPPTs, with one PV block per MPPT.

Table 4.5. Principal electrical characteristics of the JKM600N-72HL4-BDV

Parameter	STC	BNPI
Maximum power (P_{max}), W	600	660
Voltage at maximum power (V_{mp}), V	44,45	44,66
Current at maximum power (I_{mp}), A	13,50	14,78
Open-circuit voltage (V_{oc}), V	53,30	53,33
Short-circuit current (I_{sc}), A	14,19	15,49
Efficiency, %	23,23	
Temperature coefficient of V_{oc}, %/°C	-0,25	
Temperature coefficient of I_{sc}, %/°C	0,045	
Temperature coefficient of P_{mp}, %/°C	-0,29	

3.1. Power of all photovoltaic modules under STC conditions:

$$\mathbf{P_{mp\,STC} = 6 \cdot 14 \cdot P_{mp} = 84 \cdot 600 = 50,4}\ \text{kW}$$

3.2. Maximum calculated open-circuit voltage of the PV module at the minimum design temperature of minus 20 degrees:

$$\mathbf{V_{OC} = N \cdot V_{OC\,STC} \cdot \left(1 + K_V \cdot \frac{(t - 25)}{100}\right) = 14 \cdot 53,30 \cdot \left(1 - 0,25 \cdot \frac{-20 - 25}{100}\right)}$$
$$\mathbf{= 830\ V}$$

The maximum calculated open-circuit voltage does not exceed the operational voltage range of the MPPT, whose upper limit is 1000 V.

3.3. Voltage at maximum power (V_{mp}) of the PV module at the minimum design

temperature of minus 20 degrees:

$$\mathbf{U_{mp} = N \cdot V_{mp\,STC} \cdot \left(1 + K_V \cdot \frac{(t - 25)}{100}\right) = 14 \cdot 44,45 \cdot \left(1 - 0,25 \cdot \frac{-20 - 25}{100}\right) = 692\ V}$$

V_{mp} at the minimum design temperature lies within the full-load MPPT voltage range, ensuring the inverter's capability to deliver maximum power.

3.4. Voltage at maximum power (V_{mp}) of the PV module at the maximum design cell temperature of plus 70 degrees:

$$\mathbf{V_{mp} = N \cdot V_{mp\,STC} \cdot \left(1 + K_V \cdot \frac{(t - 25)}{100}\right) = 16 \cdot 44,45 \cdot \left(1 - 0,25 \cdot \frac{70 - 25}{100}\right) = 552\ V}$$

V_{mp} at the calculated maximum cell temperature is 50 V lower than the nominal value. Considering that the calculation was performed for the maximum possible operating temperature, this result is acceptable. Furthermore, the obtained V_{mp} value remains within the MPPT voltage range under full load.

3.5. Maximum short-circuit current of a single PV module at the maximum calculated cell temperature of +70 degrees:

$$\mathbf{I_{sc} = I_{sc\,STC} \cdot \left(1 + K_I \cdot \frac{(t - 25)}{100}\right) = 14,19 \cdot \left(1 + 0,045 \cdot \frac{70 - 25}{100}\right) = 14,47}\text{A}$$

Maximum short-circuit current at the maximum design cell temperature of +70 degrees Celsius under BNPI conditions:

$$\mathbf{I_{sc} = I_{sc\,BNPI} \cdot \left(1 + K_I \cdot \frac{(t - 25)}{100}\right) = 15,49 \cdot \left(1 + 0,045 \cdot \frac{70 - 25}{100}\right) = 15,8}\text{A}$$

The total short-circuit current under STC conditions does not exceed 30 A, providing a margin of more than 25% relative to the maximum permissible current at the MPPT input.

3.6. The total current at the maximum power point (Imp) of two photovoltaic

blocks (PFB) is 27 A under STC conditions and 29.56 A under BNPI conditions, which does not exceed the permissible value of 30 A at the MPPT input. Considering the climatic conditions of Uzbekistan, even during peak hours, the total current generally will not exceeding 26 A. Thus, in this configuration, a lower load on the MPPT is ensured compared to the solution based on JKM630N-66HL4M-BDV modules, which positively affects the thermal mode and reliability of the inverter's operation.

3.7. Verification of the compliance between the PV array power and the maximum allowable power MPPT considering the connection of two PV arrays to the MPPT:

$$\mathbf{P_{max\ MPPT} = 18,3\ kW < 2 \cdot P_{mp\ STC\ PVB} = 2 \cdot 14 \cdot 600 = 16,8\ kW}$$

Conclusion. As demonstrated by the presented calculations, for the Huawei SUN2000-50KTL-M 3 inverter where the configuration requires connecting two photovoltaic blocks (PVB) to a single MPPT the use of modules with a 72HL4 architecture is a more accurate and balanced solution compared to 66HL4M. Modules with 72 cells deliver lower current and higher voltage, enabling avoidance of current overload, reduction of thermal losses, and ensuring MPPT operation within the optimal voltage range with fewer photovoltaic modules (PVM) per PVB.

In virtually all cases where it is impossible to implement the "one MPPT - one PV string" scheme, a more optimal solution is the use of photovoltaic modules featuring reduced current and increased voltage. Such modules typically allow for more efficient load distribution across the inverter inputs, reduce thermal losses, and ensure MPPT operation within the optimal range.

Moreover, low-current, high-voltage modules are almost invariably the preferred choice for use in photovoltaic power plants in the private sector.

Chapter 2.3 has already provided a detailed examination of the design solution for a photovoltaic power plant with a capacity of 10 kW, based on the Huawei SUN2000-10KTL -M1-HC inverter using JKM630N-78HL4 and JKM630N-66HL4 modules. We will not revisit this topic but will note that the option with JKM630N-78HL4 proved more advantageous in terms of the combination of technical and

operational characteristics.

Note. *Photovoltaic modules from the 78HL4 and 72HL4 series are practically identical in terms of current characteristics. The increased power of the 78 HL4 module series is achieved by a higher output voltage, due to the addition of six extra silicon cells in the module structure. Therefore, the examples provided for comparison use modules from the 66HL4M series and one of the modules from either the 72HL4 or 78HL4 series depending on which best corresponds to the goal of elucidating the essence of the issue under consideration. Tables 6.6 and 6.7 present the primary electrical characteristics of the 72HL4 and 78HL4 series photovoltaic modules.*

Table 4.6. Main electrical characteristics of PV modules in the 72HL4 series

P_{mp}, W	575	580	585	590	595	600
V_{mp}, V	43,73	43,88	44,02	44,17	44,31	44,45
I_{mp}, A	13,15	13,22	13,29	13,36	13,43	13,50
V_{oc}, V	52,30	52,50	52,70	52,90	53,10	53,30
I_{sc}, A	13,89	13,95	14,01	14,07	14,13	14,19
Efficiency, %	22,26	22,45	22,65	22,84	23,03	23,23

Table 4.7. Main electrical characteristics of PV modules in the 78HL4 series

Pmp, W	625	630	635	640	645	650
Vmp, V	47,54	47,70	47,86	48,02	48,17	48,33
Imp, A	13,15	13,21	13,27	13,33	13,39	13,45
Voc, V	56,95	57,08	57,21	57,34	57,47	57,60
Isc, A	13,80	13,86	13,92	13,98	14,04	14,10
Efficiency, %	22,36	22,54	22,72	22,90	23,07	23,25

4. Design of small-scale photovoltaic power plants. Small-scale photovoltaic power plants are generally equipped with two MPPT controllers. However, due to the increase in photovoltaic module power ratings, primarily driven by rising current, it becomes difficult to design photovoltaic batteries (PVBs) with voltage near the nominal value, particularly when using both MPPT controllers.

Fortunately, for most inverters with power ratings below 6 kW, the maximum allowable power per MPPT exceeds the inverter’s nominal power.

For instance, the maximum allowable power per MPPT for single-phase Huawei

inverters rated at 6 kW or below is 6.6 kW, whereas for three-phase inverters of the same capacity, it reaches up to 8.8 kW per MPPT. This permits the use of a single MPPT, provided that the voltage requirements are met, thereby enabling the assembly of photovoltaic strings with a greater number of modules and, accordingly, ensuring a more optimal operating voltage. This solution also helps reduce costs for solar cable by decreasing the number of parallel connections. Furthermore, reducing the current in the DC circuit section decreases thermal losses in the cable by up to a factor of two, owing to the quadratic relationship between heat dissipation and current.

For example, in a three-phase photovoltaic power plant rated at 6 kW with a nominal DC-side voltage of 600 V, it is preferable to configure a single photovoltaic batterie (PVB) composed of 10 JKM600N-72HL4-BDV modules, with a maximum power point voltage (V_{mp}) under STC conditions of approximately 444.5 V, rather than constructing the system from two PVBs of 5 modules each with a voltage of 222 V.

The maximum permissible voltage of most modern single-phase inverters is 600 V, with a nominal voltage of approximately 360 V; the MPPT operating voltage range typically reaches up to 560 V.

Therefore, for single-phase photovoltaic power plants with a capacity up to 5 kW, for instance, based on eight JKM630N-72HL4-BDV modules, it is advisable to use a configuration comprising a single photovoltaic power batterie (PPB) connected to one MPPT input. It is essential to first ensure that the total peak power corresponds to the maximum permissible MPPT power rating. For such a photovoltaic power plant configuration, the PPB voltage at the minimum design temperature will be:

$$\mathbf{V_{OC} = N \cdot V_{OC\,STC} \cdot \left(1 + K_V \cdot \frac{(t - 25)}{100}\right) = 8 \cdot 57,08 \cdot \left(1 - 0,25 \cdot \frac{-20 - 25}{100}\right) = 508\ V}$$

Voltage at maximum power (V_{mp}) of the PV module at the maximum calculated cell temperature of +70 degrees:

$$\mathbf{V_{mp} = N \cdot V_{mp\,STC} \cdot \left(1 + K_V \cdot \frac{(t - 25)}{100}\right) = 8 \cdot 47,70 \cdot \left(1 - 0,25 \cdot \frac{70 - 25}{100}\right) = 340\ V}$$

This is especially important for systems in the private sector, where inverters are often installed inside residential or technical premises without active ventilation. Under such conditions, additional heat dissipation during the summer can cause excessive temperature rises both within the inverter itself and in the room, impairing thermal management and reducing equipment reliability.

This factor becomes even more critical for hybrid inverters, which are always installed indoors alongside battery storage systems.

An increase in air temperature in such an environment directly impacts the operating temperature of the battery storage system, potentially causing accelerated aging, reduced capacity, and even conditions that lead to thermal degradation. Therefore, minimizing heat dissipation through the appropriate selection of PV module configuration and optimal voltage is a fundamentally important factor in enhancing the reliability and service life of the entire system.

§4.5. Cable selection

Cable selection is one of the key factors affecting both the reliable operation of the photovoltaic power plant and the safety of its operation.

First, let us consider the solar cable on the direct current side, i.e., the section between the photovoltaic module and the inverter's DC input.

The primary technical requirements for the solar cable are as follows:

- It must be designed for long-term operation in direct current circuits with voltages up to 1500 V (DC), in accordance with the current standards for photovoltaic systems;
- Double insulation is mandatory – solar cables must have both internal and external insulation to ensure high electrical strength, protection against breakdown, mechanical damage, and environmental influences.

Thermosetting materials, such as cross-linked polyethylene (XLPE), are commonly used;

- must exhibit high thermal resistance – cable materials must endure prolonged operation at ambient temperatures up to 90°C and short-term conductor temperature

increases up to 120°C without insulation failure;

•the cable must be resistant to external influences — specifically, it must withstand ultraviolet radiation (UV), ozone, elevated humidity and condensation, as well as exposure to oils, acids, alkalis, and similar substances.

•it must possess high fire safety characteristics the cable must comply with the requirements of LSZH (Low Smoke Zero Halogen) categories and must not support combustion. Furthermore, it should emit low smoke during ignition and not release toxic gases. It must also restrict the propagation of fire when installed in bundles.

•it must have a long service life the design and materials of the cable should ensure reliable operation for at least 25 years under environmental conditions characteristic of photovoltaic installations: daily temperature fluctuations, rain, solar radiation, wind, and vibrations.

Currently, two types of solar cables are most widely represented in the Uzbekistan market: H1Z2Z2-K and PV1-F. A comparison of their main characteristics is provided in Table 3.8. For new projects, it is recommended to use the H1Z2Z2-K cable, as it offers superior operational performance and fully complies with the requirements of the contemporary European standard EN 50618. Although the PV1-F cable is produced according to the outdated standard TUV 2 Pfg 1169/08.2007, it is inferior in several parameters particularly in maximum allowable voltage, thermal resistance, and resistance to environmental exposure [43], [44].

Table 4.8. Comparison of characteristics of H1Z2Z2-K and PV1-F cables

Parameter	**H1Z2Z2-K**	**PV1-F**
Standard	EN 50618	TUV 2 Pfg 1169/08.2007
Nominal voltage, V (DC)	1500	1000
Operating temperature, °C	-40...+90	-40+90
Maximum conductor temperature, °C	+120	+120
UV resistance	High	Medium

Conductor Material	Tinned Copper (stranded, class 5)	Tinned Copper (stranded, class 5)
Insulation and Sheath Material	Cross-linked Polyethylene (XLPE)	Thermoplastic or Cross-linked Polyolefin
Double Insulation	Yes	Yes
LSZH	Yes	Not Always (Depends on the Manufacturer)
Resistance to Ozone, Moisture, Chemicals	High	Limited
Service Life	£ 25 Years	<25 Years
Suitable for Outdoor Installation	Yes (Without Additional Protection)	Yes, but only to a limited extent.

Recently, solar cables with aluminum conductors have started appearing on the market; some installers use them to reduce project costs often without proper notification or consent from the customer. This practice is unacceptable, especially in low- and medium-power systems, particularly when installing photovoltaic modules on rooftops.

Aluminum cables do not comply with the reliability and safety standards required for cable products in direct current circuits. They are prone to corrosion, exhibit increased contact resistance at connections, are sensitive to installation errors, and require regular maintenance. Under conditions of limited access, elevated temperatures, and exposure to environmental factors (UV radiation, moisture, dust), their use may lead to overheating, insulation melting, deterioration of contacts, and consequently, fire hazards.

In accordance with international standards, only copper conductors (preferably tinned) should be used on the direct current side of photovoltaic systems. Any deviation from these requirements must be agreed upon in advance with the client and be justified both technically and legally.

Table 4.9 presents the long-term permissible current values for cable type

H1Z2Z2-K depending on the installation method, for the most commonly used cross-sections - of 4 mm^2 and 6 mm^2, at a calculated ambient temperature of +60°C. The data reflect typical operating conditions for the installation of solar cables on building roofs and open sites. Given that in most cases multiple cables from different PV modules are installed, it is advisable to base calculations on the worst-case scenario the permissible current values for group (bundle) installations.

It should be noted that the provided values are approximate; for a more precise selection of current load, consulting the technical documentation of the specific cable manufacturer is recommended. The current of modern photovoltaic modules under the conditions of Uzbekistan rarely exceeds 16 A; therefore, cables with cross-sections of both 4 mm^2 and 6 mm^2 generally comply with the long-term permissible current ratings.

Table 4.9. Continuous permissible currents for solar cable H1Z2Z2-K

Cross-section, mm^2	Single installation in air, A	Single installation on surface, A	Group installation on surface, A
4	55	52	44
6	70	67	57

Nevertheless, it is recommended, whenever possible, to use cables with a cross section of 6 mm^2, as they provide not only lower losses and a greater thermal margin but also an increased contact area at connection points-MC4 connectors, fuse terminals, and other switching components. These sections are particularly prone to the risk of overheating and burning under conditions of weak or inadequate contact.

An additional advantage of using a cable with a cross-section of 6 mm^2 is the reduced voltage drop in the line. For the proper operation of the MPPT controller and the entire system, it is recommended that the voltage drop along the section from the photovoltaic module to the inverter’s DC input does not exceed 2%, and preferably — remains within 1%. This approach reduces power losses, enhances the stability of maximum power point tracking, and improves the overall energy efficiency of the installation.

From this arises the condition that limits the distance between the PV module and the inverter. If the voltage drop exceeds 2%, it is strongly recommended to increase the cable cross-section or reduce the distance between the PV module and the inverter. Using a cable with a 6 mm ^{2} cross-section instead of 4 mm ^{2} increases the permissible distance by a factor of 1.5.

Example. Calculate the voltage drop on a solar cable with a 6 mm² cross-section when connecting a photovoltaic module with an operating voltage (V_{mp}) of 600 V and a current at maximum power (I_{mp}) of 15 A, at a distance of 100 meters between the PV module and the inverter.

Resistance of the solar cable line considering the total length, including both the positive and negative conductors:

$$\mathbf{R = \rho \cdot \frac{L}{S} \approx 0,0175\ \Omega \cdot \frac{mm^2}{m} \cdot \frac{200\ m}{6\ mm^2} \approx 0,58\ \Omega}$$

Voltage drop: $$\mathbf{\Delta U = I_{mp} \cdot R = 15 \cdot 0,58 = 8,7\ V}$$

Thus, the voltage drop was approximately 8.7 V, or 1.45%.

Now, let us examine in greater detail the selection of the power cable section from the inverter to the connection point. Unlike solar cables, for which in 99% of cases the use of H1Z2Z 2-K with a cross-section of 1x6 mm^2 is sufficient, the choice of power cable demands a more careful approach. In addition to current load and permissible voltage drop, the selection of the power cable must consider the insulation material and the installation environment - whether it is an open roof, attic space, underground conduit, cable tray, or internal wiring. These conditions directly affect the selection of the cable brand and cross-sectional area.

First, it should be noted that the primary factor determining the permissible current load of a cable is the insulation aging rate, which directly depends on the conductor temperature during operation. Therefore, the current-carrying capacity of a cable is determined by the combination of the following parameters:

•Conductor material - the lower the conductor’s specific electrical resistance, the less heat is generated during current flow. Accordingly, under identical conditions, a

cable with a conductor made of a material with lower resistance (for example, copper) can carry a higher current without overheating compared to a conductor made of a material with higher resistance (for example, aluminum).

For example, the permissible current rating of a VVGng cable 4x50 mm^2 with copper conductors, when laid in air at an ambient temperature of +25°C, is 167 A. Meanwhile, for an AVVGng cable 4x50 mm^2 under the same installation conditions but with aluminum conductors, the permissible current rating is only 126 A.

- Insulation material - each type of insulation has its own allowable operating temperature. Accordingly, all else being equal, the higher the thermal tolerance of the insulating material, the greater the thermal load it can withstand, and thus the higher the current that can pass through the cable without exceeding the permissible temperature.

For example, cables with cross-linked polyethylene (XLPE) insulation, such as PvPGng(A)-HF, are rated for continuous operation at a conductor temperature of up to 90°C, with allowable short-term overheating up to 120°C. While cables insulated with polyvinyl chloride (PVC), such as VVGng, allow continuous operation only up to 7 0°C and short-term operation up to 90°C. Thus, XLPE cables can carry 10-20% more current than PVC-insulated cables of the same cross-sectional area under the same installation conditions. For example, the permissible current rating of a VVGng 4*50 mm^2 cable when installed in air is 187 A, whereas for a PvPGng(A)-HF 4*50 mim^2 cable, with the same cross-sectional area and copper conductor, it is 209 A.

- Ambient temperature the lower the ambient temperature, the more efficient the heat dissipation from the cable. This permits the transmission of higher current without exceeding the allowable conductor temperature. For cables with PVC insulation, the current-carrying capacity is specified at an ambient temperature of +25°C (when installed in air) and +15°C (in the ground), with a conductor design temperature of +7 0°C. For cables with cross-linked polyethylene (XLPE) insulation, the current-carrying capacity is standardized at an ambient temperature of +30°C (in air) and +20°C (in the ground), with a conductor design temperature of +90°C.

As ambient temperature rises, heat dissipation deteriorates, causing the cable to

reach its maximum operating temperature more rapidly [45]. Therefore, the permissible current must be reduced by applying correction factors. This consideration is particularly important when laying cables in warm environments such as rooms, attics, technical zones, and similar areas. Cables of the VVG and AVVG types with PVC insulation (see Table 4.10) are most susceptible to overheating, as they have a lower permissible conductor temperature and a steeper permissible current derating curve with increasing temperature compared to XLPE cables.

Table 4.10. Correction factors for cable currents based on air temperature

t, 0C	<-5	0	+5	+10	+15	+20	+25	+30	+35	+40	+45	+50
K	1,29	1,24	1,20	1,15	1,11	1,05	1,00	0,94	0,88	0,81	0,74	0,67

For photovoltaic power plants, the most optimal solution among the commercially available options is the use of cables with cross-linked polyethylene (XLPE) insulation PvPGng(A)-HF, which complies with the European VDE standard and is designated as N2XH-O/J. This type of cable is used in modern buildings, engineering structures, and critical sections of power supply system's where enhanced fire safety requirements apply. Decoding of the PvPGng(A)-HF cable:

- PV - insulation made of cross-linked polyethylene (XLPE), ensuring enhanced thermal and electrical strength;
- P - sheath composed of halogen-free polymer compounds, flame-retardant and free from toxic gas emissions;
- G - flexible cable featuring a multi-stranded current-carrying conductor;
- ng(A) - does not propagate fire when installed in a bundle; category A denotes the highest level of fire safety;
- HF (Halogen Free) denotes a halogen-free insulation and sheath composition with low smoke and gas emissions, complying with LSZH (Low Smoke Zero Halogen) standards.

The VVGng (or VVGng(A)-LS) cable is more commonly used in the CIS market. However, this cable is not resistant to UV radiation; its operational ambient temperature range is from -50°C to +50°C. Therefore, when installing the inverter on

the roof and routing the power cable along the roof, protection against direct sunlight must be provided. It is also advisable to incorporate a twofold reserve for current; that is, to apply a correction factor of 0.5.

Note. *A distinctive feature of photovoltaic power plants (PV plants) is that the highest current in the cable occurs during midday hours, when the generation power reaches its maximum. It is precisely during this period that the ambient temperature also reaches its peak.*

This 'symbiosis' of high currents and elevated temperature substantially increases the thermal load on the cable, necessitating a particularly careful approach to selecting the conductor cross-section and accounting for temperature correction factors in the design process.

However, copper cables are more expensive, so in practice, AVVG-type cables are more commonly used. Regarding installation conditions and correction factors, the situation is analogous to that of VVG cables. Nevertheless, the permissible current rating of AVVG cables is lower compared to VVG cables; therefore, under equal conditions, a cable with a larger cross-section is required. This is not always feasible, as most inverters' power terminals are designed specifically for copper cable connections, and there is a risk that an aluminum cable with an increased cross-section simply will not fit into the terminal clamp.

Furthermore, to ensure sealing and ease of connection, it is recommended to use a five-core cable when connecting to the inverter, which is challenging when using AVVG such cables are rarely manufactured in a five-core configuration. Additionally, at connection points, it is advisable to use tinned terminals, as the inverter is often installed outdoors, and tinning enhances contact resistance to corrosion under conditions of high humidity.

Considering all of the above, if the decision is made to use aluminum cable for economic reasons, it is recommended to connect directly to the inverter using a short section of five-core copper cable with tinned terminals, with the other end connected to the circuit breaker installed adjacent to the inverter. From the breaker to the network connection point, the use of aluminum cable is permitted (see Fig. 3.17).

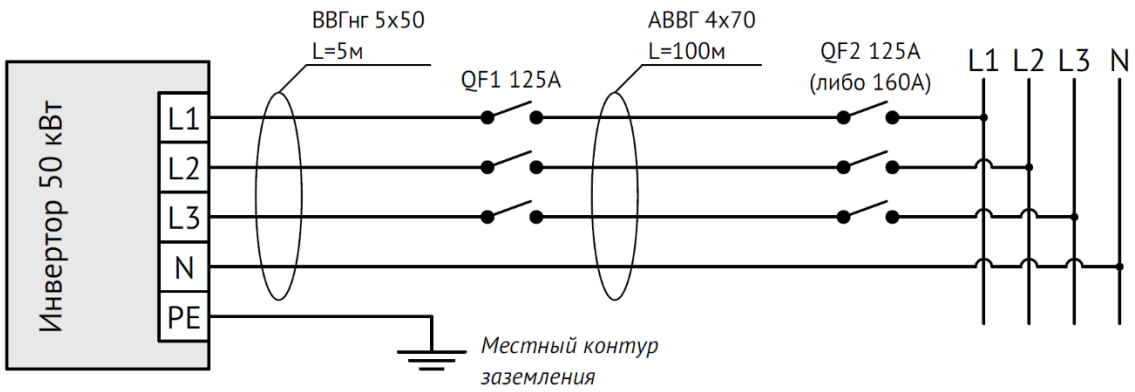

Figure 4.17. Diagram of the inverter connection to the distribution network.

The selection of the power cable is performed according to two main criteria: the permissible continuous current load and the allowable voltage drop. Traditionally, for three-phase inverters, the calculated current is determined by the following formula:

$$\mathbf{I_{cal}} = \frac{\mathbf{P_{cal}}}{\sqrt{3}\cdot\mathbf{U_{nom}}\cdot\mathbf{cos\varphi}};$$

where P_{cal} - the calculated power of the photovoltaic plant, defined as the sum of the nominal powers of all installed photovoltaic modules, considering a correction factor that accounts for the climatic characteristics of the region. Depending on the level of solar radiation and the duration of effective generation, this coefficient is usually taken within the range of 0.85-0.95; U_{nom} - nominal line voltage; $\cos\varphi$ - can be assumed to be equal to 1, since by default grid-tied inverters operate exclusively in active power generation mode.

However, it is necessary to consider the specific characteristics of Uzbekistan's power system, where the voltage in some network locations can be significantly lower than the nominal value particularly in remote rural areas or during peak load periods. According to standard settings, the inverter automatically shuts down if the voltage drops by more than 15% from the nominal value and only resumes operation after the network parameters are restored within permissible limits. In practice, this often results in prolonged inverter downtime and, consequently, generation losses. For this reason, at many facilities, undervoltage protection settings are intentionally relaxed, which, nevertheless, positively impacts the network itself, since the power generated by the

photovoltaic power plant partially contributes to an increase in voltage along the section.

Important! It is important not to confuse the relaxation of the inverter's undervoltage protection settings with that of the overvoltage protection. In the former case, expanding the permissible range of reduced voltage typically aids in stabilizing the network condition by sustaining generation, partially compensating local load, and elevating voltage on the line.

In the second case, loosening the protection settings based on maximum voltage can lead to excessive voltage rise in the grid, which is hazardous and may cause emergency equipment shutdown, overheating, failure of sensitive electronics, and in extreme cases even fire.

Therefore, when operating under elevated grid voltage conditions, it is recommended to use the P-U function automatic reduction of the inverter's active power as grid voltage increases, which helps limit further voltage rise and enhances system stability.

Under conditions of reduced voltage, for the same power rating, the current delivered by the inverter may exceed the calculated value. However, the inverter is limited by its design maximum output current (Maximum Output Current) and cannot exceed this limit. Taking this into account, when designing and selecting the power cable for a photovoltaic power plant where the total photovoltaic module power corresponds to the inverter's power rating, it is recommended to refer not only to the calculated current but also to mandatorily consider the maximum output current parameter specified in the technical specifications of the specific inverter model.

To protect the cable and inverter from overload and short circuits on the alternating current side, a circuit breaker is installed. Considering the substantially higher power of the power system relative to that of the inverter, the installation of a circuit breaker, and if necessary, a fuse at the start of the cable (on the power system side) is mandatory. This measure is necessary to ensure disconnection from the power system side in the event of cable damage along the section from the inverter to the connection point.

Table X presents the recommended cross-sections for AVVG and VVG cables under standard installation conditions, along with the nominal current ratings of circuit breakers for three-phase Huawei inverters of various power ratings. When laying cable on the roof, through an attic, or technical room with elevated ambient temperature, it is recommended to use cable with an increased cross-section considering the reduced temperature coefficients.

Table 4.11. Recommended cable cross-section and nominal circuit breaker current.

Power inverter, kW	Max. output current, A	Nominal current of the circuit breaker,	VVG	AVVG
5	8,5	15	4 mm^2	6 mm^2
10	17,0	25	6 mm^2	10 mm^2
20	33,5	40	16 mm^2	25 mm^2
30	50,4	63	25 mm^2	35 mm^2
40	67,2	80	35 mm^2	50 mm^2
50	79,8	125	50 mm^2	70 mm^2
60	100	125	50 mm^2	70 mm^2
100	160,4	200	90 mm^2	120 mm^2

For three-phase inverters, the voltage drop in the cable is calculated by the formula:

$$\Delta U_{cal} = \frac{(P_{cal} \cdot r + Q_{cal} \cdot x) \cdot L}{U_{nom}}$$

where: P_{cal} and Q_{cal} - calculated values of active and reactive power; r, x - active and reactive resistances of the cable; L - length of the cable.

Considering that inverters operate by default exclusively in the mode of active power generation, the calculation of voltage drop can be simplified by excluding the reactive component. In this case, the formula takes the following form:

$$\Delta U_{cal} = \frac{P_{cal} \cdot r \cdot L}{U_{nom}};$$

For a photovoltaic power plant where the total power of the photovoltaic modules

corresponds to the inverter's power rating, the formula can be further simplified by using the nominal (or, for some photovoltaic power plants, the maximum) current of the inverter: $\Delta \mathbf{U_{cal}} = \mathbf{I_{nom}} \cdot \mathbf{r} \cdot \mathbf{L}$;

For single-phase inverters, when calculating voltage drop, it is necessary to consider double the cable length, since the current travels from the inverter to the connection point and returns via the neutral conductor.

During the design of a photovoltaic power plant, it is essential to ensure that the total voltage drop in the direct current section from the photovoltaic modules to the inverter and in the alternating current section from the inverter to the grid connection point - is minimized and, in any case, does not exceed 5%:

$$\Delta \mathbf{U}_{\mathrm{AC}} + \Delta \mathbf{U_{DC}} < \mathbf{5}\%$$

Note. *When laying power cables underground, it is recommended to use armored cables, as they provide additional mechanical protection against external impacts. Alternatively, when using non-armored cables, it is necessary to lay them in special protective pipes or corrugated conduits that provide reliable protection against damage in the soil.*

Note. *When laying cables along overhead lines, it is recommended to use self-supporting insulated wire (SSIW), which ensures reliability, mechanical strength, and resistance to atmospheric influences.*

§4.6. Interaction of the inverter with components of the power system

During the integration of a photovoltaic power plant (PV plant) into an existing power supply system, it is essential to ensure the coordinated operation of all components of the power system. In particular, it is important to consider the interaction of the grid-connected PV plant with reactive power compensation units (RPCUs) and the diesel generator unit (DGU).

1. Influence of the PV Plant on the Operation of RPCUs. The purpose of the RPCU and its impact on losses in electrical networks were thoroughly examined in section 2.4. This section addresses the influence of the grid inverter connection point selection on the operation of the RPCU.

There are fundamentally two types of reactive power control devices, depending on the measurement point and control method:

- A reactive power control device without feedback is a device with internal measurement, meaning it does not account for its own reactive power (see Fig. 4.18 A). The distinctive feature of this design is that the system does not 'see' the reactive power compensated by its own capacitor steps. Consequently, compensation control is performed according to a predetermined algorithm, without analyzing the system's response, which may lead to overcompensation - excessive injection of reactive power into the grid.
- The feedback voltage regulator (RPCU) is an external measurement device, that is, it accounts for its own compensation (see Fig. 4.18 B). In this case, current transformers are installed after the RPCU connection point, and the system takes into account the reactive power supplied by its own capacitors. This enables more precise monitoring of the overall power factor (cosφ) and control of the compensation stages according to actual network conditions, thereby reducing the risk of overcompensation.

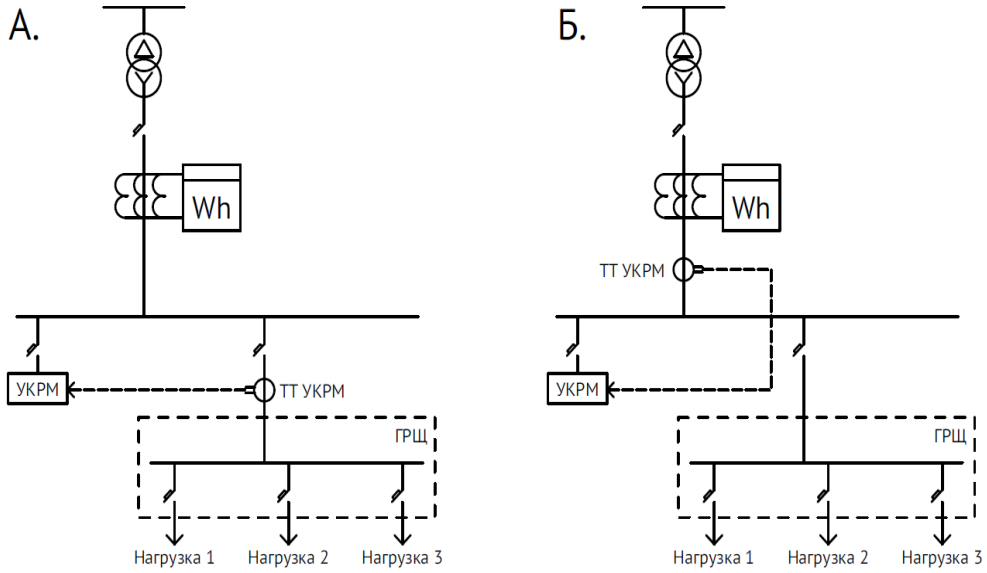

Figure 4.18. RPCU without feedback (A) and with feedback (B).

Next, we examine the RPCU with feedback, which is most commonly used when the connection point of the photovoltaic power plant is situated on the 0.4 kV busbars of the transformer substation or the input-distribution device. If the grid inverter is connected as shown in Figure 4.19, the RPCU current transformer ‘perceives’ both the load and the power generated by the photovoltaic power plant.

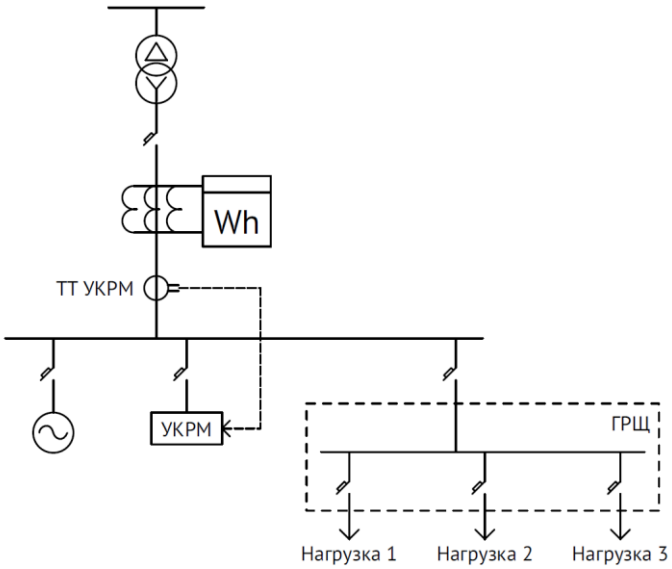

Figure 4.19. Connection of the photovoltaic power plant incorporating the RPCU current transformers within the measurement zone.

By default, the grid-connected inverter generates active power, and as generation increases, the active power flowing through the TT decreases, while the reactive power remains constant. Consequently, the power factor begins to decline, although the load conditions remain unchanged.

At a certain point, the generation of the photovoltaic power plant may exceed consumption, initiating active power export to the grid - the system's operating point will shift from the first quadrant to the fourth. In this situation, not all RPCU controllers can correctly interpret the sign and direction of the current, which may cause malfunctions, such as the false activation of additional compensation stages.

Therefore, it is necessary to use a RPCU controller that supports operation with bidirectional power flow or to modify the circuit configuration so that the RPCU current transformer measures only the load, excluding the power generated by the photovoltaic power plant (see Figure 4.20).

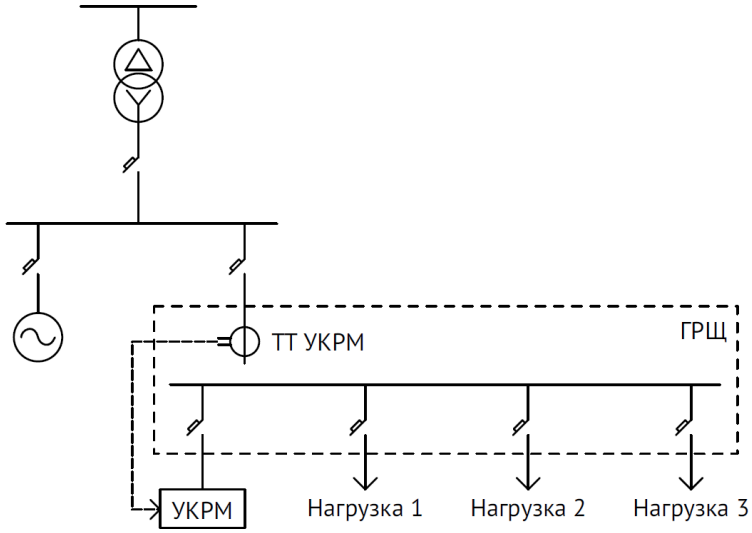

Figure 4.20. Connection of a photovoltaic power plant excluding current transformers from the UKRM measurement zone.

2. Parallel operation of a grid-connected photovoltaic power plant and a diesel generator unit. A grid inverter cannot operate without the presence of a reference voltage. In the standard configuration of a photovoltaic power plant, such a reference source is the centralized power system (CPS). However, in the event of a power outage in the centralized CPS, the reference voltage can be supplied by a diesel generator unit (DGU). It is important to note that the diesel generator unit (DGU) does not operate in parallel with the centralized electric power system (EPS); it is activated as part of an isolated power system formed by an automatic transfer switch (ATS) following the loss of voltage from the external EPS (see Figure 4.21). Therefore, the DGU can serve as a reference source for the grid inverter only if both are components of an isolated power system, disconnected from the main grid.

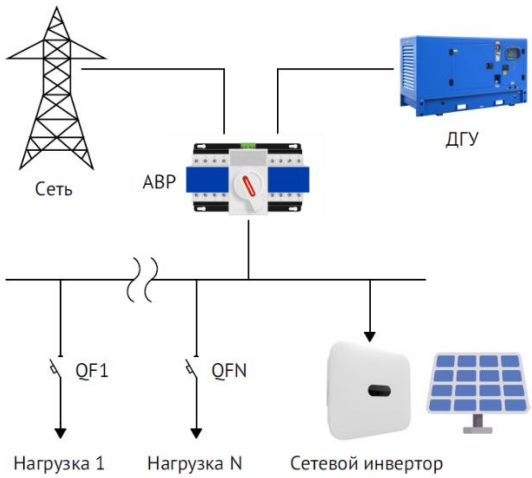

Figure 4.21. Network configuration in which the grid-tied inverter and diesel

generator set form a locally isolated power system upon disconnection from the centralized power station.

However, such an isolated system with two energy sources the photovoltaic power plant grid-tied inverter and the diesel generator set is unstable without a coordinated control system. By default, the grid-tied inverter seeks to deliver the maximum possible active power without taking into account the actual load demand. This may lead to excessive generation (see Figure 4.22), causing increased voltage and frequency in the isolated network, which may result in the emergency shutdown of the diesel generator unit (DGU) and, in some cases, its damage.

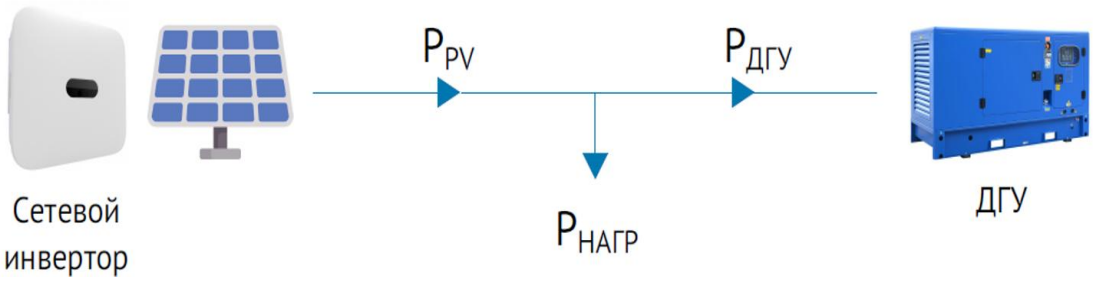

Figure 4.22. Scenario of excessive active power generation in an isolated power system.

For this reason, two technically justified solutions are possible. The first option - Connection of the grid-tied inverter before the ATS device, ensuring that in the event of a centralized power plant outage, the grid-tied inverter and the diesel generator unit are not located within the same isolated power system (see Figure 4.23).

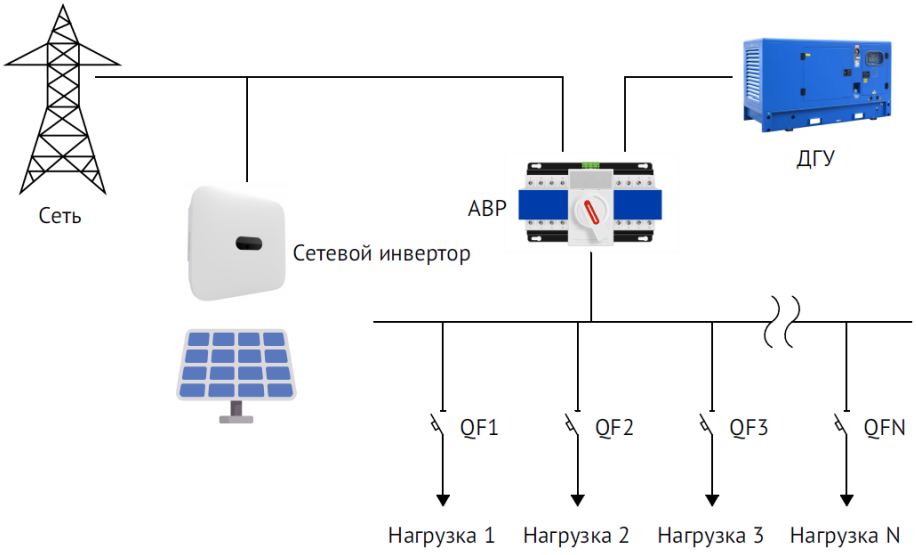

Figure 4.23. Connection diagram of the grid-tied inverter before the ATS device.

The second option involves using a dedicated control unit that limits the output power of the grid-tied inverter in accordance with the current load and the diesel generator unit's capabilities, thereby preventing excessive generation (see Figure 4.24).

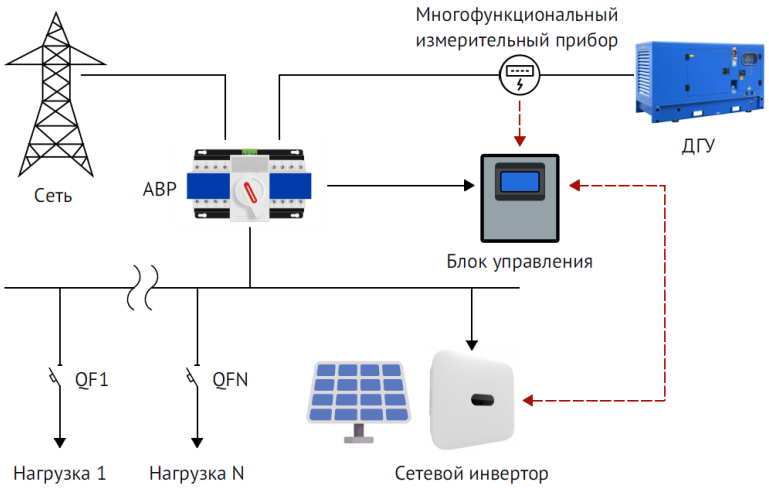

Figure 4.24. External control unit for managing power balance in an isolated power system.

3. Cooperative operation of photovoltaic power plants and voltage stabilizers. For most grid inverters, the permissible output voltage range significantly exceeds the operating range of the majority of household or industrial voltage stabilizers. Therefore, installing a stabilizer specifically to ensure correct inverter operation is usually unnecessary unless stipulated otherwise by the equipment manufacturer under warranty terms. In standard connection diagrams, it is recommended to connect the grid-tied inverter upstream of the voltage stabilizer (see Fig. 4.25).

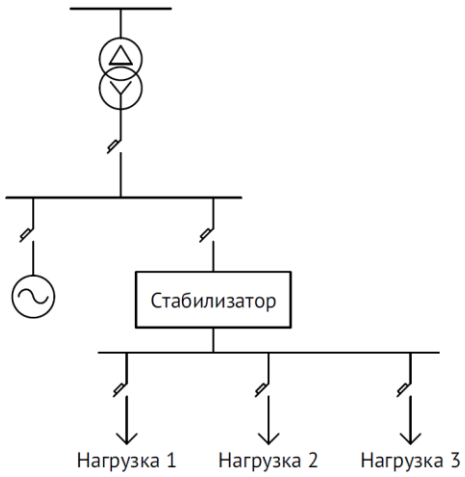

Figure 4.25. Connection diagram of the voltage stabilizer in a system with a grid-tied inverter.

Installing the stabilizer between the inverter and the grid may result in undesirable effects, especially under conditions of high generation. Specifically, the voltage at the inverter output may be maintained within permissible limits due to the stabilizer's operation, while the grid voltage increases, creating a risk of overvoltage and damage to the equipment connected to the grid. Furthermore, not all stabilizers are designed to operate in reverse power flow mode. When generation from a photovoltaic power plant passes through the stabilizer towards the grid, this may cause damage to the stabilizer.

Installing a stabilizer is justified for hybrid or autonomous (on/off) inverters, since during parallel operation with the grid, the voltage at the inverter's EPS output coincides with the grid voltage. Accordingly, installing a stabilizer can ensure stable voltage for loads connected to the EPS.

Installing a voltage stabilizer between the diesel generator unit (DGU) and the load is not recommended. It should be installed before the automatic transfer switch (ATS). This issue is especially critical during the start-up of the DGU, when the voltage is unstable and the stabilizer may attempt to compensate for voltage dips, resulting in additional current surges. Such conditions may cause generator overload, activation of protection devices, or even failure of both the stabilizer and the connected equipment.

§4.7. Grounding

Grounding is critically important for the safe operation of a photovoltaic power plant, as well as for any electrical equipment. It performs several key functions, ensuring both personnel protection and reliable equipment operation.

In photovoltaic power plant systems, grounding serves the following functions:

- Protection against electric shock – in the event of insulation failure of live parts (e.g., due to overheating, aging, or mechanical damage), grounding provides a path for fault current to flow to the earth, thereby reducing touch voltage and preventing electric shock to personnel. This is especially important in direct current (DC) systems, where leakage may not be as evident as in alternating current (AC) systems.
- Ensuring the proper operation of protection systems grounding is essential for the correct functioning of protective devices such as residual current devices (RCDs),

differential circuit breakers, and ground fault protection. Without grounding, these devices may fail to operate correctly or at all during an emergency.

- Equipment protection from over voltages photovoltaic power plant components are exposed to atmospheric and switching over voltages, particularly when installed in open areas and on building roofs. Properly executed grounding, combined with surge protection devices (SPD), allows the dissipation of discharge energy into the ground, preventing insulation breakdown and equipment damage.
- Reducing the level of electromagnetic interference - the presence of high-quality grounding contributes to the reduction of high-frequency noise and enhances the electromagnetic compatibility of system components. This is especially important for inverters, monitoring systems, controllers, and other sensitive devices.
- Functional grounding certain system elements, such as cable shields, metal enclosures, and panels, are grounded not only for protective purposes but also to ensure the proper functioning of the system itself (for example, eliminating potential differences between modules, reducing interference in measurement circuits, etc.).

Grounding errors are among the most frequent causes of failures and malfunctions of equipment in photovoltaic power plants. Incorrect implementation of the grounding system may result in uncontrolled potential differences between elements, false triggering of protective devices, impaired communication between components, and even fire hazards.

Therefore, in the design and installation of the grounding system, it is essential to comply with regulatory requirements (PUE, GOST, IEC), consider soil type, grounding resistance, contour configuration, and specific equipment placement. Accordingly, it is recommended to thoroughly review the regulatory requirements before commencing the design of the photovoltaic power plant to ensure both safety and standards compliance. Clearly, the lower the grounding contour resistance, the higher the level of the system’s electrical safety. In practice, for networks with a voltage of 0.4 kV, it is usually accepted that the resistance of the grounding device should be less than 4 ohms, ensuring reliable operation of protective devices and reducing touch voltages to a safe level.

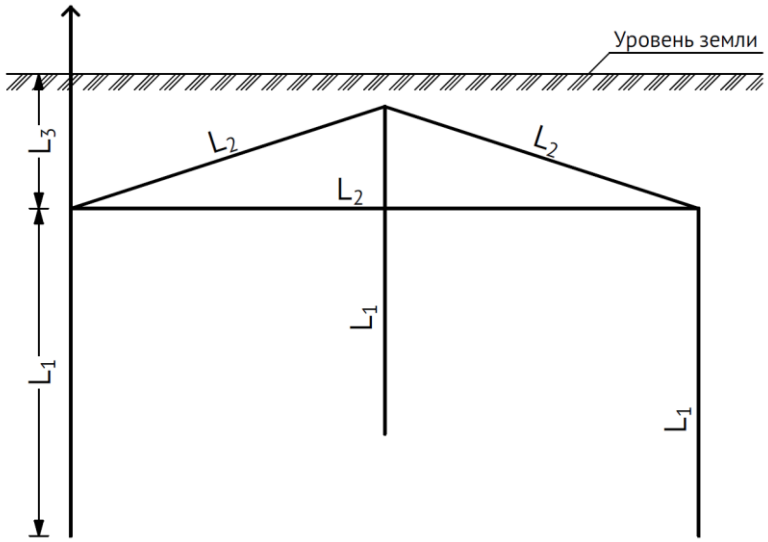

Figure 4.26. Typical grounding circuit diagram.

Figure 4.26 presents one of the most common configurations for the grounding circuit. Three vertical ground electrodes (e.g., rebar or steel angle) are installed at the vertices of a triangle.

The following may be used as grounding electrodes:

- A steel angle with a cross-section of at least 50x50 mm and a wall thickness of at least 4 mm or steel rebar with a diameter of at least 16 mm.

The length of the vertical grounding electrodes shall be at least 2.5 m (L1). After installation, they are interconnected by a horizontal grounding electrode laid at a depth of no less than 0.5 m (L3), preferably up to 1 meter, to enhance reliability during seasonal variations in soil moisture and temperature. Horizontal connectors are typically manufactured from the same angle iron, with a length (L2) not less than L1, forming an equilateral triangle. All connections are made to ensure reliable electrical contact and corrosion resistance throughout the entire service life of the grounding system.

Important! Most inverters do not operate without grounding; if it is absent, the system issues an error (Abnormal grounding) and blocks startup. Some installers attempt to circumvent this by driving short rebar into the ground or by connecting to building structures. This is categorically unacceptable, as such 'grounding' may deceive the system but does not provide a safe leakage current resistance. Consequently, the risk of electric shock, protection failure, and equipment malfunction increases.

§4.8. Lightning protection

The design of lightning protection necessitates a separate, in-depth consideration and is not fully addressed within this section. The purpose of this section is to provide a general understanding of the operational area of lightning protection components, since, in practice, there are frequent instances where a separately installed rod, extending only a few meters above the photovoltaic modules, is presented as a fully developed lightning protection system for a photovoltaic power plant spanning several tens of square meters, which is technically unfounded and does not ensure reliable protection for the entire installation.

There are two widely used methods for determining the lightning protection zone:

- Protection angle method;
- Rolling sphere method.

The protection angle method is a simplified geometric technique applicable for assessing protection zones of point objects as well as compact installations, such as photovoltaic power plants mounted on building rooftops. In such cases, it enables a rapid determination of the coverage area of individual lightning rods installed adjacent to equipment. The method is based on drawing an inclined line from a point at 0.85 of the total height of the lightning rod, at a specified angle known as the protective angle. The area within this angle is regarded as protected from a direct lightning strike (see Figure 4.27).

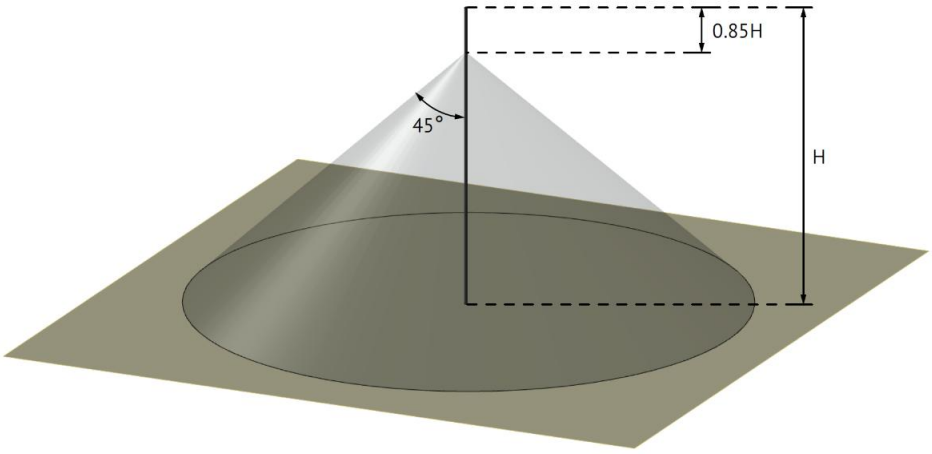

Figure 4.27. Lightning protection coverage zone using the protective angle method.

The higher the protection class, the smaller the angle and, consequently, the smaller the coverage area. For example, for objects up to 20 m in height, the angle can reach 45° under protection class III. At higher protection levels (class I-II), the angle decreases to 20-30°.

The protective angle method is not recommended for calculating lightning protection of ground-mounted photovoltaic power plants, particularly those with large surface areas, low installation heights, and distributed configurations. In such cases, it yields inaccurate assessments and does not ensure complete protection. For such facilities, the swinging sphere method is considered more accurate and reliable.

The swinging sphere method is the most universal and precise approach for determining the lightning protection zone and is applied to the calculation of protection for any category of objects, including distributed, extended, and low-lying installations, such as ground-based photovoltaic power plants. This method is particularly relevant for systems with a large number of elements situated in open areas, where other methods fail to provide a reliable assessment.

The method involves the conceptual movement of an imaginary sphere of a specified radius along the surface of the ground and equipment. The radius of the sphere is defined by the lightning protection class, in accordance with standards (e.g., IEC 62305 [38], [40]):

- Class I - 20 m
- Class II - 30 m
- Class III - 45 m
- Class IV - 60 m

All areas of the facility that the sphere cannot contact while “rolling” over are considered to be within the protection zone of the lightning rods and thus shielded from direct lightning strikes (see Figure 4.28).

The rolling sphere method enables consideration of terrain, structure elevations, and the positioning of lightning rods in three-dimensional space, making it a primary tool for designing lightning protection systems for modern facilities, including photovoltaic power plants, substations, antennas, and buildings with complex

architectural forms.

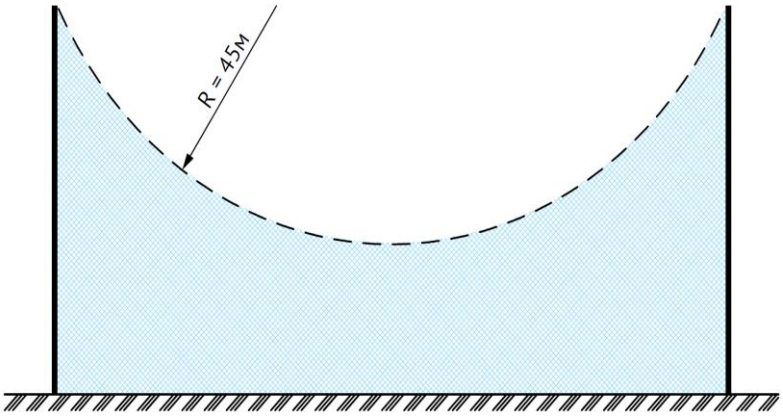

Figure 4.28. Lightning protection coverage area using the rolling sphere method.

The grounding scheme for lightning protection depends on multiple factors and necessitates a tailored approach. When installing a lightning rod on the roof, it is generally necessary to ground it to the building's main grounding system; however, it is essential first to verify that the grounding device complies with regulatory requirements. This is important to eliminate hazardous potential differences between the lightning protection system and other elements of the electrical installation, as well as to ensure reliable potential equalization within the building during a lightning strike.

If a separate grounding circuit is used for lightning protection, a minimum distance of 10 meters must be maintained from the protective grounding circuit of the electrical installation. This measure is necessary to prevent hazardous potential differences that may occur when impulse lightning current passes through the lightning protection system.

If it is not possible to maintain such a distance, both grounding devices must be united into a common grounding system or potential equalization between them must be established using conductors of the appropriate cross-section or spark gaps in accordance with the requirements of the Electrical Installation Regulations (PUE) [45].

Important! Grounding of lightning protection to building structures is prohibited unless these structures are officially included in the grounding system.

CHAPTER 5. DESIGN OF WIND POWER PLANTS

§5.1. Wind and its formation

According to RES market research, Brinkmann Consulting forecasts that approximately 1.9 TW of new wind power capacity will be installed worldwide between 2023 and 2033. According to the International Renewable Energy Agency (IRENA), the total installed wind power capacity globally reached 899 GW by the end of 2022. In line with Brinkmann's projections, around 130 GW of new onshore and offshore wind power plants were commissioned in 2023 alone, with the majority located in the Asia-Pacific region. During the period 2023–2033, the wind energy market is expected to grow at an average annual rate of approximately 6%. According to analytical estimates, by 2033 the annual capacity additions will reach around 230 GW, with about two-thirds of this capacity coming from onshore wind power plants. The rapid growth of wind energy is driven by strong policy support, including the Inflation Reduction Act in the United States, decarbonization strategies in China and the European Union, the entry of new countries into the offshore wind market, and the increasing demand for green hydrogen. These factors outweigh existing technical and economic barriers.

The use of wind energy dates back to ancient times. Initially, people utilized windmills to perform practical tasks such as pumping water and grinding grain. Archaeological evidence suggests that the earliest windmills were built in the 9th century in the Middle East, near present-day Afghanistan and Iran. These early devices featured vertical-axis designs with rectangular blades covered with fabric and were primarily used for grain milling and water pumping. Subsequently, the use of wind energy spread across the Middle East, Central Asia, China, and India. The global potential of wind energy is enormous, estimated at approximately 175,000-220,000 TW·h per year, with a total capacity of (20-25) × 10^9 kW. This is about 2.5 times greater than the current global energy consumption. However, due to technical and economic constraints, only about 5% of this potential can be practically utilized, and in reality, even a smaller fraction is currently being exploited. Wind is an atmospheric phenomenon resulting from the uneven heating of the Earth's surface and the rotation

of the Earth around its axis. It is characterized by the movement of air masses within the atmosphere. In other words, wind is a product of atmospheric circulation processes. The efficient operation of wind power systems depends directly on wind parameters, particularly its speed, pressure, and directional stability.

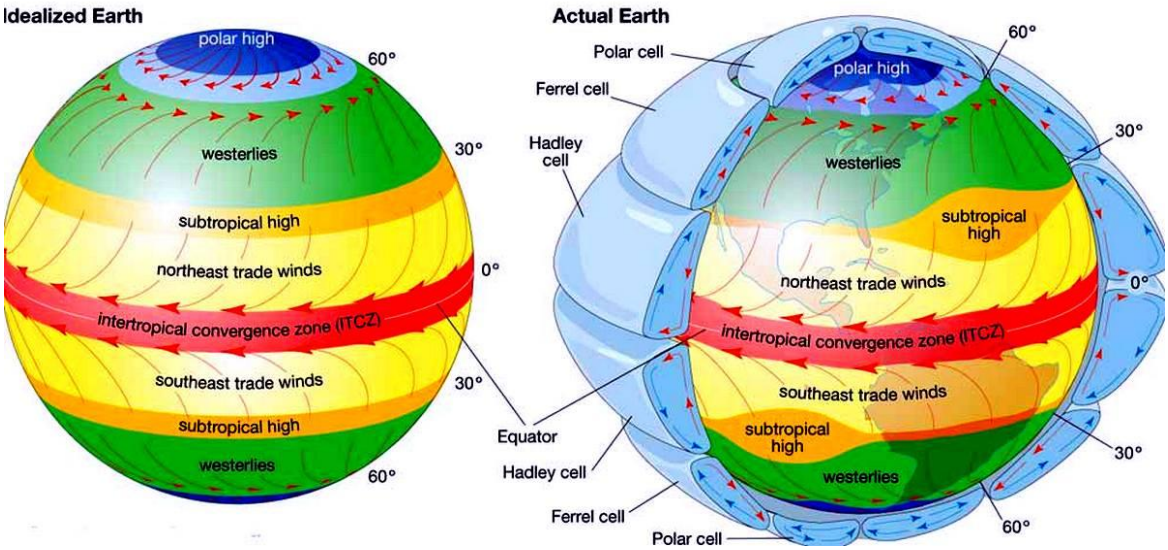

Figure 5.1. Periodic motion of air masses caused by uneven heating of the Earth's surface and the Coriolis inertial force resulting from the Earth's rotation about its axis.

Wind energy has a long history and is one of the oldest renewable energy sources utilized by humanity. The earliest simple wind-driven machines were used in Egypt and China. In particular, the remains of stone windmills dating back to the 2nd–1st centuries BC have been preserved near Alexandria in Egypt. According to historical sources (D.J. de Renzo), windmills became widespread in the Middle East by the 11th century and later appeared in Europe by the 13th century. During the Middle Ages, specific regulations governing the use of windmills were also established. In the second half of the 19th century, wind energy began to be widely utilized in the United States. During this period, more than six million small wind devices, each with a capacity of approximately 0.75 kW, were installed for electricity generation, water pumping, and various mechanical applications. Water pumping systems predominantly employed horizontal-axis wind wheels with diameters ranging from 3.7 to 4.9 meters, constructed from metal blades and equipped with tail vanes (wind vanes) to align with the wind direction. After World War II, a new stage in the development of wind energy began.

In Denmark, three experimental wind power plants with capacities of 12, 45, and 200 kW were developed and tested, capable of operating in parallel with the electrical grid. These installations were successfully operated until 1960. However, the project was discontinued after it was determined that the cost of electricity generated was approximately twice as high as that produced by internal combustion engine-driven generators.

Significant research efforts in wind energy were also carried out in the United Kingdom during the 1940s and 1950s. During this period, wind characteristics were measured at more than 100 locations across the British Isles. In 1950, the “North of Scotland Hydroelectric Board” conducted experimental studies on a wind power installation located in the Orkney Islands. The system was designed to produce 100 kW at a wind speed of 15.6 m/s and operated in conjunction with a diesel power station until 1955. However, its operation was eventually discontinued due to technical challenges encountered during installations.

The physical nature of wind motion is closely associated with the Coriolis force. The Coriolis force is the apparent force resulting from the Earth’s rotation, which causes moving objects such as air masses, water currents, and aircraft to deviate from a straight path. Together with the uneven heating of the Earth’s surface, this force plays a key role in shaping global atmospheric circulation and wind patterns.

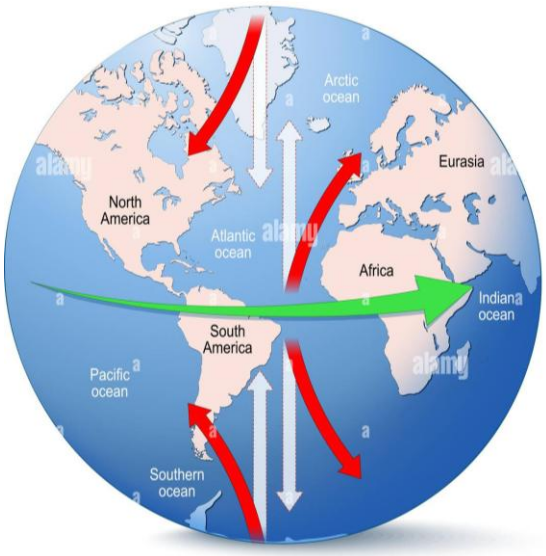

Figure 5.2. Direction of the Coriolis force.

The Earth rotates from east to west. As a result of this rotation, the trajectory of

any moving object does not appear as a straight line but rather as a deflected path. In the Northern Hemisphere, the direction of motion is deflected to the right, whereas in the Southern Hemisphere, it is deflected to the left. Wind energy is typically determined based on the airflow passing through a surface area oriented perpendicular to the wind direction, and it can be expressed by the following equation:

$$N_{wind}=0,0049\cdot\rho\cdot\upsilon\cdot A \qquad (5.1)$$

where: ρ – air density (dependent on temperature and atmospheric pressure), kg/m³; v - air flow velocity, m/s; A - cross-sectional area (swept area), m².

The amount of energy delivered by a wind energy conversion system differs significantly from the total energy available in the airflow. This is because a portion of the wind energy is lost in the rotor blades, gearbox, and generator. These losses are accounted for by the wind energy utilization coefficient (power coefficient). By considering the area perpendicular to the wind direction as the swept area defined by the rotor diameter, the power of a wind energy conversion system can be expressed by the following equation:

$$N_{turbine.power}=0,00386\cdot\ \rho\cdot\upsilon\cdot D^2\cdot\xi_{tur.}\cdot\eta_{gearbox}\cdot\eta_{generator} \qquad (5.2)$$

where: D - rotor (swept) diameter, m; $\eta_{gearbox}$ and $\eta_{generator}$ - efficiencies of the gearbox and generator, respectively; $\xi_{turbine}$ - aerodynamic energy losses in the rotor blades.

According to theoretical calculations, the power coefficient (C_p) of wind turbines can reach up to 48% under ideal conditions. However, in practice, the overall efficiency of wind energy conversion systems is lower due to mechanical and electrical losses within the system. In wind turbines, the blades are typically oriented perpendicular to the wind direction, where they convert the kinetic energy of the airflow into rotational motion of the rotor. The power output of a wind turbine primarily depends not on the number of blades, but on the rotor diameter, which determines the swept area. As the diameter increases, the swept area expands, resulting in a higher amount of captured wind energy. The power of a wind turbine is strongly dependent on wind speed and increases proportionally to the cube of the wind velocity. At the same time, increasing the number of blades may lead to higher aerodynamic drag; therefore, optimal designs usually employ 2–3 blades.

In general, the power of a wind turbine can be expressed by the following equation:

$$N_{wind.power.device}=f(\upsilon/n)$$

§5.2. Prospects for the utilization of wind energy in Uzbekistan

Extensive scientific research is being conducted in Uzbekistan to assess the potential of wind energy resources and to ensure their efficient utilization. Until recently, the gross (theoretical) wind energy potential of the country was estimated at approximately 2.2 million tons of oil equivalent (toe). However, these assessments did not fully account for the high wind energy potential of specific regions such as Navoi, Ustyurt, Bukhara, and Bekabad. Moreover, these estimates were primarily based on data obtained from actinometric stations located far from each other and were calculated for relatively low heights of 5–8 meters. In practice, however, wind energy assessments should consider heights of 25–100 meters, which are more relevant for modern wind turbine operation.

In 2013, the First President of the Republic of Uzbekistan emphasized the importance of reassessing the potential of renewable energy resources and improving their utilization efficiency through official decrees on the development of alternative energy sources. In line with these directives, in 2015, comprehensive studies were carried out in collaboration with German companies Intec-Copa and GEONET, together with JSC “Uzbekenergo,” to evaluate wind energy resources and develop a national wind energy map. Within the framework of these studies, the wind energy potential of six major regions of the country was assessed, and the feasibility of their practical utilization was evaluated. Using advanced 3D modeling techniques, German specialists developed a wind atlas of Uzbekistan.

The results of these studies identified the regions of Navoi, Bukhara, Tashkent, Kashkadarya, Samarkand, and the Republic of Karakalpakstan as the most promising areas for the installation of large-scale wind turbines. According to the research findings, the gross technical wind energy potential of Uzbekistan at a height of 80 meters is estimated to be approximately 520 GW. This significant potential demonstrates that Uzbekistan has substantial opportunities for the development of

wind energy and provides a strong foundation for expanding the use of renewable energy sources in the future.

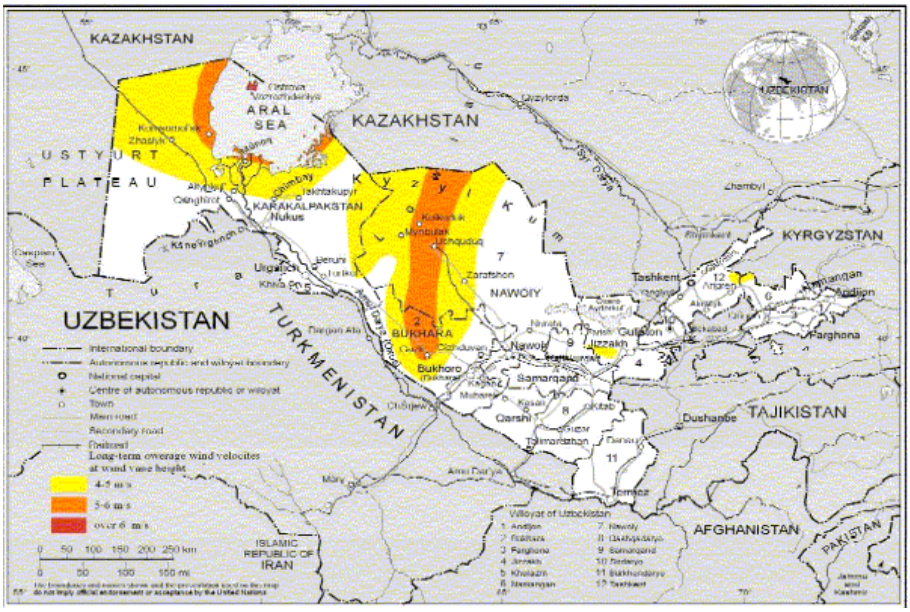

Figure 5.3. Wind energy resource map of the territory of Uzbekistan.

In Uzbekistan, a range of projects focused on the deployment of alternative energy sources are currently being implemented, alongside the continuous development of a robust regulatory and legal framework. A comprehensive assessment of wind energy potential enables a high-quality evaluation of wind resources, thereby facilitating the increased integration of renewable energy sources into the national energy system. This, in turn, contributes to enhancing the reliability of electricity supply and maintaining the country's energy balance in the long term.

During their recent visit to Uzbekistan, international consultants held a series of practical meetings and negotiations with representatives of ministries and governmental agencies. Within the framework of these discussions, agreements were reached to further strengthen cooperation in the research and implementation of modern wind energy technologies in the country. Foreign experts committed to continuing their work on the assessment of wind energy resources, sharing their knowledge and experience with local specialists, and supporting the development of national expertise in the field of wind energy.

In order to gain practical experience in electricity generation from wind energy,

the development of a pilot wind turbine project was initiated in 2011. As part of this initiative, the first experimental wind turbine in Central Asia was commissioned in 2013 in the Charvak reservoir area, located in the Bostanlyk district of the Tashkent region. The turbine has a tower height of 65 meters and a rotor diameter of 56 meters, with an installed capacity of 750 kW. Its annual electricity generation is approximately 2.3 million kW·h.

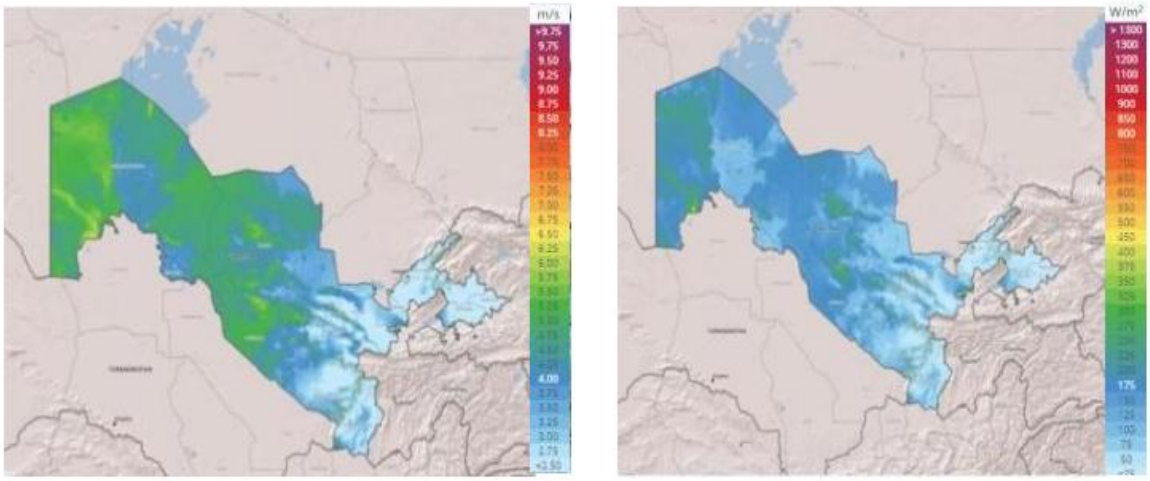

a b

Figure 5.4. Wind energy map of the region (Global wind atlas):

(a) average wind speed at a height of 10 m; (b) specific wind power density at a height of 10 m.

In recent years, particular attention has been given to the development of wind energy within the framework of large-scale investment projects. Notably, the Masdar company is currently constructing a major wind power plant in the Zarafshan area of the Navoi region. As part of this project, the initial wind power facility has already been connected to the national grid, and upon full commissioning, it is expected to supply electricity to approximately 1.5 million households.

Furthermore, an agreement has been signed between Masdar, the Ministry of Investments and Foreign Trade, and the Ministry of Energy of the Republic of Uzbekistan to increase the project's installed capacity from the initial 500 MW to 1.5 GW. This development is expected to significantly accelerate the growth of wind energy in Uzbekistan and substantially increase the share of renewable energy sources in the country's energy mix.

§5.3. International standards for wind turbines published by the International Electrotechnical Commission (IEC)

IEC 61400 is a set of design requirements developed to ensure that wind turbines are appropriately engineered to withstand risks and loads throughout their intended service life. The standard covers multiple aspects of turbine operation, including design, testing, manufacturing, installation, and ekspluatation of turbine components. Wind turbines are capital-intensive systems that are typically purchased prior to installation and commissioning. Some of these standards provide technical specifications that can be independently verified by third parties, making them essential for establishing contractual agreements related to financing, certification, and deployment of wind turbines. The International Electrotechnical Commission (IEC) initiated the standardization of international certification in this field in 1995, and the first IEC 61400 standard was published in 2001. In many cases, the IEC standards replace national standards and serve as the basis for global certification.

Small wind turbines with a swept area of up to 200 m² are covered by the simplified IEC 61400-2 standard. In some cases, IEC 61400-1 may also be applied to turbines below this threshold. At test sites such as Osterild, load and noise standards are applied during prototype development. In offshore applications, particularly in the United States, IEC standards are complemented by additional standards such as ISO and API. Key offshore standards include:

ISO 19900 — General requirements for offshore structures;

ISO 19902 — Fixed steel offshore structures;

ISO 19903 — Fixed concrete offshore structures;

ISO 19904-1 — Floating offshore structures (monohulls, semi-submersibles, spars);

ISO 19904-2 — Floating offshore structures (tension-leg platforms);

API RP 2A-WSD — Recommended practice for planning, design, and construction of fixed offshore steel platforms.

In Canada, outdated national standards were revised by the Canadian Standards Association and harmonized with IEC 61400. Efforts are ongoing to achieve global

harmonization of certification requirements for small wind turbines under the principle of “test once, certify everywhere.” International collaboration between the UK, USA, Japan, Denmark, and other countries has enabled compatibility between IEC 61400-2 and certification schemes such as the UK’s MCS and the AWEA small wind turbine standard. Wind turbines are classified based on site-specific wind conditions. During the design phase, assumptions are made regarding the wind climate affecting the turbine. Wind classes are defined by three main parameters: average wind speed, extreme 50-year wind speed, and turbulence intensity. Turbulence intensity describes the variability of wind speed over a typical 10-minute period. Wind speed generally increases with height due to vertical wind shear. Over flat terrain, this increase follows a logarithmic profile, whereas in complex terrain, flow separation may occur, leading to significantly increased turbulence.

Key IEC 61400 standards include:

- IEC 61400-1 — Design requirements;
- IEC 61400-2 — Small wind turbines;
- IEC 61400-3 — Offshore wind turbines;
- IEC 61400-4 — Design requirements for wind turbine gearboxes;
- IEC 61400-6 — Tower and foundation design requirements;
- IEC 61400-11 — Acoustic noise measurement techniques;
- IEC 61400-12 — Power performance measurements;
- IEC 61400-13 — Measurement of mechanical loads;
- IEC 61400-21 — Power quality characteristics;
- IEC 61400-23 — Full-scale structural testing of rotor blades;
- IEC 61400-24 — Lightning protection;
- IEC 61400-25 — Communication for monitoring and control;
- IEC 61400-27 — Electrical simulation models.

§5.4. Components of a wind turbine

The design and construction of wind turbines involve several important structural and technological options. These include the number of blades (typically two or three),

rotor configuration relative to the tower (upwind or downwind), blade material, manufacturing methods, and aerodynamic profiles. The hub design may be rigid, teetering, or hinged. Power regulation is achieved either through aerodynamic control (stall control) or blade pitch adjustment (pitch control). Rotor speed may be constant or variable, while yaw control can be passive (free yaw) or active (motor-driven). Generators may be synchronous or asynchronous (including doubly-fed induction generators), and transmission systems may be gearbox-based or direct-drive.

A wind power plant consists of several key components. The blades capture wind energy and drive the rotor. They are typically made of lightweight composite materials such as fiberglass or carbon fiber and are aerodynamically optimized. The rotor, consisting of blades and hub, converts the kinetic energy of the wind into mechanical energy. The main shaft (low-speed shaft) transmits this rotational energy to the gearbox and is designed to withstand loads and vibrations. The gearbox increases the rotational speed to match generator requirements. The generator converts mechanical energy into electrical energy and may be of synchronous or asynchronous type. The nacelle houses critical mechanical and electrical components, including the gearbox and generator, providing protection and facilitating maintenance. The yaw system aligns the nacelle with the wind direction using sensors and electric motors to maximize energy capture. The tower elevates the rotor and nacelle to higher altitudes, where wind speeds are stronger and more stable. It is typically constructed from steel or concrete and designed to withstand significant loads.

The control system ensures safe and efficient turbine operation through automated monitoring, real-time diagnostics, and remote control. The pitch system adjusts blade angles under high wind conditions to optimize power output and protect the turbine. Wind direction is measured using devices such as wind vanes (anemometric systems), and the control system uses this data to activate the yaw mechanism, ensuring proper turbine orientation. Overall, all components of a wind turbine are interconnected, and their optimal coordination ensures maximum efficiency in harnessing wind energy.

However, most wind turbine designs have limitations in rotational movement. The cables that transmit power or control signals from the base of the tower to the nacelle

are typically bundled together and are allowed to twist only within a specified limit as the nacelle rotates.

Figure 5.4. Main components of a wind power plant.

If these cables become excessively twisted, they may be pulled out of their anchor points, potentially causing severe damage. A limit switch is commonly used to notify the control system when the allowable twist limit has been reached. Despite these protective measures, the cables may still experience wear and degradation over time due to repeated twisting cycles.

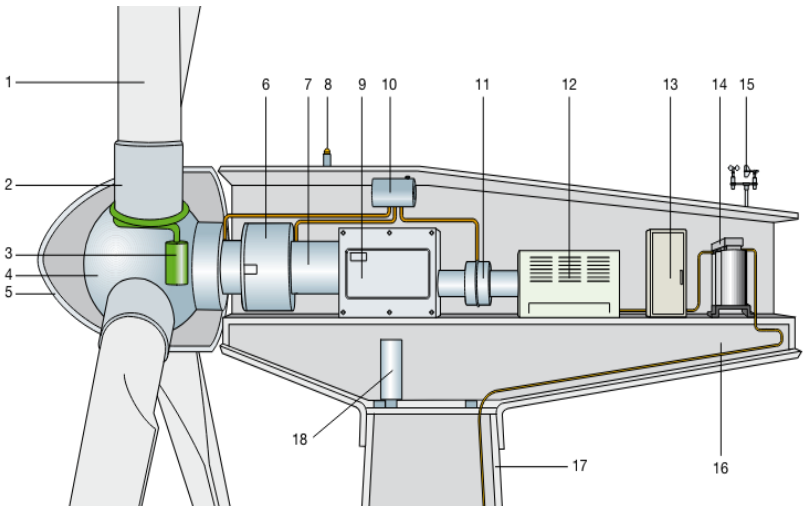

Figure 5.5. Components of a wind power plant: 1-blade; 2-blade support (blade

root); 3-pitch actuator; 4-hub; 5-spinner; 6-main bearing; 7-main shaft; 8-aircraft warning lights; 9-gearbox; 10-mechanical brakes; 11-hydraulic cooling system; 12-generator; 13-power converter and electrical control, protection, and switching equipment; 14-transformer; 15-anemometers; 16-nacelle frame; 17-support tower; 18-yaw control system.

From a cost perspective, the percentage distribution of the total cost among the various components is illustrated in Figure 5.6.

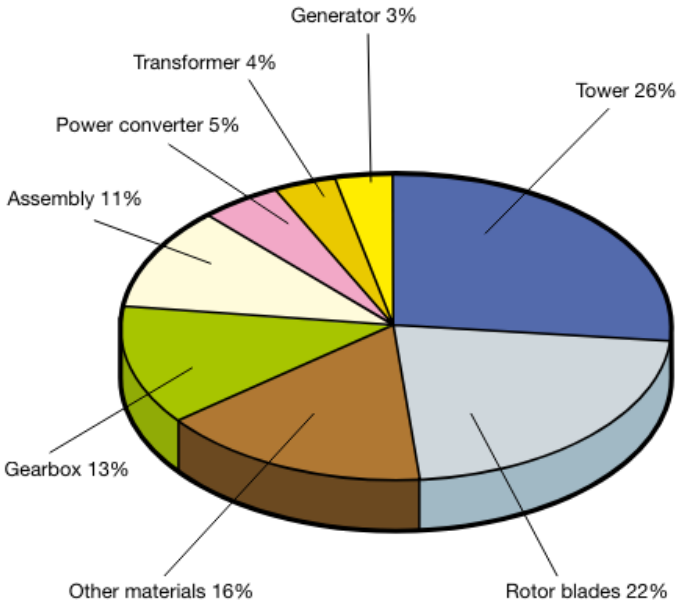

Figure 5.6. Cost Distribution of Wind Power Plant Components.

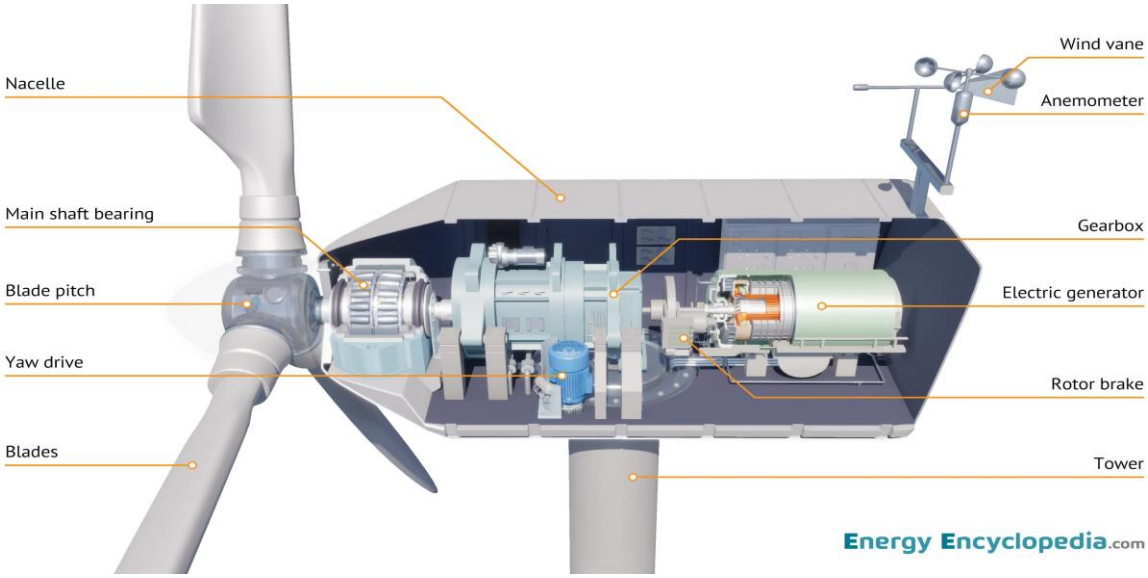

Figure 5.7. Location of the gearbox in a wind power plant.

The foundation of a wind turbine must be sufficiently strong to ensure that the turbine remains upright and stable even under the most severe and extreme operating conditions. In most cases, the foundation is constructed as a reinforced concrete pad.

The weight of the concrete is designed to provide adequate resistance against overturning under all loading conditions. In some cases, turbines are installed on rock (bedrock). In such situations, the foundation may consist of steel anchor rods embedded into deep drilled holes and fixed with cement grout. A concrete platform is used to create a level surface, while the tensile forces are primarily resisted by these anchored rods. Various types of wind turbine foundations are illustrated in Figure 5.8.

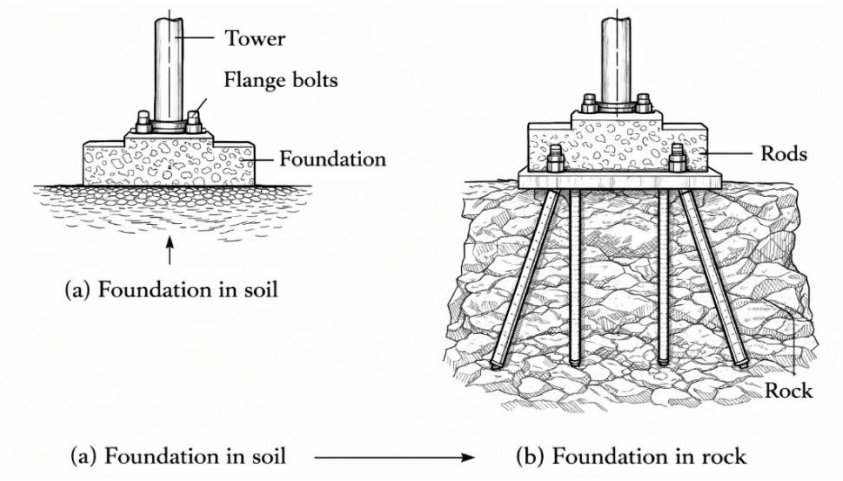

Figure 5.8. Wind turbine foundations (based on Hau, 1996).

The method used for tower installation has a direct impact on its structural design. Large-scale wind turbines are typically installed using cranes, whereas small and medium-sized turbines are often erected using self-erecting methods. One of the most common self-erection techniques involves the use of a gin pole or an A-frame positioned perpendicular to the tower. The A-frame is connected to the upper section of the tower via cables. The tower is then raised using a winch system in combination with pulleys (sheaves). In such installation methods, the base of the tower must be equipped with hinged supports, allowing it to pivot during lifting. Once the tower reaches its vertical position, it must be securely fixed using appropriate locking mechanisms. The turbine itself is typically mounted on the tower prior to erection. Various tower installation methods are illustrated in Figure 6.45.

The construction of a wind power plant generally includes the following stages:

- Construction of access roads and site clearing;
- Construction of main buildings and infrastructure required for plant operation;
- Foundation installation, delivery, and erection of selected wind turbines;

- Installation of medium- and low-voltage electrical lines, fiber-optic communication systems, etc.;
- Construction of the electrical substation;
- Testing and commissioning.

Special attention must be given to the construction of access roads and foundations. Prior to initiating earthworks, it is essential to conduct soil investigations and assess the climatic and topographical conditions of the construction site. Failure to consider these factors may lead to delays, increased costs, or even project failure. During excavation and foundation construction, heavy machinery is required, which necessitates properly designed access roads. In some cases, obstacles such as road crossings or water barriers may significantly affect construction activities. Therefore, geotechnical investigations are essential to determine soil properties and to ensure the technical and economic feasibility of the project. Subsequently, engineers aim to minimize land usage by optimizing the layout of the wind farm. Access roads must be designed to allow heavy transport vehicles to reach turbine locations efficiently, particularly during installation, operation, and maintenance stages. Specific requirements are imposed on access roads, including load-bearing capacity, slope stability, and geometric parameters. Proper soil preparation is required prior to road construction, typically involving layered compaction.

A base layer of natural gravel is followed by an additional layer of engineered aggregate to provide sufficient strength. Road width is another critical factor, as wind turbine components-especially blades, which may exceed 50 meters in length-require transportation using vehicles with large turning radii. Therefore, road curvature and turning radii must be carefully designed. These parameters are often interrelated and defined through engineering tables. Road slope is also a key design parameter. Heavy transport vehicles may experience difficulties on steep terrain; therefore, strict design limits are applied. Typically, the maximum road gradient ranges from 14% to 17%, and surface treatment (such as concrete or asphalt) may be required to ensure sufficient traction. These values may vary depending on project-specific conditions. Once installed, wind turbines are subjected to significant loads that may affect structural

stability and integrity. Therefore, accurate foundation design requires detailed geotechnical investigations for each turbine location. Soil conditions may vary from soft ground to highly resistant bedrock, and foundation design must account for these variations. Wind turbine foundations are generally classified into two main categories:

Shallow (surface) foundations-used when the soil has sufficient load-bearing capacity or when structural loads are relatively low;

Deep foundations-used when higher loads must be supported. These typically involve piles or elongated concrete elements driven into the ground, which enhance stability against tensile, compressive, frictional, and bending stresses.

Pile foundations are particularly suitable for soils with low bearing capacity, as they help prevent structural failure due to excessive loading during turbine operation. In most cases, gravity-based shallow foundations with large contact areas are used to support the combined weight of the tower, rotor, and nacelle. Due to the significant forces generated by wind loads, a large foundation area is required to ensure stability. Reinforced concrete is the primary material used for wind turbine foundations due to its strength, durability, and suitability for such applications.

Figure 5.9. Wind power plant foundation pouring process.

The geometry of onshore wind turbine foundations varies depending on multiple factors. In practice, circular geometries are often preferred due to their efficient material usage, while polygonal shapes (such as hexagonal or octagonal) are also widely used because they provide a larger contact area and better distribution of

stresses. An additional advantage of polygonal foundations is the reduced need for internal reinforcement elements, as increasing the number of sides decreases the amount of material required for structural reinforcement. A significant portion of the equipment required for turbine installation is mounted on dedicated platforms. These platforms are typically large, open polygonal areas (commonly square or rectangular), with side lengths ranging from 20 to 50 meters. During construction, heavy cranes are used to install turbine components, transformers, and other equipment. The platform is surrounded by access roads and designated storage areas for materials.

The main installation activities include assembling tower sections, mounting the nacelle onto the tower, assembling the rotor blades, and installing the rotor onto the wind turbine. As with all construction processes, strict adherence to safety standards is essential during turbine installation, particularly because operators are exposed to significant risks due to the large size, weight, and height of the components. Careful planning of the construction site is of critical importance. All materials and components must be organized efficiently to ensure unobstructed access for construction teams and to minimize crane movement time. The installation of a wind turbine typically requires two cranes. The main crane is responsible for lifting and positioning components throughout the installation process, while the auxiliary crane supports and stabilizes components during assembly, allowing the main crane to move them from a horizontal to a vertical position.

Figure 5.10. Construction process of the first wind power plant foundation.

Proper coordination between crane operators and technical personnel is especially crucial during the assembly of tower sections and rotor installation. The installation process begins with the lower section of the tower, which forms the connection point between the foundation and the wind turbine. This connection is typically achieved using a flange at the base, secured with bolts. The remaining tower sections are installed sequentially in a similar manner, with each subsequent stage performed at progressively higher elevations.

To enhance the structural stability of a wind power plant, it is essential to properly install the tower, particularly its foundation. The type of support structure selected directly influences the performance and safety of the wind turbine. The foundation is a critical element that ensures the stability and durability of the entire turbine structure.

§5.5 Wind turbine tower.

Towers serve as the supporting structures that elevate the main components of the turbine into the airflow. Typically, the tower height is at least equal to the rotor diameter, although for smaller turbines it may be significantly higher. In general, tower height should not be less than 24 meters, as wind speeds near the ground are lower and more turbulent. For example, increasing the tower height from 20 meters to 80 meters can result in approximately 5% additional energy production. Currently, the trend is toward the use of taller towers. In Europe, the average installed tower height is around 80 meters. Modern towers are equipped with internal access systems, including lifts, ladders, and intermediate platforms. Additionally, medium-voltage (MV) transformers are often installed within the tower, typically at its base. The most common types of towers used for horizontal-axis wind turbines include:

- guyed tower (truss tower);
- tubular steel tower;
- lattice tower;
- hybrid tower.

Historically, guyed towers were widely used until the mid-1980s. For example,

early wind turbines in the United States employed this type of structure. Since then, other tower designs particularly tubular steel towers have become more prevalent due to their improved structural performance and ease of installation.

Figure 5.11. View of the wind power plant tower.

Tubular towers offer several advantages. Unlike guyed (truss) towers, they require fewer supporting elements and do not include bolted connections that must be periodically tightened and inspected. Wind turbine towers are typically constructed from steel, although reinforced concrete is sometimes used. When steel is employed, it is usually galvanized or made from corrosion-resistant alloys to protect against environmental degradation.

Solid (lattice or rigid) towers were widely used in the past when turbines were relatively small (typically below the megawatt scale), but today they are rarely utilized. Their main disadvantages include significant visual impact as well as higher construction and maintenance costs. However, they do offer certain advantages: they require less material (approximately 50% of that used in a standard steel tubular tower of equivalent stiffness) and produce less shadowing (shadow flicker).

Tubular steel towers represent the most widely used solution in modern wind turbines. They are typically conical in shape, with diameters ranging from approximately 4.5 meters at the base to about 2 meters at the top. These towers are usually manufactured in 3 or 4 sections, which are assembled on-site. The length of

each section typically varies between 20 and 30 meters. The towers are primarily fabricated from rolled and welded steel plates. For modern towers exceeding 100 meters in height, the base diameter may exceed 5 meters. This presents logistical challenges, as in many countries the maximum transportable diameter by road is limited to less than 4.9 meters.

Figure 5.12. Internal view of a wind power plant tower.

Concrete towers provide an alternative solution, particularly in regions where steel prices are high (for example, in countries where steel production is limited or monopolized, such as Brazil). These towers consist of multiple prefabricated segments assembled on-site. This approach facilitates transportation due to smaller component sizes and allows for better quality control during manufacturing. However, their primary disadvantage is their significant weight, which in some cases may exceed that of the nacelle if not properly segmented. Hybrid towers are another solution adopted by several manufacturers to mitigate fluctuations in steel prices. However, their main drawback lies in the increased complexity of assembly, which leads to higher installation costs.

The tower serves to elevate the turbine blades to the desired height, enabling more efficient energy capture from higher and more stable wind flows. The main types of wind turbine towers include lattice towers, tubular towers, and guyed towers. Lattice towers are constructed from interconnected steel members forming a truss-like

structure, providing high strength with relatively low material usage.

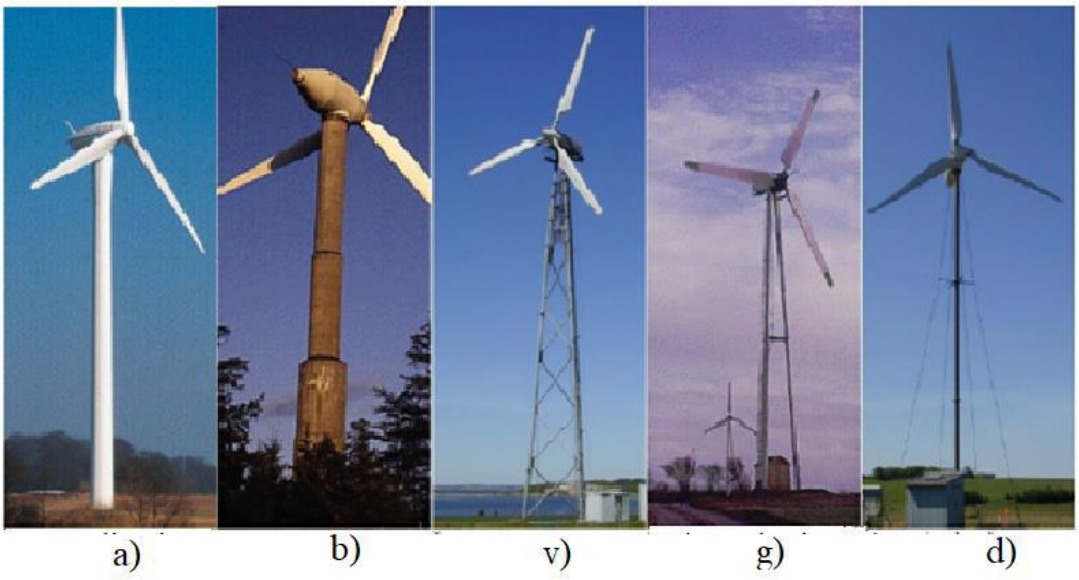

Figure 5.13. Types of towers for horizontal-axis wind turbines:
(a) tubular steel tower; (b) concrete tubular tower;(v) lattice tower;(g) tripod tower; (d) guyed (cable-supported) tower.

Lattice towers have several disadvantages. The most significant drawback is their unfavorable visual appearance, which is generally not well accepted by observers. In addition, lattice towers may pose a risk to bird populations, as their horizontal structural members can increase the likelihood of bird collisions.

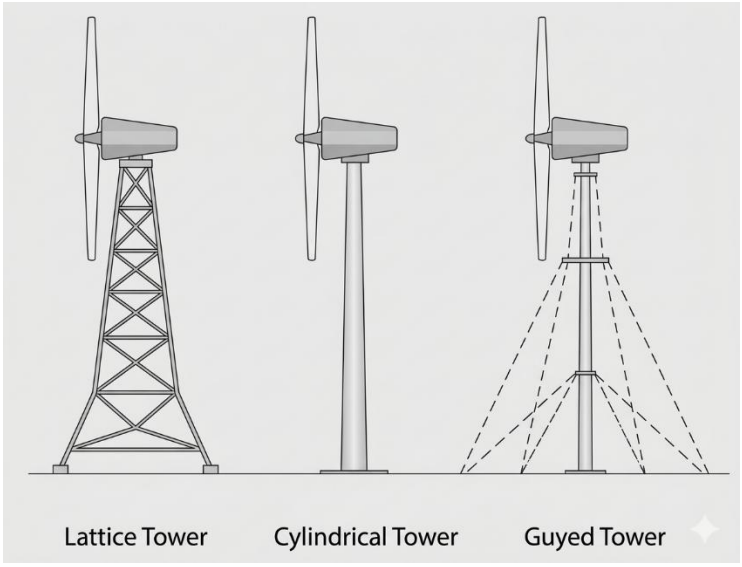

Figure 5.14. Schematic of different types of towers.

In addition, the absence of proper locking or rigid structural elements may reduce the overall durability and reliability of lattice towers. Due to these limitations, modern

wind turbine installations increasingly utilize cylindrical (tubular) steel towers.

Figure 5.15. Increase in wind turbine tower height over the years.

These towers are typically constructed by assembling cylindrical sections with lengths ranging from 10 to 20 meters. The complete erection of a single tower usually takes approximately 2–3 days. Cylindrical towers are widely used due to their streamlined, circular geometry, which results in reduced aerodynamic resistance under high wind speeds.

In small-scale wind energy systems, guyed (cable-supported) metal towers are commonly used. The use of additional guy wires reduces the overall structural weight, which in turn significantly lowers construction and material costs. Typically, the cables are arranged symmetrically in four directions and anchored at an angle of approximately 45°, ensuring tower stability. However, due to the relatively complex installation and maintenance requirements, such towers are not widely adopted for large-scale applications. Nevertheless, guyed towers are still used in certain countries, including Germany.

The loads acting on the tower increase proportionally with turbine size and power capacity. Therefore, in recent years, megawatt-class wind turbines have increasingly required towers with larger diameters and thicker walls to ensure sufficient structural rigidity. However, this trend introduces additional technical and logistical challenges, particularly in manufacturing and transportation of large tower components.

§5.6 Wind turbine blades

In wind power plants, blades (airfoils) are among the most critical functional components, and their shape, length, mass, and material properties have a direct impact on turbine performance. Proper selection of blade parameters is essential for maximizing aerodynamic efficiency and power output. Wind turbines equipped with longer blades can capture a larger volume of airflow, allowing them to generate more energy even in regions with low wind speeds compared to turbines with shorter blades. As wind speed increases, the lift force acting on the blades also increases, leading to a higher rotational speed of the rotor.

From an aerodynamic perspective, curved (airfoil-shaped) blades are significantly more efficient than flat blades. They operate effectively at higher tip-speed ratios and generate greater power output. This is due to the pressure difference created between the upper and lower surfaces of the blade: lower pressure forms on the upper surface, while higher pressure develops on the lower surface, resulting in lift generation. As a result, curved blades can typically produce 5–10% more energy than flat blades and maintain higher efficiency even at low wind speeds.

Blade mass is also an important factor. Lighter blades facilitate easier rotor rotation, reduce the cut-in wind speed, and improve overall efficiency. Additionally, lightweight structures simplify installation and maintenance processes. However, reducing mass must be balanced with maintaining sufficient material strength, as inadequate structural integrity may lead to failure.

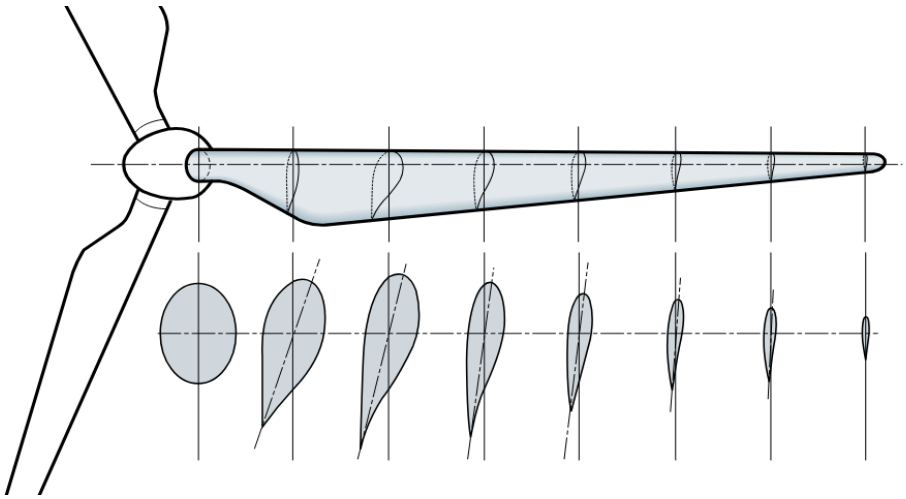

Figure 5.16. Cross-section of a wind turbine blade along its length.

Large and heavy blades may also have environmental impacts, particularly by posing risks to migratory bird populations. Therefore, modern wind turbine design must consider not only aerodynamic performance but also structural reliability and environmental safety in an integrated manner.

Figure 5.16 illustrates the typical geometry of a wind turbine blade and its cross-sections along the span. The blade is twisted from root to tip at a certain angle, with a total twist typically in the range of approximately 20–25°. Since aerodynamic forces are proportional to the square of the relative velocity, these forces increase significantly with distance from the hub. Therefore, the root section of the blade must be designed not only to ensure structural strength but also to provide sufficient lift while minimizing aerodynamic drag. In general, as in all mechanical systems, achieving an optimal balance between strength and weight is essential in wind turbine design. For each wind speed, there exists an optimal blade pitch angle at which the turbine produces maximum power, and this angle varies depending on wind speed. For instance, at a wind speed of 7 m/s, an optimal pitch angle is approximately 5°, while at around 15 m/s it increases to about 20°, and at wind speeds above 25 m/s, it may reach up to 30°. Deviations from the optimal angle result in a reduction in turbine efficiency. As airflow velocity increases, momentum exchange intensifies and thrust force grows; however, increasing the blade pitch angle reduces the effective frontal area, thereby decreasing aerodynamic resistance.

Wind turbine blades are connected to the central hub, forming the rotor assembly that converts wind energy into aerodynamic torque. In practice, three-bladed wind turbines are the most commonly used configuration. This is because a three-blade rotor provides an optimal balance between efficiency, structural weight, and dynamic stability. Increasing the number of blades does not significantly improve efficiency but increases structural weight and manufacturing costs. Moreover, additional blades can increase aerodynamic drag and reduce overall efficiency. A three-bladed rotor ensures a more uniform distribution of dynamic loads and smooth operation. The rotational speed of a wind turbine directly determines the amount of electrical energy generated. If the blades rotate too slowly, a significant portion of the wind energy remains

unutilized; conversely, excessively high rotational speeds lead to increased drag and reduced efficiency. Therefore, modern turbines operate at an optimal tip speed ratio, with maximum efficiency typically observed in the range of 6–7.

Blade material selection is also critical. Blades must be lightweight, highly durable, stiff, and resistant to environmental conditions. Modern wind turbine blades are primarily manufactured from fiber-reinforced polymer composites. In these materials, long fibers (such as glass or carbon fibers) provide high strength and stiffness, while the polymer matrix ensures impact resistance and structural integrity. Smaller blades may sometimes be made from lightweight metals such as aluminum; however, these require more frequent maintenance. Blade maintenance is generally divided into preventive and corrective types. Preventive maintenance involves regular inspection of blade condition, while corrective maintenance addresses detected damages. In modern practice, drones are increasingly used for blade inspection and maintenance operations. The selection of blade size and number is a complex engineering problem, influenced by turbine diameter, rotational speed, wind conditions, and generator requirements. Longer blades capture more wind energy but also increase weight, requiring greater torque for startup. Additionally, increasing the number of blades does not increase rotational speed but instead raises aerodynamic resistance. For this reason, three-bladed configurations are predominantly used in practice.

Figure 5.17. Transportation of wind turbine blades.

The size and number of wind turbine blades have a direct impact on both the aerodynamic and mechanical characteristics of the turbine. Smaller blades generally result in higher rotational speeds of the rotor; however, the torque generated on the

shaft is relatively low. Conversely, increasing the number of blades enhances interaction with the airflow, leading to higher torque but reduced rotational speed. For example, two-bladed wind turbines can rotate at high speeds, but they are typically unable to generate sufficient torque. In addition, such configurations often experience higher levels of vibration and noise, which may accelerate mechanical wear of components.

Four-bladed turbines, compared to three-bladed designs, provide slightly higher torque but at the cost of further reduced rotational speed. As rotational speed decreases, the gearbox system required to transmit mechanical energy to the generator becomes more complex and may operate with lower efficiency. Furthermore, each additional blade increases the overall structural weight and manufacturing cost. Therefore, considering efficiency, mechanical stability, and economic factors, the three-bladed design has been widely accepted as the optimal configuration, particularly for megawatt-scale wind turbines. Another important issue is the end-of-life management of wind turbines. According to forecasts, by 2030, up to 5,700 wind turbines in Europe may be decommissioned as part of repowering processes. Currently, nearly 90% of wind turbine components can be recycled or recovered. However, the main challenge is associated with the blades, which are made of durable composite materials designed for long service life, making their recycling process complex.

Figure 5.18. Landfilling process of wind turbine blades.

Typically, a single wind turbine blade is approximately 40 meters in length and weighs around 7 tons. Although blades account for only about 10% of the total turbine

mass, they represent a significant challenge in terms of disposal. These difficulties have raised concerns regarding the environmental sustainability of wind energy. Consequently, the development of new technologies for blade recycling, reuse, or environmentally safe disposal has become an important research and practical direction in the field of wind energy.

The disposal and recycling of wind turbine blades has become one of the most pressing challenges in recent years. The highest number of decommissioned blades has been observed in Germany and Spain, followed by Denmark. According to projections, by the end of the decade, countries such as Italy, France, and Portugal will also begin large-scale decommissioning of aging wind turbines. As a result, by 2030, the volume of blade waste is expected to reach approximately 52,000 tons per year. Based on analyses conducted by Quantis US, GE Renewable Energy has reported that recycling wind turbine blades in cement production can reduce CO_2 emissions by up to 27%, while also decreasing water consumption by approximately 13%. Currently, around 85% of wind turbines manufactured by Vestas can be recycled. However, blades remain the primary challenge, as they are made from composite materials that are not yet fully recyclable. The company is actively working on improving recyclability by analyzing the entire life cycle of wind turbines, with a particular focus on blades and nacelle components. According to future plans, the recyclability rate of blades is expected to increase from 44% to 55% by 2030, with a long-term goal of achieving 100% recyclability.

At present, approximately 80% of decommissioned wind turbines are reused in other regions, particularly in European countries such as Italy, the United Kingdom, Sweden, and Denmark. The remaining 20% are recycled or disposed of due to economic constraints. However, in the coming years, the increasing number of aging turbines and the deployment of larger, higher-capacity turbines are expected to significantly increase the volume of waste requiring disposal. In response, several countries have banned the disposal of wind turbine waste in conventional landfills. Notably, Germany, Austria, the Netherlands, and Finland have prohibited so-called “turbine graveyards.” Furthermore, European wind energy organizations have

proposed a complete ban on such disposal practices across Europe by 2025. Currently, only about 42–43% of blades can be effectively recycled, and ongoing research aims to improve this figure.

Overall, while nearly 90% of a wind turbine can be recycled, blades remain the most problematic component. They are manufactured from durable composite materials designed for long service life, making their recycling process technically challenging. Typically, a single blade is about 40 meters long and weighs approximately 7 tons, accounting for around 10% of the total turbine mass. The difficulty of managing this component has raised concerns regarding the environmental sustainability of wind energy systems.

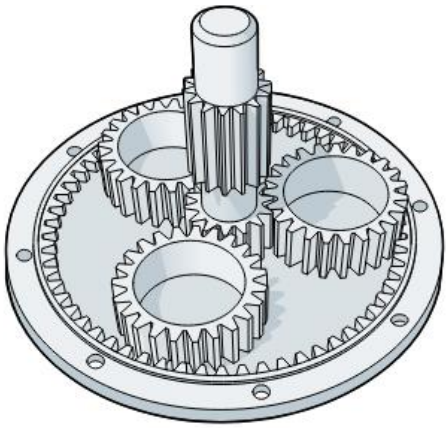

Figure 5.19. Gearbox.

An essential component of a wind turbine is the gearbox, which converts the mechanical rotational energy generated by the rotor into the higher rotational speeds required by the generator. In most wind turbines, a single-stage or multi-stage gearbox is installed between the rotor and the generator. This system plays a crucial role in efficiently converting the kinetic energy of wind into electrical energy.

The gearbox is designed to increase the rotational speed of the rotor to match the requirements of conventional generators. In some turbines, the gearbox ratio may exceed 1:100. The gearbox typically consists of one or more gear stages, which may be of epicyclic (planetary) or parallel-shaft configurations.

Braking System. In addition to aerodynamic braking, nearly all wind turbines are equipped with mechanical braking systems installed within the drivetrain. In most cases, mechanical brakes are capable of stopping the rotor under adverse weather

conditions. Furthermore, they function as parking brakes to prevent rotor movement when the turbine is not in operation.

Figure 5.20. Braking system of a wind power plant.

Various braking systems are employed in wind turbines to ensure operational safety. The most common types of mechanical brakes include disc brakes and clutch-based braking systems. These brakes are primarily used to stop the rotor during emergency conditions or maintenance operations. Wind turbines typically utilize asynchronous (induction) and synchronous generators for electricity generation. An asynchronous generator is essentially a three-phase induction machine whose operation is based on synchronous rotational speed. When the torque applied to the rotor shaft becomes driving torque and the rotational speed exceeds the synchronous speed, the machine transitions from motor mode to generator mode and begins supplying electrical energy to the grid. The relative difference between synchronous speed and actual rotational speed is referred to as slip (S). In generator mode, slip takes negative values. In squirrel-cage induction generators, slip is typically around 1%, which means they operate at nearly constant speed.

To enable variable-speed operation in systems based on induction generators, frequency converters are used. In such configurations, a converter is installed between the stator and the grid, or the rotor is supplied with variable-frequency current. As a result, the synchronous speed becomes dependent on the difference between grid

frequency and rotor current frequency, allowing speed variation of up to approximately 30%. In synchronous generators, the frequency of the induced voltage in the stator is directly proportional to the rotor rotational speed. Therefore, for variable-speed operation, a full-scale power converter is installed between the generator and the grid. In this system, the variable-frequency AC generated by the turbine is first converted into DC using a rectifier, and then inverted back into grid-frequency AC using an inverter. Using a synchronous generator with a converter system allows temporary acceleration of the rotor during sudden increases in wind speed. In this process, excess energy is stored as kinetic energy in the rotor, contributing to grid stability. Conversely, when wind speed decreases, this stored energy is released, causing a gradual reduction in rotor speed.

Wind turbines can be classified into several main categories based on generator type:

- The first type is the squirrel-cage induction generator, which operates at nearly constant speed.
- The second type is the wound-rotor induction generator, which allows a wider range of speed and torque control through external resistance.
- The third type is the doubly-fed induction generator (DFIG), which uses power electronics to achieve a wide operating range.
- The fourth type is the full-converter-based generator, typically using a permanent magnet synchronous generator (PMSG), which provides the highest level of control flexibility.

Each of these generator types has its own advantages and limitations, and the selection depends on turbine capacity, operating conditions, and control requirements. In some systems, precise control of voltage and current is required, while in others such requirements are less critical. Therefore, modern wind turbines widely employ power converters to ensure efficient energy management. It should be noted that electrical machines can generally operate both as motors and generators. When energy is supplied to the shaft, the machine operates as a motor; conversely, when energy is extracted from the shaft, it operates in generator mode. The gear ratio in the

transmission system ensures the required torque and rotational speed, while in controlled systems, these parameters are adjusted through power electronic converters.

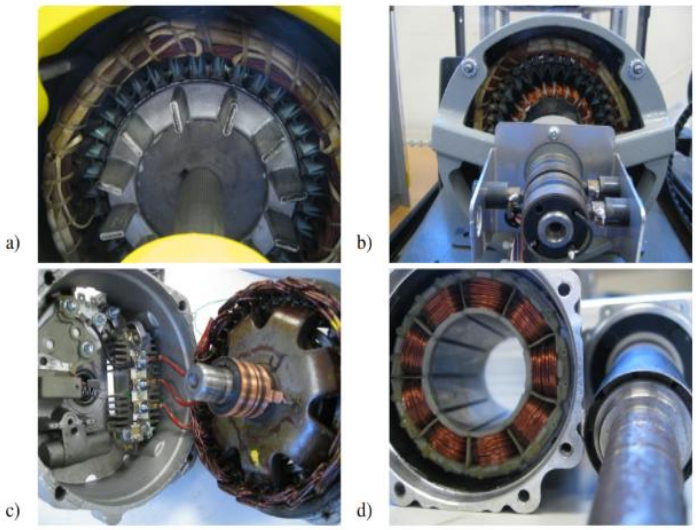

Figure 5.21. Types of generators used in wind turbines. (a) Type 1-squirrel-cage induction machine; (b) Types 2 and 3-induction generator with excitation (wound-rotor); (c) Type 4-externally excited synchronous generator; (d) Type 4-permanent magnet synchronous generator (PMSG).

The WTS generator is designed to operate without active control, where the stator outputs are rectified through a diode circuit to produce direct current (DC). The output voltage typically ranges from 6 to 25 V and depends on the turbine rotational speed as well as the strength of the excitation field. In subsequent sections of this manual, several experiments are presented to demonstrate how generator control strategies influence turbine efficiency.

Yaw System. The yaw system is a mechanism in wind turbines that rotates the rotor (the section where the blades are mounted) to align with the wind direction (see Fig. 5.22). Wind direction and speed are continuously monitored by sensors mounted on top of the nacelle. The rotor is typically oriented according to the average wind direction calculated over a 10-minute interval by the turbine control system. For horizontal-axis wind turbines, a yaw system is essential to ensure proper alignment with the wind. Smaller turbines may use a tail vane (passive yaw control), while larger turbines employ active yaw control systems. Consequently, the support tower must be properly designed to withstand torsional loads induced by yaw system operation. To

maintain alignment with wind direction, wind direction sensors (such as wind vanes) continuously measure incoming wind flow. Based on this data, the controller activates yaw motors to rotate the nacelle when necessary. However, in many turbine designs, the yaw rotation angle is limited to prevent excessive twisting of cables and mechanical components.

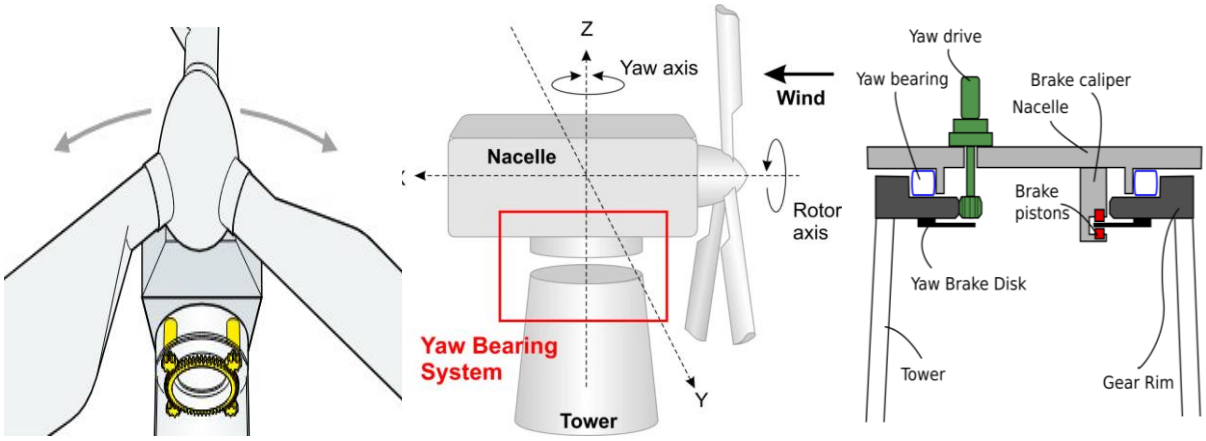

Figure 5.22. Yaw system.

The cables that transmit power and control signals from the lower section to the upper part of the turbine are bundled together and designed to allow a limited degree of rotation as the nacelle turns. If these cables are twisted excessively, they may detach from their anchoring points and cause severe damage. Therefore, a limit switch is used to signal the controller when the cable twist limit is reached. Despite this protection, cables may still experience wear over time due to repeated movements. Figure 5.22 illustrates the main elements of the yaw system in a large-scale wind turbine.

Cooling systems in wind turbines. Several types of cooling systems are used in wind turbines:

- Air cooling: This is commonly applied in small and medium-sized turbines. Heat is dissipated by directing ambient air through internal cooling surfaces of the generator using fans or air blades.
- Oil cooling: Many high-power wind generators use oil both as a cooling and lubrication medium. Oil coolers regulate the temperature of the working fluid through circulation in a radiator, and forced airflow is applied when necessary.
- Water cooling: In large wind turbines or specialized systems, circulating water is used to remove heat generated by the generator.

Offshore Wind Energy. As the name suggests, offshore wind energy refers to electricity generated by wind turbines installed in seas or large bodies of water. Over the past two decades, there has been significant interest in this technology. One of the primary reasons is the limited availability of suitable onshore sites with high wind potential, particularly in Northern Europe. Similar to onshore systems, offshore wind energy encompasses a broad range of aspects, including technology, environmental considerations, and economic factors.

Advantages of Offshore Wind Energy:

- Availability of large areas for the deployment of large-scale projects;
- Proximity to major electricity consumption centers;
- Generally higher wind speeds compared to onshore locations;
- Lower levels of natural turbulence;
- Reduced wind shear effects.

Challenges:

- High project costs due to specialized installation and maintenance vessels and more expensive support structures;
- More complex operating conditions;
- Higher installation costs and technical complexity;
- Limited accessibility for maintenance, reducing availability;
- Need for advanced corrosion protection measures.

Key Aspects in Offshore Wind Energy:

- Wind resource assessment;
- Offshore wind turbine technologies;
- External design conditions;
- Characteristics of potential sites;
- Wind farm layout and design;
- Operation and maintenance strategies;
- Marine environmental considerations;
- Economic aspects of offshore wind energy.

Offshore Support Structure Designs. Various support structures can be considered

for offshore installations. Three common types are illustrated in Figure 5.23.

Monopile Foundations: The most widely used support structure is the monopile, which consists of steel tubes with diameters ranging from 2.5 to 4.5 m. These piles are typically driven 10–20 m into the seabed, although drilling may be required in harder soils or rock formations. Seabed preparation is usually minimal, but heavy pile-driving equipment is required. Monopiles are less suitable for sea beds containing large rocks.

Gravity-Based Structures: These structures rely on their own weight (including ballast) and large base area for stability. The wide base helps resist overturning moments caused by wind loads, similar to the stability of a wide-bottomed glass. Typically, they consist of a circular base with a diameter of 12–18 m and a total weight of 500–1000 tons. The tower connection is located at the center of the base. Gravity-based structures are often made of reinforced concrete, although steel designs also exist. In some cases, the upper section is conical to break floating ice. To protect against erosion and currents, rip-rap is commonly placed around the base. The total ballast weight of such structures may exceed 1000 tons and increases nonlinearly with water depth, making them less suitable for deeper waters. Seabed preparation, often involving dredging, is required prior to installation.

Steel Gravity Structures: These consist of a vertical cylindrical steel column mounted on a flat steel base. Compared to concrete structures, they are lighter and easier to transport. Once installed, they are filled with dense ballast. Due to their lower initial weight, they are often more suitable for deeper waters, as their mass does not increase as rapidly with depth.

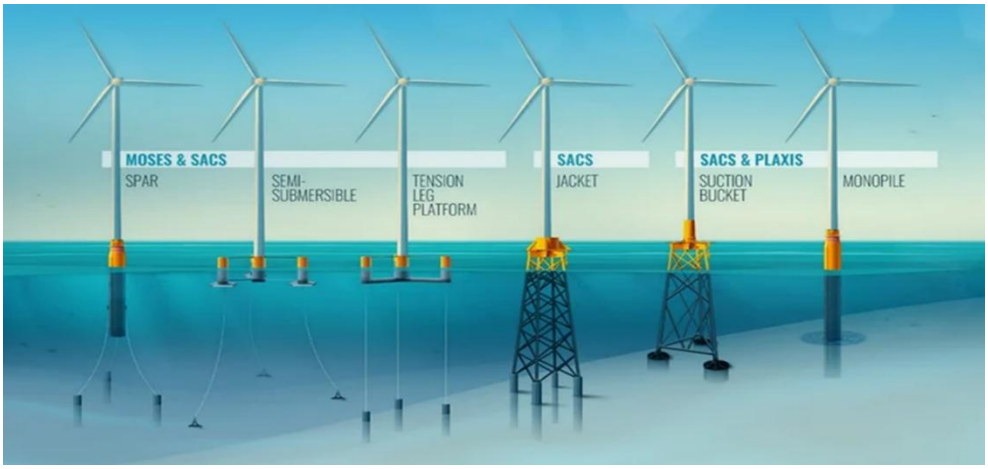

Figure 5.23. Types of pile foundations used in offshore wind power plants.

Multi-member support structures are typically constructed from three or four angled tubular elements. These elements are welded to a central tubular column and interconnected through smaller structural members. Additional shorter tubes serve as guides for relatively small piles used to secure the structure in position. One type of multi-member support structure is the tripod, as illustrated in Figure 5.6. Another widely used configuration is the jacket structure, which is a four-legged framework commonly applied in the offshore oil and gas industry. Multi-member structures require minimal seabed preparation and are well suited for installation in deeper water conditions.

§5.7 Determination of the number of wind energy systems

Let us estimate the number of wind energy systems that can be installed within a given area. Consider a scenario in which a specific land area is available for turbine placement.

Figure 5.24. Site Layout for wind power plant installation.

The total installed capacity of the wind power plant is assumed to be 730,987, and the turbine layout configuration follows a 10×10 rotor diameter spacing. Other constants required for the calculations are presented in Table 5.1.

Table 5.1. Initial data for calculations.

Parameter	Value
Rotor diameter, D (m)	50–250 m (with 10 m increments)
Air density, ρ (kg/m³)	1.23

Power coefficient, Cp	0.45
Overall mechanical and electrical efficiency, $\eta_{mech} \cdot \eta_{el}$	0.9
Available land area for onshore wind installation	730,987 km²

Using Equation (2) and the parameters listed in Table 5.1, the number of wind energy systems that can be installed within the specified area (730,987 km²) was calculated for different rotor diameters. The results are presented in Table 5.2.

Table 5.2. Number of wind turbines as a function of rotor diameter within a 730,987 km² Area.

Rotor Diameter (m)	Number of Turbines (Aligned Rows)	Number of Turbines (Staggered Layout)
50	2,923,948	3,376,284
60	2,030,519	2,344,642
70	1,491,810	1,722,594
80	1,142,167	1,318,861
90	902,453	1,042,063
100	730,987	844,071
110	604,121	697,579
120	507,630	586,160
130	432,537	499,450
140	372,953	430,649
150	324,883	375,143
160	285,542	329,715
170	252,937	292,066
180	225,613	260,516
190	202,489	233,815
200	182,747	211,018

210	165,757	191,399
220	151,030	174,395
230	138,183	159,560
240	126,907	146,540
250	116,958	135,051

From Table 5.2, it can be observed that as the rotor diameter increases, the number of turbines that can be installed within a given area decreases significantly by approximately 25 times across the considered range.

The design of wind energy systems and wind power plants must be carried out by legal entities and individuals authorized to perform such activities in accordance with established regulations. For highly complex and unique wind power projects, the client, together with relevant research and specialized organizations, must develop specific technical requirements reflecting the design, construction, and operational characteristics of the facility. These technical requirements should include:

- Topographical characteristics of the site and surrounding area;
- Wind and climatic conditions of the installation site;
- Geological structure;
- Soil composition, condition, and physical-mechanical and electrical properties;
- Seismic conditions;
- Hydrogeological conditions;
- Geodynamic and engineering-geological processes, including predictions of their changes during construction and operation;
- Requirements for the quality and quantity of generated energy;
- Grid connection or consumer requirements;
- Requirements related to electromagnetic signal propagation;
- Visual and noise impact requirements;
- Environmental protection measures;
- Requirements related to air and maritime traffic safety.

Mandatory Expertise and Commissioning Stages

The following types of expert evaluations must be conducted:

- State environmental expertise;
- Industrial safety expertise;
- Hydrotechnical structures expertise.

The acceptance of wind energy equipment by the client is carried out in the following stages:

1. Incoming inspection of equipment;
2. Acceptance of installed components after assembly;
3. Commissioning and adjustment works;
4. 72-hour continuous system testing and pilot operation;
5. Trial operation under nominal conditions (minimum 30 days continuous operation);
6. Warranty testing (overlapping with Stage 5);
7. Final commissioning and acceptance for operation.

When selecting and installing electrical cables, fire safety requirements must be strictly observed. The use of flammable polyethylene-insulated cables is prohibited. Copper-conductor cables are recommended for wind energy systems. Control, monitoring, signaling cables, and power cables from generators to distribution systems must be made exclusively of copper conductors. In areas where cables may be exposed to damage by rodents or other animals, armored cables and protective conduits must be used. If cables are installed without protective pipes or channels, their routes must be clearly marked using warning tapes or specialized cable coverings.

CHAPTER 6. DESIGN OF HYDROELECTRIC POWER PLANTS

§6.1 Methods of utilizing energy of low-head water flows

The concept of “small river” is interpreted in various ways. Hydrographic criteria that allow distinguishing small watercourses among rivers of a given region are conditional and not sufficiently precise; they depend on historical and geographical traditions. Moreover, the classification of watercourses into various categories (small, medium, large) is often also linked to the type of use of their resources.

The most widely used method for classifying rivers is by hydrological characteristics. For example, according to GOST 19179-73, rivers with a length of up to 100 km and a catchment area of up to 2,000 km² are classified as small rivers. GOST 17.1.1.02-77 divides watercourses into categories, with small rivers being those with a catchment area not exceeding 20,000 km² and a low-water discharge not exceeding 5 m³/s. According to SP 33-101-2003, rivers with a catchment area from 1,000 to 5,000 km² are considered small rivers.

In other hydrological classifications, the criterion is the mean annual discharge value. The problem of classifying rivers by size also depends on the characteristics of the terrain relief. This is confirmed in scientific works: for example, small mountain rivers of the North Caucasus are those with lengths of 10–25 km, as well as rivers with lengths over 10 km and catchment areas up to 100 km².

The following are also proposed as classification criteria for rivers: the relative depth of the river (relative to the width of the watercourse), the degree of drainage of groundwater layers. A small river is usually defined as a watercourse with an open catchment area, i.e., one that does not fully capture water flow from all subsurface layers in the active water exchange zone. In studying hydropower resources, rivers are also classified by their potential capacity: watercourses with a capacity not exceeding 2,000 kW in flatlands and not exceeding 1,700 kW in mountain conditions are classified as small rivers.

Intensive and often inappropriate use of small river resources, increasing pollution, depletion of water reserves, and even degradation require environmental protection measures. The set of these measures mainly depends on the nature of the

impact of economic activities on watercourses. From this perspective, small rivers differ significantly from medium and large rivers.

While large and medium rivers mainly suffer from the effects of local (point) pollution sources, small rivers are more frequently polluted due to dispersed (diffuse) pollution sources. This situation can also serve as an additional criterion for classifying rivers as small.

Thus, small rivers are generally understood as watercourses in a given region with the following characteristics:

- length does not exceed 200 km;
- catchment area up to 5,000 km²;
- discharge up to 50 m³/s;
- have unique hydrological processes;
- limited opportunities for the use of natural resources;
- pollution mainly arises from sources distributed along the length of the river and its basin.

Consumers use electric energy mainly for lighting, heating i.e., for heating greenhouses, electrification of pump stations supplying water, electrification of stationary and mobile irrigation units, creating a microclimate in incubators and livestock farms, and other purposes. The following are considered as initial indicators for determining the efficiency of electrification:

- cultivation of agricultural products by crop type in physical and monetary terms per land area and plowed land;
- livestock numbers by animal type in physical and monetary terms, production of livestock products;
- number and capacity of electric motors, electrical apparatus, and equipment by sector and process, value of electrical installations (substations, transmission networks, mechanisms), annual energy consumption by all sectors of the economy [27], cost per 1 kW of capacity, number of service personnel, labor costs before and after electrification for producing agricultural products, electrification level of farms — all of this characterizes the possibilities of electrifying production processes [27].

For electricity consumers with small hydropower potential, small and micro hydroelectric power plants (HPPs) operating on low-head water flows within their intake are considered ecologically clean and economically efficient. The efficiency of the power supply system can be significantly increased depending on technical solutions [28]. Both foreign and domestic scientists have used several methods to utilize the energy of low-head water flows.

Iranian researcher Y. Yassi (Iranian Research Organization for Science and Technology) developed an experimental prototype of a high-speed rotating micro-HPP water wheel (Fig. 6.1) [31]. This device is designed for installation in a pipe with high-pressure incoming water. For effective operation of the device, the water flow rate during the experiment was 420 m³/hour, and the output power was approximately 20 kW [31].

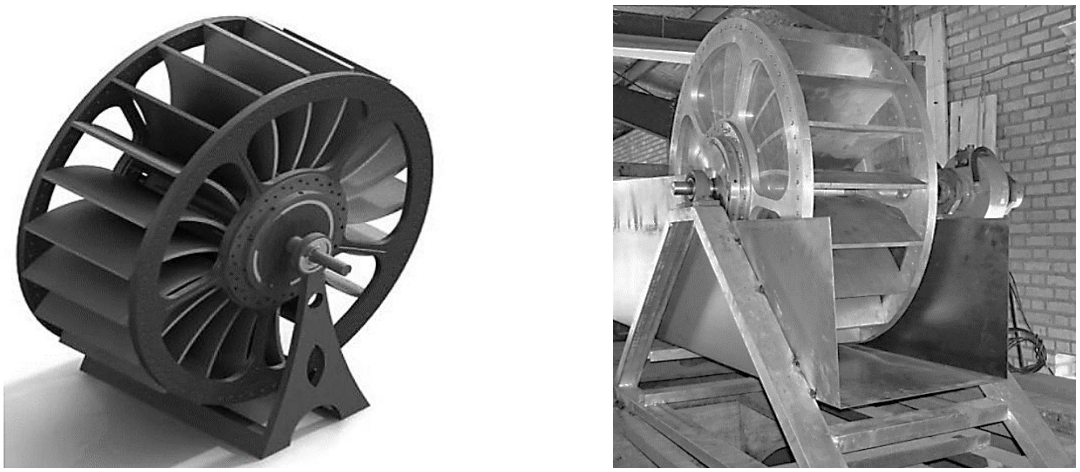

a) Model of a high-speed rotating micro-HPP water wheel

b) Operation process of high-speed rotating micro-HPP

Fig. 6.1. Models of a high-speed rotating micro-HPP water wheel developed by Y. Yassi.

German scientists F. Weichbrodt, S. Dimke, J. Hadler, and P. Freller (University of Rostock) published an article “Large-Scale Model Tests of a Floating Energy Converter” (Großmaßstäbliche Modellversuche mit einem schwimmenden Energiewandler), describing a micro-HPP in the form of a catamaran that is fixed on the water surface (i.e., floats on water). The efficiency coefficient of the device does not exceed 30% (see Fig. 6.2) [29].

Fig. 6.2. Micro-HPP created by F. Weichbrodt, S. Dimke, J. Hadler, P. Freller.

Researchers Olivier Cleynen, Emeel Kerikous, and Stefan Hoerner from Germany (Otto-von-Guericke-Universität) developed a free-flow water wheel micro-HPP. Laboratory experiments on a prototype water wheel showed mechanical power measurements using average time, and blade inclination angles of β=10° were accepted. The highest power was achieved when the optimal blade angle β=10° was used. In this case, power decreases as the rotational speed slows due to changes in water flow in the longitudinal downstream direction of the channels [30].

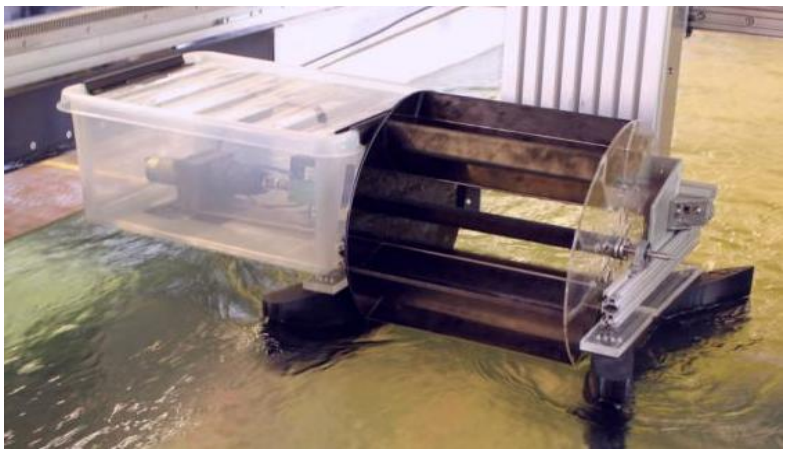

Fig. 6.3. Free-flow micro-HPP developed by Olivier Cleynen, Emeel Kerikous, and Stefan Hoerner.

The micro-HPP design developed by D. Müller (Queen's University Belfast, UK) for low-head water flows is shown in Fig. 6.4 [33-35]. The screw-blade micro-HPP shown in Figs. 6.4-a and b requires the impeller blades to be directed perpendicular to

the water flow. The direction of the water flow is of great importance here. The complex-design micro-HPP developed by D. Müller has an installed capacity of 2 kW. Moreover, the manufacture of these devices is complex and costly [33-35].

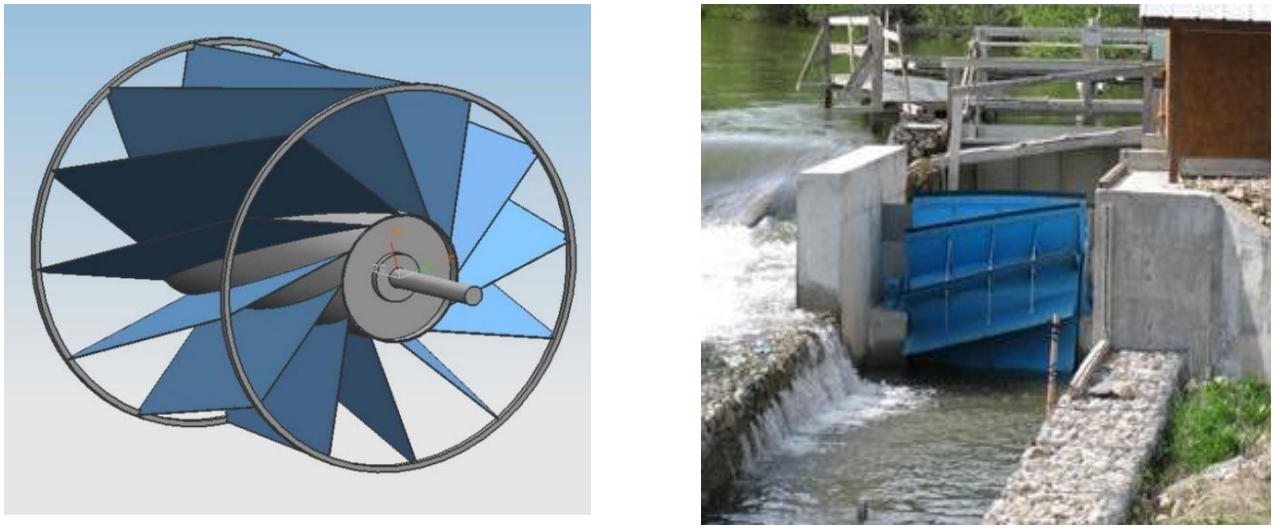

a) Screw-blade micro-HPP model *b) Screw-blade micro-HPP in operation*

Fig. 6.4. Micro-HPP model developed by D. Müller.

Pakistani scientists F.U. Khan, A. Ahmed, U.K. Jadoon, and F. Haider developed a floating water wheel micro-HPP. The optimized floating water wheel was tested in open conditions in a channel with a flow velocity of 1 to 1.2 m/s. At a flow velocity of 1.2 m/s, electricity was generated with a maximum power of 0.6 kW. Losses in the system of the micro-HPP developed by Pakistani scientists depend on the efficiency and incorrect placement of the electric generator. Power generation of electricity in low-head waters can reach up to 1 kW depending on flow velocity [32].

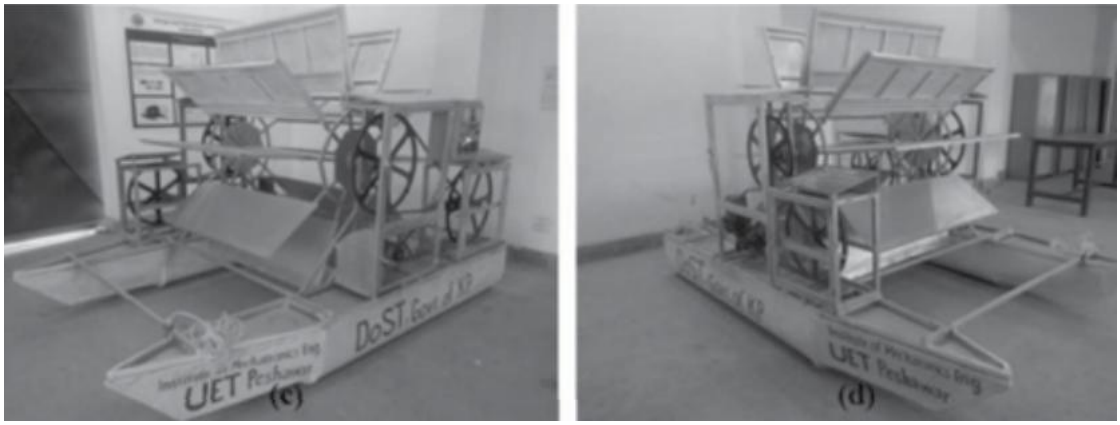

Fig. 6.5. Prototype of the optimized floating water wheel developed by Pakistani scientists F.U. Khan, A. Ahmed, U.K. Jadoon, F. Haider [32].

In D.B. Qodirov's doctoral dissertation, research was conducted and a device was developed to improve the energy efficiency of a water wheel-type micro-HPP operating in low-head water flows.

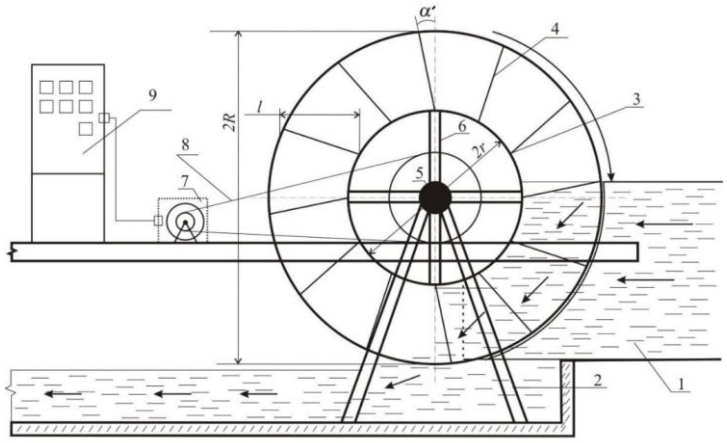

Fig. 6.6. Water wheel-type micro-HPP developed by D.B. Qodirov [36; 37].

1 – water flow; 2 – device mark; 3 – housing holding the water flow; 4 – blade; 5 – shaft; 6 – steel core; 7 – generator; 8 – belt drive; 9 – electric power control unit; α' – corresponding angle.

In it, the surface area of the blade section that interacts with water as a result of the water wheel rotation, touching the water surface at an angle α, increases as the blade is submerged and decreases as the blade exits the water. The constructive dimensions of the developed device are compact and convenient to use. The quality indicators of electricity produced (voltage and frequency) using a micro-HPP prototype were checked, and as a result, a production capacity of 10.4 kW was achieved [36].

A.B. Mamadzhanov conducted scientific research to improve the energy efficiency of a gravitational vortex micro-HPP. The gravitational vortex micro-HPP is considered highly efficient for generating electricity in low-head water flows of 0.7–3 m. It is based on achieving high values of tangential velocity and driving torque by fully forming an air vortex at the center of the vortex inside a cylindrical basin. The efficiency indicator was analyzed according to the initial velocity of water entering the basin, and the optimal tangential inlet angle of the water inlet channel to the basin was determined to be α=45° [38].

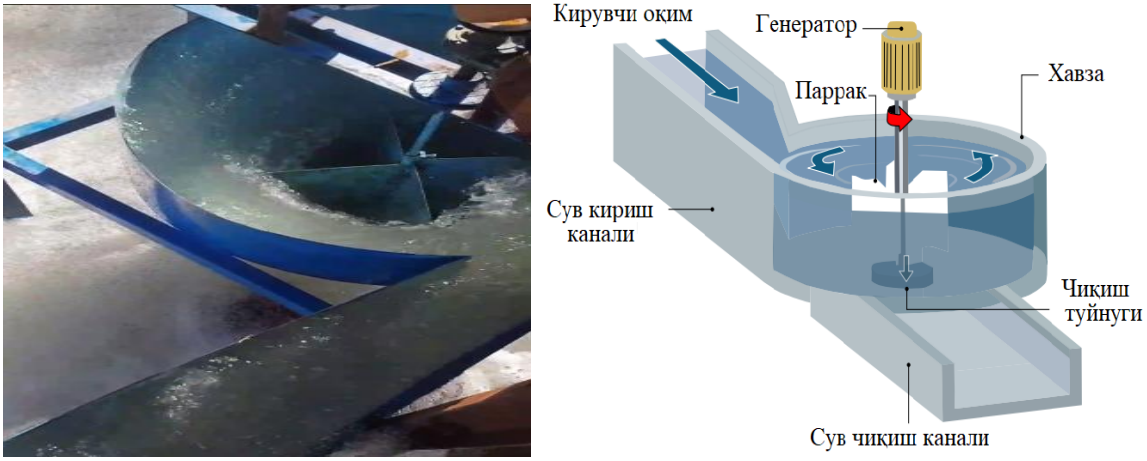

Fig. 6.7. Gravitational vortex micro-HPP developed by A.B. Mamadjanov [38].

In O.U. Zokhidov's doctoral dissertation on “Improving the efficiency of electricity consumption in mining enterprises based on alternative energy sources” scientific research was conducted on a micro-HPP operating in low-head water flows. In this work, an automated control unit and scheme with a microcontroller for automatic control of the operating modes of a phase-rotor asynchronous generator micro-HPP was developed. The micro-HPP generated a power of 20 kW [39].

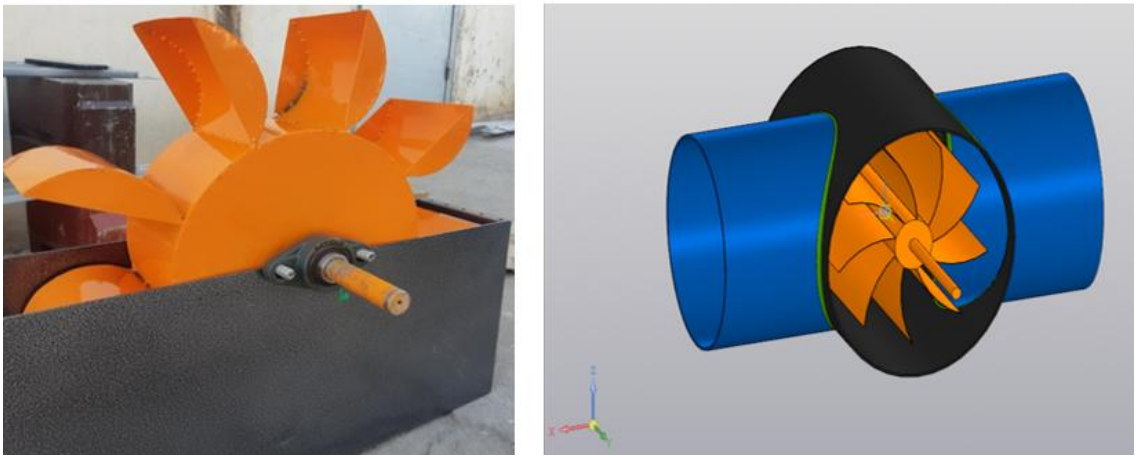

Fig. 6.9. Phase-rotor asynchronous generator micro-HPP developed by O.U. Zokhidov [39].

The ongoing research is an important issue for the further development of the field. However, in the practical work being done on developing and improving hydraulic turbines, no research has been conducted on improving screw turbines. These turbines represent a new direction compared to conventional turbines that have been in

use in recent years. The advantages of the Archimedes turbine over other types of turbines are its lower maintenance costs, mechanical ease of use, and the fact that it is a good choice for places where other types of turbines cannot be used [40].

A number of methods and scientific works of leading scientists who have conducted research in the energy field on developing small and micro-HPPs, improving the efficiency of existing ones, and developing new types of special energy-efficient hydroturbine designs were reviewed and analyzed. As a result of scientific research and literature analysis, it should be noted that hydropower is the main stable and ecologically harmless type among renewable energy sources, since water energy is an ecologically cheap and high-quality energy source for generating electricity.

Regarding the positive characteristics of micro-HPPs, it is worth noting separately that large hydroelectric power plants are often stopped or operated at relatively low capacities when the water level drops. That is, they operate at maximum capacity only when there is sufficient water. In turn, micro-HPPs are extremely convenient and provide good results in efficiently utilizing the low water flow that large hydroelectric power plants or large hydro-units cannot fully use.

§6.2 Determination of hydropower resources

In simplified form, the technical capacity is determined by the following formula:

$$N_{technical} = \eta_{HPP} (1 - \mu_Q) (1 - \mu_H) N_{section} \quad (6.1)$$

where: μ_Q – total flow (water discharge) losses (in fractions of the standard flow); μ_H – total head (height) losses (in fractions of river gradient); $N_{section}$ – theoretical capacity of the river section where development is feasible; η_{HPP} – efficiency coefficient of the HPP (usually taken as 0.82).

Flow losses are associated with:

- flow losses through turbine guide vanes, gate seals, etc. (usually doesn't exceed 1%);
- losses due to additional evaporation from the reservoir surface;
- filtration (seepage) losses from the reservoir (approximately 2%);

• losses due to limitations in the useful volume of the reservoir and the throughput capacity of hydroturbines (determined by installed capacity).

Head losses arise from:

• changes in the levels of the upper and lower pools due to changes in water discharge and flow regulation (up to approximately 20% of the river gradient);

• losses in water conveyance structures (grilles, channels, turbine water passages, etc.) and reservoir backwater curves (up to 10%).

If the upper section of the river is not worth developing due to its low capacity, the theoretical capacity of the river section is determined as:

$$N_{section} \approx 0.86\ Nt_{heoretical} \quad (6.2)$$

The technical energy is then: Etechnical = 8760 × Ntechnical (6.3)

where Ntechnical-8760 is the number of hours per year.

A micro-HPP with a capacity of 5 kW can provide electricity to individual small farms located far from population centers and centralized power grids. Electricity with a capacity exceeding 10 kW creates the opportunity to establish small enterprises for processing agricultural products.

The energy potential of micro and small HPPs, depending on the amount of water discharge, must be determined for the minimum discharge in the cold period, as well as for the nominal discharge corresponding to the required capacity in the warm period.

The capacity of micro and small HPPs is determined by the following formula:

$$P=Q\times(H_v-H_p)\times n\times g \quad (6.4)$$

where: P – power, kW; Q – water discharge through the turbine, m^3/s; H_v – geometric height between the upper and lower pool, m; H_p – hydraulic losses in pressure pipes, m; n – efficiency coefficient (0.5...0.7); g – free-fall acceleration (9.8 m/s^2).

The river cadastral chart (Fig. 6.10) is a graph showing the dependence of hydrological and energy indicators of a river on distance. The distance is usually measured from the mouth (estuary) of the river.

This graph usually displays the following data:

• longitudinal profile of the river at low-water (summer-autumn low water)

level;

- graph of changes in the catchment area;
- graph of changes in the multi-year average water discharge;
- sometimes replaced by the annual runoff norm graph;
- longitudinal profiles of river banks – left and right banks separately;
- graph of changes in theoretical capacity;
- specific (unit) capacity graph.

Such a cadastral chart is of great importance in assessing hydropower resources along the river, selecting HPP locations, and performing technical-economic calculations.

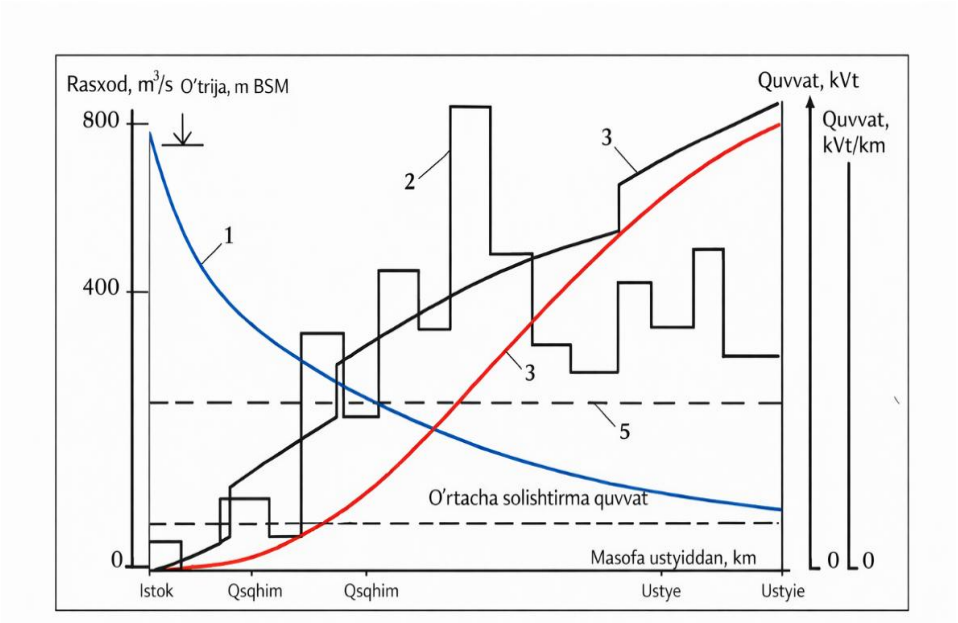

Fig. 6.10. River cadastral chart:

1 – longitudinal profile of the river; 2 – multi-year average water discharge; 3 – theoretical capacity; 4 – specific capacity; 5 – average value of specific capacity.

§6.2. Structure and operating principle of a hydroelectric power plant

What is called water energy or hydropower is the energy of moving or falling water, which is also used, among other things, for generating electricity. People have been using this energy source for thousands of years for example, the energy of water flow was actively used to rotate water mill wheels, in woodworking and pottery. Today, the energy of water flow is converted into electrical energy using special

facilitieshydroelectric power plants.

A hydroelectric power plant (HPP) is a structure used to convert the kinetic energy of water flow movement into electrical energy.

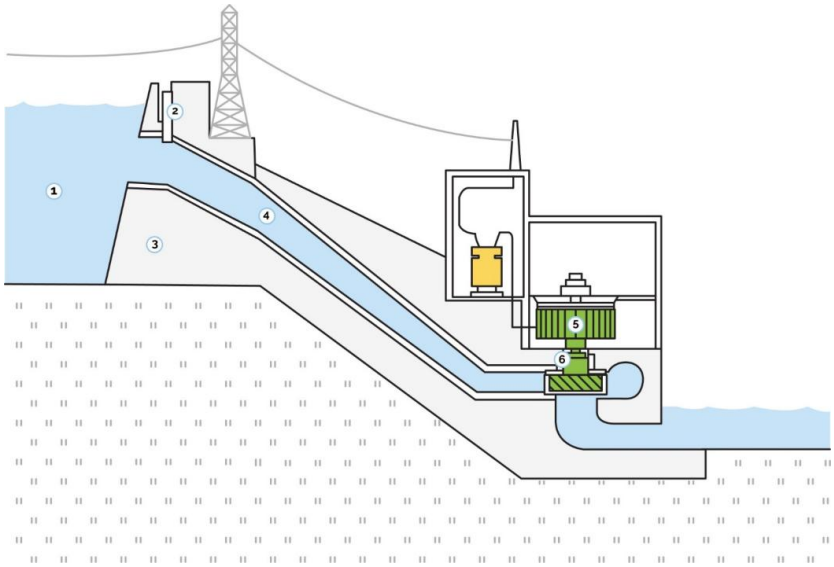

Fig. 6.11. Structure of a hydroelectric power plant:

1-reservoir; 2-gate; 3-dam; 4-water conveyance structures; 5-hydrogenerator; 6-hydroturbine

The main structures of an HPP are the dam and the station building. The dam blocks the river, raising the water level, while the station building contains hydroturbines, electric current generators, and other equipment. The hydroturbine together with the generator connected to it forms a hydro-unit. In a hydroelectric power plant, electricity is generated as a result of the action of pressurized water flow on the hydroturbine blades, causing the rotor of the connected hydrogenerator to rotate.

The operating principle of an HPP is based on converting the kinetic energy of water flow movement into electrical energy. The dam creates a height difference between the water levels above and below it. When water is released through the water conveyance structures, it begins to move with considerable velocity and gains kinetic energy. When such a water flow passes through the hydroturbine blades, they begin to rotate, and as a result the kinetic energy of the water flow is converted into the mechanical rotational energy of the hydroturbine. Then the rotation is transmitted from the hydroturbine to the hydrogenerator rotor, which rotates and produces electrical

energy.

Classification of Hydroelectric Power Plants. Hydroelectric power plants can be of various types depending on the method of converting water flow energy into electrical energy and the relative location of the main blocks of the hydroelectric power plant:

Pumped-storage hydroelectric power plants (PSHPs) deserve special attention. They consist of a storage reservoir, a lower feed reservoir, and a PSHP building housing hydrogenerators and pumps, or reversible hydro-units. A PSHP generates electricity in the same way as a regular HPP — by the movement of water from the storage reservoir under pressure through the impellers of hydroturbines but a PSHP also has the ability to accumulate energy. During hours when there is excess electricity in the grid or when electricity prices are low, a PSHP consumes energy from the grid to pump water from the feed reservoir back to the storage reservoir using the installed equipment.

Hydroelectric power plants are also classified by installed capacity into large (50 MW and above) and small (less than 50 MW) types.

The advantage of small HPPs is that many sites are suitable for their placement. This plays an important role in creating regional own generator capacities and reducing the energy shortage in the region where the small HPP is being built.

1. Run-of-river hydroelectric power plants. Run-of-river HPPs belong to the category of dam HPPs. The main feature of such plants is that the HPP building with the machine hall is located within the dam structure. Thus, the HPP building simultaneously serves the function of a dam, i.e., it bears the water pressure. Such a layout provides significant savings in concrete, which reduces the cost of building the plant. Run-of-river HPPs are built on flat rivers and create relatively small heads (usually not exceeding 30 meters).

2. Dam hydroelectric power plants. For dam HPPs, it is characteristic that the HPP building with the machine hall is located outside the dam structure. The river channel is completely blocked by a dam, and the HPP building is usually located behind the dam, at its lower end. In such power plants, water is delivered to the turbines

through special water conduits. This layout allows the hydroelectric power plant to operate at higher heads from 30-40 meters to 200–300 meters.

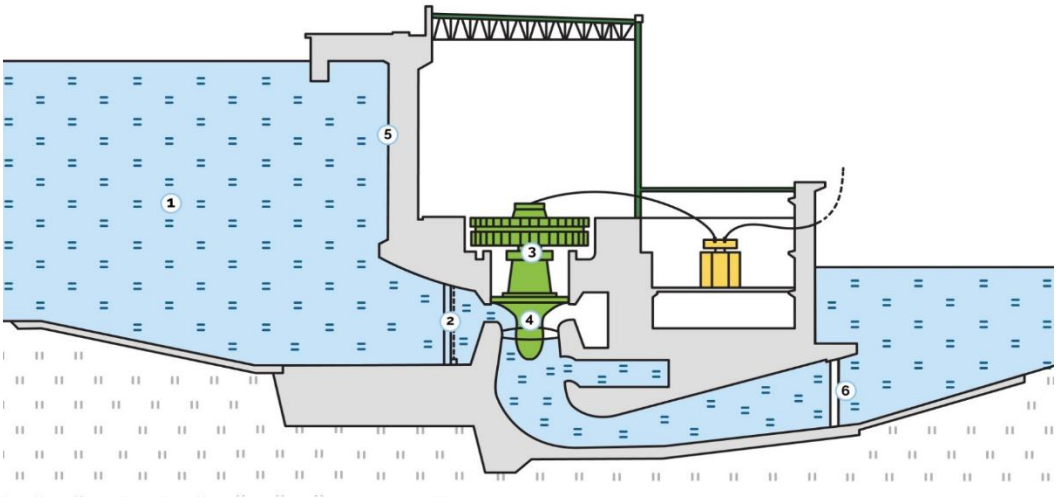

Fig. 6.2. Structure of a dam hydroelectric power plant:

1-reservoir; 2-gate; 3-hydrogenerator; 4-hydroturbine; 5-dam; 6-water conveyance structures.

3. Diversion hydroelectric power plants. Diversion HPPs are characterized by diverting part of the water flow from the main channel. The diverted water is directed through a canal or conduit to the diversion HPP building with the machine hall. There, the force of the moving water acts on the hydroturbine blades and is converted into electrical energy. The water is then returned to the river downstream.

The difference between diversion and dam HPPs is that the former systems do not block the river with a dam to create pressure, but instead use the natural flow velocity of rivers and the geographical location of water conduits. It should be noted that diversion plants may use a small dam or intake structure to ensure an adequate amount of water entering the conduit.

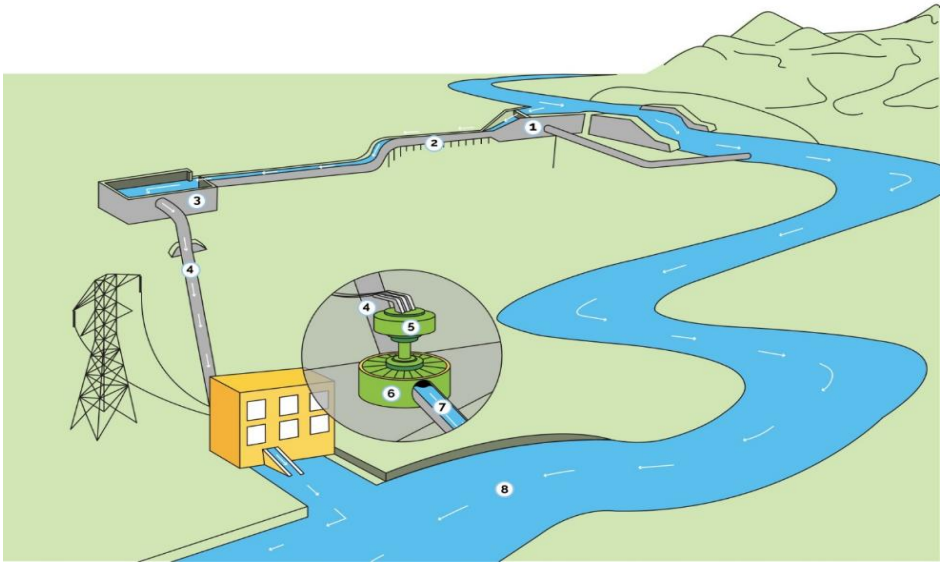

Fig. 6.2. Main nodes of a diversion HPP:

1-intake structure; 2-diversion canal; 3-pressure basin; 4-pressure canal; 5-hydrogenerator; 6-hydroturbine; 7-discharge canal; 8-river.

4. Dam-diversion hydroelectric power plants. Dam-diversion plants combine the positive features of both dam and diversion HPPs. Dam-diversion HPPs are characterized by the presence of a dam blocking the river channel and subsequent extraction of water from the channel through a conduit. Such a combination allows for additional increase in the pressure of the water flow and maximum efficient use of the high gradient of the river channel.

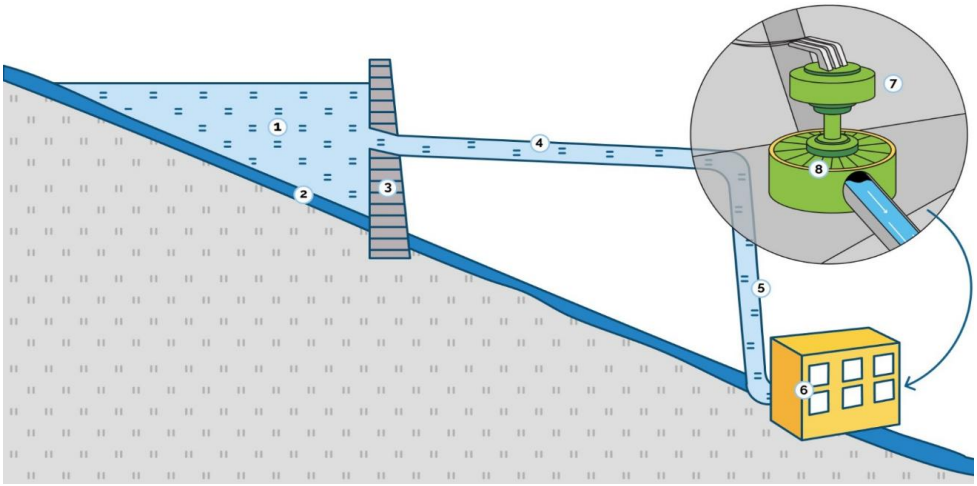

Fig. 6.2. Structure of a dam-diversion HPP.

1-reservoir; 2-natural level of the river; 3-dam; 4-diversion pipe conduit; 5-turbine pipe conduit; 6-HPP building; 7-hydrogenerator; 8-hydroturbine.

5. Water conduit type hydroelectric power plants. Dam-diversion plants combine the positive features of both dam and diversion HPPs. Dam-diversion HPPs are characterized by the presence of a dam blocking the river channel and subsequent extraction of water from the channel through a conduit. Such a combination allows for additional increase in the pressure of the water flow and maximum efficient use of the high gradient of the river channel.

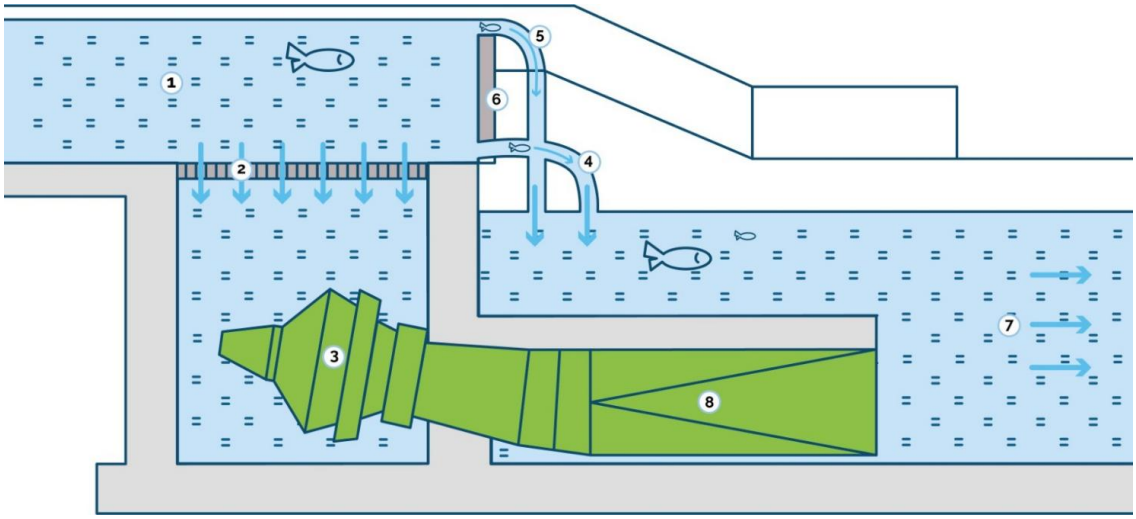

Fig. 6.2. Water conduit type hydroelectric power plant.

1-upper pool; 2-horizontal filtration barrier; 3-submerged hydroturbine with generator; 3-fish passage channel; 4-excess water flow; 5-normal gate position; 6-lower pool; 7-water discharge after passing through turbine.

Selection of Micro-HPP Location and Scheme. The selection of location and scheme for installing a micro-HPP depends on natural conditions as well as the capabilities and needs of the future user. Farms and peasant households, as well as some tourist destinations, are usually located in mountain valleys and gorges, near rivers and streams.

Therefore, the site for a micro-HPP is usually selected in an area close to the place of residence. Site selection for a micro-HPP begins with measuring the water discharge and determining the available head (pressure height).

There are approximately 130 companies worldwide engaged in the production and supply of hydroturbines and hydrogenerators, as well as low-capacity hydro-units [47; 49]. Most companies produce conventional turbines: adjustable-blade turbines (Kaplan

turbine); radial-axial turbines (Francis turbine); bucket turbines (Pelton turbine).

A few companies also produce propeller turbines and cross-flow (double-action) Banki turbines. Only individual enterprises produce exotic turbines-Straflo, diagonal-flow (Turbo) turbines.

Analysis of manufacturers shows:

• axial turbines are produced for heads from 2–5 to 30–80 m, in vertical, horizontal, and G-shaped configurations (for units);

• radial-axial turbines are designed for heads from 10–20 to 500–600 m, with horizontal or vertical shaft;

• bucket turbines are produced for heads from 30–50 to 500–1000 m, with horizontal or vertical configuration;

• cross-flow turbines are produced for heads from 2–5 to 100–200 m only with a horizontal shaft.

In designing hydroelectric power plants, turbine selection is carried out by determining their main parameters (water discharge, efficiency coefficient, rotation speed, head). Composite graphs showing turbine characteristics are also used to create favorable operating conditions for turbines and according to their various operating modes. Composite graphs showing turbine characteristics help in improving operating efficiency and correctly selecting turbines (Fig. 6.11) [40; 55].

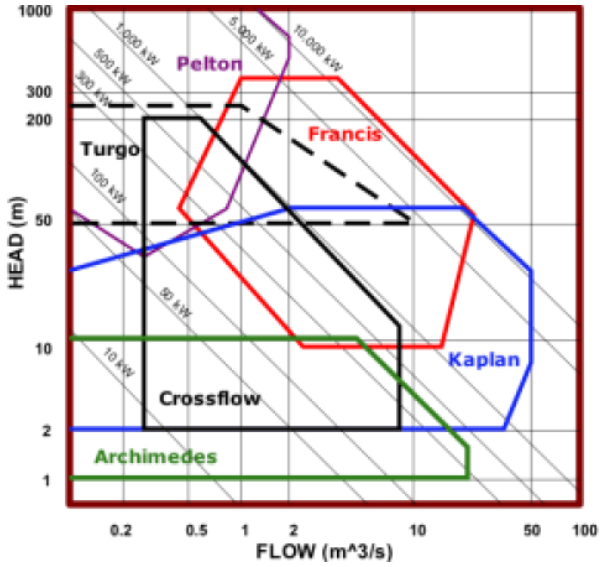

Fig. 6.11. Composite chart of hydroturbines [54, 56, 40].

From the composite chart of turbines shown in Fig. 6.11, it can be seen that

Archimedes screw hydro turbines are adapted for low-head water flows and, unlike other turbines, can achieve high-efficiency power output even at a head height of 0.1 m.

In calculating and selecting turbines, the head height H, power N, and efficiency coefficient η are the main parameters. The head height of the turbine is calculated by the following formula [57;]:

$$\boldsymbol{H = H_{st} + \frac{\alpha_1 \cdot v_1^2}{2 \cdot g} - \frac{\alpha_2 \cdot v_2^2}{2 \cdot g} - h_q} \qquad (6.1)$$

where $H_{st} = Z_1 - Z_2$ is the difference in levels of the supply and receiving water containers; v_1, v_2 are the flow velocities entering and exiting the system; h_q – head lost in water supply, pipes where the turbine is placed, and external resistances; g – free-fall acceleration.

The power of the water flow is calculated using the following formula:

$$\boldsymbol{N_w = \frac{\gamma \cdot Q \cdot H_f}{1000}} \qquad (6.2)$$

where Q – water discharge; H_f – flow head; γ – specific weight.

$$H_f = H_{st} + \frac{\alpha_1 \cdot v_1^2}{2 \cdot g} - \frac{\alpha_2 . v_2^2}{2 \cdot g} \qquad (6.3)$$

The power generated at the turbine shaft is calculated using the following formula:

$$N_T = \frac{\gamma \cdot Q \cdot H_s}{1000} \cdot \eta_T \qquad (6.4)$$

where η_T is the total efficiency coefficient of the turbine impeller [57].

Site planning and organization scheme. Designing a small hydroelectric power plant (SHPP) is a complex and multi-stage process that requires thorough analysis and planning. An important aspect of this process is the site planning and organization scheme, which involves determining the location of all necessary facilities and infrastructure, as well as assessing the impact on the environment.

The first step in designing an SHPP is site selection. This stage involves studying

hydrological, geological, and ecological conditions. The following factors must be taken into account: 1) access to water resources; 2) electricity generation potential; 3) impact on the ecosystem; 4) proximity to existing power grids; 5) access for construction and maintenance.

After site selection, a topographic survey must be conducted, which enables the creation of a detailed map of the area. This helps in subsequent design, as it is necessary to take into account the terrain, the presence of natural and artificial obstacles, as well as existing infrastructure.

The next step is to develop the site planning and organization scheme. It should include:

- location of hydraulic structures (dams, reservoirs, intake structures);
- design of buildings and structures (generator, transformer substations);
- road infrastructure for access to facilities;
- zones for storing materials and equipment;
- planning of environmental protection zones.

In design, it is necessary to take into account regulatory requirements and standards governing the construction of hydroelectric power plants. This includes compliance with environmental standards as well as safety and reliable operation requirements. An important aspect is Environmental Impact Assessment (EIA). This process involves analyzing potential negative consequences for the ecosystem, such as changes in water balance, impact on flora and fauna, as well as possible social consequences for the local population. The results of the EIA must be taken into account in developing design solutions.

After completing all preliminary design stages, public hearings must be held where local residents and stakeholders can express their opinions and suggestions. This is an important step that allows for consideration of public opinion and minimization of possible conflicts.

Upon completion of this design stage, it is necessary to prepare technical documentation that includes all calculations, schemes, and plans, as well as the justification of decisions made. This documentation will serve as the basis for obtaining

construction permits and subsequent project implementation.

After preparing the technical documentation, the next step is to develop design solutions for all elements of the small hydroelectric power plant. This includes:

Hydraulic structures: Design of dams, intake structures, and channels that ensure the necessary water level for plant operation.

Electrical equipment: Selection and design of generators, transformers, and distribution equipment used for converting and transmitting electrical energy.

Control systems: Development of automated control systems ensuring efficient and safe plant operation.

In designing hydraulic structures, hydraulic calculations must be taken into account, which help determine the optimal dimensions and shapes of the structures to achieve maximum efficiency. This includes: calculating water flow, determining the head level, and analyzing possible floods and other natural phenomena.

After completion of design, it is necessary to proceed to construction: preparation of the construction site, construction of hydraulic structures, installation of electrical equipment, testing and adjustment of control systems.

During the construction process, it is important to comply with technological processes and safety standards to minimize risks and ensure high quality of work. Regular inspections and monitoring of all construction stages must also be conducted.

After completion of construction work, the commissioning and adjustment phase begins. This includes:

- testing all systems and equipment;
- checking the operation of generators and transformers;
- training staff serving the plant.

The commissioning and adjustment work is very important, as it allows for identifying and correcting possible deficiencies before the plant is put into operation. After all tests are successfully completed, the small hydroelectric power plant can be commissioned.

Power supply systems. Designing a small hydroelectric power plant (SHPP) is a complex and multi-faceted process that requires taking into account many factors.

SHPPs are an important source of renewable energy and can make a significant contribution to the sustainable development of regions. In this section, we will review the main stages of SHPP design, from initial research to equipment selection.

1. Preliminary research. Before starting design, a number of preliminary studies must be conducted to help determine the feasibility of constructing an SHPP. The main stages of preliminary research include:

- Assessment of hydrological conditions: analysis of data on water resources, including water levels, flow velocities, and seasonal fluctuations.
- Study of geological conditions: assessment of soil conditions and their ability to support the HPP structures.
- Ecological assessment: analysis of environmental impact, including flora and fauna, and possible changes in the ecosystem.
- Socioeconomic assessment: study of the impact on the local population, including possible relocations and changes in lifestyle.

2. Site selection. Selecting a site for SHPP construction is one of the most important stages of design. The following must be taken into account:

- Access to water resources: availability of a river or stream with sufficient volume of water.
- Topographic conditions: terrain relief that may affect the design of dams and other structures.
- Proximity to energy consumers: the location of the SHPP should be convenient for connection to power grids.
- Minimizing impact on the ecosystem: choosing a site with minimal impact on the environment.

3. Design of hydraulic structures. Hydraulic structures form the basis of an SHPP and include:

- Dams: structures that create a reservoir and regulate the water level.
- Conduits: structures that enable directing water flow to the turbines.
- Turbines: devices that convert the kinetic energy of water into mechanical energy.

• Generators: equipment that converts mechanical energy into electrical energy.

4. Equipment selection. Equipment selection for an SHPP depends on many factors, including:

• Type of turbines: choice between hydraulic, axial, or radial turbines depending on flow characteristics.

• Generator capacity: determining the required capacity to meet electricity needs.

• Control systems: selection of automated systems for monitoring and controlling plant operation.

5. Design of electrical systems. The electrical systems of an SHPP play a decisive role in ensuring reliable transmission and distribution of electrical energy. The main aspects of electrical system design include:

• Transformation systems: design of transformer substations to increase or decrease voltage according to grid requirements.

• Electrical circuits: development of connection schemes for generators, transformers, and distribution equipment.

• Protection systems: implementation of protective devices to prevent overloads and short circuits.

• Automation: use of modern technologies for automatic control and monitoring of plant operation.

6. Construction and installation. SHPP construction involves several stages, each requiring careful planning and coordination:

• Site preparation: clearing and leveling the area for construction.

• Construction of hydraulic structures: building dams, channels, and other structures.

• Equipment installation: installation of turbines, generators, and electrical systems.

• Testing: testing all systems and equipment to ensure reliability and safety.

7. Operation and maintenance. After completing construction and commissioning of the SHPP, it is necessary to ensure its efficient operation and regular

maintenance:

- Performance monitoring: continuous monitoring of plant operating parameters to identify possible problems.
- Scheduled maintenance: regular inspection and replacement of equipment to prevent breakdowns.
- Staff training: preparation of qualified specialists for plant management and maintenance.

8. Ecological and social aspects. Designing and operating an SHPP must take into account ecological and social aspects:

- Environmental impact assessment: regular studies to minimize negative impact on the ecosystem.
- Interaction with local population: informing and involving local residents in processes related to the project.
- Social programs: development of initiatives aimed at supporting local residents and developing the region.

Thus, designing a small hydroelectric power plant requires a comprehensive approach that takes into account technical, ecological, and social aspects. Each stage of design and construction must be well thought out to ensure efficient and safe operation of the plant.

CHAPTER 7. DESIGN OF BIOGAS POWER PLANTS

§7.1. Biogas production units and their operation process.

Modern techniques and technologies are opening up prospects for the use of renewable energy sources. Directing scientific and practical work toward this field helps reduce the consumption of fossil fuels.

Bioenergy is a renewable energy source, and energy is obtained through the processing of agricultural and household waste. The primary type of energy produced is biogas, while the secondary type is electrical energy. Considering that Uzbekistan is a country with a developing agricultural and agro-industrial sector, bioenergy will remain a rapidly developing branch of the energy industry in the future.

Figure 7.1. View of the world's largest biomass-fired power plant.

The plant generates energy by burning 1000 m³ of biofuel per hour. The lower (base) diameter of the combustion boiler is 8.5 m, while at a height of 40 m, the upper diameter reaches 24 m. To supply the plant with biofuel, 120 cargo transport trucks are used per day. The plant can also use coal as a fuel.

Biomass and its composition.

Biomass is a term that unites the origin of all organic substances found in the plant and animal world. Biomass is divided into primary types plants, animals, microorganisms, and others and into secondary types, which are formed after long-term processes of transformation into other kinds of fuels, as well as by-products

generated during biomass processing and materials produced throughout the life activities of humans and animals.

Figure 7.2. Biofuel feedstocks:

a – biofuel plantations established from willow trees; b – peat formation as a result of long-term biological processes of plant matter.

In turn, wastes are also divided into primary wastes generated during the processing of primary biomass (fodder, stems and leaves, shavings, distillery residues, branches) and secondary, which include products of the physiological metabolism of humans and animals.

In addition, in some European countries, fast-growing plants are used as raw materials for electricity generation in order to prevent excessive deforestation. For example, in Sweden, special fast-growing willow plantations are cultivated for biomass (Fig. 7.2a). The area allocated for willow cultivation is determined in accordance with the biomass fuel demand of biomass-based power plants. Such plants, in addition to biomass, can also use peat formed after long-term biological processes of biomass and other fuels as biological fuel (Fig. 7.2b).

Biomass represents a broad range of renewable energy resources and includes wood, industrial, agricultural, and household wastes. It can be utilized as an energy source through combustion, gasification, pyrolysis, and biochemical processing to produce alcohol or biogas. Each of these processes has a specific field of application depending on the intended purpose. According to some data, the contribution of energy obtained from biomass to the global energy sector is about 12%. In the countries of the

European Union, energy derived from biomass accounts for only 3% of total energy consumption; however, in some countries, such as Austria-12%, Sweden-18%, and Finland-23%.

Primary biomass consists of plants that grow naturally on land and in water. Biomass is formed as a result of photosynthesis; that is, solar energy is accumulated in the mass of growing plants through photosynthesis. The energy efficiency of photosynthesis averages about 5%.

For the purpose of energy production, primary biomass is used as a fuel that can substitute traditional fuels. Primary biomass includes forest resources, wood-processing industry residues, and agricultural waste.

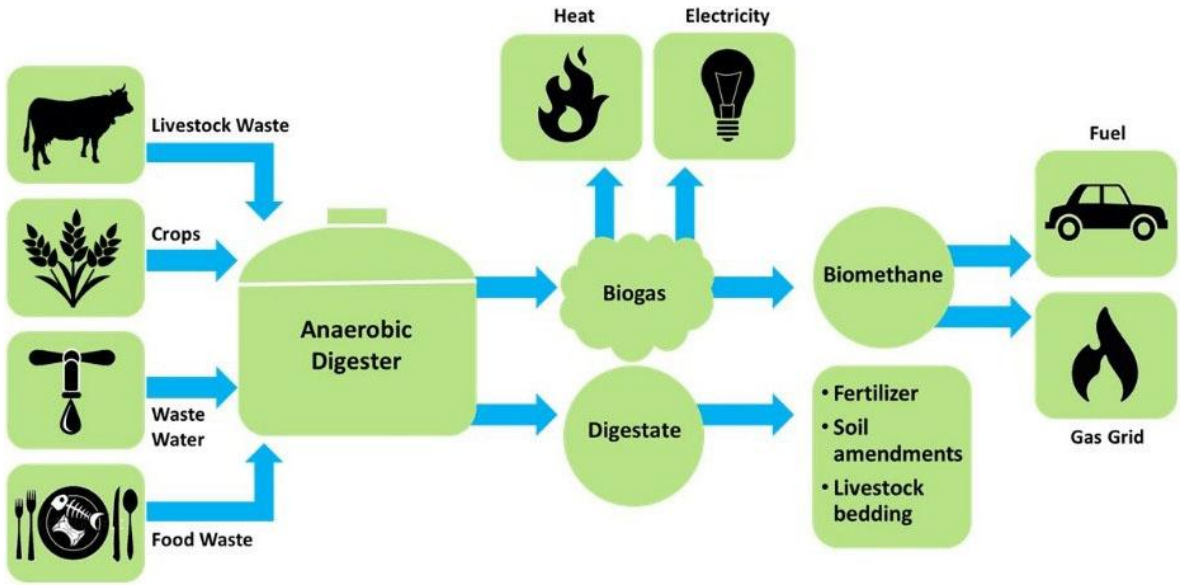

Figure 7.3. Stages of energy production from biomass.

In Uzbekistan, irrigated agricultural lands are mainly occupied by cotton, grain, tobacco, sunflower, and melon crops. To date, the stalks of cotton have been partially used as raw material in the production of alcohol, paper, and several construction materials. The stalks of the remaining plants are either discarded or burned. These agricultural residues can also be used as biomass, i.e., biofuel.

Biomass energy is considered one of the most promising sources of renewable energy and is a clean and renewable form of energy produced from organic matter (plants and animals). Biomass-based energy systems are distinguished not only by the wide availability of raw materials but also by their ability to produce both heat and

electrical energy. Biomass is widely used for the production of heat and electricity as well as chemical feedstocks using various conversion methods. The most common biomass resources include wood, wood shavings (sawdust), straw, agricultural residues, food processing waste, forestry residues, crops, municipal waste, and wastewater (Figure 7.4).

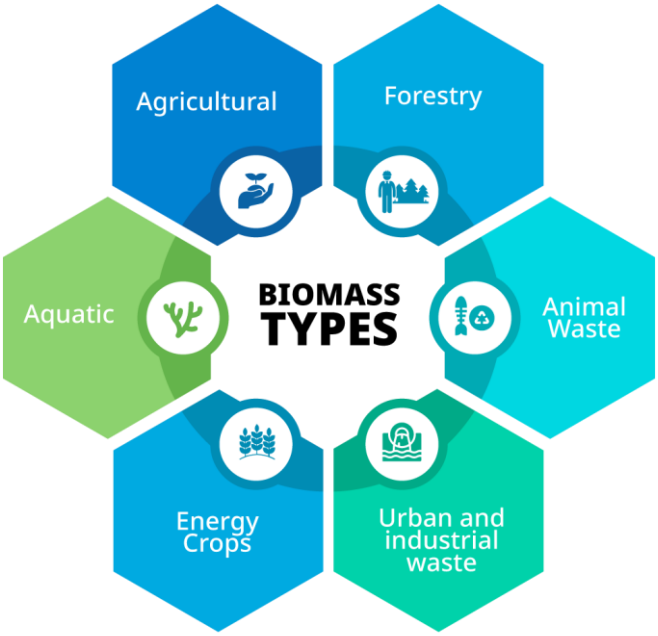

Figure 7.4. Biomass sources.

Unlike other sustainable energy sources, biomass can directly produce fuels along with chemicals. Indeed, biomass is a suitable alternative to fossil fuels, as it is a non-fossil organic material that stores internal chemical energy and helps reduce greenhouse gas emissions released into the atmosphere. Its annual global energy potential is estimated to be 200-500 EJ. Biomass supplies about 14% of the world's energy and is classified as a clean, renewable, continuous, and dispatchable energy source with significant growth prospects. Its use for energy purposes is widespread and well established worldwide.

Biomass is a renewable energy source consisting of forest and agricultural plant residues, wastewater sludge, organic matter, and other organic wastes that can be used for the production of biofuels and electricity. Municipal solid waste (MSW) is a type of biomass, mainly composed of residues from food, paper, plastic, wood, textile, metal, and glass products. It also includes certain hazardous wastes such as electric

bulbs, batteries, automotive parts, and discarded pharmaceuticals. MSW is considered a source of environmentally friendly energy (biogas, biofuel) [89].

§7.2. Anaerobic digestion process of organic biomass.

Anaerobic decomposition is the process in which organic waste is broken down by bacteria in an oxygen-free environment into gaseous fuel. The process occurs in several stages, during which organic substances are sequentially converted into simpler organic compounds. The final product is biogas, which consists of a mixture of methane, carbon dioxide, and small amounts of carbon monoxide gases. Biogas is also known by several other names, such as swamp gas, sewage gas, fuel gas, and wet gas. In India, it is commonly referred to as "gobar gas." Table 7.1 below presents the main gaseous components of biogas and their proportions.

Table 7.1. Composition of biogas

№	Constituents	Formulae	Proportion in percentage
1	Methane gas	CH_4	50-65
2	Carbon dioxide	CO_2	30-45
3	Hydrogen	H_2	1-3
4	Nitrogen	N_2	0-5
5	Oxygen	O_2	0.01
6	Hydrogen sulphide	H_2S	1-2

The treatment of any slurry or sludge containing a large amount of organic matter utilizing bacteria and other organisms under anaerobic condition is commonly referred as anaerobic digestion.

Anaerobic digestion consists of the following three phase.

(i) Hydrolysis phase,

(ii) Acid formation phase

(iii) Methane formation phase

Hydrolysis. Large molecules are breakdown into smaller size by enzymes which in turn are decomposable by bacteria. The organic substances such as polysaccharide,

protein and lipid are converted into mono-saccharide, peptide, amino acids, and fatty acids. Then they are further converted into organic acids (acetate, propionate and butyrate). Cellulytica bacteria help to reduce chains and branches. Cellulytica bacteria is of two types mesophilic (30°- 40°) and thermophilic (50°- 60°).

Acid formation. Acid phase which simple organic materials are converted into simpler acids such as volatile fatty acids. Acetic acid is one common by-product of digestion of fats, starch and proteins. Methane bacteria are strictly anaerobic and can produce methane either by fermenting acetic acid to from methane and carbon dioxide, or by reducing carbon dioxide to methane using hydrogen gas. Acetic acid is to react with methanogenic bacteria resulting in methane formation. Acetic acid accounts for 70 % of methane produced.

Methane formation. Methanogenic bacteria react with acetic acid, ethanol, carbon dioxide and hydrogen to produce methane. Methane forming bacteria slowly, in about 14 days at 25°C complete the digestion. The remaining indigestible matter is referred as “slurry”.

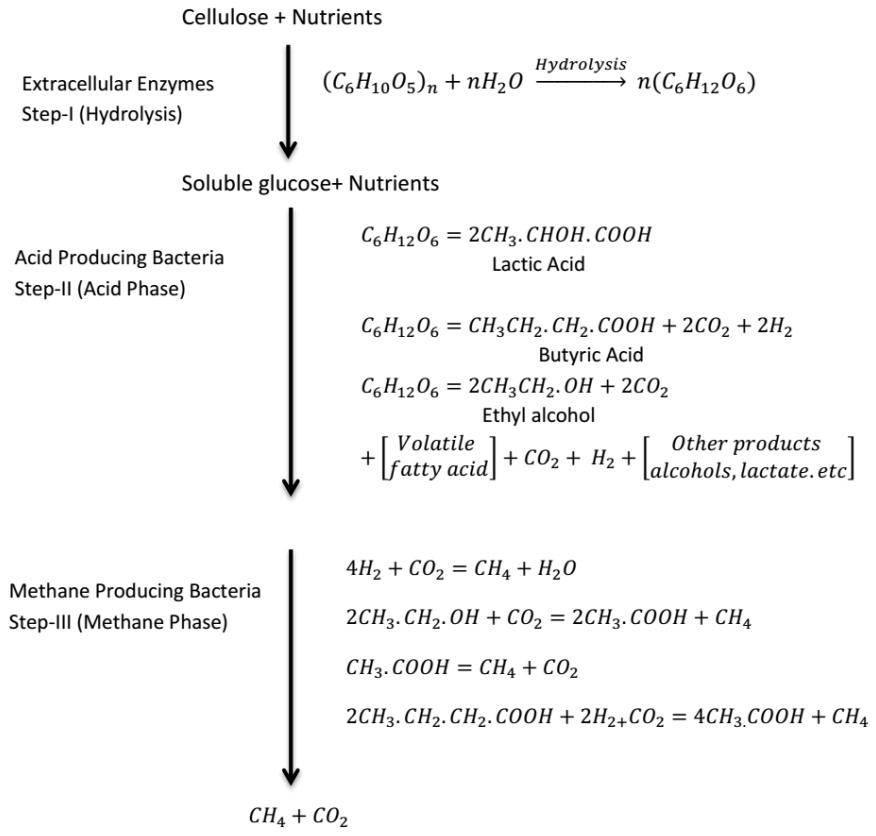

Figure 7.4. Details of biochemistry of anaerobic digestion process.

Biogas production involves different physical, chemical and biological process for conversion of biodegradable organic materials to energy rich gas. Below, some of the parameters affecting the process are discussed.

C/N ratio. The ratio of carbon to nitrogen present in the feed material is called C:N ratio. It is a crucial factor in maintaining perfect environment for digestion. Carbon is used for energy and nitrogen for building the cell structure. Optimum condition for anaerobic digestion to take place ranges from 20 to 30:1. This means the bacteria use up carbon about 20 to 30 times faster than they use up nitrogen.

When there is too much carbon in the raw astes, nitrogen will be used up first and carbon left over. This will make the digestion slow down and eventually stops. On the other hand, if there is too much nitrogen, the carbon soon becomes exhausted and fermentation stops. The nitrogen left over will combine with hydrogen to form ammonia. This can kill or inhibit the growth of bacteria specially the methane producers.

Temperature. Temperature affects the rate of reaction happening inside the digester. Increase in the ambient temperature increases the rate of reaction thus increasing the biogas production as well. Methane bacteria work best at a temperature of 35 ° - 38 °C. The fall in gas production starts at 20 °C and stops at a temperature of 10 °C. Studies hawed that 2.25 m^3 of gas was produced from 4.25 m^3 of cattle dung every day when the digester temperature was 25 °C. When the temperature rose to 28.3 °C the gas production was increased by 50 per cent to 3.75 m° per day.

Retention time. It is the theoretical time that particular volume of feedstock remains in the digester. In other words, retention time describes the length of time the material is subjected to the anaerobic reaction. It is calculated as the volume of digester divided by the feedstock added per day and it is expressed in days. Under anaerobic condition, the decomposition of the organic substances is slow and hence need to keep for long time to complete the digestion. In case of Indian digesters, where the feed stock is diluted with equal composition, so demarcation prevails between solid and liquid. In this case, biomass in the form of bacteria is washed out; hence the solid retention time (SRT) is equal to hydraulic retention time (HRT).

Loading rate. Loading rate is defined as the amount of raw material fed to the digester per day per unit volume. If the reactor is overloaded, acid accumulation will be more obviously affecting daily gas production. On the other hand, under loading of digester have negative impact in designed gas production.

pH or hydrogen ion concentration. To maintain a constant supply of gas, it is necessary to maintain a suitable pH range in the digester. pH of the slurry changes at various stages of the digestion. In the initial acid formation stage in the fermentation process, the pH is around 6 or less and much of CO_2 is given off. In the letter 2-3 weeks times, the pH increases as the volatile acid and N_2 compounds are digested and CH_4 is produced. The digester is usually buffered if the pH is maintained between 6.5 and 7.5. In this pH range, the micro – organisms will be very active and digestion will be very efficient. If the pH range is between 4 and 6 it is called acidic. If it is between 9 and 10 it is called alkaline. Both these are detrimental to the methanogenic (Methane production) organisms.

Total solid content. The raw cow dung contains 80-82% of moisture. The balance 18-20% is termed as total solids. The cow dung is mixed usually in the proportion of 1:1 in order to bring the total solid content to 8-10%. This adjustment of total solid content helps in digesting the materials at the faster rate and also in deciding the mixing of the various crop residues as feed stocks in biogas digester.

Table 7.2 below presents the optimal values of the key parameters required for biogas production.

Table 7.2. Optimum conditions for biogas production

Parameters	Optimum value
Temperature	30 – 35 ^oC
pH	6.8 – 7.5
C/N Ratio	20 – 30:1
Solid content	8 – 10 %
Retention time	20 – 50

Bio-energy is a critical issue for multiple reasons besides environmental concerns

such as i) to guarantee energy security through a more diversified energy mix and less reliance on imported fossilenergy carriers, ii) the sustainable use of natural resources as well as iii) the need to revitalize rural economies. Thus, an increased share of renewable energy is mandatory in energy system to satisfy the mentioned issues besides reducing greenhouse gases (GHG) emission.

The waste-to-energy concept is being highly promoted as a part of the efforts into sustainable development in energy sector. The use of forest and agricultural residues aswell as other biomasswaste fromagricultural and industrial activities for bio-energy production (mainly electricity and heat) plays a key role in the energy system and it is expected to increase over the next few years. However, the discontinuous availability and the relatively high maintenance and logistic costs hinder the economic convenience of biomass for large scale energy production. Therefore, numerous efforts are being carried out to make the whole process achievable from an economic approach.

Production of heat and electricity from woody residues either from forest or agricultural activities could considerably increase the contribution to energy security, reduce GHG emission and add value to waste materials. Indeed, it is a common practice in factories such as pulp mills where pulp is generated together with heat and electricity. Different studies evaluated the potential quantities of available forest biomass residues for energy production in countries such as Portugal or Uganda. According to them, only if cogeneration is implemented the wood fuel resource should be sufficient to satisfay the required capacity demand. However, special attention must be paid into the biomass-supply competition with pellets production, one of the largest internationally traded solid biomass commodities for energy purposes mainly derived from wood residues.

Sara González-García and Jacopo Bacenetti [92] analyzed the production of electricity and heat from woody biomass generated as a result of forestry and agricultural activities in Italy, taking into account different production scenarios and types of end use. This is because the total forest area in the country amounts to 10,467,000 hectares, covering approximately 34.7% of Italy’s territory. Although a variety of management systems exist for forests, shelter cut (high forest) in

combination with natural regeneration is widespread. In this case, woody residues (mainly tops and brances), produced during logging operations, can be used for bio-energy applications. Accordingly, the main objective of the study was to reduce the demand for fossil fuels by expanding small-scale biomass-based heat energy production systems in Italy. The analysis evaluated the energy potential of biomass obtained from fast-growing energy crops such as willow and poplar plantations, as well as from natural forests and conventional poplar plantations. The results of the study were compared with the conventional energy production scenario in Italy, namely the profile of electricity and heat generation based on natural gas.

In this study, the functional unit selected for evaluating the environmental profile is 1 kWh of electricity produced in a cogeneration (combined heat and power) system based on the Organic Rankine Cycle (ORC). The electricity generation efficiency of the ORC system is assumed to be 20%, while the thermal efficiency of the boiler is taken as 85%, and these values remain constant regardless of the biomass source. The CHP is mainly constituted by two different sections. The first one is characterised by a biomass boiler (thermal power of 6.047 MW) fed with the woody biomass while the second section is mainly constituted by a ORC turbine with 1 MW of electric power. The Organic Rankine Cycle's principle is based on a turbogeneratorworking as a conventional steam turbine to transform thermal energy into mechanical energy and finally into electric energy. Instead of generating steam from water, the ORC system vaporises an organic fluid, characterised by a molecular mass higher than that of water (e.g., HCFC-123 with a molecular weitght of 152.9 g·mol−1),which leads to a slower rotation of the turbine, lower pressures and no erosion of the metal parts and blades.

At the CHP plant, the heat produced by the biomass boiler is transferred, using a diathermic oil (310–315 °C and 6 bar), to the ORC where is transformed in mechanical power and, through a electrical generator, in electricity. More in details, the organic fluid vapor rotates the turbine, which is directly coupled to the electric generator. Afther that, the exhaust vapor flows through the regenerator, where it is then condensed in the condenser and cooled by the cooling circuit. The thermal energy used in the district heating is recovered at the condenser. The district heating distribution grid

considered is around 1.5 km-length and presents a lifespan of 30 years.

Figure 7.6 below shows the upstream system boundaries corresponding to the four scenarios considered as baseline cases in the study. While all the electricity produced is directly supplied to the Italian national grid, only 16 % of the total heat generated is delivered to meet the heating demand of a nearby hospital and school. The remaining 84 % of the heat is considered as unrecovered waste.

Scenario 1 (Sc1) is based on the consideration of residues from natural regeneration forestry and industrial activities as feedstock. These stands are naturally managed i.e., they are handled under low management intensity. The forest stands are untouched forests with a history of limited management. Thus, no activities are performed throughout the lifespan (>60 years) after initially diversifying the forest structure. Biomass extracted is mostly dedicated as raw material (roundwood) for furniture sector. Wood residues such as tops and branches are recovered in the harvesting activities as well as throughout the lifespan of the plantation. In this scenario, these residues are considered as raw material for bio-energy production (see Fig. 7.6 a). Firstly, wood residues are chipped into the forestry using a self-propelled chipper and after they are transported to the bio-energy plant. Residues from furniture production activities are also considered and chipped in the plant. In this scenario, the entire environmental burdens of the multifunctional process (only derived from logging operations) are allocated to the main product (roundwood). Therefore, wood residues are considered waste and free of environmental burdens except with regard to forest residues chipping and chip wood transport.

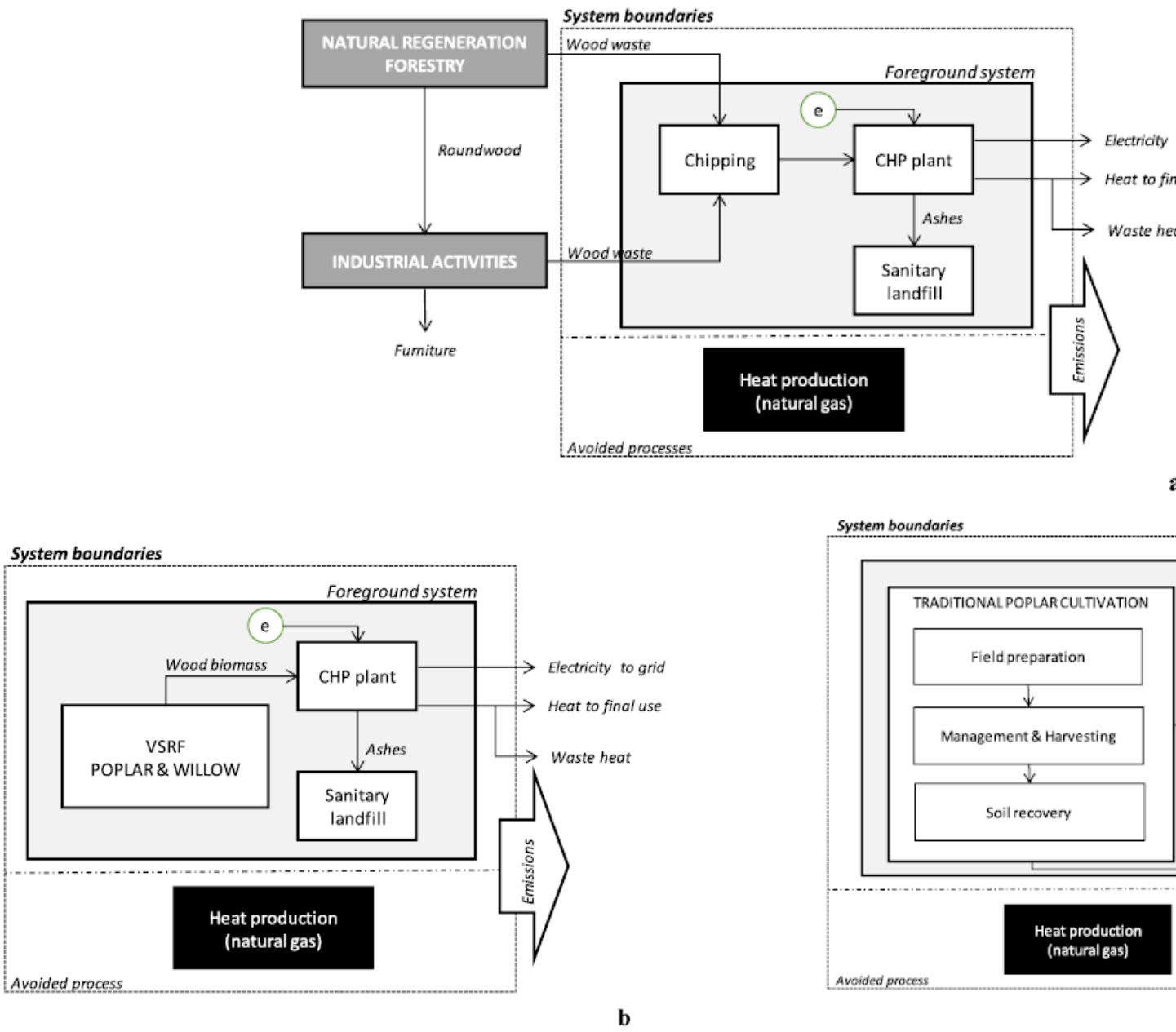

Figure 7.6. System boundaries for the modelled bio-energy systems producing the same amount of bio-energy (heat and electricity).

Scenario 2 (Sc2) and Scenario 3 (Sc3) consider the biomass from VSRF stands of poplar and willow species, respectively, as feedstock for heat and power generation (see Fig. 7.6 b). The management of VSRF plantations has been considered within the system boundaries considering all processes performed in the stands from field preparation and management, harvesting and field recovery at the end of the lifespan of the plantations (approximately ten years in both species). It is important to highlight that as difference to forest stands dedicated to roundwood production for industrial uses, all the produced biomass (including wood residues such as branches, stools and leaves) is recovered and sent to bio-energy production. The total trees are felled, and directly chipped on the field by means of a forage harvesters equipped for a specific header.

Scenario 4 (Sc4) is based on the valorisation of forest residues derived from traditional poplar stands which are mainly dedicated to the production of roundwood for pulpwood and furniture production. Wood residues are managed in the same way as in Sc1, being chipped in the power plant before their combustion in the CHP unit. All forest operations carried out in the stands have been computed within the foreground system boundaries (see Fig. 1c). Thus, organic fertilisation, ploughing, harrowing and planting have been considered as part of field preparation activities. Herbicide and pest control, mechanical weed control, irrigation (if necessary, depending on the climatic conditions) and harvesting at the end of the lifespan (12 years) have been included in stand management and harvesting stage. Finally, field recovery after the harvesting is also performed with a forestry shredder.

Within each scenario, avoided processes have also been accounted since it is assumed that biomass combustion allows savings of natural gas for heat production. Therefore, the production of the amount of heat sent for final use in the surroundings (hospital and school) considering the combustion of natural gas in a domestic boiler has been contemplated.

According to the main findings from this study, LCA methodology can be considered as a valuable and useful tool to support decision making strategies under an environmental approach, specifically for systems under development such as the ones reported in this study. However, additional research should be performed not only in

the environmental pillar of the sustainability but also in the social and economic ones to obtain a full overview. Moreover, attention must be paid in these categories different than climate change and fossil depletion (the ones that are subject of great public debate), considerably affected by air pollutant emissions derived from biomass combustion mostly when dedicated energy crops are considered.

In the study conducted by Eirik Ogner Jåstad et al. [93], a partial equilibrium model (Balmorel) was employed to analyze the district heating and electricity markets of Northern Europe, covering Norway, Sweden, Finland, Denmark, the Baltic states, Poland, and Germany. The model is designed to minimize the costs of heat and electricity production and supply with hourly time resolution. The study focuses on the role of wood biomass in energy generation under different carbon pricing scenarios. To assess the emission impacts associated with the use of wood biomass, emissions from fossil fuels under a least-cost biomass deployment scenario were compared with a counterfactual case in which biomass is not used at all for electricity and heat production. Subsequently, the emission reduction effect of using wood biomass for heat and power generation was compared with the effect of using the same amount of biomass to substitute fossil fuels in the transport sector.

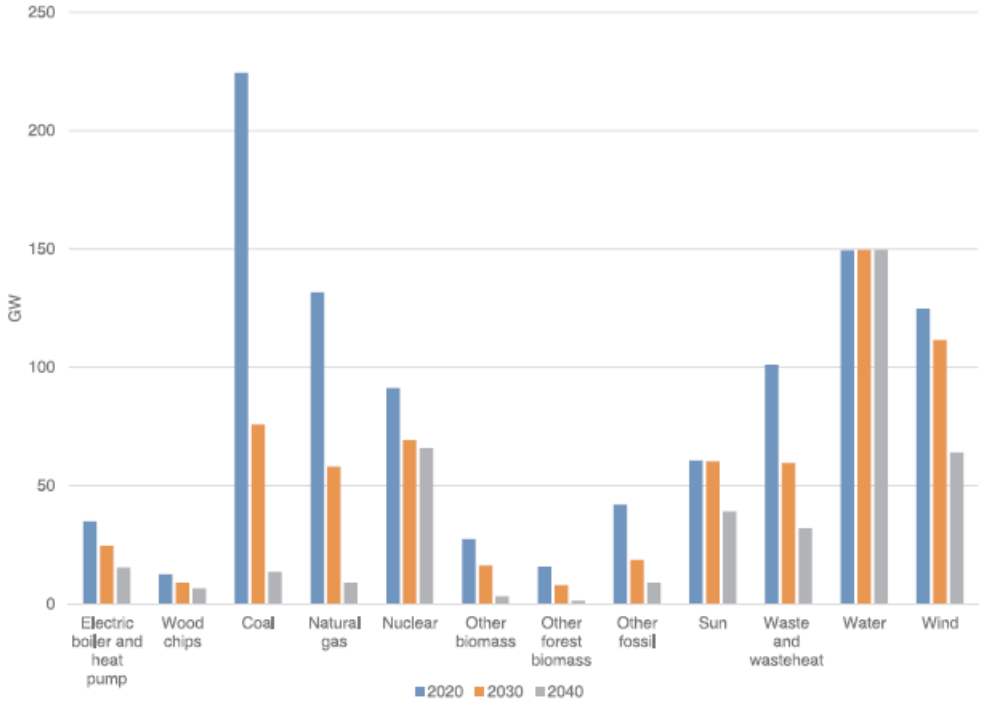

Figure 7.7. Exogenous installed electricity and heat generation capacities by fuel/technology (GW), divided by fuel.

Energy production in Balmorel happens with upper bounds on exogenously or endogenously defined production capacities. Planned capacities, both commission and decommission, are exogenously included in the model, while future investment possibilities are endogenously chosen by the model when market prices cover capital costs and variable production costs. The exogenously installed capacities are show in Fig. 7.7; the exogenously defined capacities decline over time for all technologies except for hydropower technologies. Decommission of installed capacities follows published phase-out strategies and expected techno-economical lifetimes. It is assumed that the nuclear power plants in Belgium and Germany will be fully decommissioned between 2020 and 2030, which follows known closure plans.

Due to decommission of existing plants, Balmorel needs to invest in new production units for fulfilling the consumption shown in Table 7.3. The optimization model estimates investments according to the techno-economically most profitable technology available in order to meet the demand. The final consumption of heat and electricity shown in Table 7.3 is equal for all scenarios.

Table 7.3. Assumed consumption of heat and electricity (TW·h/year).

	Electricity demand 2020–2040	**Heat demand 2020–2040**
Germany	530	116
Denmark	32	33
Estonia	7.7	5.0
Finland	82	79-76
Lithuania	6.5	7.7-6.0
Latvia	11	6.0
Poland	144	66-88
Sweden	131	90-85
Norway	121	13-15
Belgium	83	Heat sector not included
France	448	
Netherlands	111	
United Kingdom	311	
Total	**2018**	**415-428**

This table presents the projected amounts of heat and electricity consumption. Electricity demand remains constant in all years, while heat demand is expected to increase within a certain range for some countries.

The model version used in this study covers supply and demand of district heating and electricity in Norway, Sweden, Finland, Denmark, Estonia, Latvia, Lithuania, Germany, and Poland, and supply and demand of the electricity in Belgium, France, the Netherlands, and the United Kingdom. Each country consists of one or more regions. The model version uses a total of 24 electricity regions, whose borders are similar to the NordPool regions [93], see Fig. 7.8 for the regional division for the Nordic countries.

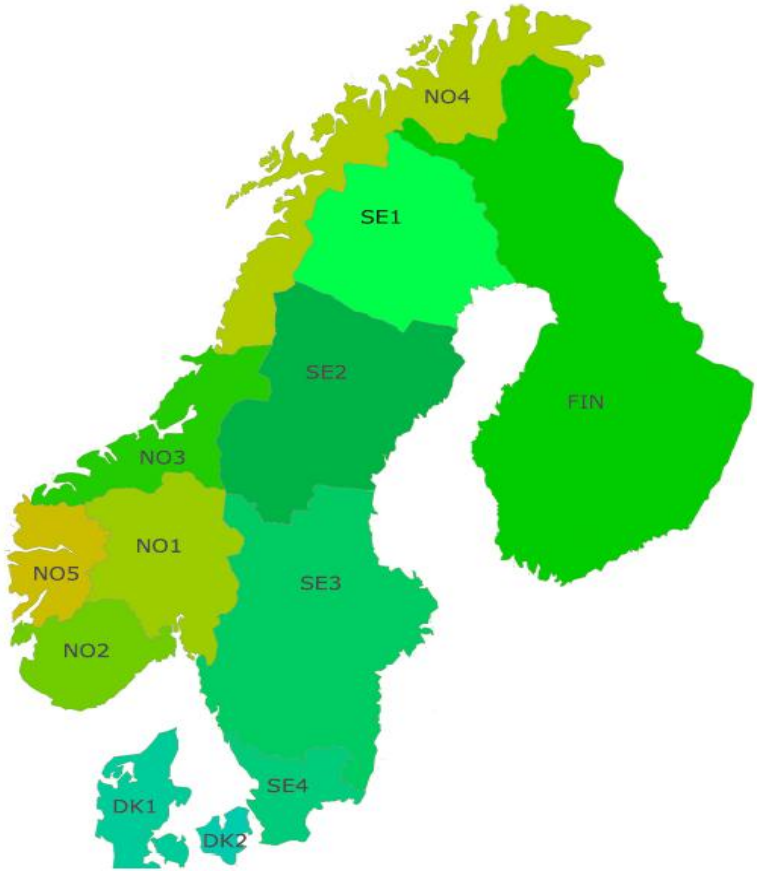

Figure 7.8. Regions in the Nordic countries, in addition is Germany divided into 4 regions and Estonia, Latvia, Lithuania, Poland, Belgium, France, the Netherlands, and the United Kingdom dividend into one region each.

Furthermore, in this study, a cost-minimization version of the Balmorel model is applied, in which the objective is to meet a given energy demand at the lowest possible cost. The objective function of the model includes the following cost components: fuel costs, operation and maintenance costs, reservoir and operating costs for hydro storage, transmission costs, investment annuity costs for expanding electricity and heat generation, transmission and storage capacities, as well as taxes. The most important constraint in the Balmorel model is the energy balance constraint. This constraint ensures that, for each time step and subregion, the sum of energy consumption,

production, transmission, losses, and storage is equal to zero.

Based on the detailed modeling of electricity and heating systems, the researchers concluded that the use of wood biomass for heat and power generation primarily contributes to reducing natural gas-based electricity production by 2040. Furthermore, under all analyzed carbon pricing scenarios, biomass continues to play a significant role in the supply of heat and electricity. When excluding wood chips as an energy source for heat and electricity production the total system costs increase by 0.2–0.7 % and the average heat prices increase by 8–20 % in 2030.

The impacts on the heat price are low in some countries and substantial in others, such as Sweden and Finland. Increased use of woody biomass would, to some extent, replace wind power, coal power, and electricity used in district heating systems. As such, we can conclude that using wood chips for power and heat reduces emissions from fossil fuels, but the model results show that the magnitude of emissions reductions depends on the assumed carbon price and technology mix in the heat and power sectors.

The substitution effects of woody biomass decline with increasing carbon price and is lower in 2040 than in 2030. This is due to the overall decrease in the share of fossil fuels in the energy system in 2040. For the Northern European energy system (Poland, Germany, and the Nordic and Baltic countries) the optimal use of wood chips reduces the fossil carbon emissions by 7–19 million tonnes CO_2eq in 2030 (4–27 % emission reduction). In 2040, the corresponding reductions are in the range 10–17 million tonnes CO_2 eq (7-43 % emission reductions). If wood chips are not included as a fuel option in the model simulations, the use of heat storage capacity increases up to 24 % more than when biomass is included.

Due to the large availability of bio-waste in Morocco, electricity generation from biomass energy can help mitigate these challenges and compensate for the decline in wind and solar power generation during sunny, rainy, and windless periods. In this regard, Meisam Mahdavi et al. [94] assessed the feasibility of hybrid electricity generation systems utilizing biomass, wind, and solar energy in the village of Tazuta and rural areas of the city of Fes in Morocco.

Expensive energy import bills, an upward trend of petroleum prices, and growing energy demand due to economic development, industrialization, population growth,

urbanization, and improvement of living standards has pushed Morocco to utilize renewable energies as alternative energy sources.

Power generation of a solar and wind unit is very uncertain and this issue reduces the power system stability, in which hybrid utilization of these renewables and certain biomass energy resources can help the system stabilization.

Biomass can directly generate electric energy and heat via the common method of combustion or indirectly can be used to produce biofuels using gasification, anaerobic digestion, and fermentation.

The following figures present a comparison of the total costs of different electricity generation methods (Fig. 7.9), the amount of water required for energy generation from biomass (Fig. 7.10), and the volume of CO_2 emissions for all energy generation methods (Fig. 7.11).

From Fig. 7.9, it can be observed that employing biomass power plants beside other kinds of renewable energy technologies for electricity generation is more economic than utilization of only wind turbines or hybrid PV and wind units.

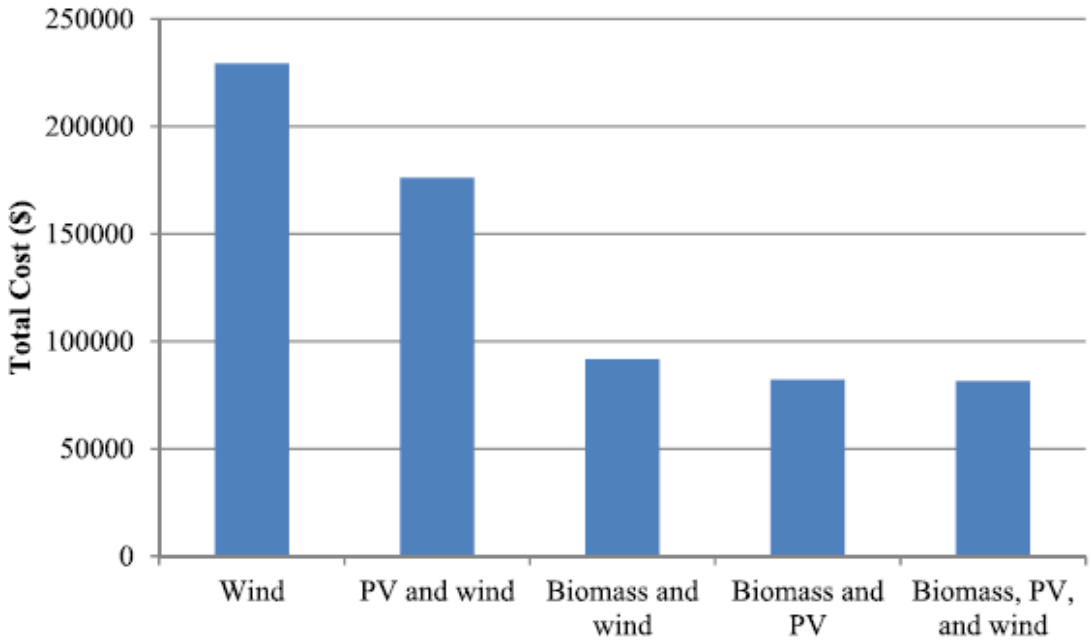

Figure 7.9. Total cost of different generation technologies.

The main reason for this is that biomass energy production does not require the installation of batteries and converters, while wind and photovoltaic systems require such equipment, which leads to additional costs.

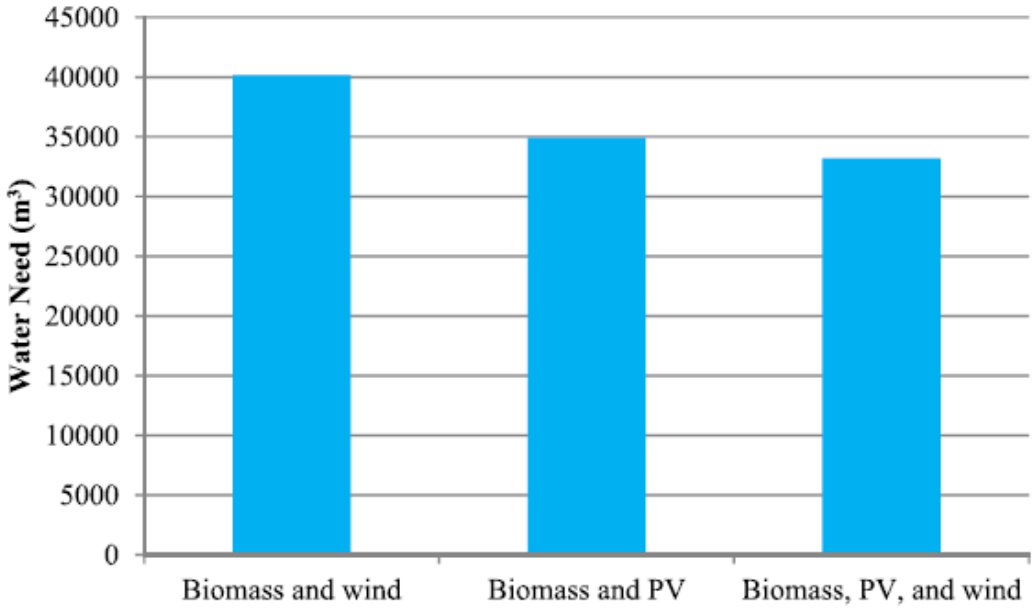

Figure 7.10. Water needs of different generation methods including biomass.

Figures 7.10 and 7.11 above indicate that, in hybrid generation systems combining biomass, solar, and wind energy, both water consumption and carbon dioxide (CO_2) emissions are significantly lower compared to other electricity generation methods involving biomass. These results suggest that such a three-source hybrid system represents a more sustainable electricity generation option with minimal impact on water resources and the environment.

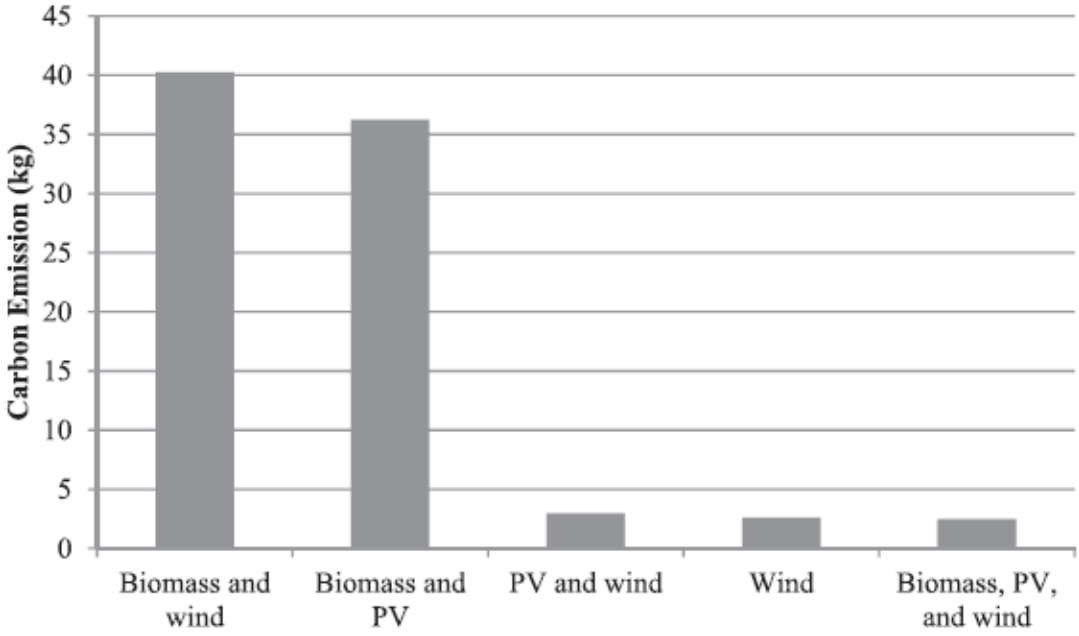

Figure 7.11. Carbon emission of all generation methods.

Fig. 7.12 indicates the share of each electricity generation technology in satisfying the load of both regions when biomass, PV, and wind units are operated simultaneously. Also, Fig. 7.13 shows graphically how the proposed system is meeting

the total daily load demand.

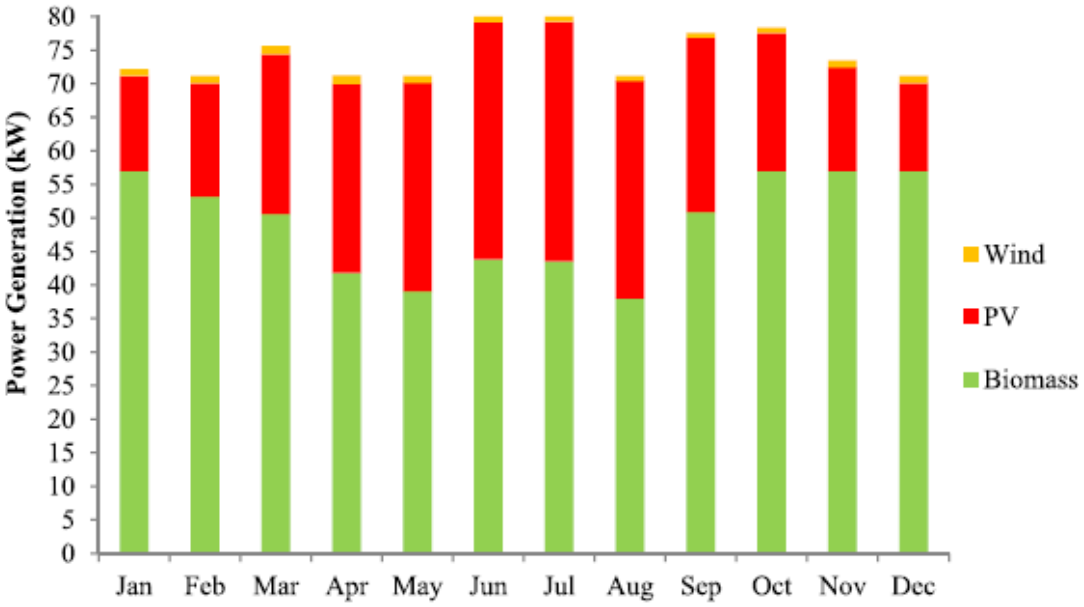

Figure 7.12. Electric power generation during the year.

As observed in Fig. 7.12, the electricity generated by the biomass meets the majority of monthly power demands. The reason is that the wind power generation strongly depends on wind speed that is so variable parameter not only throughout the year, but during the month, week, and even day. Also, PV power generation experiences a slight decrease in rainy seasons such as January, February, November, and December due to low solar irradiation because of rainy and cloudy conditions.

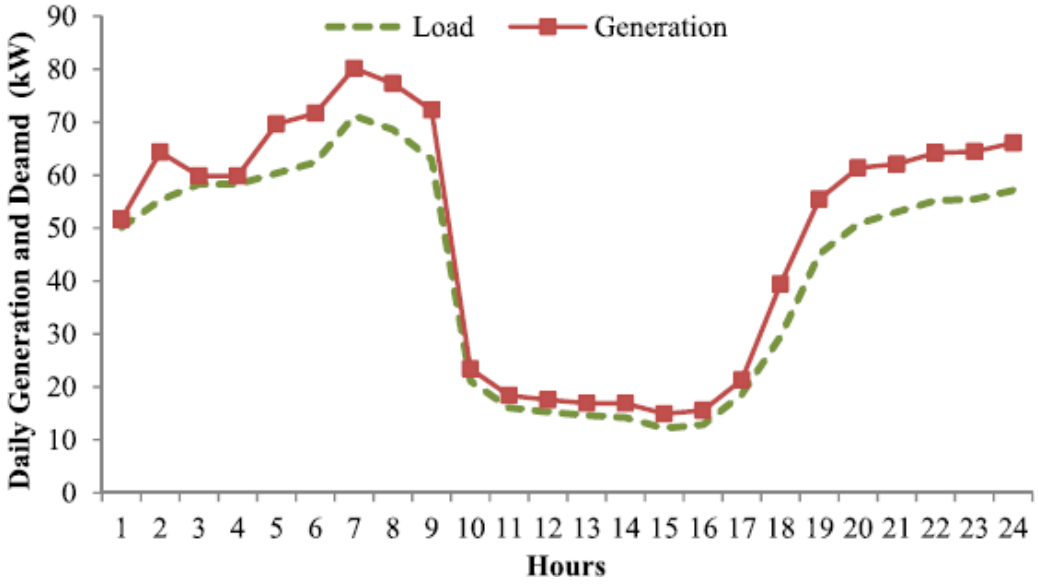

Figure 7.13. Daily generation profile versus total daily load demand.

According to the study results, the hybrid uses of biomass power plants, wind turbines, and photovoltaic systems in the village of Tazuta and the rural areas of Fes in

Morocco enables cheaper electricity generation and reduces atmospheric emissions compared to the operation of wind turbines alone and other hybrid generation scenarios. The construction of biomass power plants and PV modules reduced the number of expensive wind turbines in the hybrid case. For these reasons, biomass could satisfy almost two-third of total power demand of Tazouta and Fez regions compared to 33 % and 2 % of PV and wind generation, respectively. Biomass power plants can provide stable energy for consumers during the year and the moments without sunshine and wind blow. The operation of biomass plants with wind and solar units is necessary to provide a permanent and uninterruptable electric energy supply.

§7.3. Biogas: composition, formation process, and yield.

In addition to obtaining energy through the direct combustion of biological waste, biogas can also be produced. Biogas is a product formed as a result of fermentation (anaerobic digestion) of various biological materials in an oxygen-free environment. Biogas is a mixture of gases. Its main components are methane (CH_4) – 55–70%, carbon dioxide (CO_2) – 28–43%, and small amounts of gases such as hydrogen sulfide (H_2S) at about 500 ppm, as well as other gases. On average, when 70% of 1 kg of organic matter is biologically decomposed, it is converted into 0.18 kg of methane, 0.32 kg of carbon dioxide, 0.2 kg of water, and 0.3 kg of non-decomposed residue. The gases produced during fermentation can be used for heating houses and water, cooking food, and other purposes. In particular, the use of biogas in rural areas located far from main energy networks provides many conveniences for the rural population.

The production process of biogas and organic fertilizers takes place in special bioreactors called methane tanks. Biogas, which is considered a forgotten fuel source, was first used in ancient China. Therefore, China currently holds a leading position in the world in biogas production. In the mid-1970s, nearly one million methane tanks were constructed and put into operation in this country. At present, their number has exceeded 20 million. In the People’s Republic of China, 30% of national energy consumption is covered by biogas.

India holds the second place in the world in biogas production. In the 1930s, the first national program in the world for the development of biogas production

technology was adopted in India. By the late 2000s, the number of methane tanks constructed in rural areas of India had exceeded 1 million. As a result, the energy supply and sanitary-hygienic conditions of several villages improved, deforestation due to tree cutting in forests significantly decreased, and soil quality was enhanced. Today, the daily biogas production in India exceeds 2.5–3.0 million m^3.

A national biogas company was established in Nepal and it is actively operating. Biogas facilities installed in 8 livestock farms in Japan are being successfully operated.

Preliminary calculations show that from 1 ton of plant biomass mixed with waste, 350 m^3 of gas (methane, hydrogen) can be produced.

From the manure of one cow, up to 4.2 m^3 of biogas can be obtained per day. The energy of 1 m^3 of biogas is equivalent to the energy of 0.6 m^3 of natural fuel gas, 0.74 L of oil, 0.65 L of diesel fuel, 0.48 L of gasoline, and others. The use of biogas helps save fuel oil, coal, electricity, and other energy sources used for power generation. The implementation of biogas systems improves the environmental conditions of livestock and poultry farms as well as their surrounding areas.

How much gas can be obtained from one kilogram of manure? Considering that 26 liters of gas are required to boil 1 liter of water, it has been determined how much water can be boiled using gas obtained from the following wastes:

- from 1 kg of cattle manure: enough to boil 7.5–15 liters of water;
- from 1 kg of pig manure: enough to boil 19 liters of water;
- from 1 kg of poultry manure: enough to boil 11.5–23 liters of water;
- from 1 kg of legume straw: enough to boil 11.5 liters of water;
- from 1 kg of potato stems: enough to boil 17 liters of water;
- from 1 kg of tomato stems: enough to boil 27 liters of water.

One of the advantages of biogas is that it allows the production of heat and electrical energy anywhere.

The bioconversion process of waste, in addition to solving the energy problem, also addresses two other issues. First, digested manure increases the yield of agricultural crops by 10–20% compared to ordinary manure. Second, during the digestion process, weed seeds, various microbial compounds, helminth eggs, and unpleasant odors present in large quantities in manure are eliminated.

Biogas production systems and their operation. The schematic design and structural-technological parameters of biogas plants depend on the volume of processed raw materials, the properties of the substrate being digested, the thermal and moisture conditions, the methods of loading and fermentation, and a number of other factors. The main component of a biogas plant is a hermetically sealed reactor equipped with a heat exchanger (with a heat carrier water heated up to 50–60 °C), as well as devices for feeding and discharging manure and for removing the produced gas (Fig. 7.14).

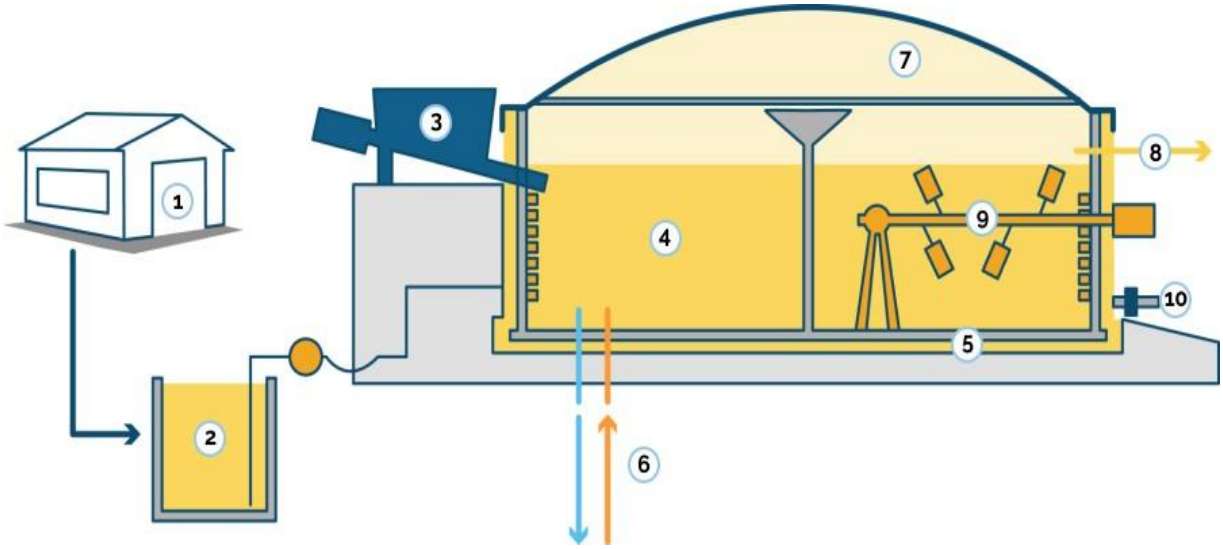

Figure 7.14. Schematic of a biogas production plant.

1 – liquid biomass production; 2 – tank for collection and homogenization of liquid raw material; 3 – solid raw material feeding unit; 4 – methane tank (methantank); 5 – system for supplying and discharging hot water for heating the unit; 6 – gas holder; 7 – biogas outlet; 8 – mixing mechanism; 9 – biomass discharge.

Biogas is produced in specialized biogas plants. Inside such systems, an oxygen-free (anaerobic) environment is maintained, where bacteria convert biomass into biogas. Biogas plants are diverse, and their design depends on local conditions as well as the quantity of raw materials used for biogas production. Below, some designs of biogas plants are considered.

The main components of a biogas production system are the biomass receiving units and the methane tank (methantank). The methantank, in turn, consists of a bioreactor and a gas holder. In the biomass receiving units, the biomass is prepared for anaerobic digestion and, if necessary, undergoes preliminary treatment. After that, the

prepared biomass is fed into the bioreactor.

The bioreactor is a waterproof and airtight vessel equipped with a special device for feeding biomass. An anaerobic environment is maintained inside it. The bioreactor is equipped with mixing devices to ensure uniform decomposition of biomass throughout its volume. To maintain optimal conditions for the digestion process, a temperature of approximately 40°C is sustained inside the reactor. Additionally, the bioreactor is provided with a special pipe for discharging the biomass after the completion of the digestion process.

The gas holder is a hermetically sealed steel vessel that collects the gas produced during the digestion process. It is equipped with a gas outlet pipe designed to discharge biogas from the holder.

Figure 7.15 presents a simplified schematic of a biogas reactor. According to the scheme, the raw material a mixture of water and manure is fed into the bioreactor. The amount of substrate should fill up to 90% of the bioreactor volume. The substrate is retained in the bioreactor for 7–12 days. The produced gas is burned for various purposes or can be converted into thermal or electrical energy.

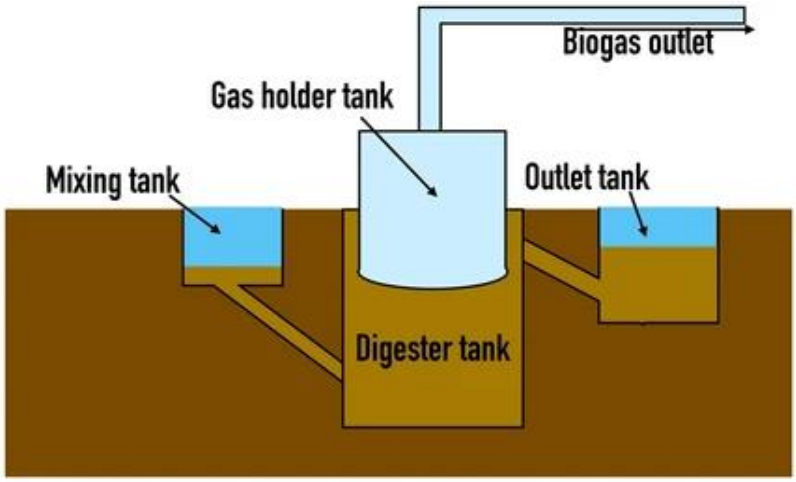

7.15. Simplified diagram of a biogas reactor.

The spent raw material is removed from the bioreactor, and the reactor is then refilled with fresh substrate. The use of biogas has the following advantages:

– biogas is considered a carbon-neutral fuel compared to CO_2, and its use prevents the increase of methane emissions into the atmosphere that would otherwise result from the uncontrolled decomposition of organic waste.

– the fertilizers obtained from digested biomass have significantly higher value

than the initial raw materials;

– the recycling of nutrients on farmers' lands in an environmentally safe and economically beneficial way is an advantage of anaerobic digestion of solid biomass for biogas production;

– human health improves due to the reduction of environmental pollution;

– it provides household conveniences even in remote rural areas;

– it increases soil fertility;

– it enables the utilization of waste;

– it reduces dependence on external energy sources.

At present, small-scale bioreactors are being installed that produce approximately 6-8 m^3 of biogas and 100–120 liters of fertilizer per day.

Figure 7.16. A biogas production unit operating on organic waste from the YOSHQ farm, affiliated with the Bukhara Oil Refinery, located in Qaravulbozor district of Bukhara Region.

The picture shows one of the existing biogas plants in our country, with a total capacity of 300 m^3.

Economic efficiency of biogas plant operation. The economic efficiency of biogas plants is determined by the method of obtaining high-quality organic fertilizers, biogas (methane), and vitamin supplements (B_{12}) used as feed additives for animals and poultry, all of which are produced during the processing of organic waste. It also depends on the amount of biomass processed per unit volume of the plant. Many

studies indicate that this efficiency is largely influenced by the quality and quantity of products obtained from the processing of organic waste.

The economic efficiency of biogas production plants is best evaluated during the calculation phase based on the type and quality of products obtained from them, such as high-quality organic fertilizers, biogas, or vitamin supplements, and by the profit generated from their sale. In addition, it is necessary to consider the significant reduction of toxic gases emitted into the atmosphere during the anaerobic digestion of organic waste. However, in biogas plants, there is still no established methodology for calculating the cost of the environmental impact of greenhouse gases that are captured during the recycling of organic waste and prevented from being released into the atmosphere, which is considered a negative limitation (anomaly). In biogas systems, the cost of high-quality processed organic waste is considered as the profit obtained from its sale. In this case, it is appropriate to compare one ton of organic waste with mineral fertilizers in terms of application rates to soil and plants. The bio slurry consists mainly of water (over 88.5%) and dry organic matter (11.5%). If a 10 m^3 bioreactor designed for cattle waste operates continuously under thermophilic conditions, the processed bio slurry can provide, per day, directly applicable organic nutrients such as nitrogen (2–3 kg), phosphorus (1.6 kg), potassium (3.6 kg), sodium (0.96 kg), and calcium (1.28 kg) for soil application. If technological conditions in bioreactors are fully maintained, on average up to 3 m^3 of biogas per day can be obtained from 1 m^3 of useful reactor volume.

The construction and operation of anaerobic treatment facilities for organic waste should be organized and applied in enterprises and organizations where economic efficiency is determined based on the amount of daily organic waste generated. Such enterprises include: a) In agriculture: cattle farms, poultry farms, pig farms, horse stables, and agricultural plant waste storage sites; b) Greenhouses producing root and plant residues; c) Food processing enterprises: alcohol, beer, and sugar factories; fish, meat, milk, fruit, and vegetable processing plants; bakery production enterprises; and in recent years, plants processing high-water aquatic plants cultivated in drainage areas to reduce soil salinity; d) Municipal wastewater treatment plants; e) Rural settlement waste collection sites.

Rural bioreactors are medium-capacity bioreactors (capable of processing up to 10 tons of organic waste per day) that can be constructed and commissioned at low cost through community cooperation (hashar) and the use of local materials. Such systems not only fully meet the demand of rural households for mineral fertilizers but also provide additional electricity supply and enable the capture of harmful gases released into the atmosphere. The natural processing of organic waste (anaerobic digestion, which can be considered 99.99% natural fermentation) and its complete return to nature results in immeasurable economic benefits. It is well known that living organisms depend on daily nutrition. The composition of food entering the human body determines its physiological and intellectual development as well as life expectancy. Even minor disturbances in dietary patterns (small changes in the composition of fresh and dried fruits, root crops, and vegetables, etc.) can reduce human immune resistance. The main reason for this is the contamination of the ecological environment with small amounts of radionuclides, toxic elements, nitro compounds, pesticides, antibiotics, and hormones. The main cause of this problem is the return of previously used substances, which are mixed into organic waste and not properly processed before being returned to the plant ecosystem. This factor defines the main economic efficiency of anaerobic processing.

REFERENCES

1. Decree of the President of the Republic of Uzbekistan No. UP-158 dated September 11, 2023, ‘On the Strategy "Uzbekistan - 2030".
2. https://minenergy.uz.
3. Allaev K.R. Modern Energy Sector and Prospects for Its Development. Tashkent: Fan va texnologiyalar, 2021. - 951 p.
4. Gerasimov V.G. et al. Electrical Engineering Handbook. Volume 3. Generation, Transmission, and Distribution of Electric Power. Moscow: MEI, 2004. - 964 p.
5. Product Catalog of the Joint-Stock Company SP AO «UZKABEL». Tashkent, 2021. - 464 p.
6. IEC 60364-5-52:2009. Low-voltage electrical installations – Part 5 -52: Selection and erection of electrical equipment – Wiring systems. Geneva: International Electrotechnical Commission, 2009. - 214 p.
7. https://solar.huawei.com/.
8. https://www.solaxpower.com/.
9. GOST R IEC 60050-121-2010. International Electrotechnical Vocabulary. Part 121. Electromagnetism. Moscow: Standartinform, 2011. – 42 p.
10. R.R. Avezov, A.Yu. Orlov. Solar Heating and Hot Water Supply Systems. Tashkent: Fan, 1988. - 288 p.
11. N.R. Avezova, R.R. Avezov, A.U. Vokhidov. Resource Indicators of Flat Solar Water Heating Collectors. Methodology for Calculating the Main Thermal, Techno-Eco- nomic, and Environmental Indicators of Solar Collectors // LAP-Lambert Academic Publishing - Saarbrücken, Germany, 2016. – 93 p.
12. GOST 32144–2013. Electric Energy. Electromagnetic Compatibility of Technical Equipment. Standards for Electric Energy Quality in General-Purpose Power Supply Systems. Moscow: Standartinform, 2014. – 16 p.
13. M. Mirzaboev, Q. Rasulov. Solar Battery Elements. Tashkent: Uzbekistan, 1979. – 23 p.

14. https://globalsolaratlas.info/.

15. A.M. Mirzabaev, T.A. Makhkamov, O.R. Sytdykov, Sh.M. Mirzabekov, Sh.I. Dungbaev. Development of Solar Energy in Uzbekistan and Methods for Its Promotion. Issues of Energy and Resource Conservation. Tashkent: Fan va texnologiyalar, 2017, No. 1-2, pp. 182–186.

16. I.A. Yuldoshev, M.Q. Sultonov, F.M. Yuldashev. Solar Energy. T.: Bookany Print, 2022. – 338 p.

17. M.M. Mirzabaev, K. Rasulov, A. Komilov, A. Iskanderov, S.T. Tashhodzhaeva. Characteristics of physical processes in photoconverters based on silicon and gallium arsenide under concentrated solar radiation. T.: Fan, 1986. – 144 p.

18. R. Verduci, V. Romano, G. Brunetti, N. Yaghoobi Nia, A. Di Carlo, G. D'Angelo, C. Ciminelli. Solar Energy in Space Applications: Review and Technology Perspectives. Advanced Energy Materials, 2022. DOI: 10.1002/aenm.202200125.

19. J. Li, A. Aierken, Y. Liu, Y. Zhuang, X. Yang, J. H. Mo, R. K. Fan, Q. Y. Chen, S. Y. Zhang, Y.M. Huang, Q. Zhang. A Brief Review of High Efficiency III-V Solar Cells for Space Application. Frontiers in Physics, 2021, Vol. 8, Article 631925. DOI: 10.3389/fphy.2020.631925.

20. IEC 60904-1:2020. Photovoltaic devices – Part 1: Measurement of photovoltaic current- voltage characteristics. Geneva: International Electrotechnical Commission, 2020. - 64 p.

21. IEC 60904-3:2019. Photovoltaic devices – Part 3: Measurement principles for terrestrial photovoltaic (PV) solar devices with reference spectral irradiance data. Geneva: International Electrotechnical Commission, 2019. -44 p.

22. IEC 61853-1:2011. Photovoltaic (PV) module performance testing and energy rating – Part 1: Irradiance and temperature performance measurements and power rating. Geneva: International Electrotechnical Commission, 2011. — 42 p.

23. IEC 61853-2:2016. Photovoltaic (PV) module performance testing and energy rating – Part 2: Spectral response, incidence angle and module operating temperature measurements. Geneva: International Electrotechnical Commission, 2016.

— 50 p.

24. IEC 61215-1:2016. Terrestrial photovoltaic (PV) modules – Design qualification and type approval – Part 1: Test requirements. Geneva: International Electrotechnical Commission, 2016. – 62 p.

25. IEC 61215-2:2016. Terrestrial photovoltaic (PV) modules – Design qualification and type approval – Part 2: Test procedures. Geneva: International Electrotechnical Commission, 2016. – 9 p.

26. A.M. Mirzabaev. RENEWABLE ENERGY SOURCES AND UTILIZATION TECHNOLOGIES. T.: Fan Ziyosi, 2023. — 244 p.

27. M.M. Koltun. Optics and Metrology of Solar Cells. Moscow: Nauka, 1985. – 280 p.

28. https://www.jinkosolar.com/.

29. Akram M. Mirzabayev, Temur A. Makhkamov, Shakhnoza A. Mukhamadova, Lazizakhon R. Makhkamova, Sanobar N. Avliyakulova. Effect of Surface Soiling on the Energy Output of Monocrystalline Photovoltaic Modules. International Scientific and Technical Conference ‘Challenges and Solutions for the Efficient Use of Alternative Energy Sources’. ProceedinHz. Karshi, 2024. pp. 526– 530.

30. Mohan, N., Undeland, T. M., Robbins, W. P. Power Electronics: Converters, Applications, and Design. – 3rd ed. – Hoboken, NJ: Wiley, 2022. – 832 p.

31. Rashid, M. H. Power Electronics: Devices, Circuits, and Applications. – 5th ed. Hoboken, NJ: Pearson, 2023. – 1072 p.

32. Andreev, V.D., Zharkov, Yu.D. Power Electronics: A Textbook for Universities. Moscow: Akademiya, 2010. – 544 p.

33. SUN2000-(3KTL-10KTL)-M1 High Current Version User Manual. –2025. Huawei Digital Power Technologies Co., Ltd.

34. NFPA 70: National Electrical Code (NEC) – 2023 edition. Article 690: Solar Photovoltaic (PV) Systems. Includes requirements for circuit sizing and overcurrent protection, specifically clauses 690.8(A)(1) and 690.8(B)(1), detailing factors of 1.25 and 1. 56 for fuse/ conductor sizing. Quincy, MA: National Fire Protection Association, 2023.

35. IEC 62548:2016. Design requirements for photovoltaic (PV) arrays. Geneva: International Electrotechnical Commission, 2016.

36. IEC 62109-1:2010. Safety of power converters for use in photovoltaic power systems–Part 1: General requirements. Geneva: International Electrotechnical Commission, 2010.

37. IEC 62109-2:2011. Safety of power converters for use in photovoltaic power systems – Part 2: Particular requirements for invertors. Geneva: International Electrotechnical Commission, 2011.

38. IEC 62305-1:2024. Protection against lightning – Part 1: General principles. Geneva: International Electrotechnical Commission, 2024.

39. IEC 62305-3:2024. Protection against lightning – Part 3: Physical damage to structures and life hazard. Geneva: International Electrotechnical Commission, 2024.

40. IEC 62305-4:2024. Protection against lightning – Part 4: Electrical and electronic systems within structures. Geneva: International Electrotechnical Commission, 2024.

41. A.M. Mirzabaev, T.A. Makhkamov. Issues of Integration of Photovoltaic Power Plants into the Electric Power System. Problems of Energy and Resource Saving. Special Issue No. 87. Tashkent: Fan va texnologiyalar, 2004. pp. 365–377.

42. Akram M. Mirzabaev, Temur A. Makhkamov, Afzalkhuja R. Kudratov, Shahnosa A. Mukhamadova, Lazizakhon R. Makhkamova. The impact of the grid invertor’s connection point on the operational efficiency of a photovoltaic power plant. International Scientific and Technical Conference ‘Problems and Solutions for the Effective Use of Alternative Energy Sources.’ ProceedinHz Collection. Karshi, 2024. pp. 477–480.

43. EN 50618:2014. Electric cables for photovoltaic systems. Brussels: CENELEC, 2014 (incorporating Corrigendum 2015).

44. TÜV 2 PfG 1169/08.2007. Requirements for cables for use in photovoltaic systems (PV1-F). Cologne: TÜV Rheinland, 2007.

45. Electrical Installation Regulations (PUE), Seventh Edition. Moscow: ENAS NC Publishing House, 2003. 557 pp.

46. Burton, T., Sharpe, D., Jenkins, N., Bossanyi, E. *Wind Energy Handbook*. 2nd ed., Wiley, 2011.

47. Hau, E. *Wind Turbines: Fundamentals, Technologies, Application, Economics*. Springer, 2013.

48. Manwell, J.F., McGowan, J.G., Rogers, A.L. *Wind Energy Explained: Theory, Design and Application*. Wiley, 2010.

49. Paraschivoiu, I. *Wind Turbine Design: With Emphasis on Darrieus Concept*. Polytechnic International Press, 2002.

50. Gasch, R., Twele, J. *Wind Power Plants: Fundamentals, Design, Construction and Operation*. Springer, 2012.

51. Mathew, S. *Wind Energy: Fundamentals, Resource Analysis and Economics*. Springer, 2006.

52. Hansen, M.O.L. *Aerodynamics of Wind Turbines*. 3rd ed., Earthscan, 2015.

53. International Renewable Energy Agency. *Renewable Capacity Statistics 2023*. Abu Dhabi, 2023.

54. International Energy Agency. *World Energy Outlook 2023*. Paris, 2023.

55. Global Wind Energy Council. *Global Wind Report 2024*. Brussels, 2024.

56. Brinkmann Consulting. *Global Wind Market Forecast 2023–2033*.

57. International Electrotechnical Commission. *IEC 61400-1: Wind Turbines – Design Requirements*. Geneva, 2019.

58. International Electrotechnical Commission. *IEC 61400-2: Small Wind Turbines*. Geneva, 2013.

59. International Electrotechnical Commission. *IEC 61400-3: Offshore Wind Turbines*. Geneva, 2019.

60. International Organization for Standardization. *ISO 19900: Offshore Structures – General Requirements*.

61. API. *API RP 2A-WSD: Planning, Designing and Constructing Fixed Offshore Platforms*.

62. Rezaeiha, A., Kalkman, I., Blocken, B. Effect of solidity on the performance of vertical axis wind turbines. *Energy Conversion and Management*, 2017.

63. Castelli, M.R., Englaro, A., Benini, E. The influence of blade geometry on

Darrieus wind turbine performance. *Journal of Fluids Engineering*, 2011.

64. Musial, W., Butterfield, S., Ram, B. Energy from offshore wind. *Energy Policy*, 2006.

65. Hansen, M.O.L., Sørensen, J.N. Aerodynamic analysis of wind turbines. *Progress in Aerospace Sciences*, 2008.

66. O‘zbekiston Respublikasi Energetika vazirligi. *Qayta tiklanuvchi energiya manbalarini rivojlantirish konsepsiyasi (2020–2030)*.

67. “O‘zbekenergo” AJ, GEONET, Intec-Gopa. O‘zbekiston shamol energetikasi atlasi. Toshkent, 2015.

68. Vestas Wind Systems. *Wind Turbine Technology Overview*.

69. GE Renewable Energy. *Wind Turbine Technical Documentation*.

70. Quantis. *Lifecycle Assessment of Wind Turbines and Recycling Technologies*.

71. Пашковскаya Е.Е., Сивеев Т.М., Дубина Д.С., Илин С.В. Разработка схемы размещения ветряной энергоустановки на площадке ветроэлектростанции оценка выработки ветроэлектростанции//Современные научные исследования: актуалные вопросы, достижения и инновации– 2021 – С. 83 – 85

72. Проектирование гидроэлектростанции / С.В. Евдокимов [и др.]. — Самара: Самарский государственный технический университет, ЭБС АСВ, 2019. — 87 с.

73. A.Davirov, N.Abdug‘aniyev. MikroGES charxpalagi parraklarining optimal burchagini aniqlash bo‘yicha dastlabki tadqiqotlar // “Qishloq va suv xo‘jaligining zamonaviy muammolari” XX – yosh olimlar, magistrantlar va iqtidorli talabalarning ilmiy-amaliy anjumani to‘plami, Toshkent, 2021 y., 25-26 may.

74. D.Kodirov, Kh.Muratov, A.Davirov, J.Normuminov, B.Mamadjanov, A.Shukuraliyev, I.Berdiyorova, and Sh.Musayev // Study on the effective use of solar and hydro energy for powering agriculture and water management, IOP Conf. Series: Earth and Environmental Science 1142 (2023) 012029 IOP Publishing doi:10.1088/1755-1315/1142/1/012029

75. Y. Yassi Experimental Study of a High Speed Micro Waterwheel // Iranian Journal of Mechanical Engineering, Vol. 14, No. 1, March. 2013. Pages: 33-47

76. F.Weichbrodt, S.Dimke, J.Hadler, P.Fröhle Großmaßstäbliche

Modellversuche mit einem schwimmenden Energiewandler // 29334. Dresdner Wasserbaukolloquium 2011: Wasserkraft – mehr Wirkungsgrad + mehr Ökologie = mehr Zukunft, Pages:291-299

77. Cleynen, O., Kerikous, E., Hoerner, S., & Thevenin, D. (2017). Influence of flotation bodies on the power characteristics of a free-stream water wheel. Computational and Experimental Methods in Multiphase and Complex Flow IX 55-60.

78. G.Müller, C.Wolter The breastshot water wheel: design and model tests / Proc. ICE Eng. Sustain ability , Vol. 157, Issue E S4, 2004, Pages:203 – 212.

79. Müller, G., & Kauppert, K. (2004). Performance characteristics of water wheels. Journal of Hydraulic Research, 42(5), 451–460

80. Müller, G., Denchfield, S., Marth, R., & Shelmerdine, R. (2007). Stream wheels for applications in shallow and deep water. Proc. 32nd IAHR Congress, Venice C (2c, Paper 291).

81. Khan, F., Ahmed, A., Khan, U., & Haider, F. (2015). Modeling, simulation and fabrication of an undershot floating waterwheel. J. Eng. and Appl. Sci., 34(2), 55–69.

82. D.B.Qodirov Past bosimli suv oqimlari uchun energiya samarador mikrogidroelektrstansiya // Texnika fanlari bo‘yicha falsafa doktori(PhD) avtoreferati. Toshkent 2018. 41 bet

83. D.Qodirov., A.Davirov., R.Qobilov. Kichik gidroelektrstansiyalarni loyihalashtirish// Mashinasozlik ilmiy-texnika jurnali, Andijon, 2022 yil, 1120-1126-bet

84. A.B.Mamadjanov. Gravitatsion girdobli mikrogidroelektr stansiyaning energiya samaradorligini oshirish // Texnika fanlari bo‘yicha falsafa doktori(PhD) ilmiy darajasini olish uchun yozilgan dissertatsiya ishi. Toshkent 2023. 131 bet

85. O.U.Zoxidov. Konchilik korxonalarida muqobil energiya manbalari asosida elektr energiya iste’moli samaradorligini oshirish// Texnika fanlari bo‘yicha falsafa doktori(PhD) ilmiy darajasini olish uchun yozilgan dissertatsiya ishi. Toshkent 2023. 140 bet.

86. Yoosef Doost, A.; Lubitz, W.D. Archimedes screw turbines: A sustainable

development solution for green and renewable energy generation-a review of potential and design procedures. Sustainability 2020, 12, 7352.].

87. https://rreda.ru/industry/acquaintance/res-hydro/

88. Scott C. Simmons, Chris Elliott, Mike Ford, Adrian Clayton, William David Lubitz // Archimedes screw generator powerplant assessment and field measurement campaign// Energy for Sustainable Development 65 (2021) 144-161

89. Q.Латипов, С.Эргашев, Гидравлика ва гидромашиналар оʻқув қоʻлланма Тошкент 1986

90. Имомов Ш. Ж., Усмонов К.Э. Биогаз: экология ва органик ўғит / жамоа. Тошкент, Адабиёт учқунлари, 2016 – 240 б. Номограмма

91. Sara González-García, Jacopo Bacenetti. Exploring the production of bio-energy from wood biomass. Italian case study. Science of the Total Environment 647 (2019), pp 158–168

92. Eirik Ogner Jastad et al. The role of woody biomass for reduction of fossil GHG emissions in the future North European energy sector. Applied Energy 274 (2020), 115360.

93. NordPool. Historical Market Data. Available at: http://www.nordpoolspot.com/historical-market-data/; 2018.

94. Meisam Mahdavi et al. Hybrid biomass, solar and wind electricity generation in rural areas of Fez-Meknes region in Morocco considering water consumption of animals and anaerobic digester. Applied Energy 343 (2023) 121253.